

SKB R-20-17

ISSN 1402-3091 ID 2078915 September 2025

Methodology for site descriptive and safety assessment transport modelling of the bedrock at Forsmark

Sten Berglund, HydroResearch AB

Anna-Maria Jakobsson, Jan-Olof Selroos Svensk Kärnbränslehantering AB

James Crawford, Kemakta Konsult AB

Paolo Trinchero, Amphos 21 Consulting S.L.

This report is published on www.skb.se
© 2025 Svensk Kärnbränslehantering AB

Preface

A series of methodology reports support the programmes for investigation and modelling during the execution of planned underground constructions at Forsmark. The series includes the following disciplines: geometric modelling of ground elevation and regolith, deterministic geological modelling, discrete fracture network (DFN) modelling, rock mechanics modelling, thermal properties modelling, integrated hydrological and hydrogeological modelling, hydrogeochemical modelling, and transport modelling. Report numbers (ID), acronyms and titles are shown below. The acronyms are recommended for internal referencing.

ID	Acronym	Title				
R-20-10	DGMM	Methodology for deterministic geological modelling of the Forsmark site. Application to the development of the final repository for spent nuclear fuel				
R-20-11	DFNMM1	Methodology for discrete fracture network modelling of the Forsmark site Part 1 – concepts, data and interpretation methods				
R-20-13	RMMM	Methodology for rock mechanics modelling of the Forsmark site				
R-20-14	HGMM	Methodology for hydrological and hydrogeological modelling of the Forsmark site				
R-20-15	НСММ	Methodology for hydrochemical modelling of the Forsmark site				
R-20-16	ERMM	Methodology for elevation and regolith modelling of the Forsmark site				
R-20-17	TRPMM	Methodology for site descriptive and safety assessment transport modelling of the bedrock at Forsmark				
R-20-18	THPMM1	Methodology for modelling of thermal properties of the Forsmark site Part 1 – Recommended data and interpretation methods				
R-20-19	THPMM2	Methodology for modelling of thermal properties of the Forsmark site Part 2 – Background and methodology development				

The present report provides the methodology for transport modelling. It covers transport modelling of the bedrock (geosphere) performed during both site investigations, resulting in a site descriptive model, and safety assessments, where simulations of radionuclide transport and associated doses are a central component. In particular, the methodology report focuses on how the site-specific parameters measured within the bedrock transport properties programme are interpreted, evaluated and further developed into recommended input parameters for the radionuclide transport modelling in the safety assessment. The parameterisation of radionuclide transport models is another important part of the methodology proposed in the report.

The work presented in this report was initiated by Jan-Olof Selroos (SKB) and performed by a project group led by Anna-Maria Jakobsson (SKB). The following persons have contributed as authors and/or internal reviewers: Anna-Maria Jakobsson, Martin Löfgren, Niko Marsic, Jean-Marc Mayotte, Jan-Olof Selroos, Henrik Widestrand and Per-Anders Ekström (SKB), James Crawford and Karin Norrfors (Kemakta Konsult), Johan Byegård and Kersti Nilsson (Rejlers), Sten Berglund (HydroResearch), Björn Gylling (Gylling GeoSolutions), Paolo Trinchero (Amphos 21 Consulting), Eva-Lena Tullborg (TerraLogica) and Antti Poteri (Posiva).

Abstract

The objective of this report is to present an updated methodology for construction of site descriptive models of bedrock transport properties and for geosphere transport modelling in forthcoming safety assessments of nuclear waste repositories at the Forsmark site. In the methodology, a conceptual model is developed for organising identified small-scale ("microstructural") features of importance for transport retardation of released radionuclides. This consists of a description of the various geological materials and features comprising the geosphere and how they are organised along flowpaths hosted in the rock. The conceptual model is then intended to be used as a basis for defining a simplified modelling parameterisation (transport classes) for use in numerical models of radionuclide transport. The methodology addresses both the interpretation of experimental data and the further analyses where a set of transfer factors are applied to obtain parameters that represent present and future site conditions relevant for the safety assessment calculations of radionuclide transport.

The report begins with a background of the Forsmark site and repository projects, including an overview of the associated licensing processes and the site descriptions and safety assessments produced to date. Bedrock transport modelling is introduced, and the main modelling tasks are outlined. The background description also summarises the currently available data, earlier review comments and modelling terminology. The report then explores the theory, modelling concepts, processes, and parameter definitions that constitute the basis for the SKB transport modelling. Furthermore, transport modelling concepts and codes are presented and discussed, as well as the parameterisation of radionuclide transport models and interactions with other modelling disciplines.

The methodology for developing site descriptive transport models of bedrock materials and structures is detailed in the report, introducing different types of building blocks to be used when structuring models on different scales. The site descriptive modelling is to a large extent developed and delivered in terms of the retardation model, which is a descriptive model that consists of fracture types and other geological units/materials and associated transport parameters identified as typical for the site. The identification and description of fracture types and other model components is carried out in a process that requires inputs of geological, hydrogeological and hydrogeochemical data and models.

The conceptualisation of fracture types in the retardation model is based on a multilayer description of the rock matrix including fracture coatings, alteration rims associated with the fracture, and the underlying unaltered rock matrix (referred to as fresh rock). Material properties of the different rock and alteration types comprising the retardation model are determined in laboratory and field investigations using the Forsmark site and site-specific materials wherever possible. The report also provides a methodology for using inputs from data sources in the open literature in cases when parameters needed for the safety assessment transport modelling cannot be obtained from site data.

The main retardation parameters of interest for radionuclide transport modelling are the porosity, effective diffusivity and sorption partitioning coefficients (K_d) of the geological materials included in the modelling. In the proposed methodology, a correction is applied to material property parameters for effects relating to *in-situ* compression (pore compression and anion exclusion), as well as to laboratory measurement data for deviations relating to stress relaxation and damage incurred during sampling. Whereas the radionuclide transport modelling is the main recipient of retardation parameters, these parameters are also needed for transport calculations performed within hydrogeological (density-driven flow) and hydrogeochemical (e.g. penetration of dilute water) modelling.

The K_d value that quantifies sorption has a special status given that it is not only dependent on the identifiable material properties of the rock itself, but also conditional on the groundwater composition which is expected to vary in space and time throughout the geosphere over safety assessment timescales. The approach for assigning site-specific K_d values is based on a transfer factor approach which accounts for deviations in groundwater chemistry relative to a small number of representative compositions used in the laboratory investigations.

In the transfer factor methodology, K_d values measured in the laboratory for reference materials (fresh and altered rock, fracture coatings and fracture-filling materials) and groundwater types are extrapolated to safety assessment conditions with the aid of numerical models of the principal sorption mechanisms, i.e. surface complexation and cation exchange. In the proposal for the use of

transfer factors it is reasoned that the simulation of relative deviations (i.e. normalising simulated K_d values to a reference) yields transfer factors that cancel parameter biases and more reliably scale site-specific measurements of K_d across groundwater compositions than the direct use of uncalibrated literature models derived for simpler mineral systems.

The flow-related parameters, which form the other main category of transport parameters, are directly interpreted from the hydrogeological modelling, i.e. from particle tracking simulations in groundwater flow models. The report provides an overview of methods for calculation of flow-related parameters in different types of flow models and briefly discusses analyses of advection phenomena that may need to be carried out in support of forthcoming transport modelling.

In the methodology for radionuclide transport modelling, a division of the flowpaths where transport takes place into segments and the use of so-called transport classes are proposed. The division into segments and transport classes involves a description of how transport properties vary both spatially and temporally (primarily due to varying water chemistry). The report provides a methodology for identifying and describing transport classes based on a geospatial database and the fracture types in the retardation model. In the final step of the modelling methodology, procedures for assigning transport classes and thereby retardation parameters to flowpath segments are presented.

Sammanfattning

Syftet med denna rapport är att redovisa en uppdaterad metodik för framtagandet av platsbeskrivande modeller av bergets transportegenskaper och för transportmodellering av geosfären i kommande säkerhetsanalyser av kärnavfallsförvar i Forsmark. I den föreslagna metodiken utvecklas en konceptuell modell som används för att strukturera beskrivningen av de småskaliga geologiska enheter som befinns vara viktiga för retardationen av radionuklidtransport. Beskrivningen innefattar diverse geologiska material och hur dessa uppträder längs flödesvägar i berget. Modellen används sedan som utgångspunkt för en förenklad beskrivning och modellparametrisering i termer av så kallade transportklasser i säkerhetsanalysen. När det gäller transportparametrar innefattar metodiken både den primära tolkningen av experimentella data från platsundersökningar och de fortsatta utvärderingarna där överföringsfaktorer används för att ta fram parametrar som kan användas för att representera framtida förhållanden i säkerhetsanalysens radionuklidtransportmodellering.

Rapporten inleds med bakgrundsbeskrivningar av platsen Forsmark och de förvarsprojekt som bedrivs där, inklusive översiktliga beskrivningar av pågående tillståndsprocesser och de platsbeskrivningar och säkerhetsanalyser som hittills producerats. Vidare ges en introduktion till SKB:s transportmodellering av berget och de viktigaste modelleringsuppgifterna inom detta område. Rapporten sammanfattar tillgängliga platsdata, erhållna granskningskommentarer och den terminologi som används i rapporten. Dessutom ges en överblick av teori, modelleringskoncept, processer och parameterdefinitioner som ligger till grund för SKB:s transportmodellering. Rapporten beskriver även modelleringskoncept och beräkningsverktyg, samt parametrisering av transportmodeller och interaktioner med andra modelleringsdiscipliner.

Metodiken för utveckling av platsbeskrivande modeller av berget och dess ingående strukturer beskrivs relativt detaljerat, varvid introduceras ett antal olika typer av modellkomponenter (byggstenar) som används för att strukturera och beskriva platsen på olika skalor. Den platsbeskrivande modelleringen bedrivs och levereras till stor del i form av den så kallade retardationsmodellen, vilket är en beskrivande modell som består av spricktyper och andra geologiska enheter och material som identifierats som typiska för platsen samt tillhörande transportparametrar baserade på platsdata. Identifiering och beskrivning av spricktyper och andra modellkomponenter görs i en process som till stor del bygger på indata från andra ämnesområden, främst data och modeller från geologi, hydrogeologi och hydrogeokemi.

Konceptualiseringen av spricktyper i retardationsmodellen utgår från en flerlagerbeskrivning av det angränsande berget, där lagren från sprickväggen räknat kan utgöras av sprickbeläggningar, omvandlingszoner och den underliggande och av omvandlingsprocesser opåverkade delen av bergmatrisen. Materialegenskaperna hos de olika typerna av geologiska material som ingår i retardationsmodellen bestäms i laboratorie- och fältundersökningar som i största möjliga utsträckning nyttjar platsen Forsmark och platsspecifika material därifrån. Rapporten innehåller dock även metodik som beskriver hur andra datakällor i den vetenskapliga litteraturen ska användas i de fall då parametrar som behövs i säkerhetsanalysens transportmodellering inte kan erhållas från platsdata.

De viktigaste parametrarna för radionuklidtransportmodelleringen är porositeten och den effektiva diffusiviteten hos bergmaterialen, samt sorptionsfördelningskoefficienterna (K_d) för relevanta kombinationer av radionuklider, geologiska material och vattensammansättningar. I den föreslagna metodiken beskrivs hur transportparametrar korrigeras för kompression *in-situ* (porkompression och anjonexklusion) och även hur korrektioner tillämpas för att hantera effekter av provtagning (spänningsavlastning och mekaniska skador). Även om radionuklidtransportmodellering är den huvudsakliga mottagaren av retardationsparametrar ska det noteras att dessa parametrar även används i transportberäkningar inom hydrogeologi (densitetsdriven strömning) och hydrogeokemi (exempelvis analyser av nedträngning av jonsvaga vatten i berget).

 $K_{\rm d}$ -värdet för sorption beror av både bergets egenskaper och grundvattnets sammansättning, av vilka den senare kan förväntas variera i både tid och rum i geosfären inom säkerhetsanalysens modellvolymer och tidsperspektiv. Metodiken för tilldelning av platsspecifika $K_{\rm d}$ -värden vid varierande vattenkemi är baserad på användning av överföringsfaktorer som tar hänsyn till variationer i grundvattenkemin i förhållande till mätningar gjorda med ett urval av representativa vattensammansättningar i laboratorieundersökningar. $K_{\rm d}$ -värden som mätts i laboratoriet extrapoleras för referensmaterial (berg och sprickmineral) och grundvattentyper till förhållanden i säkerhetsanalysen baserat på numerisk modellering av de viktigaste sorptionsmekanismerna (ytkomplexering och katjonbyte).

De flödesrelaterade parametrarna utgör den andra huvudgruppen av transportparametrar som används i radionuklidtransportmodelleringen. Dessa parametrar produceras inom den hydrogeologiska modelleringen, genom partikelspårning längs flödesvägar från det aktuella förvaret till ytsystemet (biosfären). I rapporten ges en översikt över metoder för beräkning av flödesrelaterade parametrar i olika typer av grundvattenflödesmodeller och en kortfattad beskrivning av tänkbara stödjande analyser av advektiv transport som kan behöva göras i samband med framtida transportmodellering.

I metodiken för radionuklidtransportmodellering föreslås en uppdelning av flödesvägen där transport sker i segment och en användning av transportklasser vid parametrisering av modeller. Indelningen i segment innebär en beskrivning av hur transport- och sprickegenskaper varierar både spatialt och temporalt (främst beroende på varierande vattenkemi). Rapporten redovisar en metodik för identifiering och beskrivning av transportklasser baserat på den geospatiala databas som kommer att byggas upp inom platsmodelleringen och retardationsmodellens spricktyper. I modelleringsmetodikens sista steg beskrivs hur transportmodellens segmentindelade flödesvägar tilldelas transportklasser och därmed även retardationsparametrar.

Contents

1	Introduction	
1.1	Background	
1.2	Overview of transport modelling	
1.3	Objectives, use and contents of the report	12
1.4	Related documents	15
2	Overview of prerequisites and earlier modelling	16
2.1	Site conditions and existing models	
	2.1.1 Surface and bedrock conditions at Forsmark	
	2.1.2 Existing and planned nuclear waste repositories	
2.2	Transport modelling tasks	
2.3	Previous site investigation and modelling	
	2.3.1 The spent fuel repository (SFK)	
	2.3.2 The SFR extension project (PSU)	
	2.3.3 Other contributions	
2.4	Overview of transport properties data	
2.5	Summary of review comments from SSM	
	2.5.1 The SFK review processes	
	2.5.2 SFK review comments and SKB response	
	2.5.3 The PSU review and comments	
2.6	Terminology	35
3	Transport modelling concepts, processes and parameters	
3.1	Overview of processes and concepts	
3.2	Radionuclide transport in rock fractures	
	3.2.1 Advection and dispersion	
	3.2.2 Pathway simplification	
	3.2.3 Fracture aperture	
3.3	Radionuclide retardation and decay	
	3.3.1 Matrix diffusion	
	3.3.2 Sorption	
	3.3.3 Decay/ingrowth	
3.4	Colloid facilitated and gas phase transport	
3.5	Reactive transport modelling concepts	
	3.5.1 Travel-time based reactive transport models	
	3.5.2 Continuum models for reactive transport	
	3.5.3 DFN models for reactive transport	
3.6	Parameters for transport modelling	53
4	Development of retardation models	
4.1	Introduction	
	4.1.1 Background and applications	
	4.1.2 Conceptual understanding of the zonation of altered rock in the geosphere	
4.2	Overview of existing retardation model	
	4.2.1 Rock types	
	4.2.2 Fracture types	
	4.2.3 Deformation zones	
4.3	Updated methodology and retardation model	
	4.3.1 Transport domains	
1 1	4.3.2 Retardation components comprising microstructural units	
4.4	Parameterisation of building blocks	
	4.4.1 Demarcation of transport domains	
	4.4.2 Assigning retardation data to transport domains	
	4.4.3 Proposal for specification of sorption properties for retardation components	
	updated model	/4

4.5 Basis for identification of fracture types					
	4.5.1	Overview of basic requirements and issues related to the retardation model			
	4.5.2	Conceptualisation based on identified retardation components			
	4.5.3	Proposed workflow for defining fracture types and deformation zone structures	77		
4.6	Summa	ry	80		
5	Daviva	tion of retardation parameters	01		
5.1		y for estimating effective diffusivity and porosity			
3.1	5.1.1				
	5.1.1	Overview of pore-scale solute retardation properties			
		Small-scale laboratory results			
	5.1.3	Correlation between parameters			
	5.1.4	Medium-scale and large-scale spatial variability			
	5.1.5	Lab-to-field transfer factor			
<i>5</i> 2	5.1.6	Anion exclusion.			
5.2		etation of sorption properties from site-specific data			
	5.2.1	Estimation of equilibrium $R_{\rm d}^0$ values from laboratory experiments			
	5.2.2	Estimation of reference K_d^0 values for geosphere sorption			
	5.2.3	Sorptive surface areas, CEC, and mafic mineral content of site-specific rocks			
	5.2.4	Relations between surface area, mineralogy, and sorptivity			
<i>5</i> 2	5.2.5	Aggregation of sorption data and extrapolation to geosphere reference condition			
5.3		plation of K_d values to application conditions	113		
	5.3.1	Overview of modelling approach			
	5.3.2	Mechanistic models for calculation of chemistry correction factors			
	5.3.3	Anchoring of modelled data to reference K_d values for studied groundwater type			
	5.3.4	Estimation of Smart K_d for colloids			
	5.3.5	Estimation of Smart K_d for radioelements lacking measurement data			
~ A	5.3.6	Estimation of Smart K_d for fracture coatings	122		
5.4		ry and overview of transport property parameter specification for safety assessments			
	5.4.1	Effective diffusivity and diffusion accessible porosity			
	5.4.2	Sorption properties	125		
	5.4.3	Verifying <i>in-situ</i> experiments			
6	5.4.3	Verifying in-situ experiments	126		
6 6.1	5.4.3 Derivat		126 127		
	5.4.3 Derivation Introduction	Verifying in-situ experiments tion of flow-related parameters ction	126 127 127		
6.1	5.4.3 Derivation Introduction Overview	Verifying in-situ experiments	126 127 127 127		
6.1 6.2	5.4.3 Derivation of the second of the secon	Verifying in-situ experiments	126 127 127 127 129		
6.1 6.2	5.4.3 Derivation Introduction Overvier Flow-reference 6.3.1	Verifying in-situ experiments	126 127 127 127 129 129		
6.1 6.2 6.3	5.4.3 Derivation Introduction Overvier Flow-ref 6.3.1 6.3.2	Verifying in-situ experiments	126 127 127 127 129 129 131		
6.1 6.2	5.4.3 Derivation Introduction Overvier Flow-reference 6.3.1 6.3.2 Example	Verifying in-situ experiments	126 127 127 129 129 131 133		
6.1 6.2 6.3 6.4	5.4.3 Derivation of the second of the secon	Verifying in-situ experiments	126 127 127 127 129 129 131 133		
6.1 6.2 6.3	5.4.3 Derivation of the following of the following flow-reference of the fl	Verifying in-situ experiments	126 127 127 127 129 129 131 133 136 136		
6.1 6.2 6.3 6.4	Derivation Introduction Overvier Flow-ref 6.3.1 6.3.2 Example Transp Overvier 7.1.1	Verifying in-situ experiments	126 127 127 127 129 129 131 133 136 136 136		
6.1 6.2 6.3 6.4	5.4.3 Derivation of the property of the prope	Verifying in-situ experiments	126 127 127 127 129 129 131 133 136 136 136 138		
6.1 6.2 6.3 6.4	5.4.3 Derivation Introduction Overvier 6.3.1 6.3.2 Example Transp Overvier 7.1.1 7.1.2 7.1.3	Verifying in-situ experiments	126 127 127 129 129 131 133 136 136 136 138 141		
6.1 6.2 6.3 6.4	5.4.3 Derivation Introduction Overvier 6.3.1 6.3.2 Example Transp Overvier 7.1.1 7.1.2 7.1.3 7.1.4	Verifying in-situ experiments	126 127 127 129 129 131 133 136 136 138 141 142		
6.1 6.2 6.3 6.4 7 7.1	5.4.3 Derivat Introductovervie Flow-re 6.3.1 6.3.2 Example Transp Overvie 7.1.1 7.1.2 7.1.3 7.1.4 7.1.5	Verifying in-situ experiments	126 127 127 129 129 131 133 136 136 136 138 141 142 145		
6.1 6.2 6.3 6.4	5.4.3 Derivat Introduction Overvier Flow-ref 6.3.1 6.3.2 Example Transp Overvier 7.1.1 7.1.2 7.1.3 7.1.4 7.1.5 Framew	tion of flow-related parameters	126 127 127 129 129 131 133 136 136 136 138 141 142 145 145		
6.1 6.2 6.3 6.4 7 7.1	5.4.3 Derivation of the properties of the prope	tion of flow-related parameters ction Exercise of processes and scales Elated parameters and pathway tracing. Methodology for quantification of parameters Pathway delineation in different codes. Les of supporting analyses Exercise of radionuclide transport modelling. Model domains and modelling methodology. The spent fuel repository (SR-Site and PSAR SFK). The SFR repository (SR-PSU and PSAR SFR). Biosphere models and interface to the geosphere Future directions and implications for modelling methodology. Vork for geosphere numerical transport modelling. Introduction to DFN modelling.	126 127 127 129 129 131 133 136 136 136 138 141 142 145 145 145		
6.1 6.2 6.3 6.4 7 7.1	5.4.3 Derivation of the properties of the prope	tion of flow-related parameters ction we of processes and scales elated parameters and pathway tracing Methodology for quantification of parameters Pathway delineation in different codes less of supporting analyses wort simulations we of radionuclide transport modelling. Model domains and modelling methodology The spent fuel repository (SR-Site and PSAR SFK) The SFR repository (SR-PSU and PSAR SFR) Biosphere models and interface to the geosphere Future directions and implications for modelling methodology work for geosphere numerical transport modelling. Introduction to DFN modelling. The continuum approximation	126 127 127 129 129 131 133 136 136 136 138 141 142 145 145 145		
6.1 6.2 6.3 6.4 7 7.1	5.4.3 Derivation Introduction Overvier Flow-ref 6.3.1 6.3.2 Example Transp Overvier 7.1.1 7.1.2 7.1.3 7.1.4 7.1.5 Framew 7.2.1 7.2.2 7.2.3	tion of flow-related parameters ction we of processes and scales elated parameters and pathway tracing Methodology for quantification of parameters Pathway delineation in different codes es of supporting analyses ort simulations we of radionuclide transport modelling. Model domains and modelling methodology The spent fuel repository (SR-Site and PSAR SFK) The SFR repository (SR-PSU and PSAR SFR). Biosphere models and interface to the geosphere Future directions and implications for modelling methodology ork for geosphere numerical transport modelling. Introduction to DFN modelling The continuum approximation The time domain random walk approach	126 127 127 129 129 131 133 136 136 136 138 141 142 145 145 145 146 146		
6.1 6.2 6.3 6.4 7 7.1	5.4.3 Derivation Introduction Overvier Flow-ref 6.3.1 6.3.2 Example Transp Overvier 7.1.1 7.1.2 7.1.3 7.1.4 7.1.5 Framew 7.2.1 7.2.2 7.2.3 Toolbox	Verifying in-situ experiments tion of flow-related parameters ction we of processes and scales Plated parameters and pathway tracing Methodology for quantification of parameters Pathway delineation in different codes les of supporting analyses ort simulations we of radionuclide transport modelling Model domains and modelling methodology The spent fuel repository (SR-Site and PSAR SFK) The SFR repository (SR-PSU and PSAR SFR) Biosphere models and interface to the geosphere Future directions and implications for modelling methodology vork for geosphere numerical transport modelling. Introduction to DFN modelling The continuum approximation The time domain random walk approach x for numerical modelling.	126 127 127 129 129 131 133 136 136 138 141 142 145 145 145 145 146 147		
6.1 6.2 6.3 6.4 7 7.1	5.4.3 Derivation of the property of the prope	tion of flow-related parameters ction we of processes and scales elated parameters and pathway tracing. Methodology for quantification of parameters Pathway delineation in different codes. les of supporting analyses wort simulations wort simulations word radionuclide transport modelling. Model domains and modelling methodology The spent fuel repository (SR-Site and PSAR SFK) The SFR repository (SR-PSU and PSAR SFR). Biosphere models and interface to the geosphere Future directions and implications for modelling methodology. Fork for geosphere numerical transport modelling. Introduction to DFN modelling. The continuum approximation The time domain random walk approach x for numerical modelling. Radionuclide transport modelling.	126 127 127 129 129 131 133 136 136 136 138 141 142 145 145 145 146 147 147		
6.1 6.2 6.3 6.4 7 7.1	5.4.3 Derivation Introduction Overvier Flow-reference 6.3.1 6.3.2 Example Transp Overvier 7.1.1 7.1.2 7.1.3 7.1.4 7.1.5 Framew 7.2.1 7.2.2 7.2.3 Toolbor 7.3.1 7.3.2	tion of flow-related parameters	126 127 127 129 129 131 133 136 136 136 138 141 142 145 145 145 146 147 147		
6.1 6.2 6.3 6.4 7 7.1	5.4.3 Derivation Introduction Overvier Flow-reference 6.3.1 6.3.2 Example Transp Overvier 7.1.1 7.1.2 7.1.3 7.1.4 7.1.5 Framew 7.2.1 7.2.2 7.2.3 Toolbor 7.3.1 7.3.2 7.3.3	tion of flow-related parameters	126 127 127 129 129 131 133 136 136 136 138 141 142 145 145 145 145 147 147 149 150		
6.1 6.2 6.3 6.4 7 7.1	5.4.3 Derivation Introduction Overvier Flow-reference 6.3.1 6.3.2 Example Transp Overvier 7.1.1 7.1.2 7.1.3 7.1.4 7.1.5 Framew 7.2.1 7.2.2 7.2.3 Toolbox 7.3.1 7.3.2 7.3.3 Identifier	Verifying in-situ experiments	126 127 127 129 129 131 133 136 136 136 138 141 142 145 145 145 145 145 145 145 146 147 147 149 150 153		
6.1 6.2 6.3 6.4 7 7.1	5.4.3 Derivation Introduction Overvier Flow-reference 6.3.1 6.3.2 Example Transp Overvier 7.1.1 7.1.2 7.1.3 7.1.4 7.1.5 Framew 7.2.1 7.2.2 7.2.3 Toolbor 7.3.1 7.3.2 7.3.3	tion of flow-related parameters	126 127 127 129 129 131 133 136 136 136 138 141 142 145 145 145 145 145 145 146 147 147 149 150 153 154		

	7.4.3	Step 3 – Define transport classes and retardation data	154
	7.4.4	Step 4 – Define statistics of transport classes by drivers	
	7.4.5	Step 5 – Basis for assigning transport classes to pathline segments	
	7.4.6	Step 6 – Handling new information	
	7.4.7	Step 7 – Implementation in radionuclide transport models	
7.5	Handli	ng of other transport processes	
	7.5.1	Bedrock wells in transport modelling	
	7.5.2	Transport of radionuclides in the gas phase	
	7.5.3	Colloid facilitated transport	
7.6	Interac	tions with other transport modelling	
Refe	erences .		162
Ann	endix A	Derivation of transfer factors	181
		ation for surface complexing solutes	
		ation for cation exchanging solutes	
		or a single CEC-dominating mineral	
		or multiple CEC-contributing minerals	
App	endix B	Handling of uncertainties related to transfer factor calculations	197
		ng of measured $R_{\rm d}^0$ values to reference $K_{\rm d}^0$ values for specific rock types	
		ng of uncertainties related to the chemistry correction factor	
App	endix C	Prototype calculation examples for the chemistry transfer factor	202
C.1		examples involving a single anchor	
C.2		dimensional extrapolations based on multiple anchors	
C.3		K _d estimates based on detailed groundwater modelling	
C.4		tion of Smart K_d for radioelements lacking measurement data	
App	endix D	Transport modelling using the time domain random walk approac	h215

1 Introduction

1.1 Background

SKB, the Swedish Nuclear Fuel and Waste Management Company, is responsible for managing radioactive waste generated by nuclear power plants and associated activities in Sweden. The Swedish programme for handling radioactive waste, which also includes waste from other sources such as health care, consists of systems and facilities for transport and disposal of waste. Different types of waste are distinguished by their different levels and longevities of radiation and hence impose different requirements on protective measures in connection with handling and on intermediate and final repository facilities. The waste management system is under development and SKB is currently in the process of seeking legal permits for several new components of the system.

The Forsmark area (Figure 1-1), located about 120 km north of Stockholm, is a key location for SKB, as the site for both operating and planned waste disposal facilities. Specifically, Forsmark hosts the SFR repository for low- and intermediate-level nuclear waste, which is planned to be enlarged, and it is also the intended site for the planned repository for spent nuclear fuel from the Swedish nuclear power plants. Site investigation and modelling activities have been carried out at Forsmark in the 1970s and 1980s for the planning of the nuclear power plant and the first stage of the SFR repository, and in more recent years (from 2002) for the spent fuel repository and the extension of SFR.

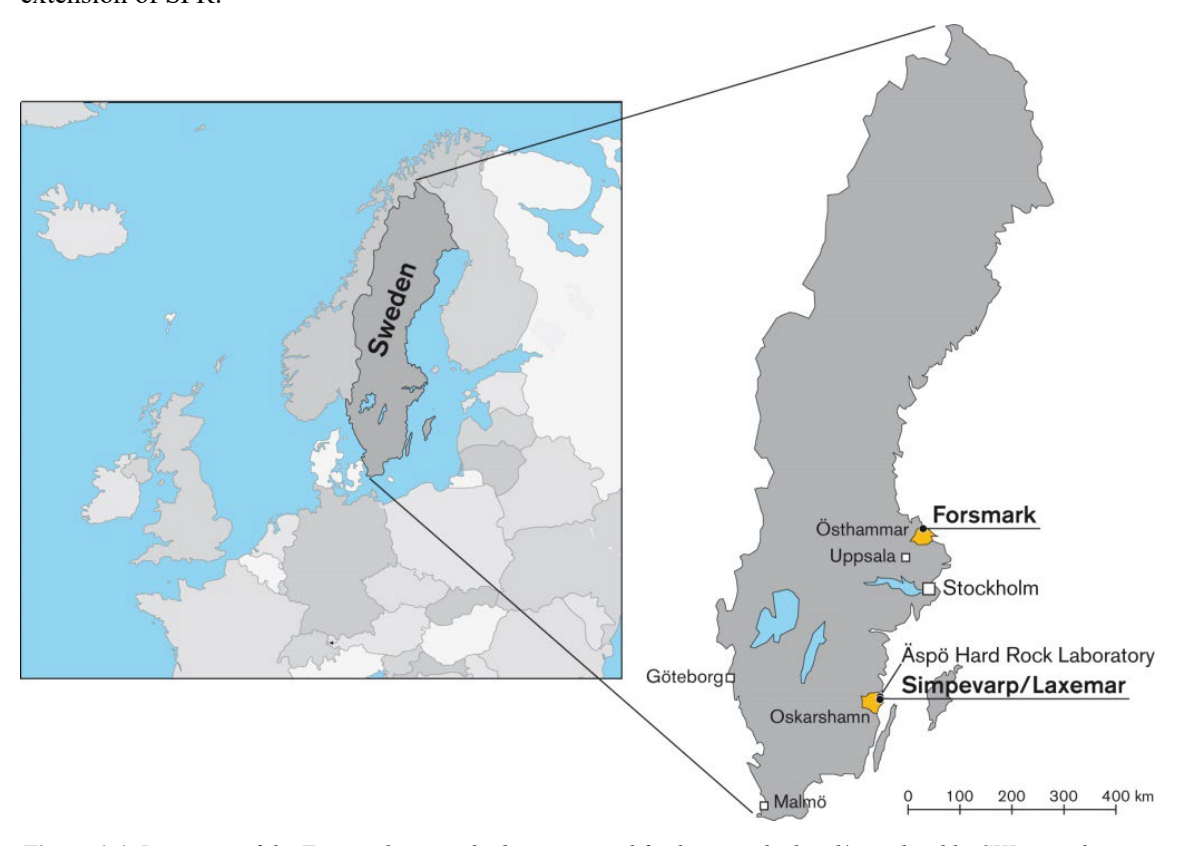


Figure 1-1. Locations of the Forsmark site and other areas and facilities studied and/or utilised by SKB's nuclear waste management programme. These include the site investigation areas for the spent fuel repository (Forsmark, Laxemar-Simpevarp), operating nuclear waste facilities (SFR in Forsmark and the Clab interim storage in Simpevarp), and the underground research laboratory at Äspö.

Provided that the legal permits required to start construction activities are obtained, the SFR extension and spent nuclear fuel repository projects will proceed with their next stages, which involve underground construction works and detailed site investigations in and from shafts, tunnels and rock caverns in the repositories. This implies that new Forsmark site data will be collected for site descriptive modelling and other modelling activities that use site data. In addition, new modelling needs arise. Updated site descriptive models based on data from detailed site investigations and ongoing long-term site monitoring provide inputs to the analyses of consequences of repository construction and operation and post-closure safety that are needed to support future license applications.

This report describes methodology for modelling bedrock transport properties and processes in forthcoming site descriptions and assessments of post-closure safety. The report, internally often referred to as TMM (Transport Modelling Methodology) or TRPMM, when it needs to be distinguished from the corresponding reports for thermal modelling, is an update and extension of an earlier report produced before the start of the site investigations for the spent fuel repository in the early 2000s (Berglund and Selroos 2004). In agreement with common SKB terminology, the present report refers to the SFR extension project as PSU and to the spent fuel repository project as SFK. Furthermore, KBS-3 denotes the multi-barrier repository concept to be used for disposal of the spent nuclear fuel (e.g. SKB TR-11-01¹).

1.2 Overview of transport modelling

To illustrate the sequence of modelling tasks and links between them, the SFK repository is used as an example to describe the roles of the site descriptive model (SDM) and safety assessment (SA) modelling efforts. Surface-based site investigations were performed at Forsmark and Laxemar-Simpevarp and resulted in SDM reports (SKB TR-08-05 and SKB TR-09-01, and underlying reports). After Forsmark was chosen as repository site, a safety assessment denoted SR-Site (SKB TR-11-01) was performed and constituted a part of the application for Forsmark as the site for a KBS-3 repository.

The previous modelling methodology report (Berglund and Selroos 2004) was published prior to the initiation of the site investigations and SDM work for the spent fuel repository. In addition, a report describing the strategy for laboratory measurements and development of a retardation model was presented (Widestrand et al. 2003), which served as an input to the modelling methodology. SDM reports for the Transport discipline were subsequently produced for the two sites (Crawford 2008, Crawford and Sidborn 2009), with supporting reports describing site data evaluation and development of a retardation model for each site (Byegård et al. 2008, Selnert et al. 2009a).

The retardation model provides a description of the site in terms of the properties of identified fracture types and deformation zones and surrounding unfractured rock. This means that the retardation model includes all site-specific complexities considered relevant and describes the site as realistically as possible. Applying the retardation model for SA applications thus typically implies necessary simplifications; in SR-Site, these simplifications and abstractions were presented in Crawford (2008) and informed the subsequent radionuclide transport calculations performed as part of SR-Site (SKB TR-10-50).

Here, the overall workflow of the forthcoming SDM and SA modelling is summarised, together with the links to the present modelling methodology report (TMM). The workflow is presented in Figure 1-2, where the red boxes represent the transport modelling activities, i.e. SDM-SAR and SAR corresponding to the SDM and SA steps, and the baseline modelling preceding these two steps. The baseline model describes and summarises the knowledge of the site at the start of the construction phase.

¹ For SKB reports without named authors, the report number is used instead of publication year when referring to them in the text.

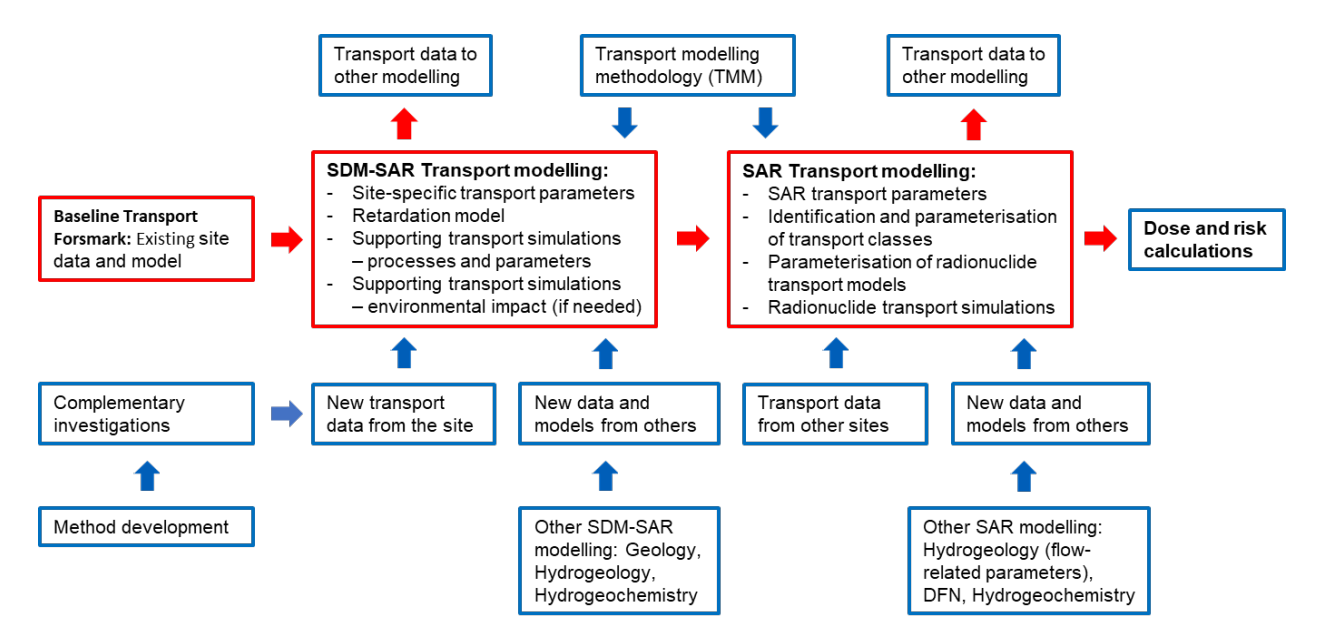


Figure 1-2. Workflow for site descriptive and safety assessment transport modelling. SDM-SAR and SAR are used as generic names of the site descriptive model and the safety assessment, respectively.

Also shown in the figure is the input from TMM to the SDM-SAR and SAR modelling, i.e. the TMM is to provide the modelling methodologies to be adopted in these two efforts. The expected products of the SDM-SAR and SAR are indicated in the respective red boxes, and the usage of the SAR in subsequent steps indicated by the blue boxes; the two main usages are hence modelling of future site development, and modelling of radionuclide dose and risk.

The lower part of the figure shows the different inputs to the modelling activities; specifically, new transport data may be required during the SDM-SAR stage, and such data requires complimentary investigations, which in turn may require method development. Also new data from other SDM disciplines may inform the SDM-SAR work. Additional transport data are needed for the safety assessment, in order to enable the modelling of radionuclide transport under conditions not measured or otherwise observed at the site today. Finally, also data from other disciplines are used in the SAR transport modelling.

Compared to the earlier methodology report by Berglund and Selroos (2004) and the SFK modelling actually performed (there were some deviations), there are some differences in the preconditions for the present modelling methodology. These differences include both internal and external factors and are summarised below.

- Whereas the previous report was focused on site descriptive modelling, this updated report presents a methodology for both site descriptive and safety assessment transport modelling. One reason for this decision is that a clear demarcation between the two modelling stages is difficult to define and perhaps not even needed. However, there are methodology-related issues that are decided in the planning of each safety assessment and therefore not covered in the present report. These issues may include the overall organisation of the radionuclide transport "model chain" and the specific types of input data and tools to be used.
- For the present methodology development and the forthcoming modelling, there are existing
 data and models from SFK and PSU to build on. This means that the purpose of the modelling in
 most cases is to update existing models. These updates could involve interpretations of new data
 from complementary investigations and/or re-interpretations of data from earlier investigations.

- The earlier SFK and PSU modelling also provides experience from applications of modelling methodology that may be useful when deciding what could and should be done in future modelling stages. The relation between the previous methodology report and the methodology actually applied in the site descriptive modelling for SFK is discussed in Berglund et al. (2020).
- The earlier SFK and PSU modelling reports have been reviewed by the authorities and comments from these reviews should be considered in the present methodology and future modelling. The review of the SR-Site safety assessment is presented in SSM (2018) and that of SR-PSU in SSM (2019). These are the main review reports; they are accompanied by more detailed reports dealing with specific parameters and modelling activities.
- The SFK site investigations and modelling were performed 15–20 years ago and since then both SKB-internal and external developments have been made that should be considered and used in the present methodology. Essentially, these developments fall into the partly related categories of scientific advances in investigation methods and resulting process understanding, and developments in the areas of modelling methodology and modelling tools. Some of the more important developments are listed below.
 - Improved methods for detailed characterisation of fracture surfaces and matrix pore networks provide a basis for detailed process modelling and better understanding of transport in fracture planes, fracture-matrix interactions and transport in the matrix.
 - Development of tools for integrated groundwater flow and reactive transport modelling, with applications including simulations of hydrogeochemical evolution, process-based radionuclide transport modelling, and chemistry-dependent assignment of transport parameters.
 - Development of methodology and tools for modelling solute and reactive transport in discrete fracture network (DFN) models. In recent years, this has been applied on a variety of scales, ranging from "micro-DFN" models of matrix processes to site-scale models using DFN-based groundwater flow models and including reactive transport in fracture networks (e.g. Sampietro et al. 2022).
 - The potential for simulation-aided improvements of understanding and methodologies for parameterisation and consequence calculations are further enhanced by recent developments of super-computers and associated modifications of transport codes carried out to utilise these improved tools.

1.3 Objectives, use and contents of the report

The main objective of the present report is to provide the methodological input needed to produce the site descriptive and safety assessment transport modelling to be performed in support of future applications for construction and operation licences for nuclear waste repositories at Forsmark. This means that the methodology described in this report should cover the transport modelling carried out for future site descriptive models and assessments of post-closure safety of Forsmark, as well as inputs to transport modelling serving the needs of other modelling disciplines and activities related to these license applications.

The present report is primarily focused on methodology for modelling radionuclide transport in the bedrock (geosphere), especially the interpretation and further analysis of the parameters measured within the investigation programme for bedrock transport properties and the application of these parameters in radionuclide transport simulations. However, the aim is that the methodology should be possible to adapt to fulfil also other needs, primarily to provide parameters for other types of transport modelling. The following requirements on the transport modelling methodology have been identified.

- The methodology should make use of earlier site descriptive and safety assessment models, as
 well as new site data and modelling results obtained by Transport and other disciplines since the
 completion of these earlier models.
- The methodology should consider the increasing demands associated with the stepwise licensing process, the review comments on earlier site descriptive and safety assessment models, and modelling methodologies of related disciplines (primarily Geology, Hydrogeology and Hydrogeochemistry).
- Recent advances in research and development, including improved scientific understanding of
 processes as well as new possibilities offered by improved methods and simulation tools, should
 be utilised in the development of the methodology.
- The methodology should describe the identification and description of bedrock units and structures to be included in the transport modelling. The recently developed DFN modelling methodology is an important input to this work.
- For the modelling of transport parameters, the methodology should cover the interpretation of
 site-specific data and how they are used to parameterise bedrock units and structures to form a
 site descriptive transport model, how the site-specific information is used in conjunction with
 other data and modelling results to produce the safety assessment database, and how it can be
 checked whether the transport parameters are consistent with current understanding and
 confirmatory tests.
- The methodology should describe the transport simulations required to support the modelling of transport parameters and processes, including both detailed processes in matrix and fracture planes and overarching understanding of present and future site conditions.
- The methodology should consider transport parameter needs associated with transport modelling performed by other modelling disciplines, primarily Hydrogeology and Hydrogeochemistry.

The methodology describes how the modelling should be performed in terms of what needs to be achieved, which system components, parameters and processes to consider, and what is done in the different steps that form the methodology. However, programmes and plans need to be developed to determine when different activities are to be carried out, how the different activities (transport modelling and others) are related and coordinated, and which resources are needed to do the work.

Thus, the present methodology provides a technical description of the modelling that informs future modellers of what needs to be done and constitutes a basis for both general and detailed planning. In addition, the methodology report is intended to inform also others, both within and outside SKB, about the modelling to be performed, and to provide a structured description that can be reviewed internally (preferably together with similar reports from other modelling disciplines) and externally.

Figure 1-3 presents an overview of the site descriptive and safety assessment transport modelling to be performed in future stages of the repository licencing processes and related modelling carried out within other disciplines. The figure also indicates where in the present report methodology for each transport modelling activity is provided.

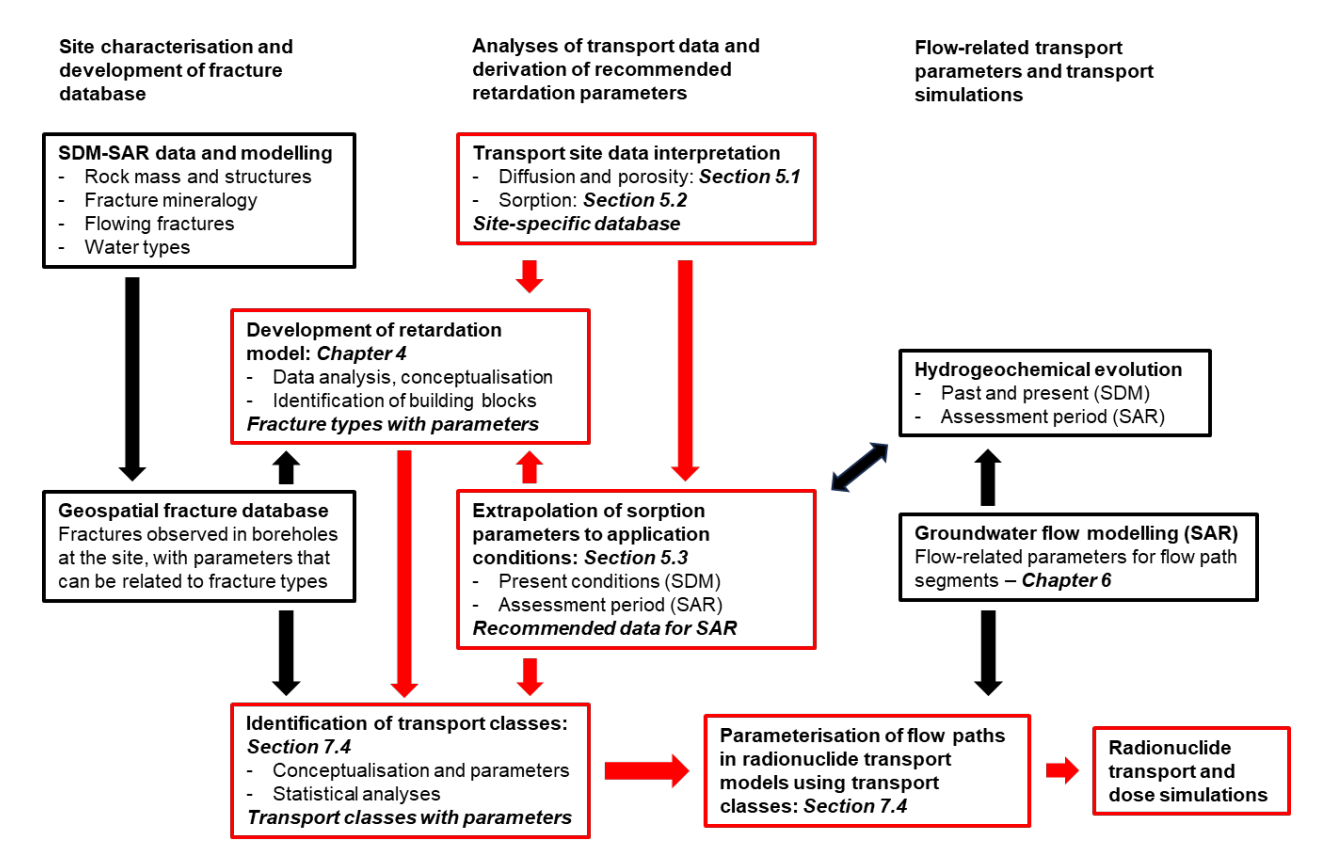


Figure 1-3. Overview of transport modelling activities and where they are described in the present report (red boxes), related modelling activities and entities (black boxes), and interactions between them (arrows).

This report is organised as follows. The present introductory chapter is followed by Chapter 2, which provides more background information on a variety of prerequisites and conditions of importance for transport modelling at Forsmark. Chapter 3 describes the concepts, processes and parameters that form the basis of the modelling methodology. Chapters 4 and 5 present the methodology for developing the retardation model and the derivation of the associated retardation parameters, respectively. It may be noted that Chapter 5 covers both the site-specific parameters obtained from interpretations of data from the site investigations (to be included in the database for the site) and the parameters resulting from further analyses considering also future site conditions (to be delivered as recommended parameters for safety assessment transport modelling).

Chapter 6 provides a brief account of the methodology for derivation of flow-related parameters, which are produced by Hydrogeology using particle tracking in groundwater flow models. Transport simulations are described in Chapter 7, where the methodological content is focused on the identification and parameterisation of transport classes, and their application in radionuclide transport models. Note that the methodology chapters covering the retardation model and the retardation parameters, i.e. chapters 4 and 5, respectively, both contain summary sections (sections 4.6 and 5.4).

1.4 Related documents

In addition to the earlier modelling methodology report (Berglund and Selroos 2004) and the supporting description of strategy for measurements and retardation model development (Widestrand et al. 2003), the following categories and specific documents have been identified as related to the present report.

Other modelling methodology reports. Methodology reports with focus on site descriptive modelling have been published or are under production for several other modelling disciplines. The methodologies of largest importance for the transport modelling are those for deterministic geological modelling (Hermanson and Petersson 2022), discrete fracture network (DFN) modelling (Selroos et al. (2022), integrated hydrological and hydrogeological modelling (Odén et al. 2025) and hydrogeochemical modelling (to be published as SKB report R-20-15).

Programme for laboratory and field investigations of transport properties. A programme for the forthcoming complementary site investigations of transport properties is under production. This programme corresponds to the earlier measurement strategy document by Widestrand et al. (2003), with some differences in scope, contents and intended use caused by the different needs at the present stage of the site investigations.

Site investigation and modelling programmes for the repository projects. These internal programme documents have recently been completed for both SFK and the SFR extension project (PSU). For SFK, two multi-disciplinary investigation programmes are presented, one focusing on the initial construction phase, during which accesses, central area and the first tunnels at repository depth are built, and one preliminary programme for the repository construction and operation phase.

Documentation of earlier site investigations, site descriptive modelling and safety assessments. Reports describing earlier SFK and SFR/PSU modelling, results as well as how they were produced, constitute an important input to the present work. Overviews of modelling and data reports are presented in Chapter 2.

Method descriptions. These documents describe investigation methods and how they are implemented in SKB site investigations. A programme for development of investigation methods and associated updates of method descriptions is carried out within SKB.

Baseline Forsmark and preparatory modelling activities. The Forsmark baseline description, which will be presented in a main report (SKB R-24-01) and a set of supporting discipline-specific reports, will provide valuable inputs to forthcoming site descriptive transport modelling, especially when it comes to new data and modelling results from others. However, directly transport-related activities and hence the implications for the present report are very limited. Concerning preparatory activities, it is worth mentioning that safety assessment modelling methodologies and tools are tested in an ongoing programme that includes some of the concepts discussed in the present report as well as related aspects of hydrogeological and hydrogeochemical modelling.

2 Overview of prerequisites and earlier modelling

2.1 Site conditions and existing models

2.1.1 Surface and bedrock conditions at Forsmark

The Forsmark site is located in the northern part of the County of Uppsala and the Uppland province in central Sweden, in the municipality of Östhammar and about 120 km north of Stockholm. During the period 2002–2008, extensive site investigations were performed at Forsmark to collect data for the SDM developed for the SFK licence application. SDM-Site is the last in a series of Forsmark site descriptive models produced during these site investigations and is reported in the SDM-Site main report SKB TR-08-05. More recently, site investigations were performed for the SFR extension (PSU) project. The results of these investigations are reported in the SDM-PSU main report SKB TR-11-04.

Figure 2-1 presents an overview of the Forsmark site, illustrating its coastal location, current lakes, wetlands and streams, and existing nuclear facilities (SFR and the Forsmark nuclear power plant). The SFK repository is planned to be built in the area southeast of the nuclear power plant, with its surface facility located just south of the water intake canal. The Forsmark area constitutes a typical coastal site on the shoreline of the Baltic Sea in northern Uppland. Post-glacial land uplift, in combination with the flat topography, implies fast shoreline displacement that has resulted in a very young terrestrial system containing several recently formed shallow lakes and wetlands.

Forsmark is situated below the highest coastline, and when the latest deglaciation took place the area was covered by c. 150 m of water. The closest shore/land area at that time was situated c. 80 km to the west of Forsmark. The first parts of Forsmark emerged from the sea around 500 BC. The process of shoreline displacement has strongly affected landscape development and still causes a continuous and relatively predictable change in the environment and the conditions affecting a variety of hydrological, hydrogeological, hydrogeochemical and related processes. Shoreline displacement has important implications also for groundwater flow and transport modelling of the bedrock. Note especially the deeper (i.e. darker blue) parts of Öregrundsgrepen outside Forsmark, which in the future will host relatively long-lived lakes and constitute discharge areas for groundwater flow.

The Forsmark area is characterised by a crystalline bedrock that belongs to the Fennoscandian Shield formed 1.85 to 1.89 billion years ago. Tectonic lenses, in which the bedrock is less affected by ductile deformation, are enclosed in between ductile high-strain belts. The so-called candidate area (Figure 2-2) is located in the northwestern-most part of one of these tectonic lenses. This is the area where SKB plans to build the SFK repository, and consequently also the area where most of the site investigations for this repository were performed. As shown in Figure 2-2, the tectonic lens in Forsmark extends from northwest of the nuclear power plant south-eastwards to the area around Öregrund. The figure also shows that the SFR repository is located just outside the lens, separated from the lens by a major deformation zone called the Singö zone.

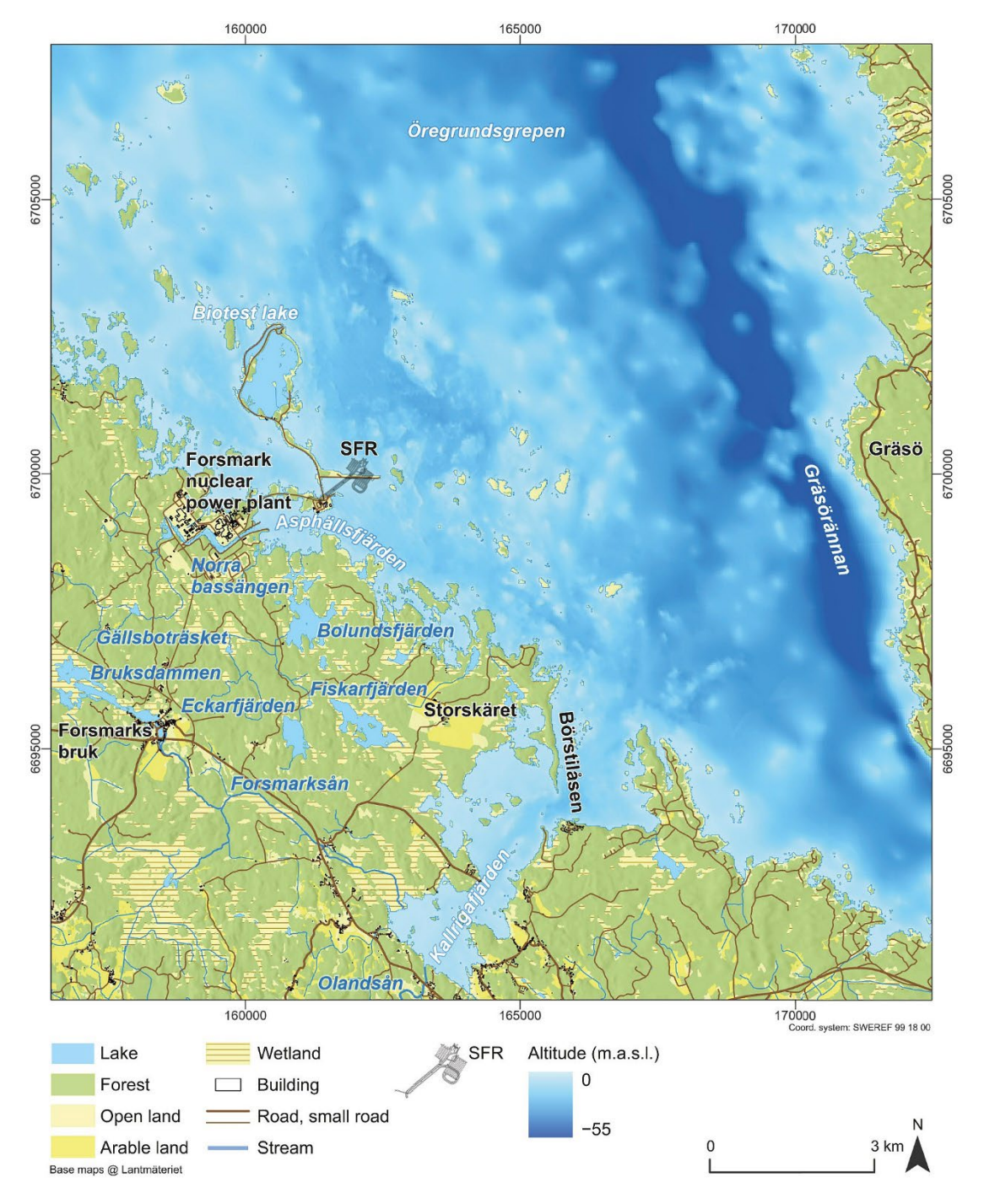


Figure 2-1. Overview of Forsmark showing the present shoreline and bathymetry of Öregrundsgrepen, lakes, wetlands, and existing nuclear facilities. Both the existing part and the planned extension of SFR are shown (figure from SKB TR-23-06).

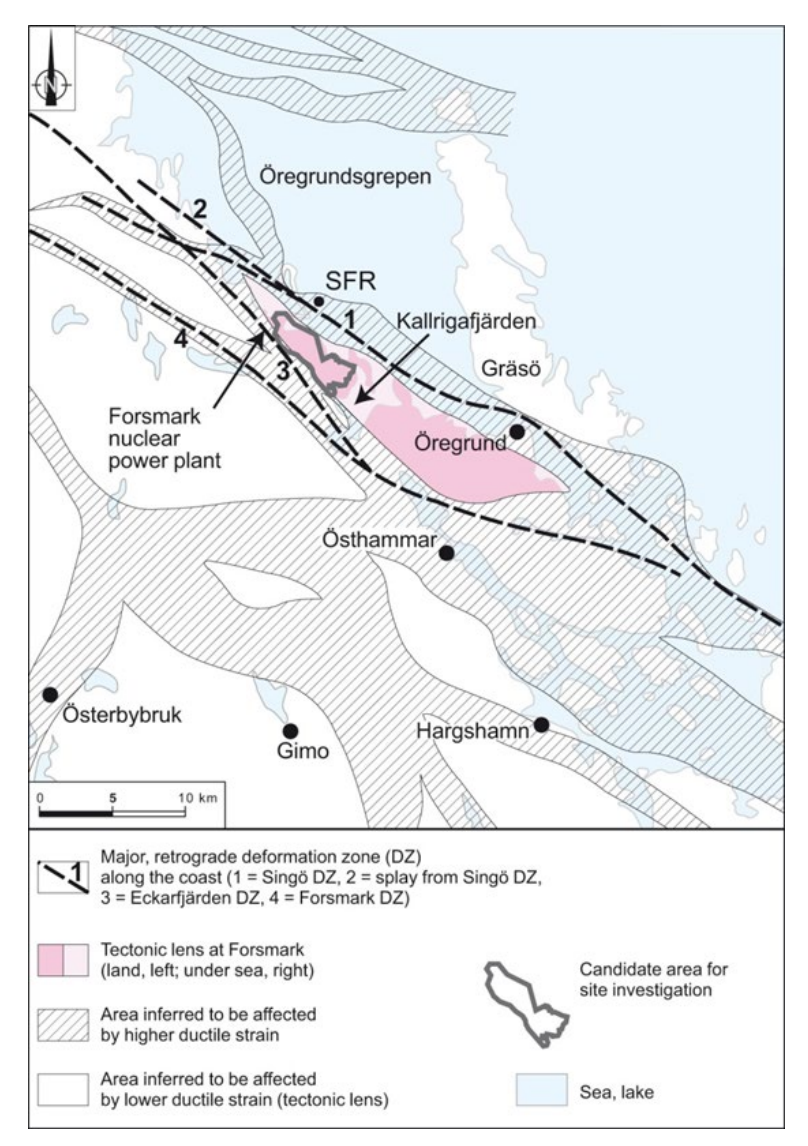


Figure 2-2. The tectonic lens with the major deformation zones (DZ; broken lines) at Forsmark and the candidate area of the site investigation for the spent fuel repository. Nearby areas affected by strong ductile deformation are also shown (figure from SKB TR-08-05).

Three major sets of deformation zones with distinctive orientations have been recognised in the geological modelling of the bedrock. In addition to vertical and steeply dipping zones, there are also zones gently dipping southeast and south. These gently dipping zones are more frequent in the southeastern part of the candidate area (volume) for the spent fuel repository and have higher hydraulic transmissivity than vertical and steeply dipping deformation zones at the site. The frequency of fractures is very low below approximately 300 m depth compared to what is observed in the upper part of the bedrock in the northwestern part of the candidate area, which is the "target area" where the spent fuel repository is planned to be located (e.g. SKB TR-08-05). In addition, the rock stresses are relatively high compared to typical conditions in Swedish bedrock.

The target area differs from the regional pattern also when it comes to the hydrogeological and related solute transport properties. Highly permeable structures are associated with the complex network of gently dipping and sub-horizontal, open and partly open fractures in the upper part of the bedrock. This means that the upper 100 to 150 metres of the bedrock overlying the volume intended for the spent fuel repository contain many highly transmissive (water-conducting) fractures extending in the horizontal plane, which results in hydraulic connections over relatively large distances. Conversely, the deeper bedrock has very low permeability and few transmissive fractures.

At the proposed repository depth (c. 470 m), the average distance between transmissive fractures (as defined by the applied threshold value) is more than 100 m according to the results of the surface-based site investigations.

The surface water and shallow groundwater in Forsmark are characterised by relatively high pH-values and concentrations of major constituents, especially calcium and bicarbonate. The hydrogeochemical site investigations of the bedrock show that groundwater in the uppermost 100 to 200 m of the bedrock displays a wide range of chemical variability, with chloride concentrations in the range 200 to 5,000 mg/L suggesting influence of both brackish marine water and meteoric (from recent precipitation) waters. At depths between 200 and 800 m, the salinity remains essentially constant (5,000–6,000 mg/L) and the water composition indicates remnants of water from the Littorina Sea that covered Forsmark between 9,500 and 5,000 years ago. At depths between 800 and 1,000 m, the salinity increases to even higher values.

Many descriptions of the Forsmark site have been published during the 20-year period that passed since the publication of the first SFK SDM report, ranging from the detailed and extensive SDM-Site report (SKB TR-08-05) to overviews (e.g. in Berglund and Lindborg 2017), and descriptions focusing on specific modelling disciplines such as transport properties and related conditions (e.g. Crawford 2008). There is no need to repeat more details from these descriptions in the present report, although Forsmark transport properties data and modelling obviously will be discussed on several occasions in the remainder of this report. Instead, a very brief description is given below, based on figures illustrating model integration within the SFK and SFR model volumes.

Figure 2-3 provides a presentation of the site understanding resulting from site descriptive modelling within several disciplines. Specifically, it contains series of cross-sections through the northwestern part of the investigation area at Forsmark showing the integrated understanding of the site at the completion of the SFK site investigations. These cross-sections are obtained through integration of a multitude of modelling activities, including geological modelling (fracture domains), rock mechanics (horizontal stress model), hydrogeological modelling (hydrogeological DFN model of connected fractures) and hydrogeochemical modelling (spatial distribution of reference waters).

In a similar way, Figure 2-4 gives an integrated presentation of modelling results and site understanding developed during the site descriptive modelling for the SFR extension. The upper figure is a side view facing west showing the conceptual hydrogeological model, including the interconnected flowing fracture network and potential flowpaths towards the Central block due to inflow to the existing SFR facility or borehole pumping during the SFR site investigation. The vertical deformation zones contained in the northern and southern "boundary belts" connect the Baltic Sea to the bedrock and may thus act as potential positive hydraulic boundaries for inflow to the planned SFR extension. The strip of land is the "SFR Pier", cf. below.

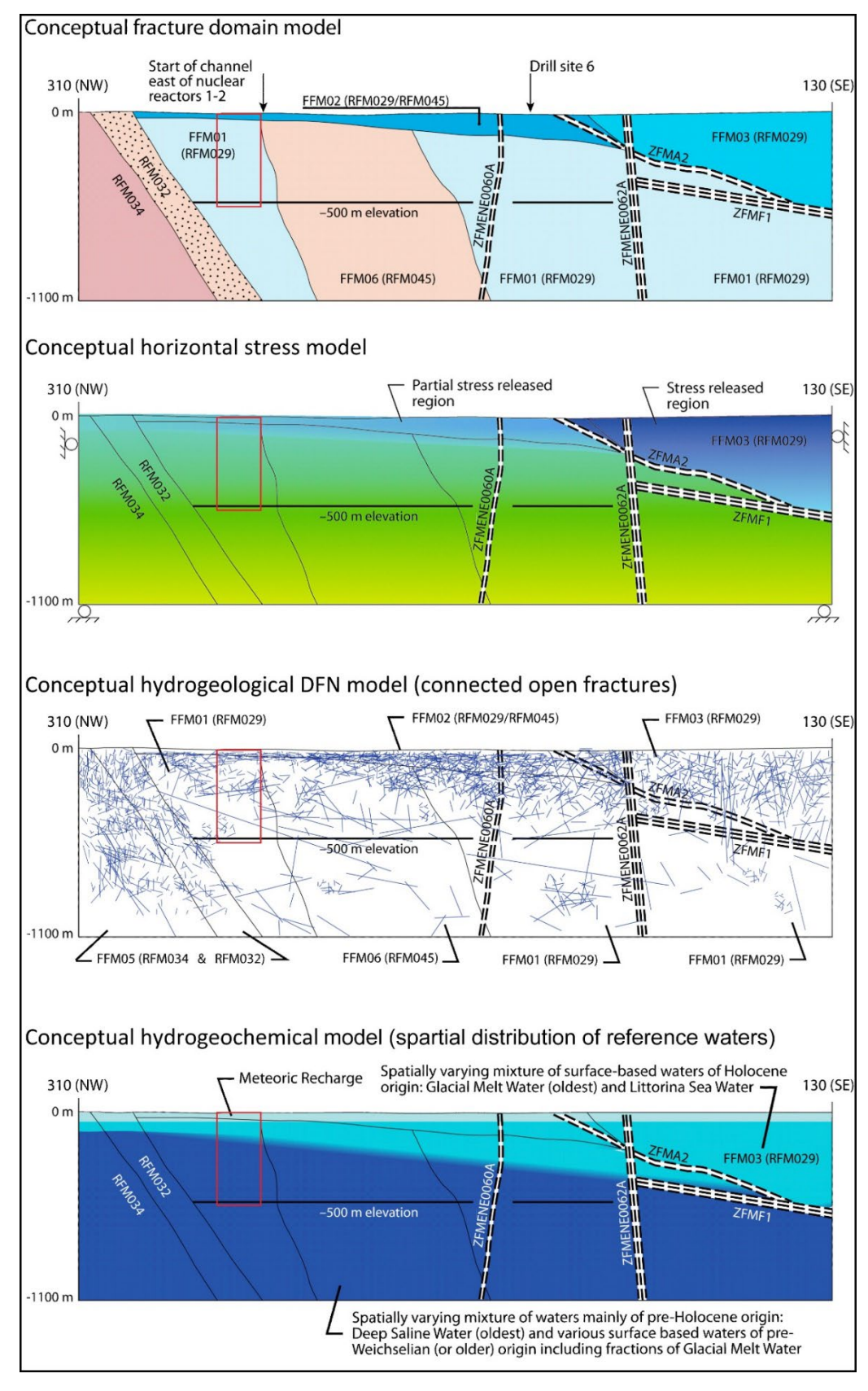
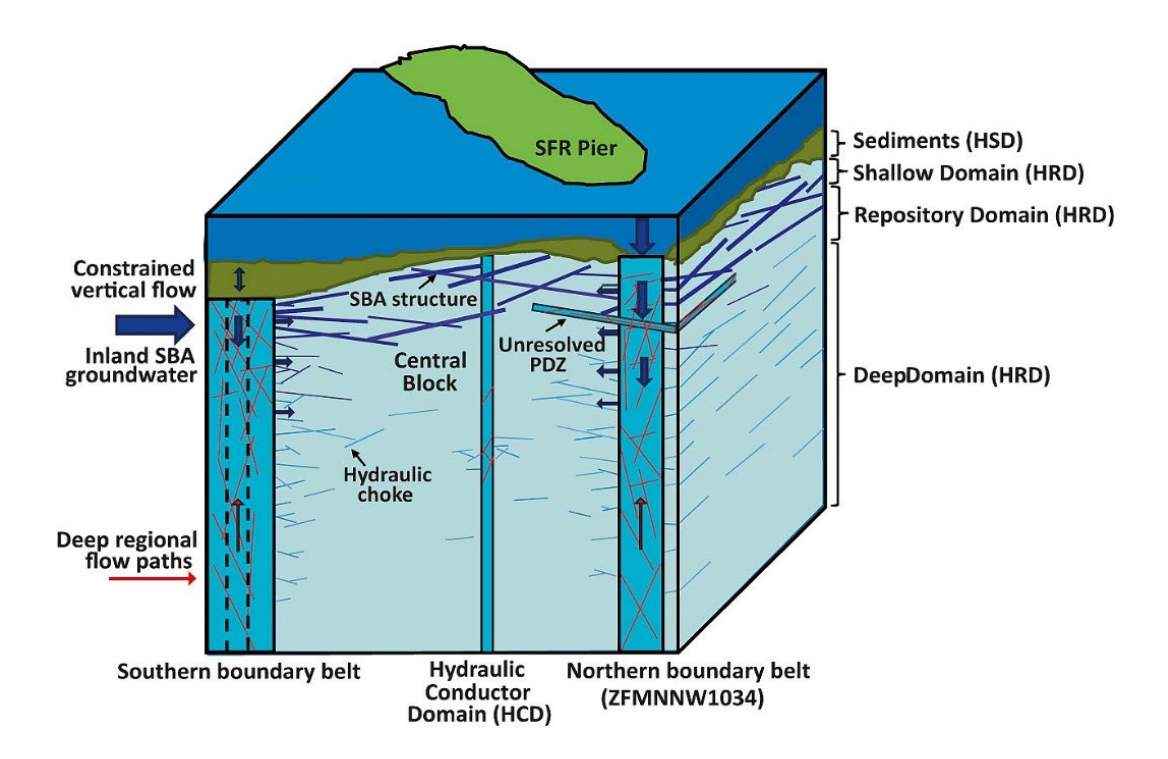


Figure 2-3. A cross section through the northwestern part of the SFK site investigation area at Forsmark showing the integrated understanding of the site at the completion of the site investigations. The red rectangles indicate the SFK access volume, i.e. the bedrock volume where ramp and shafts will connect the SFK repository deposition areas to the ground surface (from Follin 2019).



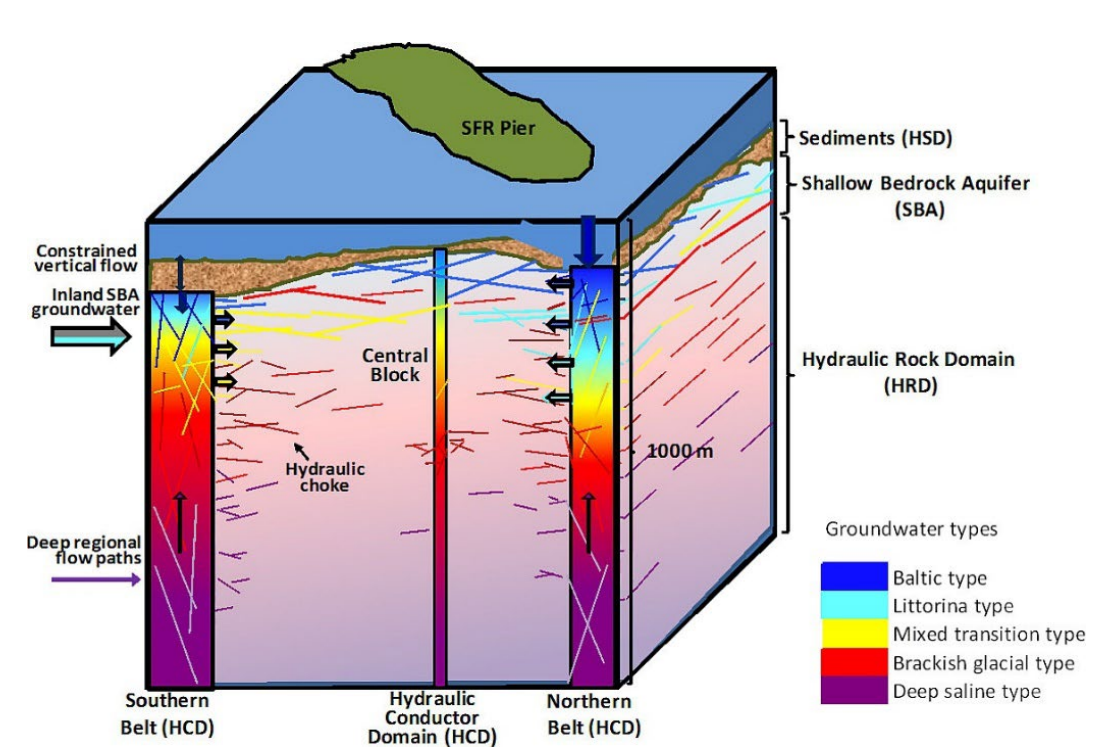


Figure 2-4. Upper: Conceptual block model incorporating the major geological and hydrogeological features of the investigated SFR rock volume. The horizontal and vertical dimensions of this model are approximately 1.5 km by 1.1 km. Lower: Conceptual block model incorporating the major hydrogeological and hydrogeochemical features of the investigated SFR rock volume. The different groundwater types are indicated by the colour scheme displayed on the right-hand side. The deep saline groundwater, which is indicated by lilac, is not present as a dominant groundwater type in the SFR bedrock volume.

2.1.2 Existing and planned nuclear waste repositories

As mentioned above, there already exists an underground repository for short-lived, low- and intermediate-level operational waste at the Forsmark site, i.e. the SFR facility. The SFR construction works started in 1983 and the facility became operational in 1988. The waste is

stored in rock caverns situated in the bedrock at c. 60 m depth below the seabed in the bay Öregrundsgrepen just off the Forsmark harbour. The vaults are accessed via tunnels that descend from an island called "Stora Asphällan", where also the SKB and SFR office buildings and the Forsmark harbour are located (Figure 2-5).

SKB is in the process of extending the SFR repository. Specifically, the plan is to create an entirely new section directly adjoining the existing underground facility, see Figure 2-5. The extension will primarily be used for decommissioning waste from Sweden's nuclear facilities, consisting of reactor components, scrap metal, concrete and other building materials. The new section for decommissioning waste will be built at larger depth than the vaults of the present SFR-1, at roughly 120 m below the seabed, where studies have shown that suitable bedrock for the purpose exists. The construction licence application for the SFR extension was submitted in March 2023 and approved in November 2024.

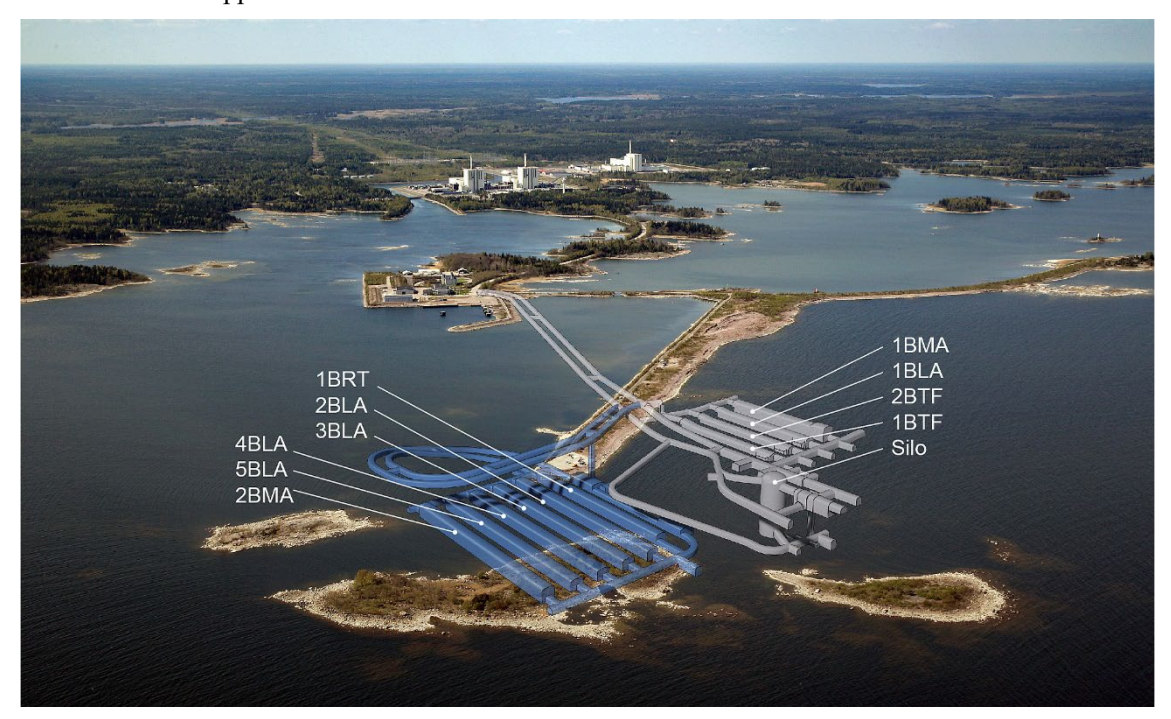


Figure 2-5. Perspective view of the Forsmark-SFR area from the southeast with the existing SFR facility indicated to the right (grey) and the planned expansion to the left (blue). The SFR Pier, the access tunnels from the surface facility in the Forsmark harbour, and the nuclear-power reactor buildings are also shown.

According to SKB's plans, a final repository for long-lived, high-level nuclear waste (spent nuclear fuel) will be constructed with accesses from the mainland just south of the nuclear power plant and southwest of the SFR facility. Figure 2-6 shows a cross-sectional view of the surface and subsurface parts of the spent fuel repository. The subsurface parts of the repository consist of accesses (ramp tunnel and shafts) from the surface, the central area containing of a number of rock vaults, and a network of tunnels along which the waste-containing canisters are to be placed. Altogether, it is estimated that the repository tunnels will occupy an area of 3–4 square kilometres at a depth of about 470 metres. The construction of the spent fuel repository is also pending license approval by the authorities. The construction licence application was submitted in January 2025 and is the latest step in the legal process that started with the first SFK/KBS-3 application in 2011 (which included SDM-Site and SR-Site).

When the accesses have reached repository depth, work will commence on developing the central area that includes the lower stations for the various shafts and underground caverns that furnish various kinds of services and infrastructure. These comprise seven c. 100 m long rock caverns and are encircled by service and ventilation tunnels. From the central area, a first loop of transport tunnels will be driven to the first disposal area where main and deposition tunnels are established. Initially, these first tunnels will be used for preparations and execution of demonstration and system integration and co-functionality tests to showcase application of developed detailed site characterisation and deposition technologies.

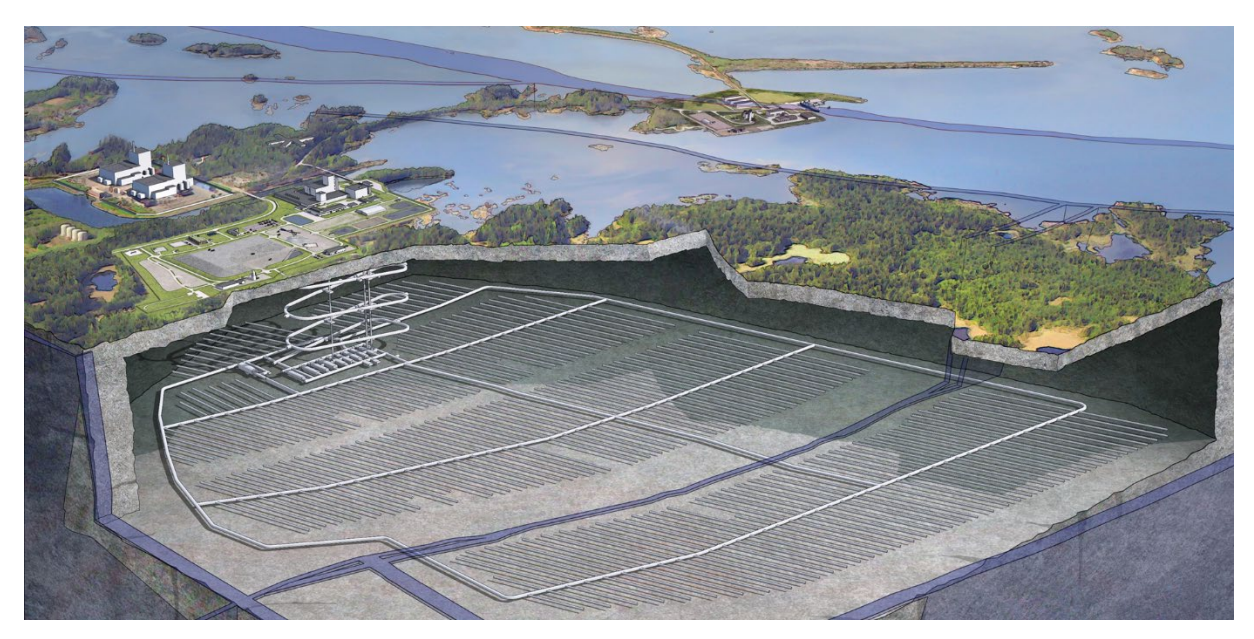


Figure 2-6. Cross-sectional view of the planned repository for spent nuclear fuel (SFK), with the nuclear-power reactor buildings to the left, the planned surface facility above the access tunnel loop, and the SFR peninsula to the right in the background.

2.2 Transport modelling tasks

Concerning preconditions and requirements upon the transport modelling to be performed in support of forthcoming site descriptions and safety assessments, it is noted that its overall objectives are related to analyses of either the conditions in the surroundings of the repository or within the repository itself. Without specifying discipline-specific responsibilities, the main overall transport modelling tasks for which transport parameters and/or simulations are needed can be outlined as follows.

- Transport of radionuclides and other pollutants from the repository to the surface system/biosphere and other potential exposure points (e.g. bedrock wells), for calculations of radionuclide doses to humans and other biota, and assessments of other consequences of transport from the repository.
- 2. Transport of safety-relevant chemical species from the surface or sources elsewhere to the repository, thereby affecting the repository environment, with modelling being used as a basis for evaluation of safety indicators.
- 3. Transport of chemical species (major and minor species and tracers such as isotopes) for assessment of past, present and future hydrogeochemical conditions and their evolution on a variety of scales ranging from those of repository components to the entire site and its local and regional surroundings.

Additional tasks can be identified, such as modelling performed for evaluation of disturbances from construction, including consequences of groundwater drawdown and related solute transport, evaluation of field experiments, investigations performed for improving site understanding, and others. Modelling tasks also include other entities than solutes being transported, primarily gases and colloids and other particles.

In the safety assessment, an integrated account of transport from the surface to the repository, and from the repository to the surface system, is strived for. When transport along recharge flowpaths is considered, main interests include major chemical evolution, and transport of specific harmful substances jeopardising repository integrity. Transport along discharge flowpaths is mainly focused on transport of radionuclides but also transport of other constituents emanating from the repository structures and potentially affecting chemical evolution downstream should be considered.

The main task of the Transport discipline (or "Bedrock transport properties") in the site descriptive modelling is to provide the site-specific input to the development of retardation parameters for radionuclide transport simulations in the analysis of post-closure safety. This includes presentation and delivery of interpreted parameter values, as well as site information that could serve to support

further analysis of parameters and representation of processes in radionuclide transport models. In addition, Transport should provide parameters and supporting information for modelling of transport processes within other disciplines, primarily Hydrogeology and Hydrogeochemistry.

Concerning transport parameters, it should be noted that the site-specific information is not the only input utilised when producing parameters for radionuclide transport simulations. As part of the safety assessment, the site-specific database is extended in various ways to obtain data also representing radionuclides, materials and conditions not considered in the site investigations. There is no clear demarcation between site descriptive modelling and safety assessment when it comes to the processing of site data. The retardation model (see Chapter 4) is a central delivery from the site descriptive modelling. This model summarises the site understanding and is intended to serve as a starting point for further analyses in the safety assessment.

In addition to the retardation parameters, flow-related transport parameters are used in the parameterisation of transport models. These parameters are obtained from groundwater flow simulations performed by Hydrogeology. However, supporting analyses of advective transport and flow-related parameters may need to be carried out by or in cooperation with Transport to address issues related to, for instance, heterogeneity and upscaling. Depending on needs and who is performing the analyses, studies of this kind may or may not be reported in future Transport SDMs. In the present document, advection and flow-related parameters are discussed in Chapter 6.

2.3 Previous site investigation and modelling

Earlier stages of the SFK and SFR extension (PSU) projects leading up to the applications submitted in 2011 and 2014, respectively, consisted of site investigations, site descriptive modelling and assessments of post-closure radiological safety. Site data and models were also used to provide input to repository design and assessment of the environmental impact of repository construction and operation. However, for the Transport discipline safety assessment modelling was by far the most important end-user of site data and models produced. This will be the case also in forthcoming SDMs and safety assessments.

Site investigations and site descriptive modelling were organised in terms of seven disciplines (provided "surface system modelling" is considered as just one), which produced discipline-specific reports as the final products of their data interpretations and modelling. These reports were then summarised and integrated into a main report for each version of the site descriptive model. The safety assessments also had a structure with a main report and underlying reports presenting specific parts of the assessment in more detail. In this case, the first level of underlying reports was not organised in terms of geoscientific disciplines; the structure of reporting was determined by the different analyses required by practise and regulations to be included in a safety assessment.

Excluding pre-studies not involving actual site investigations and focusing on Forsmark, the main activities and references generating the presently available site understanding and related simulation models are summarised in the following subsections. Note that new applications concerning the next step in the licensing processes, which is to obtain licenses to start construction works, have been submitted for both the SFR extension and the SFK repository. Construction works for both repositories have started. Furthermore, the associated safety assessment reports, the so-called PSAR reports, have been published in the SKB Technical Report (TR) series (cf. below for detailed references).

2.3.1 The spent fuel repository (SFK)

Site investigations

Extensive bedrock and surface system investigations were performed at the Forsmark site during the period 2002–2008. Investigations included borehole investigations in connection with drilling, execution of laboratory programmes, such as the long-running programmes for measurements of transport parameters, and long-term monitoring (repeated measurements of, primarily, hydrogeological and hydrochemical parameters). A monitoring programme based on installations from the site investigations and later complementary installations is still running; this programme includes groundwater flow measurements in selected packed-off sections in boreholes.

The overview map in Figure 2-7 shows objects of particular interest for the reporting of site investigations and modelling in connection with SFK. Specifically, the terms "candidate area" and "target area" are frequently used in SFK-related reporting. The numbering of drill sites corresponds to that of the core-drilled boreholes; drill cores from some of these boreholes have been sampled for laboratory investigations of transport properties. Note that the map also shows the surface projections of inclined boreholes, thereby indicating the bedrock volumes investigated around the different drill sites.

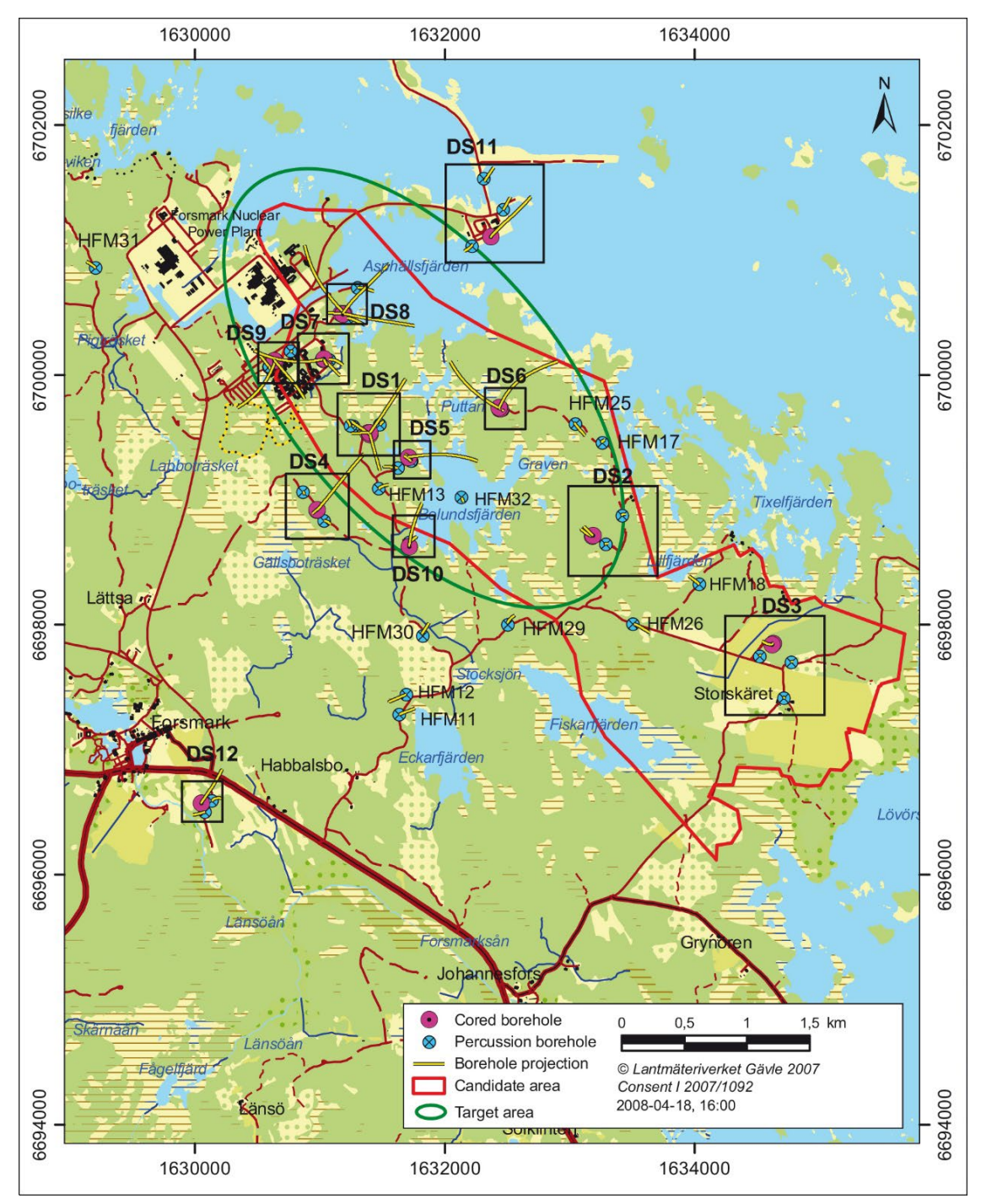


Figure 2-7. The Forsmark candidate area (bounded by red line) with the target area in the north-western part (circled in green) and the locations of drill sites (DS) with core-drilled boreholes (KFM) and percussion-drilled boreholes (HFM). The drill sites are labelled DS1 to DS12, where the numbering corresponds to that of the coredrilled borehole(s) at each site (for example, boreholes labelled KFM01 are located at DS1). The projection of each borehole on the ground surface (due to inclination) is also shown (figure from SKB TR-08-05).

Data from the site investigations were presented in a large number of mostly activity-specific reports (published in the SKB P series). Monitoring is reported regularly, usually in annual reports. Data are integrated and evaluated in the context of site descriptive modelling. There is virtually no interpretation or modelling performed as part of the data reporting, except for investigations performed to answer specific questions or when modelling is part of the data generation (such as when hydraulic testing is performed). The administrative structure of the site investigations is provided by a set of standard documents, including method descriptions (MD) and activity plans (AP).

Site descriptive modelling

Site descriptive modelling is concerned with the present state of the site, site development leading up to this present state ("site history"), and ongoing processes of importance for describing future site conditions in the assessments of environmental impact (a 100-year perspective) and long-term safety (a million-year perspective). No modelling of future site conditions has been performed in the SDMs produced to date. However, this might be changed in forthcoming site descriptions, which may be extended to cover the whole construction and operation period, thereby providing early input to the environmental impact assessment (and repository design).

The final version of the Forsmark SDM produced for the 2011 SFK licence application is called SDM-Site Forsmark and is reported in "Site description of Forsmark at completion of the site investigation phase. SDM-Site Forsmark" (SKB TR-08-05). Bedrock transport properties is one of the SDM disciplines; Chapter 10 in the main SDM-Site report summarises the site descriptive modelling of transport properties. The main underlying investigation and modelling reports are Selnert et al. (2008), Byegård et al. (2008) and Crawford (2008).

Assessment of post-closure radiological safety

Safety assessments are performed according to an established procedure that consists of a number of steps producing pre-determined types of analyses and associated reports. These steps include description of the initial state (based on the SDM), identification and description of scenarios, qualification of data to be used in modelling (to large extent based on the SDM), and description and modelling of processes that affect repository safety. The safety assessment included in the 2011 SFK application is called SR-Site and is reported in "Long-term safety for the final repository for spent nuclear fuel at Forsmark. Main report of the SR-Site project" (SKB TR-11-01, consisting of three volumes).

It may be noted that SR-Site is an SKB-internal name. In the "official" report structure, it is referred to as F-PSAR SFK. PSAR stands for Preliminary Safety Assessment Report, which is preliminary in relation to later assessment reports to be presented as a series of SAR (Safety Assessment Report).

Transport modelling is a cornerstone of the assessment of post-closure radiological safety. This concerns primarily the calculations of radionuclide transport and doses. However, also transport of specific chemical components to or towards the repository and transport of background chemistry in the area in general constitute important transport modelling tasks. In the present context, the most important "second-level reports" are the SR-Site "Radionuclide transport report" (SKB TR-10-50), "Data report" (SKB TR-10-52) and "Geosphere process report" (SKB TR-10-48). Additional data and modelling reports of potential relevance for the current description are summarised below.

As mentioned above, also the post-closure safety assessment reports associated with the forthcoming construction license application have been published (December 2022). This safety assessment is referred to as PSAR SFK, and the reports are in most cases only slightly updated versions of the corresponding SR-Site reports. The differences compared to the SR-Site reports are clearly indicated in the PSAR reports. The title of the main report is "Post-closure safety for the final repository for spent nuclear fuel at Forsmark. Main report, PSAR version" (SKB TR-21-01), whereas the most important second-level reports are the "Radionuclide transport report, PSAR version" (SKB TR-21-07), the "Data report, PSAR version" (SKB TR-21-06), and the "Geosphere process report, PSAR version" (SKB TR-21-04). Although in many cases not much different from their SR-Site counterparts, they constitute the latest SFK safety assessment reports and should be used when seeking up-to-date information on any aspect of the SFK assessment.

Later investigations and modelling

After the conclusion of the main surface-based site investigation at Forsmark, i.e. the one performed to support the 2011 SFK licence application, some complementary investigations that primarily cover needs associated with the SFK repository have been performed. Focusing on the bedrock and additional information of relevance for bedrock transport properties, two main types of data have been collected: (1) data from the ongoing monitoring programme, primarily hydrogeochemical, hydrogeological and groundwater flow data from bedrock boreholes, and (2) data from investigations in the access volume, i.e. where ramp and shafts between ground surface and repository level are planned to be located.

Monitoring data are evaluated within the framework of the baseline description, whereas the investigation data from the access volume have been summarised, and in some cases also modelled (primarily the geological data) within a specific activity. A report presenting the then existing (as of 2018) knowledge of the access volume was produced by a multi-disciplinary modelling group: "Multidisciplinary description of the access area of the planned spent nuclear fuel repository in Forsmark prior to construction" (Follin 2019). No new data on transport parameters have been obtained in the access volume investigations. However, various types of supporting data and models (e.g. geology and fracture mineralogy) have become available. The post SDM-Site investigations also include complementary drilling campaigns elsewhere in Forsmark. Transport-relevant data produced within these and other recent (and some less recent) activities are described in Section 2.4.

2.3.2 The SFR extension project (PSU)

Site investigations and site descriptive modelling

Compared to the site investigations for SFK, those performed to produce data for the analyses of the extension of SFR were limited, both in terms of geoscientific disciplines included and the modelling volume considered. Specifically, the bedrock investigations were for most disciplines focused on a relatively small rock volume near the existing SFR repository. Site investigations and site descriptive modelling of the bedrock included geology, rock mechanics, hydrogeology and hydrogeochemistry, whereas no investigations or modelling of transport properties were performed.

Starting with the investigation for the existing SFR facility in the early 1980s, a series of drilling campaigns and other investigations have been carried out in the SFR area. Figure 2-8 shows boreholes from different campaigns, which are colour coded by investigation project/period. Note that cored and percussion-drilled boreholes in the SFR area are labelled KFRXX and HFRXX, respectively, whereas the corresponding notation used in the SFK investigations is KFMXX (cored) and HFMXX (percussion-drilled). The map in Figure 2-8 also indicates the regional and local model areas utilised in the site descriptive modelling for the SFR extension project. So far, no sampling of cores from the SFR area for investigations of transport properties has been performed.

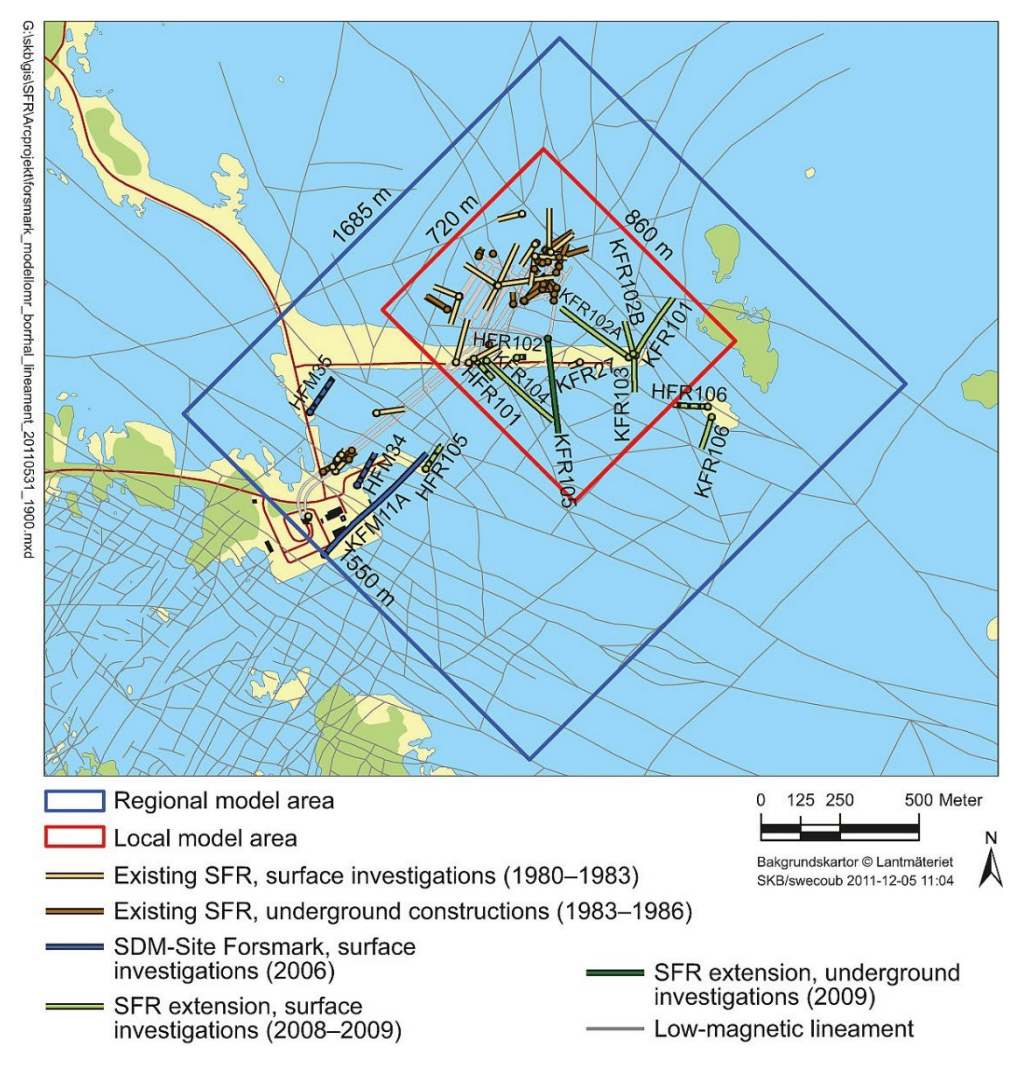


Figure 2-8. Map showing boreholes, i.e. the horizontal component of inclined boreholes, from different time periods of site investigations in the SFR area. Boreholes are colour coded by investigation project/period. Cored boreholes (KFRXX) are in solid colour and percussion (HFRXX) boreholes have black dots. The map also contains the regional model area for which updated models were developed for the SFR extension project. The local model area has a higher data intensity, which permitted a higher resolution in the deformation zone model.

The title of the main SDM-PSU report, where bedrock transport properties are not included is "Site description of the SFR area at Forsmark at completion of the site investigation phase. SDM-PSU Forsmark" (SKB TR-11-04). It should be noted that whereas the site investigations for the extension of SFR were focused on the rock volume where the new storage facilities are planned to be built, the post-closure safety assessment, including the radionuclide transport modelling, considered both the existing SFR and the planned extension (Figure 2-5). Of importance for forthcoming investigations and modelling is also the fact that the existing SFR contains boreholes from tunnels and rock caverns that already before start of construction provide access to monitoring data and data from underground site investigations.

Assessment of post-closure radiological safety for PSU

The safety assessment of the extended SFR, SR-PSU (or F-PSAR SFR), was a part of the 2014 PSU licence application. The activities and reporting follow the same formal structure as those in SR-Site, although report contents and titles differed slightly in some cases. The main SR-PSU report is "Safety analysis for SFR. Long-term safety. Main report for the safety assessment SR-PSU" (SKB TR-14-01). The most important second-level reports in the present context are considered to be the "Radionuclide transport report" (SKB TR-14-09), "Data report" (SKB TR-14-10) and "Geosphere process report" (SKB TR-14-05). To provide input to the radionuclide transport and dose calculations, modelling of transport parameters was carried out as part of the safety assessment. Additional references are provided below.

The construction license application for the SFR extension was submitted in March 2023. A similar set of reports as in SR-PSU was published in connection with this application: the main report "Post-closure safety for SFR, the final repository for short-lived radioactive waste at Forsmark. Main report, PSAR version" (SKB TR-23-01), the "Radionuclide transport and dose calculations, PSAR version" (SKB TR-23-09), and the "Data report, PSAR version" (SKB TR-23-10). No geosphere process report was produced specifically for PSAR SFR; the SR-PSU report (SKB TR-14-05) was used also in PSAR.

The differences between SR-PSU and PSAR SFR appear to be somewhat larger than those between SR-Site and PSAR SFK. The main developments since SR-PSU are summarised in the first chapter of the main PSAR report (SKB TR-23-01, Section 1.5.2). For the radionuclide transport modelling these developments involve changes in both input data and models (SKB TR-23-09, Section 1.3.2).

Later site investigations and modelling

Similar to SFK, continued data collection during the period after completion of SDM/SR-PSU has taken place by means of (1) the ongoing programme for long-term monitoring of Forsmark, which includes surface-based and underground hydrogeochemical and hydrogeological measurements in the SFR area, and (2) investigation campaigns in "old" and/or new SFR boreholes. Complementary drillings have been made from the SFR Pier (KFR117–121, Nilsson 2021) and underground from tunnels in SFR (KFR90-91, Nilsson 2024). Potential transport-relevant data from these boreholes will be acquired and assessed in forthcoming SDM work.

2.3.3 Other contributions

In addition to the SFK and PSU projects, SKB is also pursuing a third repository project, referred to as SFL, which deals with long-lived low- and intermediate-level waste. No site has been selected for this repository, and it is therefore not considered further in the present Forsmark-centred context. However, it should be noted that a safety evaluation (SE-SFL), mostly based on data from SKB's site investigations at Laxemar, has been produced (SKB TR-19-01), and that this work includes developments within transport modelling methodology that may be of interest for the present report (e.g. Trinchero et al. 2018a, Joyce et al. 2019). Other relevant developments have taken place in research activities organised by SKB and others; specific references will be given where appropriate.

2.4 Overview of transport properties data

Almost all site data on bedrock transport properties available from Forsmark were acquired during the site investigations for SFK. Site data were evaluated and modelled, and the results were presented as the SDM-Site retardation model and SDM transport model in Byegård et al. (2008) and Crawford (2008), respectively. This section provides a summary of Forsmark site investigations, site data and associated references, primarily those from the SFK investigation but also some related to more recent monitoring data.

The laboratory programme for measurements of transport properties on Forsmark rock samples is reported in Selnert et al. (2008). There is also a set of additional data reports describing investigations of transport properties. To give an idea of the amounts and types of data available for the development of the SDM-Site retardation model, a summary table from Crawford (2008) is included below (Table 2-1). The table shows how many samples of different geological units and materials (rock, fractures, deformation zones) that have been subject to measurements with different investigation methods. The table includes only methods for measurements of "primary transport data", i.e. data on porosity and diffusion and sorption parameters, whereas supporting data from other disciplines are not included.

Table 2-1. Rock sample data included in the retardation model. Note that a rock sample is considered as one sample-ID (e.g. KFM01A_103 m). BET and CEC measurements are performed on two different crushed size fractions, whereas batch sorption measurements are performed on up to three size fractions for a number of different radionuclides and water types (from Crawford 2008, Table 4-5)

Method	Total samples	Number of rock type samples	Number of fracture type samples	Number of samples representative of deformation zones
Porosity (water saturation)	211	182	-	29
РММА	13	5	1**	6
Electric resistivity (lab)	163	142	-	21
Through diffusion	72	50	-	22
BET (crushed rock)	46	29	12	5
BET (whole core)	4	4	_	_
CEC	9	4	2(3)	3
Batch sorption (crushed rock)	17	6	6	4
Batch sorption (whole core)	4	4	_	_

^{*} Including rock samples with faint to weak oxidation.

For those in search of more detailed information, a particularly useful summary of transport data and their usage in the site descriptive modelling is provided in Appendix 3 of the SDM-Site main report (SKB TR-08-05, Table 6 in Appendix 3). This table summarises data types, from which borehole data were obtained, references to data reports, and how the data were used. It constitutes a basis for the presentation in the remainder of this section.

The radionuclide transport modelling for assessment of post-closure repository safety is the main user of site investigation transport data. Transport data and modelling are discussed in the main SR-Site (SKB TR-11-01) and SR-PSU (SKB TR-14-01) reports, as well as in a number of "main references" and "additional references" produced within these safety assessments.

In particular, the SR-Site Data report (SKB TR-10-52, PSAR version: SKB TR-21-06) is very useful since it provides descriptions, discussions, analyses and selections of data that could represent the Forsmark site in, for instance, complementary site modelling and methodology development. In the SR-Site Data report, transport properties data are discussed primarily in sections 6.7 "Flow related migration properties" and 6.8 "Non-flow related migration properties".

In the following, a summary of available Forsmark transport properties site data is presented. For a complete account of the site investigation data reports, the reader is referred to the sources above. Here, only a few key references are given, which in most cases concern data summary and/or evaluation reports. Following the transport data description, some comments and references regarding supporting data from other disciplines are provided. The summary of transport data consists of data from the following types of measurements.

- Laboratory porosity, diffusion and sorption measurements, including formation factor data interpreted from measurements of electrical resistivity, and supporting BET (specific surface area) and CEC (cation exchange capacity) data.
- *In-situ* formation factor data from electrical resistivity measurements in boreholes, which are used to assign diffusion parameters.
- Groundwater flow measurements by tracer dilution methods.
- Single-well injection-withdrawal tests (SWIW).
- Multi-well tracer tests.

The Forsmark laboratory investigations of bedrock diffusion and sorption parameters are described in Selnert et al. (2008), which also contains measurements of associated supporting parameters such as BET and CEC. Although most of the laboratory investigations are fully described in the

^{**} Porosity measured orthogonally across an annealed fracture surface.

Selnert et al. (2008) report, there are some additional reports describing specific laboratory activities (PMMA and laboratory resistivity measurements). These reports are not listed here (cf. references above). Since sorption data also from the Laxemar-Simpevarp area were used in SR-Site, the corresponding laboratory investigations report for that site (Selnert et al. 2009b) is also relevant in the present context.

Detailed information about sampling locations and samples is readily available in the various data reports, where especially the appendices of Selnert et al. (2008) contain much useful information about the investigations at Forsmark. Table 2-2 shows which boreholes contributed data on which parameters in the site investigations for SFK and SFR. The SFK data are presented in terms of drill sites and boreholes (cf. Figure 2-7), whereas SFR data is limited to *in-situ* electrical resistivity data (ER *in-situ* in the table) from two boreholes (cf. Figure 2-8).

Note that Table 2-2 shows only the boreholes providing transport data, and that there are more boreholes at several of the drill sites (cf. Figure 2-7 and the detailed maps of drill sites in SKB TR-08-05). The table shows that data on parameters such as porosity are available from many boreholes, whereas fewer boreholes contribute with data on sorption and supporting parameters (BET and CEC). In the site descriptive modelling, transport data are grouped and evaluated in terms of primarily geological characteristics (e.g. rock type and alteration), in order to enable "extrapolation" of sample data to the descriptive model of the whole site (see Chapter 4).

Determination of the formation factor through interpretation of borehole resistivity logs was used together with laboratory methods to obtain diffusion parameters, and a series of data reports was produced during the SFK site investigations. Löfgren (2015) presents an evaluation undertaken to improve the understanding of the method and to address issues raised in the review of the SFK license application. Data from the SFR area are presented in Löfgren (2014), which also includes recommendations for the assignment of diffusion parameters in the SR-PSU transport simulations.

Table 2-2. Boreholes from which samples have been taken for measurements of SFK transport parameters and specification of which parameters have been measured on samples from each borehole. TDE stands for through-diffusion experiments, ER for electrical resistivity (measured both in the laboratory and *in-situ* and interpreted in terms of diffusion parameters), BET quantifies the specific surface area, and CEC stands for cation exchange capacity. ER *in-situ* refers to a method where ER data are obtained directly in boreholes (no core sampling); such measurements were made in both SFK and SFR boreholes

Drill site	Borehole	Porosity	TDE	ER lab	ER in-situ	Batch- <i>K</i> d	BET	CEC
DS1	KFM01A	Х	Х	Х	Х	Х	Х	Х
	KFM01B	Χ	Χ	X		Χ	X	X
	KFM01D				Χ			
DS2	KFM02A	X	Χ	X	Χ	Χ	X	Χ
DS3	KFM03A	Χ	Χ	X	Χ	Χ	Χ	
	KFM03B	Χ						
DS4	KFM04A	Χ	Χ	X	Χ	Χ	Χ	
DS5	KFM05A	X	Χ	X	Χ	Χ	Χ	X
DS6	KFM06A	X	Χ	X	Χ	Χ	Χ	
	KFM06B	X				Χ	Χ	
DS7	KFM07A	Χ	Χ		Χ	Χ	X	X
DS8	KFM08A	X	Χ	X	Χ		X	
	KFM08C	X		X	Χ			
DS9	KFM09A	X		X			X	
DS10	KFM10A							Χ
SFR	KFR102B				Χ			
SFR	KFR105				Х			

Groundwater flow measurements have been performed by tracer dilution methods using two types of equipment/installations, i.e. permanent borehole installations and the mobile dilution probe equipment. The measurements in permanently installed borehole sections are still performed regularly as a part of the Forsmark monitoring programme. Andersson et al. (2019) presents an evaluation of the groundwater flow monitoring campaigns carried out during the period 2005–2017. The analysis resulted in some modifications of the measurement programme. An earlier evaluation is presented in Nordqvist et al. (2008), which includes groundwater flow measurements at several SKB sites.

Tracer tests with injection and extraction of tracer in the same borehole section, i.e. single-well injection-withdrawal tests (SWIW, also referred to as push-pull tests) were carried out in several borehole sections during the Forsmark SFK site investigations. The aim of the SWIW tests is to measure retardation parameters under *in-situ* conditions. The SWIW tests performed at Forsmark have been summarised and evaluated in Chapter 6 of the Forsmark SDM-Site transport report (Crawford 2008), and they have also been subject to a more detailed model-based evaluation (Nordqvist 2008).

Multi-well tracer tests with injection and extraction/monitoring of tracer breakthroughs in different borehole sections were performed during the SFK site investigations at Forsmark. The results of these tests were also discussed in Chapter 6 of the SDM-Site transport report (Crawford 2008), and in a compilation and evaluation report covering tracer tests at several SKB sites (Hjerne et al. 2010). Two of the SFK tracer tests were focused on assessing relatively large-scale connectivity based on transport of non-sorbing tracers (sorbing tracers were used along one flowpath), whereas one test involved non-sorbing and several sorbing tracers on a somewhat smaller scale.

In addition to the transport data briefly presented above, the SFK transport modelling was based on a wide range of data and models produced by others. These inputs included a variety of information on geological and geochemical characterisation, including fracture mineralogy and porewater characterisation, as well as hydrogeological and hydrochemical data. Concerning geological and geochemical characterisation data, reports covering important data types, such as data on mineralogy, petrophysics, petrographics, and geochemistry are listed in SKB TR-08-05. Sandström and Stephens (2009) presents a compilation of these types of data for use in the SR-Site assessment.

Fracture mineralogy was a central input to the development of the SDM-Site retardation model. A summary and analysis of the SFK site investigations of fracture mineralogy is presented in Sandström et al. (2008), whereas quantitative mapping of fracture minerals and statistical analysis of the resulting data are found in Eklund and Mattsson (2009) and Löfgren and Sidborn (2010), respectively. It should also be noted that additional fracture mineralogy data are available from the PSU site investigations (Sandström and Tullborg 2011, Sandström et al. 2011).

Finally, bedrock porewater compositions were studied during the Forsmark site investigations, primarily to obtain information on past and present interactions between fractures and matrix. Waber et al. (2009) summarises and analyses the SFK site investigations for the SDM-Site modelling. Furthermore, investigations of porewater compositions have been carried out in two boreholes drilled after the SFK investigations within the planned access area for the SFK repository (Waber and Smellie 2012) and in a new borehole on the SFR Pier (Eichinger and Iannotta 2024).

2.5 Summary of review comments from SSM

2.5.1 The SFK review processes

SKB activities within nuclear waste management, including operation of the existing system for waste handling and planning and licensing of new facilities, are subject to supervision by the authorities. In particular, the Swedish Radiation Safety Authority (Sw: Strålsäkerhetsmyndigheten, abbreviated SSM) and environmental authorities on various levels, from local (the municipality) to national (the Swedish Environmental Protection Agency, Sw: Naturvårdsverket), are the main supervisors of operation, monitoring and legislation of active and planned components of the Swedish nuclear waste management system.

The authorities review applications and programmes produced by SKB, and the comments and requirements arising in such processes are important inputs to the planning for forthcoming site

investigations and modelling activities. When establishing new nuclear facilities, planning and reporting follows a stepwise process based on requirements in the radiation protection and environmental legislations, implying that SKB needs to submit increasingly detailed safety analysis reports.

- First, applications to construct, own and operate the facility are submitted to SSM and the Land and Environment Court. The Government decides on permissibility and licensing, and then conditions are determined by SSM and the court.
- Before construction of a nuclear facility can commence, a preliminary safety analysis report (PSAR) must be approved by SSM.
- When systems and processes in the facility have been tested and work as intended, a safety analysis report (FSAR) is submitted, as a part of an application for starting trial operation.
- Before a facility can be put into regular operation, the safety analysis report must be supplemented with experiences from trial operation (this report is referred to as SAR) and approved by SSM.

As explained above, both projects that involve repositories at Forsmark have submitted construction licence applications (including PSAR) to SSM, i.e. the second stage of this process, and the application for the SFR extension has been approved by the Authority.

2.5.2 SFK review comments and SKB response

The final version of the main review report on the SR-Site safety assessment was published in January 2018 (SSM 2018), when SSM submitted its statement to the Government. Since SDM-Site is a major input to SR-Site, the report also covers components of the site descriptive modelling, especially the overall description of the present Forsmark site that contributes to the "initial state" part of the safety assessment and the review of input data and other inputs to the transport calculations used as a basis for the consequence calculations of dose and risk.

Some comments in SSM (2018) are of general character and merely express views on which are the important issues and the main uncertainties of a certain parameter or model and what is the general status of a certain discipline. Others are more specific and describe shortcomings of the analyses presented to date and what needs to be done to overcome them. The specific comments address a variety of topics, from laboratory methods to numerical models used in safety assessment calculations. In some cases, they call broadly for further investigations of a certain phenomenon or subject area, whereas other recommendations are quite specific in terms of what SSM wants SKB to do.

The main SSM comments on sorption in Section 7.3.3 of SSM (2018) are summarised below. The SSM comments have been extracted, translated and in some cases commented or "interpreted", which means that the statements below are not the exact words of the Authority.

- Based on the expert review reports (cf. below) and earlier reviews, SSM states that few large changes in recommended K_d values have been made, but that the development of K_d values has become more systematic and transparent. According to SSM, it remains after these reviews that a significant proportion of the K_d values still is not based on data from site-specific materials. However, SSM notes that even more important uncertainties arise from the fact that crushed bedrock materials (rather than intact bedrock) are used in the sorption experiments. SSM also remarks that there are still questions about the significance of sorption on fracture-filling materials. These are general comments provided by SSM. No specific suggestions or requirements are formulated, but comments clearly reflect areas and issues where the Authority expects SKB to make improvements.
- The effects of leachate of cement components from the repository on groundwater chemistry and sorption parameters have been addressed during the review process. SSM comments that the issue of these high-pH waters is not of great importance for safety assessments but urges SKB to more convincingly show that such conditions are limited in space and time and therefore insignificant, or to investigate the impact of cement leachate and high-pH groundwater in experiments. This is one of several SSM comments that address relations between chemistry and sorption parameters.

- SSM encourages further development and application of supporting thermodynamic sorption models (also called mechanistic or process-based models), since this type of modelling could improve the understanding of how sorption is affected by various environmental factors and thereby increase the confidence in the selection of K_d values. However, SSM also concludes that K_d values selected taking hydrogeochemical conditions into account in most cases provide the best solution for radionuclide transport calculations in connection with deposition of nuclear waste. These comments encourage SKB to continue presently ongoing development efforts in the areas of thermodynamic and chemistry-conditioned K_d models (also called "smart" or "dynamic" K_d).
- Concerning the sorption database, SSM finds that significant gaps still exist. Although the use of
 analogues has enabled SKB to present a complete sorption dataset, SSM judges additional
 efforts in coming stages necessary to improve the ability to quantify site-specific sorption.
 Specific suggestions for improvements are given below and in the expert review report by
 Bertetti (2014). These suggestions concern both modelling and experiments.
- The Authority emphasises that the establishment of appropriate distributions for use in probabilistic calculations needs special attention. A more explicit handling of spatial and temporal variations in chemical conditions affecting sorption could be useful for improving the precision in calculations by narrowing K_d intervals down. This comment also focuses on effects of chemical changes on K_d values and involves suggestions for improvements of this aspect of the K_d parameterisation procedures.
- SSM finds that there are deficiencies in the sorption measurements, e.g. insufficient control of redox conditions. One consequence of these deficiencies is that measured site-specific data on redox sensitive elements could not be used in the modelling. Other shortcomings noted by the SSM experts are that the control of the partial pressure of CO₂ (pCO₂) and pH was insufficient. These parameters are important for the sorption of actinides. SSM therefore proposes that new sorption experiments with better control of chemical conditions are carried out. Experiments may also be needed to complement the site-specific database in other ways, e.g. to cover materials and water types not included or included with only very little data support. In any case, the main implication of the SSM comments is that it appears necessary to organise a laboratory programme for complementary sorption measurements.

Detailed comments are provided in the expert review report by Bertetti (2014), which is the primary background report on sorption parameters that was produced during the SFK review. The Bertetti (2014) review found the development of K_d values adequate for SR-Site but also noted "substantive data gaps" that should be addressed. One such gap emphasised in the review report is the lack of site-specific sorption data at site-relevant conditions for reduced actinide elements and technetium. The review was concluded by providing two specific recommendations for further modelling and experimental studies: (1) SKB should conduct limited surface complexation modelling to evaluate the sensitivity of the sorption of actinides to changes in pH and pCO₂, and (2) SKB should be strongly recommended (by SSM) to conduct a limited set of sorption experiments under site-relevant conditions that include variations in and control of pH and pCO₂. The radioelements studied should include Tc, Np and U, with Th and Pu as options.

Matrix diffusion and associated parameters such as porosity, diffusivity, formation factor and the maximum penetration depth for diffusion are discussed in Section 7.3.5 of the SR-Site review report (SSM 2018). The programme for measurements of these parameters included both laboratory measurements on rock samples and *in-situ* measurements in boreholes. Specifically, *in-situ* measurements of electrical resistivity are used to obtain formation factor values, which are estimated using supporting hydrochemical data. This method is relatively new and measures diffusion indirectly. SSM provided several comments on this method, especially in the early review stages; these comments were addressed in the evaluation presented in Löfgren (2015).

An expert review focused on the handling of matrix diffusion was performed by SSM (Haggerty 2012). Based on this review, SSM requested complementary analyses from SKB. These requests and the responses from SKB are summarised in the main SSM review report (SSM 2018), where SSM also states that SKB provided the information needed and that the uncertainties identified in Haggerty (2012) were investigated to sufficient extent.

In Section 7.3.5 of SSM (2018), the Authority also offers some additional diffusion-related comments, which primarily concern the implications of porewater chemistry data collected by SKB (Waber et al. 2009) for the understanding of matrix diffusion (and vice versa). SSM notes that these data provide no quantitative information on diffusion but might contribute to the understanding of the effects of matrix diffusion on groundwater composition in long-term perspectives. In the porewater chemistry studies, certain patterns and variations depending on depth and the distance to water-conducting fractures are observed that likely would not exist in absence of diffusive transport. Variations in matrix porewater composition should also be studied to better understand the long-term development of groundwater salinity.

As indicated above, SKB has responded to SSM comments and requests on numerous occasions during the review process. These responses have taken different forms, ranging from short answers to specific questions to extensive complementary studies involving modelling that resulted in published reports. Specifically, some of the more extensive and important complementary studies of transport parameters considered the *in-situ* formation factor measurements (Löfgren 2015) and the modelling of retardation processes in the matrix (Löfgren and Crawford 2014, Crawford and Löfgren 2019).

2.5.3 The PSU review and comments

The review of the PSU license application and SR-PSU followed the same overall procedure as the SFK/SR-Site review summarised above and produced a similar set of review reports. The main review report on the SR-PSU safety assessment was published in 2019 (SSM 2019), and the external expert review reports from the initial and main review stages were merged into two series of compilation documents published as SSM reports. Among these compilation documents, review comments on bedrock transport parameters are mainly found in the report "Review of handling of K_d -values used for near- and far-field analyses in the safety assessment SR-PSU" (by F. Paul Bertetti), which is included in SSM (2017). The comments on sorption in this expert review concern the use of analogues, needs for additional sorption data on specific elements, how parameters are represented in probability distributions, traceability of correction factors, and conservatism in K_d values.

2.6 Terminology

This section summarises terminology associated with site investigations and site descriptive modelling, both general and specific for Forsmark (Table 2-3), and terminology related to transport modelling, including processes, parameters and a set of concepts defined for the purposes of the present description of transport modelling methodology (Table 2-4). The terminology in Table 2-3 is mostly based on earlier SDM reports, whereas that in Table 2-4 is from the laboratory strategy report produced in the planning of the SFK site investigations (Widestrand et al. 2003) or based on the present report.

Table 2-3. Basic terminology of site descriptive modelling, including geology/geometry that constitutes the common framework for the bedrock modelling disciplines

Term	Definition	Reference*				
Site investigations and modelling						
Site descriptive model (SDM)	A synthesis of observations of the current state of the site and of the understanding of past and ongoing processes providing an integrated description of the geology, rock mechanics, thermal properties, hydrogeology, hydrogeochemistry, bedrock transport properties and surface system properties of the site.	Based on TR-11-01				
Candidate area/volume for SFK	The candidate area refers to the area at the ground surface that was recognised as suitable for a site investigation, following the feasibility study work for the spent fuel repository. The extension at depth is referred to as the candidate volume (Figure 2-7).	Based on TR-08-05, R-07-45				
Target area/volume for SFK	The target area/volume refers to the northwestern part of the candidate area and the rock volume beneath that was selected during the site investigation process as potentially	Based on TR-08-05, R-07-45				

	suitable for hosting a final repository for spent nuclear fuel (Figure 2-7).	
Access area/volume for SFK	The access area comprises the area where the ramp and shafts of the spent fuel repository are planned to be located, and it also envelopes all other parts of the surface access infrastructure for this repository. The extension at depth is referred to as the access volume.	Based on R-17-13
Prioritised area for the SFR extension site investigation	The prioritised area for the site investigation performed for the SFR extension project is located north of the area selected for the final repository for spent nuclear fuel, in an area that is below the sea and southeast of the existing SFR (SKB TR-11-04, Figure 1-1).	Based on TR-11-04
Geological and geometric	cal modelling	
Rock unit	A rock unit is defined based on the composition, grain size and inferred relative age of the dominant rock type. Other geological features including the degree of bedrock homogeneity, the degree and style of ductile deformation, the occurrence of early-stage alteration (albitisation) that affects the composition of the rock, and anomalous fracture frequency also help define and distinguish some rock units.	TR-08-05, R-07-45
Rock domain	A rock domain refers to a rock volume in which rock units that show specifically similar composition, grain size, degree of bedrock homogeneity, and degree and style of ductile deformation have been combined and distinguished from each other. Different rock domains at Forsmark are referred to as RFMxxx.	TR-08-05, R-07-45
Deformation zone	Deformation zone is a general term that refers to an essentially 2D structure along which there is a concentration of brittle, ductile or combined brittle and ductile deformation. Deformation zones at Forsmark are denoted ZFM followed by two to eight letters or digits. An indication of the orientation of the zone is included in the identification code.	TR-08-05, R-07-45
Fracture zone	Fracture zone is a term used to denote a brittle deformation zone without any specification whether there has or has not been a shear sense of movement along the zone.	TR-08-05, R-07-45
Fracture domain	A fracture domain is a rock volume outside deformation zones in which rock units show similar fracture frequency characteristics. Fracture domains at Forsmark are denoted FFMxx.	TR-08-05, R-07-45
Discrete fracture network (DFN) model and modelling	DFN modelling refers to a process where a fractured rock mass (the natural fracture system) is equivalently and quantitatively represented as a population of individual, fracture-like, idealised tabular objects, including their geometrical and physical properties. The DFN model is the recipe for creating a numerical system of fracture objects in which the mechanical, flow and transport processes taking place in fractures are represented explicitly in a discrete system.	Based on R-20-11
Fracture set	Based on one or several properties, geological fractures may be grouped into "fracture sets". Traditionally, the term "set" has been used almost exclusively for categorising fractures according to their orientation (e.g. "NW set", "subhorizontal set").	Based on R-20-11

^{*} R-07-45: Stephens et al. 2007, R-17-13: Follin 2019, R-20-11: Selroos et al. 2022

Table 2-4. Terminology for transport modelling. References to specific chapters in the present report indicate that the concept in question is discussed there, not necessarily that the exact definition given in this table can be found there

Term	Definition	Reference*
Transport processes a	nd parameters	
Matrix diffusion	Transfer of radionuclides or other dissolved solutes by diffusion, a process resulting from the Brownian motion of molecules, which leads to a net mass flow from regions of high concentration to regions of low concentration. Matrix diffusion can lead to mass flux between the flowing fracture, the surrounding rock matrix, and the adjacent inplane stagnant water zones. The directions of these fluxes (e.g. into or out of the flowing fracture) depend on the concentration gradients.	Updated from R-03-20
Sorption	A collective name for a set of processes by which solutes become attached by physical or chemical reactions to solid surfaces within the geosphere. The term is taken to include processes that are reversible over the time scales of relevance to performance assessment.	R-03-20
Immobilisation	Processes by which solutes become irreversibly incorporated within immobile solid phases in the geosphere over the time scales of relevance to performance assessment.	R-03-20
Retardation	Reversible processes (sorption and matrix diffusion) that delay the time taken for solutes to traverse the geosphere.	R-03-20
Retention	In R-03-20* defined as the combined effect of retardation and immobilisation processes. Now commonly used as a generic term referring to the collective effect of processes that delay solute transport, with or without immobilisation.	Updated from R-03-20
Storage porosity	The storage porosity of the rock is the total volume of water filled voids in the rock that are directly accessible and can store migrating solute. It includes pores that are connected to the wider fracture/pore system as well as dead-end pores that do not contribute directly to diffusive transport although can function as a storage capacity for migrating solute.	
Transport porosity	The transport porosity is the porosity of the rock that has a direct influence on diffusive transport and permeability by way of the geometric formation factor. The transport porosity is always less than the storage porosity which additionally includes dead-end pores that do not contribute to diffuse transport.	
Total porosity	The total volume of voids in the rock including all connected (grain boundaries, microfractures, hydrated interlayers of clay minerals) and non-connected voids (solution pores, etc.).	
Transport modelling m	ethodology	
Retardation model	The retardation model is an interpreted description, including interpreted data, of retardation properties for the typical rock units and structures at a site (different types of rock, fractures and deformation zone components). It is the final product of the site investigations and site descriptive modelling of bedrock transport properties.	
Transport domain	Large-scale building blocks of the retardation model that represent significant volumes of the host rock, e.g. sparsely fractured rock near the repository and upper rock near the ground surface, through which flowpaths intersect on their way from the repository to the surface system, or	This report, Chapter 4

vice versa. Examples of transport domains include deformation zones, the sparsely fractured rock (in specific named rock volumes), near surface sheet joints, etc.

Retardation component

Small-scale building blocks of the retardation model defined as the various distinct geological material types that constitute the basic components when constructing the model, and for which retardation data are provided. Examples of retardation components are fracture coatings, altered rock, intact (fresh) rock, fault gouge and breccia.

This report, Chapter 4

Microstructural unit

A microstructural unit represents a cohesive assembly of closely interconnected retardation components, exhibiting collective attributes and functions within identified fracture types and deformation zone structures. A microstructural unit may consist of one or more retardation components. An example of a microstructural unit is a fracture featuring a fracture mineral coating with an associated alteration rim overprinting fresh rock in a 3-layer configuration.

This report, Chapter 4

Fracture type

Fracture types are groups of fractures with common characteristics (e.g. the same microstructural model) that based on geological and/or other information are considered typical for the site or transport domains at the site. A fracture type may consist of one or more microstructural units and may include features in its description (e.g. continuously variable material properties, variable width alteration rim, etc.) that require further abstraction to transport classes before use in numerical models

This report, Chapter 4

Structural elements of deformation zones

Recurrent features of the deformation zones considered typical for the site or transport domains at the site, including materials commonly abundant in deformation zones as well as those deemed less common, although potentially contributing to the total retardation capacity of the deformation zones.

This report, Chapter 4

Transport class

A transport class is a simplified "basis set" of combined microstructural units that can be used directly in numerical transport modelling. For the simplest fracture types, there may be a 1:1 match between the fracture type and the corresponding transport class. For more complex fracture types, e.g. fracture types with spatially variable alteration properties, the corresponding transport classes could be abstractions designed for mathematical convenience. The transport class simplifies the properties of the fracture type for modelling purposes (e.g. a fixed width layered structure with piecewise constant material properties assigned from spatially averaged properties as described in the description of fracture type). Transport classes can be used directly in a transport model to directly represent identified fracture types or combined with other transport classes to model a more diverse range of fracture types. These may be identical to or changed relative to the fracture types in the retardation model.

This report, Chapter 7

^{*} R-03-20: Widestrand et al. 2003

3 Transport modelling concepts, processes and parameters

3.1 Overview of processes and concepts

Most long-range transport of dissolved species to or from the repository will occur by advection in open and water conducting fractures. Advective transport exists only if there are water conducting fractures that are connected to each other in a large-scale network that permits flow. Such a network is typically represented using the concept of a Discrete Fracture Network (DFN). This network will also be connected to open and water saturated fractures where the water is stagnant or has an insignificant conducting capacity. Moreover, the network effect and differences in transmissivity between fractures could lead to significant channelling, to which also internal fracture variability might contribute.

Open, or partly open fractures that are connected to the DFN, whether they are water conducting or non-conducting, cut through the heterogeneous crystalline bedrock. Crystalline rock typically contains both inter-granular and intra-granular porosity, with the proportion of each varying depending on the rock type. Inter-granular porosity consists of water-filled voids at grain boundaries, formed due to differential expansion of minerals during crustal uplift. Intra-granular porosity, on the other hand, consists of microcracks transecting otherwise non-porous mineral grains. Collectively, these water-filled void spaces are referred to as the rock matrix porosity. For typical permeability ranges of bedrock at Forsmark (see e.g. Vilks 2007) the matrix porewater may be considered effectively stagnant (Ferreira and Nick 2024).

There may also be microfractures below the size considered in the discrete fracture network that additionally contribute to the matrix porosity although these typically have the highest intensity in the vicinity of fracture surfaces. Solutes advected with the flowing groundwater can diffuse into and out of the rock matrix. In situations where there is a higher concentration in the flowing water relative to the rock, this can drive a net flux of solute into the rock matrix. When the concentration in the flowing water subsequently decreases, the concentration gradient is reversed, and there can be a net out-flux of solute from the rock matrix back into the flowing fractures. This process is typically very slow, and it leads to long tailing in radionuclide breakthrough curves (Neretnieks 1983, Haggerty et al. 2000).

If the solutes are sorbing they may sorb on the mineral surfaces adjoining the rock matrix porosity and their transport will be retarded. The lower part of Figure 3-1 shows a minor deformation zone that cuts through the host rock. The light blue lines represent fractures that are flow bearing while the black lines, for the purpose of the present report, can be taken to represent open non-conductive fractures (micro fractures in the upper magnified image) whereof some connect to the flowpaths. The upper part of Figure 3-1 shows an illustration of the altered wall rock associated with the flow bearing fractures, as well as alteration and deformation products within the fracture.

The matrix porosity consists of different types of pore space, predominantly grain-boundary pores and microfractures, but also solution pores and ruptured fluid inclusions. The diffusion into the accessible pore space of the rock matrix is in turn an important retention process for radionuclides and contaminants in general. Radionuclides can interact with and sorb on different mineral surfaces in the rock matrix to varying degrees which contributes to their transport retardation. These processes are discussed in more detail in Section 3.3, Chapter 5 and appendices A–C.

The open or partly open fractures of the fracture network that host flowpaths do not typically feature a fracture plane of simple geometry, with a constant water-filled aperture. This is partly due to natural roughness of the fracture surface and small lateral offsets between opposing fracture surfaces (related to shear processes) giving a variable aperture, and partly due to fracture infillings, fault gauge and/or fracture coatings. These can be described as rock alteration products that have accumulated in the fracture plane over the usually many millions of years that have passed since the fracture was formed, or small pieces of the rock matrix that have been broken off in brittle deformation.

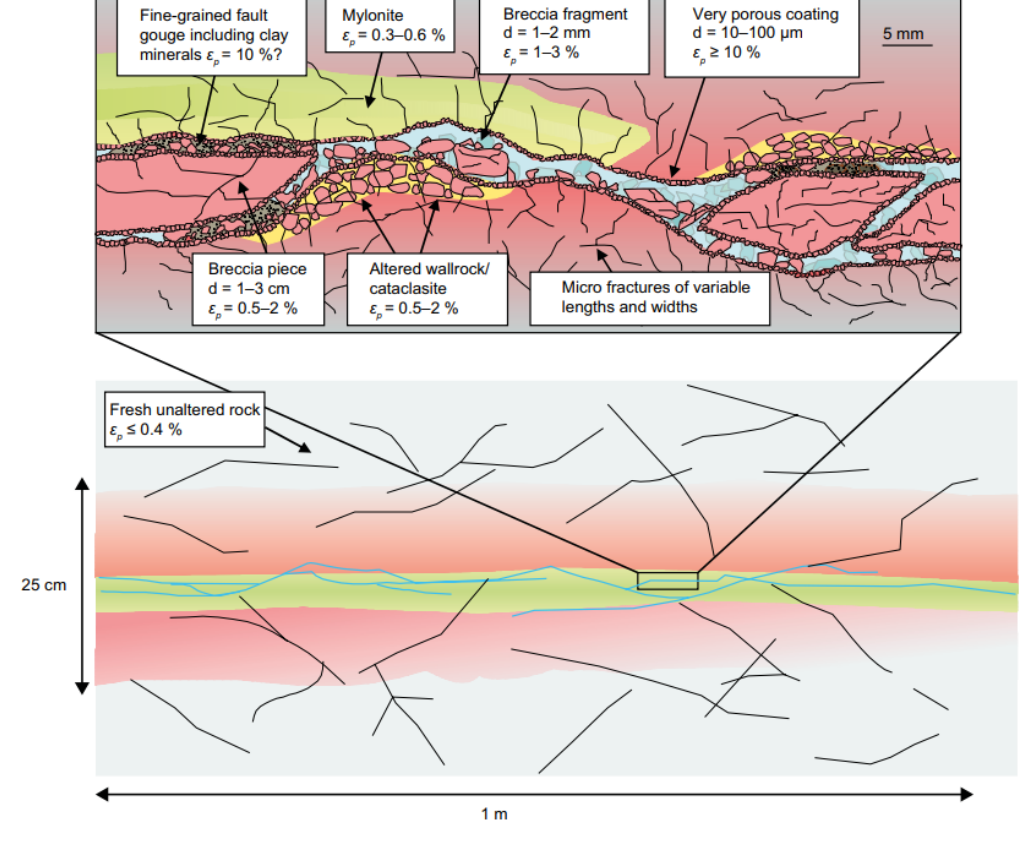


Figure 3-1. Schematic illustration of a generalised transport path in cross-section based on the conceptual model developed in the TRUE Block Scale project for a minor deformation zone. Illustration reproduced from Andersson et al. (2002).

Fracture infillings and fault gauge will obstruct the water flow. In some parts of the fracture plane the water flow may be relatively fast, whereas in other parts it will be slow and sometimes effectively stagnant. Solutes that diffuse into effectively stagnant zones in flow bearing fractures can access additional wetted surface area for matrix diffusion within the stagnant zone. Such stagnant water may be part of relatively unconstrained "pockets" of fracture water in the fracture plane. It may also be associated with water-filled microporosity of the fracture infillings or fault gauge.

Diffusion from flowing water to stagnant water within the fracture plane is a very similar process to diffusion normal to the fracture plane, from flowing water to the microporosity of the rock matrix (Crawford 2008, Appendix I). In transport modelling, these fundamentally three-dimensional processes can sometimes be simplified into a coupled set of notionally one-dimensional processes. Specifically, it turns out that diffusion from the flowing water can take different complex paths and sometimes be decomposed into a sequence of one-dimensional processes, such as from the flowing water to the nearby stagnant water and subsequentially to the bordering rock matrix, see for example (Mahmoudzadeh et al. 2013). In Sanglas et al. (2024) the effects of diffusion into stagnant water in a fracture of variable aperture are shown to be small under the conditions investigated.

For some solutes, diffusion into non-conductive but open fractures that intersect the flowpath may be an important mechanism for retardation. For non-sorbing anionic species, which have a low tendency to diffuse into the rock matrix due to anion exclusion processes, the diffusion into these dead-end fractures might be particularly relevant for the purposes of safety assessment calculations. In fact, anionic species are often the greatest dose contributors and their discharge, which is sometimes close to the regulatory limit, could potentially be reduced as a result of these diffusive processes.

Such non-conductive fractures may also constitute an important part of the groundwater solute storage capacity. From the non-conducting fracture, the solutes may diffuse further into the rock matrix that surrounds the fracture, where sorption on mineral surfaces may also occur. Therefore, these non-conductive fractures could be seen as providers of additional pools of surface area available for rock matrix diffusion. An additional complexity is that there is no conceptual

difference between a relatively large micro-fracture in the rock matrix and very small open but non-conductive fracture that is part of the discrete fracture network. As such, the DFN can be seen as a modelling construct where fractures above and below an arbitrary size threshold are classified as either being part of the DFN or belonging to the matrix porosity.

An aspect that adds complexity to transport in fractured media is the multi-scale nature of the underlying processes and related features. For instance, sorption of charged species in the matrix might be driven by electrostatic forces occurring within a few nanometres from the charged mineral surface, matrix pore sizes range from nanometre to millimetre scale, single fracture sizes are of the order of a few decimetres to some tens of metres, and transport pathways are often on the kilometre scale. Explicitly accounting for this broad range of scales, e.g. using multi-scale modelling frameworks, is impractical. For this reason, appropriate upscaling methods are required to parameterise long-range transport models.

Radionuclide transport modelling is typically carried out along fixed streamlines or transport pathways (Selroos and Painter 2012, Posiva 2012, Trinchero et al 2020). This is further discussed in Section 3.2.2. Besides the evident computational advantage, streamline-based approaches are particularly suited for these types of simulations since the underlying numerical or semi-analytical approaches are not affected by numerical dispersion and thus the computed breakthrough curves are not affected by artificial spurious dilution effects. Reactive transport modelling can be carried out using different approaches based on e.g. continuum approximations, DFN representations or traveltime based methods. Reactive transport modelling of the major chemical constituents (solutes) of the groundwater is typically used in an assisting role to inform radionuclide transport modelling (future groundwater states and compositional ranges as input to sorption modelling) and as part of the site descriptive modelling (Hydrogeochemistry). These different approaches are described in Section 3.5.

3.2 Radionuclide transport in rock fractures

Radionuclide transport modelling includes the migration of nuclear waste derived radionuclides and the fate of those radionuclides in the biosphere resulting in dose contributions to humans and non-human biota. Radionuclide transport modelling involves the assessment of transport through different components: i) the near-field engineering barriers, ii) the far-field host rock comprising the geosphere, and iii) the near-surface Quaternary deposits of the biosphere (see Chapter 7). In the following sub-sections, the focus is on item ii), that is, far-field radionuclide transport calculations of the geosphere. These calculations usually take the source function (i.e. radionuclide mass discharge at the near-field/far-field interface) as input and estimate the discharge at the far-field/near-surface interface as output.

3.2.1 Advection and dispersion

Advection is the phenomenon by which dissolved solutes are transported by fluid flow in flow-bearing fractures. The partial differential equation describing transport of a solute takes the form of the standard advection-dispersion equation (ADE), which for a one-dimensional flow channel can be written as:

$$\frac{\partial c}{\partial t} = -u_x \frac{\partial c}{\partial x} + D_L \frac{\partial^2 c}{\partial x^2} \tag{3-1}$$

Where C (mol/L) is the volumetric water phase concentration, u_x (m/y) is the water velocity in the principal flow direction, and D_L (m²/y) is the hydrodynamic dispersion coefficient in the longitudinal direction parallel to the flow direction.

The variability of the fracture velocity field within and between fractures leads to a spreading of the dissolved mass, which is observed both in space and in time. This phenomenon, usually referred to as hydrodynamic dispersion, has an important effect on e.g. radionuclide breakthrough curves that are characterised by earlier initial arrival times and lower peak values. Hydrodynamic longitudinal dispersion is often approximated as:

$$D_L = D_w + \alpha_L \cdot u_x \tag{3-2}$$

where α_L (m) is an empirical parameter denoted as longitudinal dispersivity and D_w is the diffusivity in water. If transport is modelled in a two-dimensional domain representative of a

fracture plane, typically one needs to considered transverse dispersion as well. Although it is generally accepted that large-scale radionuclide transport simulations can be constructed based on 1D representations of transport processes (Equation 3-1), the consideration of transverse dispersion is important when assessing the potential for diffusion into in-plane stagnant water zones in realistic heterogeneous fractures. Transverse dispersion is also important for the assessment of the transport of major geochemical components, since it is the main mechanism for mixing that does not involve matrix diffusion.

Molz (2015) stated that in any fluid flow, including groundwater flow, there is only advection and diffusion, which means that if one could reproduce the true velocity field, only molecular diffusion would be needed to model solute transport. Although theoretically true, this statement has limited practical implications because it is impossible to obtain the true velocity field, particularly in complex systems such as natural fractures. Thus, a macroscopic representation of dispersion processes is still needed. It is also worthwhile noting that Equation 3-2 is only valid under the assumption of asymptotic or Fickian conditions where the longitudinal dispersivity, α_L is constant.

Evidence of scale dependency of hydrodynamic dispersion dates back to the pioneering work of Gelhar (1993) and has been assessed in numerous scientific publications. As noted by Neretnieks (2002) this implies that the standard ADE equation does not strictly give a correct account of the impact of dispersion at different length scales since the longitudinal dispersity must be assumed constant. A detailed review of these works is however out of the scope of this report. At the network scale, the strong variation in fluid velocities, which is often controlled by the structure of the fracture network, leads to additional dispersion mechanisms. This large-scale dispersion mechanism, which is caused by the presence of different transport pathways with different velocities, is well described in Shahkarami (2017).

3.2.2 Pathway simplification

Radionuclide transport in the geosphere is typically assumed to occur along discrete and fixed pathways connecting a source location with a given compliance boundary, such as the interface between bedrock and regolith (Figure 3-2). In this conceptualisation, solute mass is transported by fluid flow along the pathway (advection), hydrodynamic dispersion takes place along the longitudinal direction only and there is no mass exchange between nearby pathways. Radionuclide retention is caused mostly by matrix diffusion and sorption in the rock matrix, although additional retention can be provided by diffusion into stagnant water where additional wetted surface for matrix diffusive uptake is available (Neretnieks 2006).

The fixed pathway simplification has three main advantages: (i) radionuclide transport calculations can be run using analytical solutions or dispersion-free numerical simulations, (ii) neglecting transverse dispersion is deemed to be cautious in terms of e.g. maximum radionuclide discharge at the outlet boundary, and (iii) it allows for the use of separate, specialised models for flow simulation and transport simulations. The main drawback of the fixed pathway representation is that it is not well suited to describe changes in the groundwater flow velocity field.

Pathway tracing is typically carried out assuming perfect mixing at fracture intersections which means that the downstream fracture segment is chosen based on a probability proportional to the outlet flux. Moreover, different DFN realisations should typically be accounted for in the analysis, and transport pathways therefore be considered as a stochastic process and handled within an appropriate stochastic framework.

Transport pathways are typically subdivided into consecutive segments. In DFN-based particle tracking simulations, each segment is assumed to lie in a single fracture plane and is delimited by the intersection with two adjacent fractures. In ECPM-based particle tracking simulations the physical meaning of a segment is however more ambiguous. The advantage of the segment-based representation is that full pathway heterogeneity can be accounted for, including different retention models in different segments. How pathway parameterisation is carried out is an open question, which is discussed in some detail in Section 7.4. If the level of granularity of the underlying groundwater flow model is used, then deterministic *rock types* can be used. If heterogeneity within a single rock domain is to be taken into account, then an approach based on probabilistic sampling of *transport classes* might be adopted.

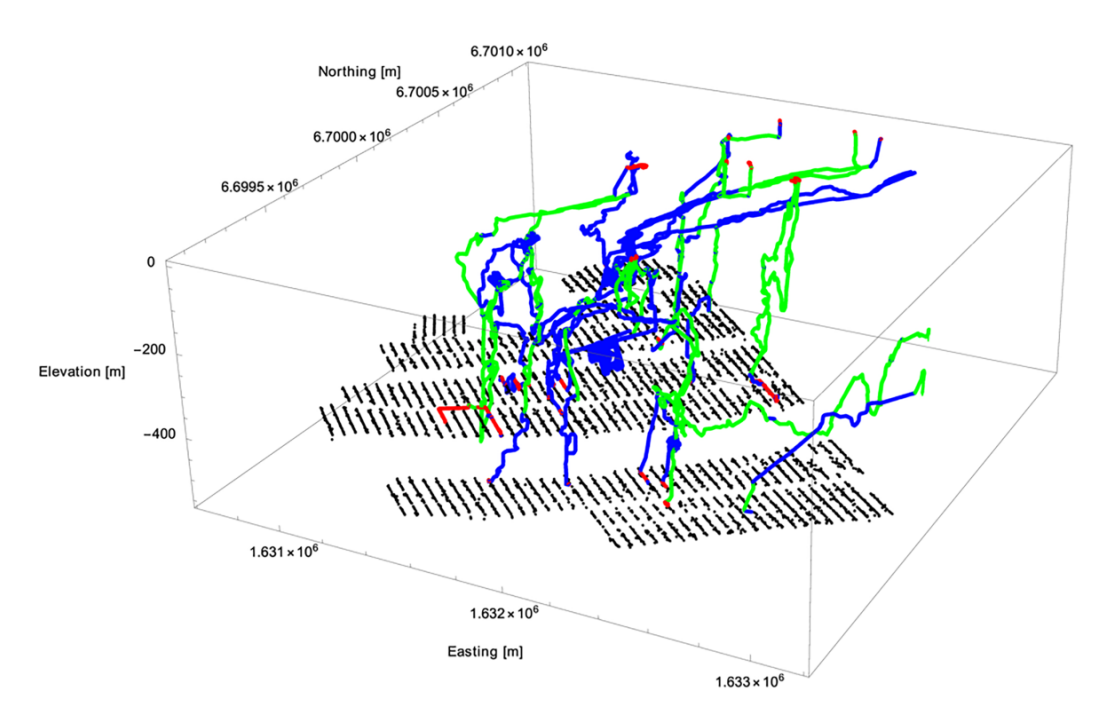


Figure 3-2. Three-dimensional representation of twenty randomly selected transport pathways computed for the so-called Forsmark growing pinhole scenario. Segments are coloured according to the type of medium: green is the Hydraulic Conductor Domains (i.e. deterministically modelled deformation zones), blue is the Hydraulic Rock mass Domain (i.e. the less fractured bedrock), and red is either tunnels (at repository depth) or soil (in the near-surface system). The black dots are the deposition holes of the planned spent nuclear fuel repository at Forsmark. Figure modified from Selroos and Painter (2012).

A pathway segment is described by two parameters: (i) the groundwater travel time (t_w) and (ii) the transport resistance. The latter is denoted as β [TL⁻¹] in Cvetkovic et al. (1999), where it is defined as

$$\beta = \int_0^{t_W} \frac{d\varepsilon}{b(\varepsilon)} \tag{3-3}$$

where ε is a dummy integration variable and b (m) is the fracture half-aperture. The transport resistance, hereinafter referred to as the F-parameter, F-factor or just as F, in line with the notation used by SKB (see Section 3.6), is the key hydrodynamic control parameter for matrix diffusion and is dependent on the travel time of water, t_w . (also referred to as advective travel time).

Depending on modelling approach, the transport resistance (β or F) can be computed either using the Lagrangian definition in Equation 3-3, as the ratio of advective travel time to the transport fracture half-aperture, or using geometric and flow information available in channel or fracture network models, where the transport resistance is defined as the ratio between flow-wetted surface area and the flow rate (e.g. Berglund and Selroos 2004, Appendix A). In the former approach, the uncertainty mainly arises from the calculation of the advective travel time performed by the groundwater flow model. This calculation depends on a number of underlying assumptions, with the most critical one being the definition of the transport aperture, as discussed in the next section. In the latter approach, flow rates can be reasonably well constrained using, for example, flow logging data, while the uncertainty primarily stems from the degree of channelling, which affects the definition of flow-wetted surface area (see Chapter 6).

In-plane longitudinal dispersion is typically expressed in form of the Peclet number:

$$Pe = \frac{L}{\alpha_L} \tag{3-4}$$

where α_L (m) is the longitudinal dispersivity coefficient and L (m) is a characteristic spatial scale. The latter is typically set equal to the transport pathway length. Further details on advection and inplane dispersion are discussed in the next sub-section.

Pathway tracing is typically done using particle tracking calculations and the underlying groundwater velocity field is taken from existing hydrogeological models. These models are either based on a DFN representation of the fractured medium or upscaled in a continuum grid using the so-called Equivalent Continuous Porous Media (ECPM) approach.

In DFN models, fluid flow along fractures is explicitly resolved and fracture features, such as aperture, are retained and explicitly used to derive segment-based values of transport resistance. For ECPM models, however, upscaling methods are required. It should be noted that models based on the pathway simplification can also include the uppermost unconsolidated regolith layers, as was done for instance in Selroos and Painter (2012). In that implementation, retention was described by a linear isotherm single-porosity model.

As mentioned previously, the transport pathway simplification has several advantages related to computational efficiency and lack of numerical dispersion. However, this simplification has important limitations in the way transient groundwater flow conditions can be handled. In fact, the only way this can be done is by changing the magnitude of velocity in a global sense, which means scaling the groundwater travel time and transport resistance by the same factor along the whole trajectory and the entire set of trajectories. This is the approach that was used in SR-Site to represent changes in groundwater flow due to higher gradients during a glacial cycle (Selroos et al. 2013). Other more realistic approaches, which are based on a piecewise representation of flow changes, require the fixed transport pathway representation to be abandoned.

3.2.3 Fracture aperture

One important aspect to consider when dealing with the somewhat abstract concept of "fracture aperture" is that real fractures are not parallel plates, as typically assumed in their mathematical representation, but rather rough and irregular. Consequently, the *geometric aperture*, defined as the pointwise distance between the two fracture walls, is characterised by a heterogeneous distribution. When modelling groundwater flow and radionuclide transport over the large spatial and temporal scales of safety assessment applications, explicitly accounting for such internal variability is unfeasible. Therefore, appropriate "equivalent" values are needed. It is noted that the term "equivalent" aperture is used here in accordance with the commonly accepted terminology of stochastic hydrology, where "equivalent" refers to averaging in physical space (Sanchez-Vila et al. 2006).

One challenge in the formulation of equivalent fracture apertures for model parameterisation is that they are problem dependent. In other words, the equivalent fracture aperture for use in groundwater flow models (*hydraulic aperture*) typically differs from the equivalent aperture required by transport models (*transport aperture*). This problem dependency has been extensively studied and documented (Silliman 1989, Tsang 1992).

The hydraulic aperture, δ_h (m), is typically defined based on the cubic law (e.g. Witherspoon et al. 1980) as the aperture that would carry the same amount of water under the same hydraulic gradient as the actual rough-walled fracture:

$$\delta_h = \left(\frac{12\mu Q}{\rho gW} \cdot \frac{L}{|\Delta H|}\right)^{1/3} \tag{3-5}$$

where μ (Pa·s) and ρ (kg/m³) are, respectively, the viscosity and density of the water, Q (m³/s) is the flowrate, W (m) is the fracture width and $\frac{|\Delta H|}{L}$ (-) is the hydraulic gradient. The equation can be rewritten in terms of fracture transmissivity, T (m²/s)

$$\delta_h = \left(\frac{12\mu T}{\rho q}\right)^{\frac{1}{3}} \tag{3-6}$$

Equation 3-5 is written here for linear flow conditions while a slightly different expression is obtained for e.g. radially converging flow. Regardless of the flow regime, in the field the hydraulic aperture is typically derived from hydraulic measurements of volumetric flow rate and pressure drop.

The transport aperture, δ_t (m), also denoted as mass balance aperture in Tsang (1992), is related to the advective travel time (t_w , y), and the F-factor (F, y/m) as

$$\delta_t = \frac{2t_{\rm w}}{F} \tag{3-7}$$

In the field, δ_t is derived from flow and tracer tests based on the volumetric flow rate and the mean transport residence time. Tsang (1992) presents a second transport aperture defined as frictional loss aperture, which is not further discussed here as it has not been used in any of the previous safety assessment applications.

One interesting piece of evidence is that the hydraulic aperture, as defined in Equation 3-5, depends on the pressure drop while the transport aperture (Equation 3-7) does not. This is especially important, as pressure drops are particularly sensitive to local small aperture values and therefore the hydraulic aperture is generally smaller than the transport aperture. This is shown in a simplified form in Figure 3-3.

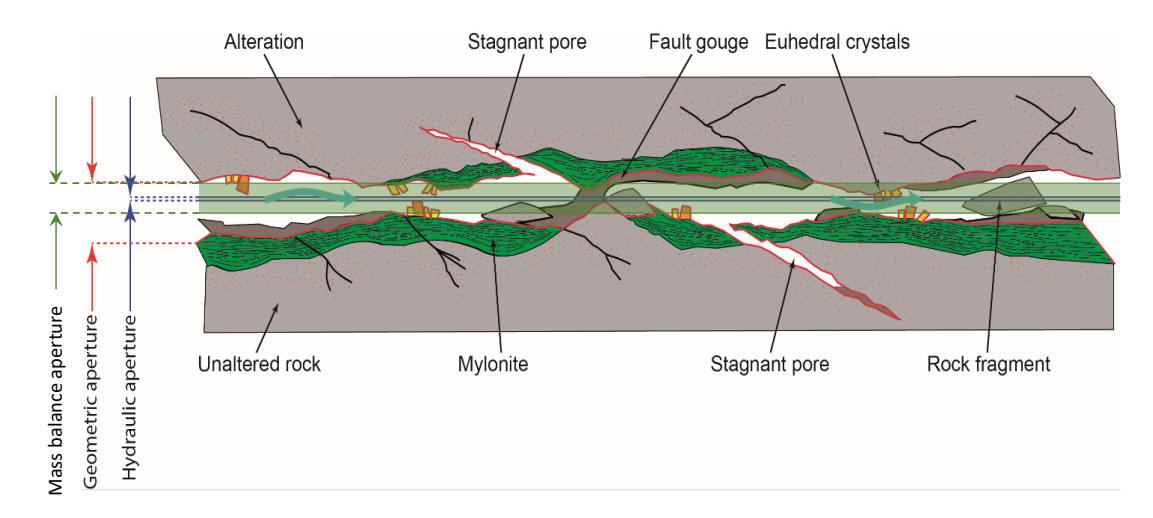


Figure 3-3. Illustration of different types of apertures. Figure modified from Selroos et al. (2022).

While fracture apertures in small, well-defined networks can be determined through field tests, in safety assessment applications DFN models must instead be parameterised using empirical rules. For instance, (i) the transmissivity is related to fracture size, (ii) the hydraulic aperture is defined according to the cubic law, and (iii) the transport aperture is established through a functional relationship with the hydraulic aperture.

In the Äspö Task Force GWFTS Task 6c (Dershowitz et al. 2003), and in the subsequent SR-Site modelling work, the following functional relationship between transmissivity and hydraulic aperture was used:

$$\delta_h \cong a_h \cdot T^{0.5} \tag{3-8}$$

According to this relationship and hydraulic experiments in the TRUE Block Scale project, $a_h = 0.46$ (an interval of 0.25 to 0.60 is also given). The relationship between the hydraulic and transport apertures is typically defined using a simple linear relationship (see Table 8-2 of the DFN modelling methodology report, Selroos et al. 2022):

$$\delta_t = a_t \cdot \delta_h \tag{3-9}$$

where a_t [-] is an empirical parameter that can be inferred from *in-situ* tracer or grout injection tests (see also Selroos et al. 2022, Table 8-2). A detailed discussion about the relationships between the different fracture apertures is provided in Hjerne et al. (2010). As a final remark, it is noted that the present section discusses the full aperture, which is denoted as δ (with various indexes), whereas in other parts of the report the fracture half-aperture, denoted as b, is often used (e.g. in transport equations).

3.3 Radionuclide retardation and decay

3.3.1 Matrix diffusion

Solutes moving along water conducting fractures may diffuse into the adjacent rock matrix. A packet of radionuclide mass that has diffused into the matrix may decay or eventually re-emerge from the matrix and move along the remaining pathway. In Lagrangian terms, the time spent by a packet of solute mass in the matrix surrounding a water conducting fracture (also known as retention time t_m) is described by the following cumulative distribution function (Painter et al. 2008):

$$P(t_m) = \operatorname{erfc}\left(\frac{\kappa_{MPG}\beta}{2\sqrt{t_m}}\right) \tag{3-10}$$

where $\kappa_{MPG} = \sqrt{D_e \phi_p R_p}$ is the material properties group, D_e (m²/y) is the effective diffusivity, ϕ_p (–) is the matrix porosity, and R_p (–) is the pore retardation factor for the rock matrix. The retention time in the matrix is equal to the total retarded travel time, t_r (y) minus the advective travel time, t_w (y):

$$t_m = t_r - t_w \tag{3-11}$$

There is a direct analogy between the retention time distribution (Equation 3-10) and the Eulerian solution for a continuous injection boundary condition (Carslaw and Jaeger 1959). From these simple analytical solutions, it is evident that the coupling between advective processes in the fracture and diffusion mechanisms in the matrix is given by the transport resistance, also referred to as F-factor and denoted as F or β (Section 3.2.2), which is thus a parameter of key importance for the simulation of contaminant transport in fractured rock.

For a non-layered matrix, the other controlling parameter, κ_{MPG} depends on specific characteristics of the rock matrix, namely the matrix retardation factor (see Equation 3-14), matrix porosity, and effective diffusion coefficient. This retardation factor depends in turn on the available pool of sorption sites in the matrix. Details on how matrix porosity should be inferred are provided in chapters 4 and 5. Although there is no unified notation, the effective diffusion coefficient is usually defined as:

$$D_e = F_f D_w = \phi_p \frac{\sigma}{\tau_n^2} D_w \tag{3-12}$$

where $F_f(-)$ is the geometric formation factor, $\sigma(-)$ is the constrictivity, and $\tau_p(-)$ the tortuosity. Methods for measuring the effective diffusivity are described in Chapter 5.

Equation 3-10 and the discussion above assume that properties of the rock matrix are homogeneous. However, both laboratory micro-characterisation studies (Voutilainen et al. 2019) and results from *in-situ* tracer tests have pointed out that the matrix is highly heterogeneous, both in terms of physical and mineralogical properties (Iraola et al. 2017).

For cases where the rock matrix has a limited accessible diffusion depth, an analytical model was proposed by (Sudicky and Frind 1982). There is no closed-form solution for this model and therefore it is usually more convenient to calculate the corresponding residence time distribution in the frequency (Laplace) domain and numerically invert the solution to the time plane. There are also frequency domain solutions for multilayer rock matrix settings where the layers are defined with piecewise constant material properties (see, e.g. Moreno and Crawford 2009, Cvetkovic 2010, Mahmoudzadeh et al. 2014).

3.3.2 Sorption

Sorption describes several mechanisms by which dissolved solutes are removed temporarily (reversible) or sometimes permanently (irreversible) from the mobile aqueous phase and incorporated on, or within minerals. These include physical and chemical adsorption, surface precipitation, co-precipitation (solid solution formation), and pure phase precipitation. In the context of radionuclide transport modelling, however, it is common to consider physical and chemical adsorption processes separately from precipitation and surface precipitation. Here, the term sorption is amended to explicitly include only those processes that can be described using an isotherm-based approach where there is a direct 1:1 relation between concentration of a solute in the aqueous phase and its corresponding concentration adsorbed to a surface either physically, electrostatically, or by covalent chemical bonding.

Dissolved solutes are frequently distributed amongst various ionic forms and can interact with and attach to mineral surfaces that possess a net charge of opposite sign. This is the most common way in which dissolved radionuclides sorb to mineral surfaces. The surface charge of minerals results from both permanent structural charge in the mineral crystal itself and atoms with unsatisfied bonds at the mineral surface reacting with water to give variably charged surface reactive groups. The interaction of ionic solutes with the permanent charge sites and the reactive surface groups may be electrostatic in nature, or due to the formation of covalent chemical bonds.

In the context of contaminant transport in fractured media, sorption takes place on minerals directly in contact with flowing water in the fracture, but also on mineral surfaces within the rock matrix which can be accessed by diffusive transport. Even though the diffusion accessible porosity of the rock matrix is typically very low (usually a fraction of a percent), the specific surface area of mineral surfaces that can be accessed is many orders of magnitude greater than that associated with the minerals lining fracture surfaces along a flowpath. When radionuclides and other contaminants carried by groundwater interact with these surfaces, the movement of the contaminant plume is retarded and pulse releases are broadened, thereby diluting the mass flux discharge to surface systems and the biosphere.

Mechanistic models used to describe the sorption processes are typically ion-exchange and surface complexation models. The other related processes of surface- and free phase precipitation are not included. This is partly due to that these processes typically cannot be handled in a conditionally constant K_d based modelling framework, and partly because they are not considered relevant at concentration levels diluted below conservatively chosen solubility limits which constrain near-field release. If simplifying assumptions are made, it may also in some cases be possible to include solid solution formation in the operative definition of the sorption processes that are modelled.

Ion exchange

Sorption by cation exchange describes the competition between different ionic species for sorption sites in reversible reactions that are fundamentally electrostatic in character. Models of cation exchange are mostly applicable for modelling sorption on fixed charge binding sites on clay minerals. The binding sites themselves derive from the electrostatic potential well formed at mineral surfaces from structural charge deficits. The charge deficit arises due to regular isomorphic substitution of lower valence cations in the crystal structure of phyllosilicate minerals (for a more detailed explanation see, e.g. Appelo and Postma 2005).

Since the negative surface charge is permanent and not affected by solution chemistry, sorption can be described as a simple stoichiometric exchange of equal quantities of ionic charge. The mass action equations describing cation exchange reactions can be written in several different ways depending on how the activity of charged sites are conceptualised in the model. A more detailed account of the different cation exchange model formalisms can be found elsewhere (e.g. Bolt 1980, Sposito 1981, 1989, Appelo and Postma 2005). Cation Exchange (CE) models are usually parameterised based on measurements of Cation Exchange Capacity (CEC) and selectivity coefficients derived for the mass action equation defining the relative affinity of positively charged species with the mineral surface charges.

Since the activity of sorbed cations is not well defined, one approach is to assume that the sorbed activities are equal to the equivalent ion fraction. This is the commonly used Gaines-Thomas convention (Gaines and Thomas 1953). Since equal amounts of charge are exchanged between the surface and the aqueous phase, the net energy expenditure required to move the sorbing and desorbing cations to and from the surface is identical and electrostatic corrections therefore do not need to be considered explicitly.

Although the formulation of cation exchange generally assumes sorption on permanently charged binding sites, the measured CEC will usually include a contribution from variable surface charge as described previously. While cation exchange at variably charged sites can be modelled in the same way as permanently charged sites at constant pH, it is usually more accurate to model them as surface complexation reactions as this allows the mass balance of variably charged sites as a function of pH to be considered. It is also common for cation exchange to occur at different locations on phyllosilicate minerals, and the cation exchange capacity may be comprised of

contributions from multiple classes of binding sites featuring different affinities and exchange capacities. This is discussed in greater detail in Appendix A.

Surface complexation

Variably charged, reactive surface groups exist at the surface of many different minerals including oxides, hydroxides, tectosilicates (such as the feldspar mineral group) and edges of phyllosilicate minerals (including biotite, chlorite, muscovite, and clay minerals). The net surface charge of these minerals changes in response to surface chemical reactions. The most important reactions in this respect are protonation-deprotonation reactions of surface exposed oxygen atoms resulting in the formation of different proportions of $-OH_2^+$, -OH, and $-O^-$ surface reactive groups. The surface charge is often described in terms of the pH_{pzc} which is the pH at which the net surface charge is zero. When considering the variable charge arising only due to reactions of surface reactive groups with H⁺ and OH⁻, it is called point of zero net proton charge (PZNPC) (Langmuir 1997 and references therein).

At pH levels lower than the PZNPC there is a net positive surface charge, whereas at higher pH levels the net surface charge is negative. At normal groundwater pH levels (7-9), the net surface charge is predominantly negative for most aquifer forming minerals and the rock matrix. The various Fe-oxide polymorphs are an exception, as they typically have PZNPC close to the pH of groundwater and therefore exhibit a tendency to neutral or slightly positive surface charge depending on the mineral under consideration. A detailed account of the surface charge of various minerals as well as techniques for its measurement can be found in (Kosmulski 2009).

Charged cations and anions dissolved in groundwater can react with the surface reactive groups in different ways and be reversibly immobilised as surface complexes. Reactions that result in the formation of covalent bonds between reactive surface groups and the sorbing solute are referred to as inner sphere surface complexes since partial or total loss of the hydration shell of the sorbing ion typically occurs and it is bound very closely to the mineral surface. Reactions involving weaker, non-covalent interactions that are predominantly electrostatic in nature, although may also involve hydrogen bonding (and where the sorbing ion retains its hydration shell), are referred to as outer sphere surface complexation reactions.

Since surface complexation reactions do not preserve surface charge in the same way as simple cation exchange reactions, electrostatic corrections are needed to account for the changes in the electrical potential that affects the distribution of ions near the mineral surface. In surface complexation (SC) models, the effect of charged surfaces is considered using *electrostatic double-layer* (*EDL*) theory (see Appendix A and references therein). In EDL theory, the electrostatic potential is conceptualised to rapidly decrease with distance from the mineral surface in an approximately exponential fashion. Due to the unbalanced charge near the mineral surface, a swarm of ions of opposite charge (*counterions*) accumulates in a layer adjacent to the surface although at a slightly greater distance than the ions that form inner sphere surface complexes. The layer containing ions sorbed at the mineral surface (*Stern layer*) together with the layer of loosely associated counterions (*diffuse layer*) are referred to as the electrical double layer.

Since the solution composition within the electrical double layer differs to that of the bulk solution, electrostatic corrections are introduced which enable one to relate concentrations at the mineral surface with those in the bulk solution. The electrostatic corrections essentially account for the additional work required to move dissolved ionic reactants and products between the surface and bulk solution. There are several different models in the literature which are used to model surface complexation processes. These differ mostly in the way the EDL is conceptualised and the localisation of charge at or adjacent to the mineral surface. A review of these different conceptualisations is beyond the scope of this report although a short account of the principal differences between the different models is given in Appendix A; for more details, the reader is referred to the texts by Dzombak and Morel (1990), Langmuir (1997), and Appelo and Postma (2005).

Sorption in transport modelling

In radionuclide transport modelling, the distribution of the sorbent between the solid and solution due to the sorption processes is commonly described with a *distribution coefficient*, K_d (m³/kg or L/g):

$$K_{\rm d} = \frac{s}{c} \tag{3-13}$$

where C (mol/L) is the aqueous concentration and S (mol/g) is the specific sorbed concentration in terms of sorbent mass. The K_d is simply a ratio of concentrations for a specific groundwater composition and is not a thermodynamically defined construct, although it can be defined in terms of thermodynamic expressions depending on the type of sorption reaction being modelled.

In transport calculations the distribution coefficient is often incorporated in a dimensionless *retardation factor*, which for the rock matrix can be defined as:

$$R_p = 1 + \frac{\kappa_{\rm d}\rho_b}{\phi_p} \tag{3-14}$$

where ρ_b (kg/m³) is the bulk density, and ϕ_p (–) is the matrix storage porosity. For sorption processes in the flow-bearing fracture, there is an analogous expression that uses a distribution coefficient specific for the minerals lining the fracture flowpath that are sorptively equilibrated on the timescale of transport:

$$R_f = 1 + \frac{d_s}{2b}(\phi_s + K_{ds}\rho_{bs}) \tag{3-15}$$

where d_s (m) is the total thickness of mineral coatings in the fracture summed over opposing fracture surfaces, b (m) is the transport half-aperture of the fracture, while ϕ_s (–), ρ_{bs} (kg/m³), and K_{ds} (m³/kg) denote the average porosity, bulk density and distribution coefficient of the fracture minerals. This is discussed more in Section 5.3.6 where an alternative formulation is given for mixed mineral contributions to the fracture retardation factor.

The K_d in safety assessment modelling is typically assumed to be conditionally constant for a given groundwater composition presumed representative of the geosphere. The use of a K_d value in safety assessment also implies sufficiently dilute concentrations of the migrating radionuclide such that the sorption isotherm is approximately linear over the modelled range of radionuclide concentration. Despite this requirement for sorption linearity, other non-linearities relating to variation of groundwater composition in the fractured-rock aquifer system can be considered when defining suitable ranges of K_d to be used in transport modelling. This is typically formalised in descriptions of "Smart K_d " (e.g. Kulik 2002) where thermodynamic sorption models are used to estimate K_d values for spatially and temporally variable groundwater compositions along a flowpath.

In the approach to Smart K_d assignment adopted in this work, mechanistic models including cation exchange and surface complexation as described above are used to anchor K_d values measured in laboratory experiments for a given reference groundwater to values appropriate for use in safety assessments. This is achieved using chemistry correction factors to account for deviating groundwater compositions due to the evolving groundwater situation in the geosphere. Details of this methodology are described in Chapter 5 and appendices A–C.

3.3.3 Decay/ingrowth

Radionuclides are unstable isotopes that decay according to a first order rate process giving rise to an exponential decay function. Most of the available radionuclide transport codes can account for radionuclide decay and ingrowth although there are subtle differences in the numerical algorithms used that are only briefly discussed here. Figure 3-4 shows the U-238 decay chain, as simplified in calculations for SR-Site (Crawford and Löfgren 2019).

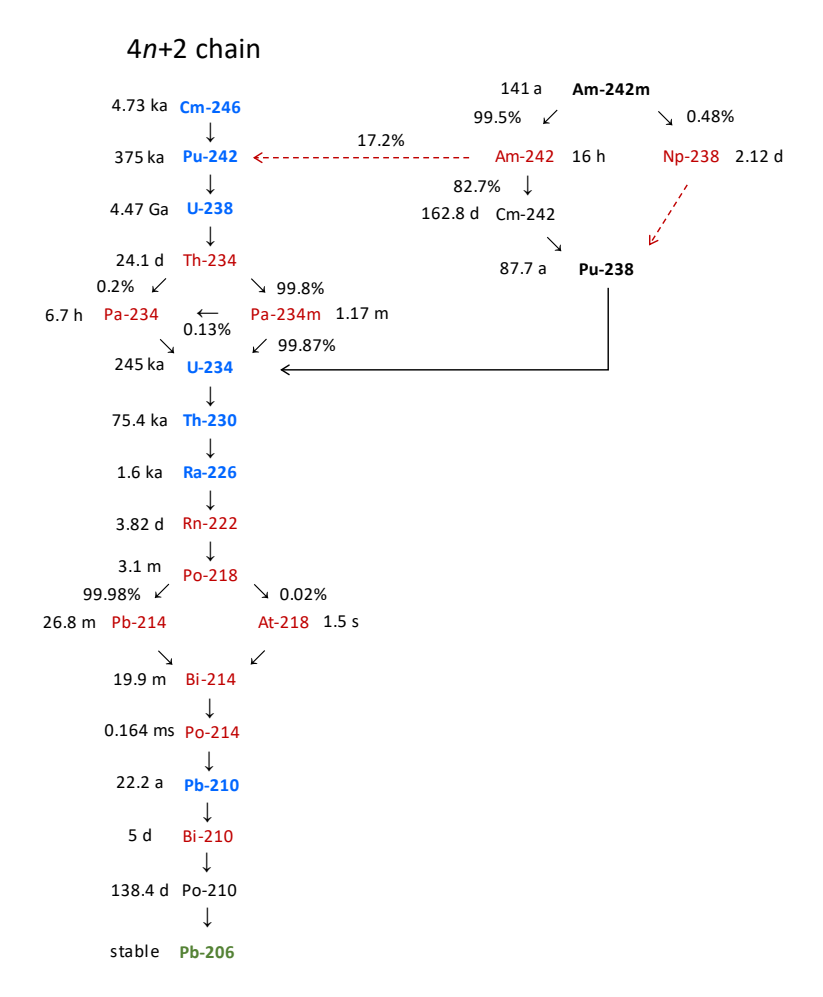


Figure 3-4. Simplification of the U-238 decay chain used in radionuclide transport calculations of SR-Site. Blue – explicitly modelled radionuclide; black – radionuclides that are part of the initial inventory, but where transport is neglected and inventory is simply added to subsequent progeny nuclide; red – radionuclides implicitly modelled assuming secular equilibrium with the parent radionuclide; green – stable isotope decay chain terminator. Figure taken from Crawford and Löfgren (2019).

Decay chains can have converging and diverging decay branches. Some of the available tools for radionuclide transport modelling cannot handle decay branches; FARF31 cannot simulate neither diverging nor converging branches, whereas MARFA and FARFCOMP can account for converging branches – see Section 7.3 for details about these computer codes. In SR-Site, most of the diverging branches were neglected as they have very short half-lives and re-converge quickly to the main decay chain. Other branches were discarded based on expert judgment, such as the decay of Mo-93 to stable Nb-93, which was neglected with the argument that it was a conservative assumption with regard to the radiological risk.

3.4 Colloid facilitated and gas phase transport

In addition to their transport in dissolved form, radionuclides can also be transported by carrier colloids in sorbed form and in the gas phase. Carrier colloid facilitated transport is an important transport mechanism that is considered explicitly in safety assessment calculations (SKB TR-21-07). Naturally occurring carrier colloids typically consist of clay platelets, micro- and nano-precipitates of various ferric oxide polymorphs, and other common secondary minerals. As noted in Chapter 5, the naturally occurring colloids are expected to be at sufficiently low concentrations that they do not contribute significantly to radionuclide transport. Carrier colloids resulting from bentonite buffer erosion during the low ionic strength waters typical of glacial advance and retreat, on the other hand, are a significant transport mechanism that is included in safety assessment transport calculations (see Chapter 7).

For gas phase mediated radionuclide transport, the focus is mostly on gas generated by corrosion of iron in repository systems. Radionuclide transport can be enhanced by the presence of a gas phase

either directly or indirectly. The direct mode of transport is in the form of gas phase components mixed with migrating H₂ gas bubbles. This, however, is only a relevant transport mechanism for C-14 and Rn-222 since they are the only radionuclides that can exist in gas form at low ambient temperatures. The second mode of transport is indirect and involves adhesion of carrier colloids (e.g. particles of bentonite) to bubbles undergoing advective transport. Although the processes by which radionuclides may be transported by this mechanism are associated with considerable uncertainty, it has been concluded in previous safety assessments (e.g. SKB TR-21-01, Section 13.8) that they are of minor importance for overall safety.

3.5 Reactive transport modelling concepts

An important input to radionuclide transport modelling in safety assessments is the predicted state of the groundwater composition as it evolves over time. To make these predictions, consideration needs to be given to the present state of the groundwater and how it is affected by infiltration of meteoric water during temperate periods, density driven flow, influence of future glacial climate cycles, land uplift, etc. These types of predictions typically require more sophisticated modelling techniques than for radionuclide transport as the major groundwater components are not diluted contaminants as is the case for radionuclides.

The current and future hydrogeochemical conditions at Formark are and will be strongly influenced by mixing processes between different groundwater types, such as marine, brackish, and meteoric water types, as well as influences from the highly saline groundwater found at increasing depths. These mixing processes affect concentration levels of major ions (including Ca²⁺, Mg²⁺, Na⁺, K⁺, CO₃²⁻, and SO₄⁻). Changes in concentrations of these solutes due to mixing may also result in precipitation-dissolution reactions to uphold chemical equilibrium and may also be affected by cation exchange processes.

Mixing processes, and the related hydrogeochemical evolution of the site, are dependent on the dual-porosity behaviour of the fractured system due to coupled matrix diffusion-sorption processes and chemical reactions involving minerals in the rock matrix. Meteoric water infiltrating through outcropping fractures, for example, may be only partly buffered chemically by fracture coating minerals, and matrix diffusion coupled with weathering reactions in the rock matrix may further change the character of the infiltrating water over a distance along recharge paths from the surface. Electrostatic effects relating to a significant electrical double layer presence at narrow pore throats in the rock matrix may also cause enrichment of cations in the matrix porewater so that the diffusive uptake of anions is simultaneously hindered. Processes related to this anionic exclusion as it relates to radionuclide transport are discussed in more detail later in Section 5.1.6.

The representation of these complex and coupled processes typically requires the use of multi-component reactive transport codes as well as appropriate approaches and methodologies. For instance, the mutual interplay between the rock matrix and the flowing fractures can be accounted for by using travel-time based (Section 3.5.1) or continuum-based (Section 3.5.2) reactive transport models, while its implementation in explicit DFN models (Section 3.5.3) is numerically challenging. The following sub-sections provide an overview of these different approaches to reactive transport modelling (RTM).

3.5.1 Travel-time based reactive transport models

In travel-time based reactive transport models the spatial coordinate is replaced by the groundwater travel time by making use of the relation between distance travelled by notional parcels of water and advective travel time (i.e. $t_w = x/u_x$). The groundwater (advective) travel time is also sometimes referred to as the kinematic groundwater age (Goode 1996). Using this relationship, the advection-dispersion equation (ADE) can be re-written in terms of a 1D travel-time based partial differential equation.

The simplification introduced by this transformation is useful since it allows complex three-dimensional problems to be decomposed into a set of computationally more tractable 1D simulations. Such approaches are often referred to as *streamtube-based* methods. The underlying assumption is that steady-state hydraulic conditions prevail and that there is no mixing between different streamtubes, i.e. no transverse dispersion between flowpaths with different flow velocities and/or compositional boundary conditions.

A notable application of this modelling concept is the Lagrangian Stochastic Advective Reactive (LaSAR) approach (Cvetkovic and Dagan 1994). The LaSAR approach implicitly recognises the stochastic nature of t_w due to the underlying uncertainty of the heterogeneous distribution of permeability values, and thus uses appropriate probability density functions (pdf) for t_w which are mapped onto related pdfs of species concentration. Applications of the LaSAR approach have been presented, where the numerical code PHREEQC (Parkhurst and Appelo 2013, Malmström et al. 2008) has been used as the geochemical calculation engine. One such application is FASTREACT, which has been developed and applied by SKB (Trinchero et al. 2014a, b).

3.5.2 Continuum models for reactive transport

In continuum-based formulations applied to fractured media, the properties of the flow bearing fractures are mapped and represented in a continuum grid. The representation of DFNs in continuum models has mostly been studied for applications focused on groundwater flow (e.g. Jackson et al. 2000). Handling mass-exchange between the flow bearing fractures and the adjacent rock matrix is not a trivial task, and different approaches have been proposed. For example, Haggerty and Gorelick (1995) and Carrera et al. (1998) proposed using multiple linear mass-transfer terms. This approach, denoted as the Multi-Rate Mass Transfer (MRMT) model, is computationally attractive and is the model used by the SKB groundwater flow modelling code DarcyTools to simulate mass exchange. However, MRMT is restricted to the simulation of non-sorbing solutes and can at most accommodate simple bi-molecular reactions (Willmann et al. 2010).

For multi-component reactive transport simulations, an alternative approach is to use Dual-Continuum formulations based on two overlapping continua: the primary continuum, which represents the flow bearing fractures, and the secondary continuum, which represents the intact rock matrix (Lichtner 2000, Lichtner and Karra 2014, Iraola et al. 2017). This approach is also referred to as the Dual Continuum Disconnected Matrix Model (DCDMM), since a block of secondary continuum grid cells can only exchange mass with the corresponding cell of the primary continuum whereas no mass exchange is allowed among different blocks of the secondary continuum. In the much-simplified case of a one-dimensional flowpath, the cell blocks of the secondary continuum may be imagined as teeth in a toothcomb-like arrangement where the primary continuum comprises the shaft of the comb. As is the case in all numerical models of limited diffusion, the innermost cells in the secondary continuum are by necessity defined to have zero flux (i.e. a reflection boundary).

The reactive transport formulation is presented in detail in Lichtner and Karra (2014) and Iraola et al. (2019) and is based on the canonical formulation provided by e.g. Steefel and MacQuarrie (1996) and Steefel et al. (2005), which expresses the mass balance equation in terms of a set of basis components. The basis component set is defined as the minimum set of chemical species that can be used to mathematically describe the composition of all other species in a chemical system. Components are fundamental quantities used to represent the chemical composition of a system. They are defined as a linear combination of chemical species, which forms a basis for describing all other species in the system. The component set is the minimum number of independent variables needed to account for the entire system composition through aqueous reactions defined by the mass action law. Separate terms are used to relate mineral and aqueous kinetic rates together with mass balances for the conservation of mass in the system defined in terms of the basis components. The mass balances in the primary and secondary continua are related by flux terms which define the mass exchange between fracture and matrix to establish continuity of species concentration across the fracture-matrix interface.

The reactive transport formulation for multiple continuum systems is also described in Lichtner and Karra (2014) and Iraola et al. (2019). The formulation is based on the canonical approach presented in e.g. Steefel and MacQuarrie (1996) and Steefel et al. (2005), which expresses the mass balance equation in terms of a set of components (i.e. linear combinations of chemical species). Coupled mass balance equations for both the fracture and matrix continua, including geochemical reactions, are formulated using these defined components. At the fracture-matrix interface, continuity of component concentration is enforced, while a standard no mass flux condition is applied at the matrix outlet. More recently, Trinchero et al. (2022) incorporated the Nerst-Planck equation into this model and demonstrated that, by leveraging the Donnan equilibrium approach, anion exclusion processes can be effectively simulated within this modelling framework.

3.5.3 DFN models for reactive transport

Despite significant advances during the last ten years (see e.g. the coupling between PHREEQC and ConnectFlow, Joyce et al. 2015a), the incorporation of large-scale multi-component reactive transport models explicitly in native DFN models remains very challenging and often unfeasible. Generating a mesh representing a large-scale DFN made up of hundreds of thousands of fractures of different size is a formidable challenge since a very careful refinement is needed to discretise incredibly complex fracture intersections. If a mass-conservation scheme is used, Voronoi-based meshing requires the adjustment of particularly complex intersections, with the drawback that it is often difficult to properly honour underlying constraints of fracture statistics. This approach also has evident limitations in terms of, e.g. the maximum number of computable fractures and range of fracture sizes.

If a finite-element scheme is used, larger DFNs can be discretised but the locally non-conservative numerical solution schemes can lead to mass balance errors that are amplified in the presence of non-linear geochemical reactions. Another aspect that is difficult to resolve is the treatment of the rock matrix, which is frequently a key component for simulation of chemical buffering processes. An explicit representation of the whole rock matrix would be problematic since it requires accommodating 2D mesh elements (representing fractures) embedded in a larger 3D mesh (representing the rock matrix), which significantly increases the model complexity. The use of a full dual-continuum approach, on the other hand, would leave unresolved the issue of how to discretise the matrix close to narrow fracture intersections.

Despite these challenging numerical and conceptual issues, considerable efforts have been made in recent years towards developing numerical tools able to accommodate geochemical reactions directly in explicitly defined DFN models. Three of these numerical tools (ConnectFlow, iCP and dfnWorks) are described more in detail in the section on modelling tools (Section 7.3).

3.6 Parameters for transport modelling

As clearly shown in the following chapters, activities that deal with derivations and further developments of parameters are central to the presented transport modelling methodology. The input parameters to the modelling are obtained from investigations performed within the Transport programme itself and from external sources. Transport parameters are used in radionuclide transport modelling and supporting modelling activities, and are also delivered to other disciplines within the site descriptive and safety assessment modelling (cf. Section 7.6).

Focusing primarily on the radionuclide transport modelling, input parameters can be subdivided into the following partly overlapping categories.

- Site investigation parameters. This category comprises the parameters that are measured in the site investigations of bedrock transport properties and then analysed and presented within the framework of the site descriptive modelling. These parameters quantify the retardation/retention properties of the rock matrix and other geological materials of potential significance for solute transport along flowpaths in fractures and deformation zones.
- Site-specific safety assessment parameters. These are the parameters that constitute the primary site-specific input to the radionuclide transport calculations in the safety assessment. The parameters are obtained from further analyses of site investigation parameters (e.g. for sorption essentially "extrapolations" to future hydrogeochemical conditions), which provide retardation parameters for the whole assessment period, and from groundwater flow modelling based on past, present and future hydrogeological site conditions, which provides flow-related transport parameters.
- Element- and nuclide-specific parameters. This category involves parameters that are not obtained from site investigations, but rather from generic databases available in the scientific literature or established by SKB or international organisations. Parameters included in this category are primarily those associated with radioactive decay. Basic diffusion parameters also belong here.

Model- and code-specific parameters. These parameters are specific to a certain
conceptualisation and/or simulation code. Examples include dispersion parameters and the
penetration depth for matrix diffusion (which to some extent are estimated based on site data).
Needs for parameters of this category could arise due to both model simplifications, e.g. a
simplified representation of mass transfer between matrix and flowing water, and increased
model complexity, e.g. addition of diffusion in stagnant water or elements of reactive transport
to the modelling.

Of these parameter categories, the remainder of this report mainly considers categories 1 and 2. These parameters can be specified in terms of two groups as described in the following:

- Parameters that characterise the retention/retardation properties of geological materials, here
 referred to as retardation parameters. These parameters quantify the diffusion and sorption
 properties of fresh (unaltered) and altered rock, fracture coatings and fracture-filling materials.
 - Effective diffusivity, D_e [L²T⁻¹].
 - Porosity, ϕ [-].
 - Sorption distribution coefficient, K_d [L³M⁻¹].

The retardation parameters are measured in the site investigations and then interpreted and associated with rock types and fracture types in the retardation model, which constitutes a major delivery from the site descriptive transport modelling. In the safety assessment modelling, the site-specific information is further analysed to obtain a delivery of parameters recommended for use in radionuclide transport calculations.

- Parameters that characterise solute transport along flowpaths in the fracture network and the
 conditions for mass exchange between the flowing groundwater in the fractures and the
 porewater in the rock matrix, here referred to as flow-related transport parameters. These
 parameters are obtained by means of particle tracking simulations in groundwater flow models.
 - Water travel time (or residence time), t_w [T].
 - F-parameter (also referred to as F-factor or transport resistance), F [TL⁻¹].

The flow-related parameters are modelled, site-specific parameters that quantify properties of flowpaths or streamtubes where advective transport takes place. These parameters are calculated in the safety assessment only, for different times during the assessment period, and constitute a key input to the radionuclide transport calculations.

The notation given in the list above is that commonly used by SKB and others in the context of radionuclide transport modelling. It is used throughout the present report, in some cases with additional symbols or indexes for clarity. Porosity is the only parameter for which the notation varies, also within SKB. Supporting parameters used in the various derivations and other equations in this report are defined where used. Concerning the flow-related parameters, it should be noted that t_w and F often are denoted as τ and β , respectively, in the scientific literature (especially in connection with Lagrangian modelling concepts). For the purposes of the discussion in the present report, these two notations are regarded as interchangeable.

The handling of transport parameters in connection with site investigations and site descriptive modelling is regulated by quality assurance procedures stated in method descriptions (MD) and activity plans (AP). A particularly important step in the data handling is that of approving a dataset for inclusion in the site database. The data to be used in safety assessment radionuclide transport modelling is selected by following a structured procedure (e.g. SKB TR-21-06, Section 2.3). The procedure and the resulting datasets are described in the "Data report" of each safety assessment (e.g. SKB TR-21-06 for PSAR SFK and SKB TR-23-10 for PSAR SFR).

4 Development of retardation models

4.1 Introduction

4.1.1 Background and applications

The retardation model describes, in a simplified manner, the capacity of the host rock to slow the advective transport of solutes being carried over long distances through flow bearing fractures. The retardation effect arises due to diffusive exchange between mobile and immobile water volumes coupled with storage in the immobile water and adsorption to mineral surfaces. Immobilisation of solutes can also occur as result of geochemical reactions including precipitation, surface precipitation, and solid solution formation, although these are not explicitly accounted for in the retardation model. The retardation model is the basis for both the site descriptive model and the safety analysis. The simplifications needed for the safety analysis are further described in Chapter 7.

The main rationale for not including these processes is that the sorbed concentration must be a monotonically increasing function of aqueous concentration. This is not generally possible for the family of precipitation-related processes as solid phase concentrations are not directly related to aqueous concentrations. An exception is made, however, for fracture coatings where exchange processes involving solid solutions can be approximately modelled using an isotherm-based approach provided the transported radionuclide is only present at trace concentrations. An overview of processes involved in the retardation model is given in sections 3.1–3.3 of the present report and in SKB TR-10-48 and SKB TR-14-05.

In this report the term "retardation model" is used as this type of model has customarily been used in conjunction with the modelling of transport and retardation of radionuclides escaping from the engineered barrier through the host rock. The presently discussed model, however, also serves various other scientific areas where the solute exchange capacity of the host rock is of interest. Some of the topic areas where the retardation model may find applications are:

- Geosphere radionuclide transport (including repository releases and naturally occurring radionuclides).
- Hydrogeochemistry (evolution of groundwater chemistry).
- Hydrogeology (salt mixing and density driven flow).
- Recharge transport (dilute waters and oxygen penetration).

Section 3.1 presents a view of fracture-adjacent rock as a layered structure with deposits of fracture minerals that coat the wall rock where the wall rock is divided into an alteration rim and a thick layer of underlying host rock. Crawford and Löfgren (2019) explored the impact of this kind of a three-layer retardation model on radionuclide transport, although with a primary focus on quantification of diffusive properties. Site-specific data from Forsmark were used as far as possible, although significant gaps were identified in the available input data. A similar three-layer retardation model was also applied in radionuclide transport calculations in support of the Finnish safety assessment TURVA-2012 (Posiva 2013a, b) and the forthcoming safety case for the operating licence application (SC-OLA; reports in preparation).

4.1.2 Conceptual understanding of the zonation of altered rock in the geosphere

The original concept for a retardation model comprised of multiple layers arose from a desire to more accurately model spatial variability both longitudinally along a transport path as well as orthogonally to the principal direction of advective transport (i.e. in the direction of diffusive uptake within the rock). The overarching idea is that by combining a sequence of different transport classes one can represent spatial variability in a statistical sense along a flowpath through the geosphere. Each transport class is intended to function as a building block in this scheme where different blocks can be combined to reflect local transport properties of the rock along a segmented flowpath. The concept of transport classes is elaborated more fully in Chapter 7.

While longitudinal variability is relatively straightforward to include in transport modelling, the inclusion of a layered rock matrix is more complex to implement in transport calculations. Modern safety assessment codes such as MARFA (Painter and Mancillas 2013, Painter et al. 2022) and FARFCOMP (SKB TR-19-06), however, can readily include both longitudinal variability and layered rock matrix representations in transport models.

A relatively simple multilayer rock matrix description is given by a three-layer representation where fracture coatings adjoin a hydrothermally or oxidatively altered zone of limited extent which overprints fresh rock. Here, a distinction is made between alteration which extends from a fracture surface into the rock matrix for only a short distance and more general metamorphic alteration which is more pervasive and is considered a unique rock type. When we speak of fresh rock in the geosphere at Forsmark and Laxemar, we therefore mean rock that is both non-oxidatively weathered and non-hydrothermally altered, although may or may not be metamorphic in character.

It is acknowledged that the view of fracture adjacent layered rock matrix is a simplification of a more disorganised reality. Although it is not feasible to model all possible rock matrix configurations at a detailed level, the relative incidence of different microstructural sub-types is worthwhile investigating as significant deviations from the ideal layered matrix configuration could have a non-negligible impact on modelled transport. The relative frequency of different alteration types (i.e. hydrothermal vs. low temperature chemical weathering) associated with the rim zone flanking flow bearing features should also be ascertained as the distinction could be important for formulation of different fracture types to be defined in the retardation model.

Here, judgement must be exercised concerning the level of detail that is necessary to model in transport calculations, particularly for statistically infrequent microstructures. The three-layer rock matrix representation was first formalised in the transport properties site descriptive model guidelines for evaluation and modelling (Berglund and Selroos 2004) as well as the strategy report for the use of laboratory methods in the site investigations programme for the transport properties of the rock (Widestrand et al. 2003). While the archetypal three-layer representation is a good foundation for defining different fracture types, the statistical representativity of this microstructure should be confirmed by more detailed examination of borehole logging and drill core data. This will require a statistical analysis of alteration types, thicknesses, symmetry, and orientations relative to modern flow bearing fractures.

The experience from the radionuclide retardation modelling in Crawford and Löfgren (2019) is that the altered layers can have large impacts on the retardation of key radionuclides in different modelling scenarios. Here, the duration and relative rate of the radionuclide release, the radionuclide half-life, the cumulative transport resistance (i.e. F-factor) and the stability of the flow field are all factors that have a strong impact on the relative role of the different layers in retarding radionuclide transport.

Assigning proportions of different fracture types is not completely straightforward, particularly if there are statistically significant fractions of the rock associated with more complex alteration microstructures than the simple three-layer concept. It is also possible for some parts of the geosphere to have simpler microstructural features. There are, for example, statistically significant regions of the geosphere where fracture coatings and hydrothermal alteration are essentially absent and where the fresh rock plays a more important role (cf. fracture type H in Figure 4-1, Section 4.2.2).

Within a single safety assessment scenario, the release of different nuclides ranges from short term pulse releases (e.g. the instant release fraction) to very long duration releases (e.g. the fuel dissolution release fraction). Key radionuclides in the safety assessment have half-lives of decades to millions of years (e.g. Crawford 2022). Groundwater flow may be relatively static, such as when the repository is submerged or inland, or highly variable during future glacial periods when the terminus of an advancing or retreating ice sheet spans the repository. Given this complexity, the retardation properties of fracture adjacent rock layers are likely to be important inputs for future safety assessments.

It is possible that too much weight was given to the undisturbed rock in the previous SR-Site safety assessment, as outlined in Haggerty (2012) and SSM (2013). The latter publication from the regulatory authorities also invited more detailed consideration of alteration layers as paraphrased here in English:

- SSM considers that SKB should produce an analysis of the effect of mineral alterations and
 fracture-filling minerals in the rock on matrix diffusion and retardation of radionuclides. The
 analysis should highlight both the processes and characteristics that could mean improved or
 deteriorated retardation relative to the base case where the undisturbed rock is considered.
- SSM considers that SKB should analyse the importance of reasonably probable variability of the rock diffusivity and its impact on radionuclide transport.

It is intended that greater focus will be given in the upcoming safety assessments to the retardation properties of the altered zone flanking flowpaths in the rock matrix. At present there is a lack of data to adequately quantify retardation processes in the altered zone to the same degree as in the undisturbed rock. This will need to be investigated further in the detailed site investigations with focused campaigns to reduce identified uncertainties.

4.2 Overview of existing retardation model

4.2.1 Rock types

In the earlier site descriptive modelling of Forsmark, the focus was on the most volumetrically significant geological rock domains (principally, RFM029 and the subordinate rock domain RFM045) within the local model as well as the target rock volume. A summary of the rock types included in the retardation model and their estimated proportions in the central geological rock domains is given in Table 4-1. A few of the minor rock types investigated in the laboratory programme have been excluded from the retardation model since they constitute less than 2 % of the rock types within RFM029 and RFM045 or are located in rock domains external to the present target area.

The principal rock types investigated in the transport laboratory programme and integrated in the retardation model were:

- 101057 (Granite to granodiorite, metamorphic, medium-grained); dominates strongly in the target volume.
- 101051 (Granodiorite, tonalite and granite, metamorphic, fine- to medium-grained); relatively frequent and regularly distributed.
- 101058 (Aplitic granite); occurs as dykes and minor bodies that are commonly discordant to ductile deformation in older rocks.
- 101061 (Pegmatite, pegmatitic granite); small amounts regularly distributed primarily as dykes and minor bodies.
- 102017 (Amphibolite); occurs as dykes and irregular intrusions.

It was assumed that the properties of flowpaths through the rock could be represented in a statistical sense by consideration of the proportions of different rock types comprising the geological rock domains without consideration of the possibility of preferential flowpaths involving specific rock types.

Table 4-1. Rock names and SKB codes for major and most common subordinate rock types found within rock domain RFM029 and RFM045. Approximate proportions (vol-%) for each rock type is also given for both rock domains (Crawford 2008, Table 4-1)

Rock name	SKB code	RFM029	RFM045
Granite to granodiorite, metamorphic, medium-grained	101057	73.6	18.0
Pegmatite, pegmatitic granite	101061	13.3	13.9
Granite, granodiorite and tonalite, metamorphic, fine- to medium-grained	101051	4.6	9.0
Granite, metamorphic, aplitic	101058	1.2	49.3
Amphibolite	102017	4.4	6.3
Granite, fine- to medium-grained	111058	1.5	1.3
Felsic to intermediate volcanic rock, metamorphic	103076	0.4	1.2
Calc-silicate rock (skarn)	108019	0.3	0.2
Quartz-dominated hydrothermal vein/segregation	8021	0.2	0.2
Diorite, quartz diorite and gabbro, metamorphic	101033	0.2	0.2

4.2.2 Fracture types

Although not ultimately used quantitatively in SR-Site, a relatively detailed account of fracture coatings was given in the site descriptive modelling (e.g. Byegård et al. 2008, Selnert et al. 2009a). For the Forsmark site, retardation models were constructed for eight different fracture types, labelled A to H based on the identity of fracture coating minerals as shown in Figure 4-1. These were intended to represent the most common identified open fractures at the Forsmark site.

The fracture coating thickness was specified to be in the range of 0 to 5 mm for the most common fracture types (see Table 4-2). Each fracture type also had a brief qualitative description of wall rock alteration and an approximate thickness given for the alteration rim, which was specified to be in the range 0 to 5 cm. The fracture coating thickness specified for some of the fracture types in Table 4-2 are large compared to the results of an analysis from drill core mapping of the fracture minerals presented in Löfgren and Sidborn (2010). As discussed further in Section 5.1.4, an average fracture coating thickness of 0.1 mm is currently thought to be reasonable for both the Forsmark and Laxemar sites.

The fracture types specified in Figure 4-1 and Table 4-2 and the other components of the SDM-Site retardation model were developed in a process where the selection of geological materials for laboratory measurements of transport parameters was done in parallel with the identification and successive refinement of the model component descriptions (Byegård et al. 2008). Since sorption and through-diffusion experiments are quite time-consuming, it was necessary to collect most samples during the initial stages of the site investigations based on early versions of the geological site models. For forthcoming complementary site investigations, if needed, fracture types from existing retardation models and well-developed supporting site descriptive models are available to guide early sampling for transport investigations, thereby enabling an improved overall investigation and modelling process.



Figure 4-1. Typical fracture surfaces of Forsmark drill core samples. Mineral abbreviations are as follows: chlorite (Chl), calcite (Ca), epidote (Ep), hematite (Hm), laumontite (Lau), prehnite (Pr), pyrite (Py), quartz (Qz). Reproduced from Crawford and Löfgren (2019, Figure 4-3).

As noted by Byegård et al. (2008), the distribution of fracture types is most significant for open fractures that are water transmissive, termed PFL-fractures. Here, the term "PFL" denotes the Posiva Flow Log, the tool for detecting flow anomalies in the site investigation boreholes. In the investigations providing input to SDM-Site, flow anomaly locations could be identified with a precision of a few decimetres. When multiple fractures were in this depth range, the most likely water-conducting one was selected based on drill core mapping. In some cases, multiple fractures were chosen which may or may not represent a more complex flow feature than a simple flow bearing fracture. Both open and partly open fractures were typically considered when making this determination (Forssman et al. 2006, Follin et al. 2007).

The distribution of fracture types associated with PFL-fractures at various elevations, both inside and outside deterministic deformation zones, is shown in Figure 4-2. This figure gives the proportion of PFL-fractures linked to different fracture types A-H in 10 m elevation intervals. Since the frequency of transmissive fractures decreases significantly with depth, many of the deeper intervals are associated with very few, or no PFL-anomalies. The statistical basis for fracture type proportions at depth intervals greater than about 400 m should therefore be considered uncertain.

Table 4-2. Thicknesses of fracture coating and alteration rim of fracture types A-H for Forsmark. Data from Byegård et al. (2008, Table 2-3)

Fracture type	Α	В	С	D	E	F	G	Н
Coating thickness (mm)	≤ 0.5	~1	≤ 0.5	≤ 0.5	0.1–2	0.1–2	1–5	0
Alteration rim thickness (mm)	0	~10	5	0	10–50	0	≥50	0

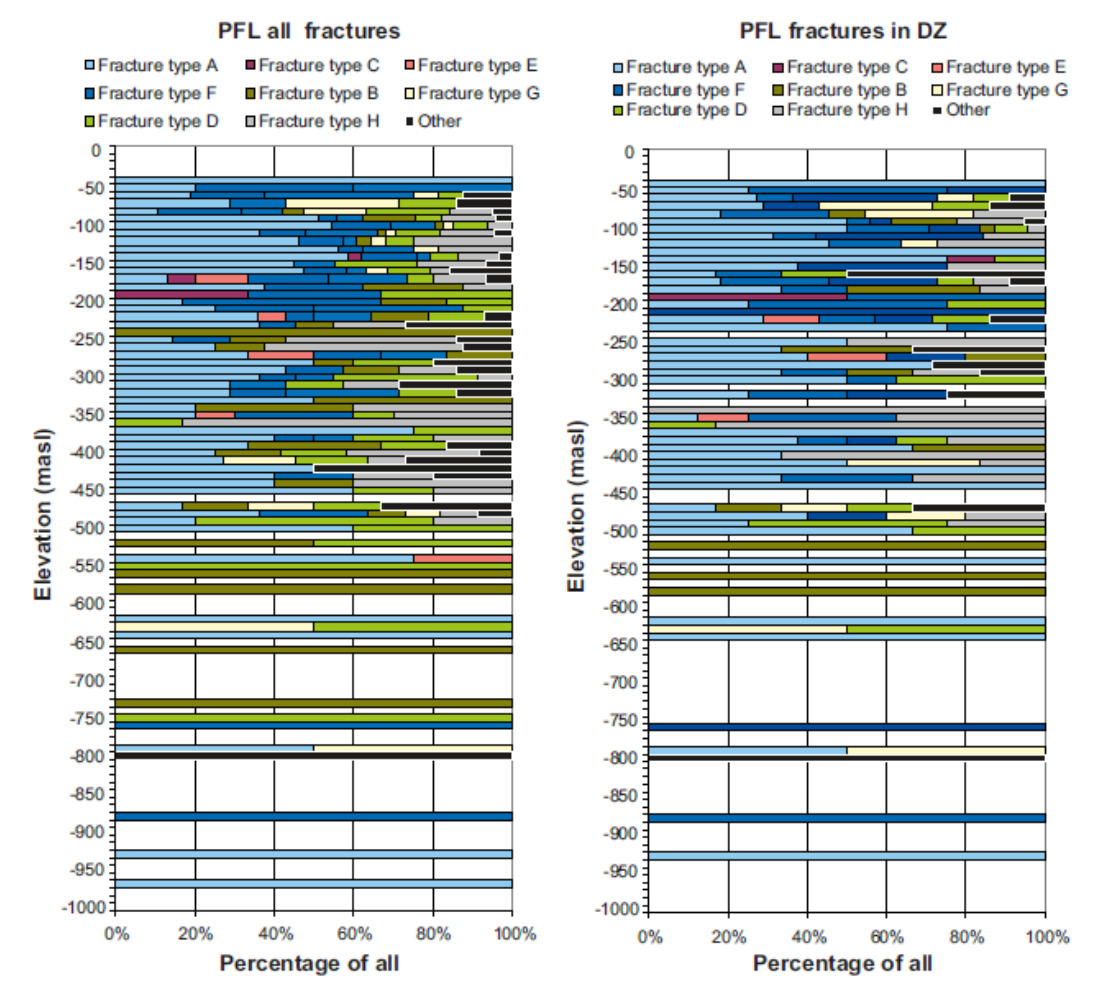
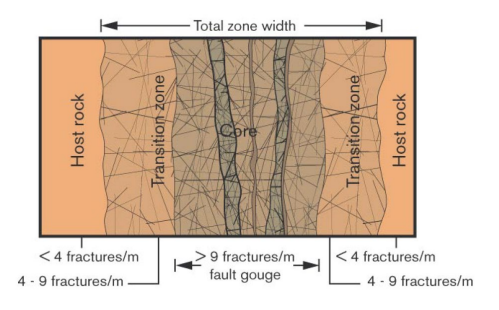


Figure 4-2. Percentages of open and transmissive PFL-fractures that were assigned to fracture types A-H (or others) per 10 m elevation interval, within deformation zones (right) and for the entire rock volume at Forsmark (left). Reproduced from Byegård et al. (2008, Figure 2-13).

In the definitions given in Byegård et al. (2008), there was no association between fracture types and different rock types and the classification was based on identified fracture minerals. This implies that different site-specific rock types could be assigned randomly to the undisturbed rock layer for the rock types in the retardation model produced for SDM-Site. Furthermore, the type of alteration was not specified in detail beyond a yes/no indication of its existence and approximate maximum thickness. It is noted that an alteration zone was assessed as being absent from fracture types A, D, F, and H and only associated with fracture types B, C, E, and G.

4.2.3 Deformation zones

In Byegård et al. (2008), some illustrative examples were given for how deformation zones (DZ) and associated microstructural units might be included in a site-specific transport retardation model. While acknowledging that it was difficult to parameterise deformation zones on account of their intrinsic complexity, a basic organising principle was an underlying assumption of brittle deformation giving rise to a transition zone of relatively high hydraulic transmissivity and a non-transmissive core zone as illustrated in Figure 4-3A. Based on this premise, three possible transport modelling representations of increasing complexity were developed as shown in Figure 4-3B.



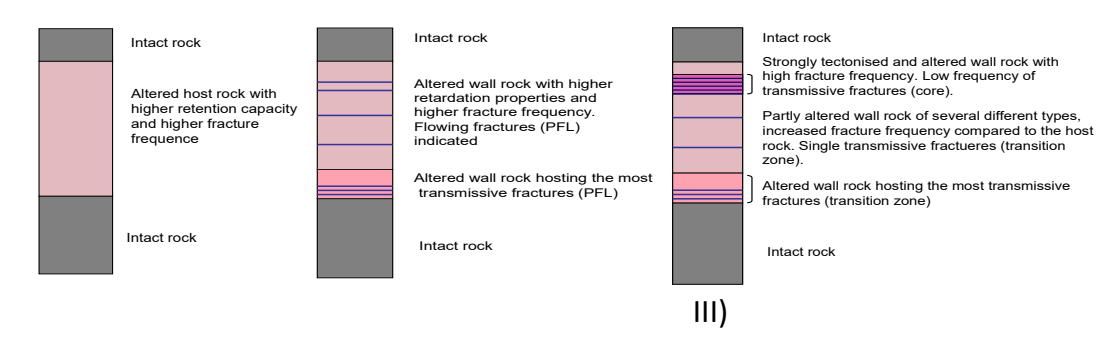


Figure 4-3. Basic organising principle for creating a transport retardation model for deformation zones (DZ), consisting of: A) schematic illustration of a brittle deformation zone according to SKB definition (after Munier et al. 2003); B) alternative descriptions of deformation zone structures (taken from Byegård et al. 2008) consisting of I) a single zone with higher fracture frequency and retardation capacity than surrounding rock, II) a zone divided into high- and low-transmissive units, and III) a variation including an explicitly defined core zone as well as high- and low-transmissive units.

In the simplest version shown in Figure 4-3B(I), it was proposed that DZ-specific retardation properties could be ascribed to the whole zone in an average sense recognising simply that the zone would be associated with flowpaths featuring higher transmissivity than the surrounding non-DZ rock and where the wall rock would have enhanced retardation characteristics relative to the previously defined fractures belonging to the sparsely fractured rock (cf. Table 4-2). A slightly more sophisticated model alternative shown in Figure 4-3B(II) was based on the notion of dividing the deformation zone into high transmissive and low transmissive units with different retardation properties assigned to the different units. The most complex model representation shown in Figure 4-3B(III) additionally considered the possibility of core and transition zones.

While the model variants shown in Figure 4-3B depict some possible approaches to establishing a retardation model for deformation zones, no guidance or recommendation was given in Byegård et al. (2008) for how this should be carried out in a practical sense. An implicit assumption in the proposal was that the transmissive regions of deformation zones could be populated with fracture types corresponding roughly to those defined for the sparsely fracture rock, although hosted in rock with more pervasive alteration.

Four different structural elements were identified as being typically recurrent features of the deformation zone host rock. These are given in Table 4-3 and include materials which are commonly abundant in deformation zones as well as those that were deemed less common, although potentially contributing to the total retardation capacity of the deformation zones in a non-negligible fashion. The identification of these units was based on macroscopic observations of altered parts of the drilled rock cores during the initial phase of the rock sampling for the laboratory programme. In the previous description of deformation zones these structural elements were hypothesised as occurring individually or together within a deformation zone.

A feature that is unique to deformation zones that typically is not found in sparsely fractured rock is the presence of cataclasite or mylonite zones of alteration which may or may not be found adjacently to hydrothermally altered wall rock. Both are metamorphic, being formed under conditions of intense pressure and deformation at elevated temperatures, although they differ in their formation process and resultant textures.

Mylonite is formed through ductile shearing, prior to uplift where temperatures and pressures are high enough for rocks to deform in a plastic manner without fracturing. It is characterised by a well-developed foliation, often exhibiting a banded or streaked appearance with alignment of the long axes of mineral crystals in the direction of deformation. Mineral grains in mylonite are usually recrystallised and of smaller grain size than in the original rock. Mylonite zones are usually associated with large faults that have been subjected to significant tectonic movement.

Cataclasite, on the other hand, forms through brittle deformation typically at shallower depths relative to mylonite. In this process, the rock is intensely fractured and crushed since temperatures are not high enough for plastic deformation. The rock consists of broken fragments of the original rock and fine-grained material cemented together by hydrothermally formed secondary minerals. Cataclasite does not typically exhibit a strong foliation, and its texture is more disordered.

Both materials may occur in deformation zones, although cataclasite is generally associated with shallower near-surface faults where brittle deformation is dominant and typically forms a part of the fault core, i.e. the central part of the fault filled with crushed rock material as indicated in Figure 4-3.

Table 4-3. Main identified structural elements residing in deformation zones that have been included in the retardation model. The estimated occurrences given in the table are subjective judgements by Byegård et al. (2008) and were not based on rigorous statistical analysis

Strongly altered (tectonised and partly incohesive) wall rock described in the report as "fault rock". Altered rock fragments with varied mineralogy dependent on host rock. Chlorite, saussurite and clay are generally present. Estimated occurrence: sparsely occurring



Sealed fracture networks mainly consisting of breccia and cataclasite. Different fracture fillings such as laumontite + calcite, epidote, chlorite.

Estimated occurrence: relatively common



Quartz dissoluted rock (vuggy rock).
 Estimated occurrence: sparsely occurring



Oxidised wall rock (mainly medium or strong degree of 4) alteration).

Estimated occurrence: relatively common



4.3 Updated methodology and retardation model

The steps involved in developing an updated methodology for the retardation model are shown in Figure 4-4 and explained in the following paragraphs. The development of an updated retardation model in the continued site investigations will build in part on the previously existing model developed in SDM-Site described above and the analyses presented in Crawford and Löfgren (2019). As a first step, the existing models should be evaluated in the context of relevant newly acquired data. An attempt should be made to assess the availability and sufficiency of the various inputs which might be needed to improve or update the models. This information can then be used to guide updated activity planning for the laboratory and field programme. Using detailed borehole maps and BIPS images, a database of identified flow-bearing fractures at different depths should be created to obtain a statistical basis for identification of typical fracture types and deformation zone structures. In addition, information on sealed fractures should be included since these may be reactivated in the future.

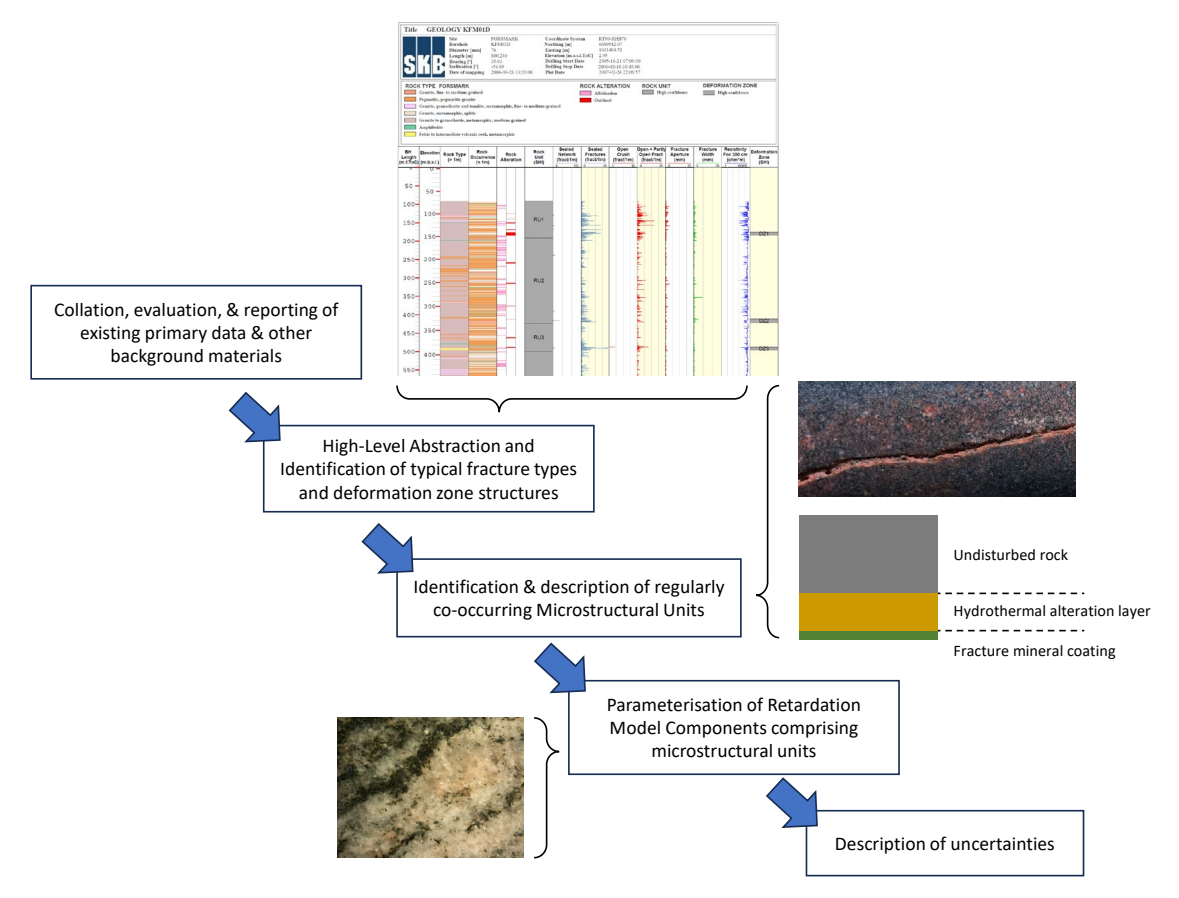


Figure 4-4. Proposed methodology for development of the updated site-specific, transport retardation model.

In this report, retardation components are defined as the various distinct geological material types which comprise the retardation model. At a higher level of abstraction, different identified fracture types and deformation zone structures are constructed from combinations of one, or more microstructural units. A microstructural unit represents a cohesive assembly of closely interconnected retardation components, exhibiting collective attributes and functions within identified fracture types and deformation zone structures. These constitute the foundational building blocks from which varied and complex fracture types are constructed, featuring potential correlations between material property parameters of their constitutive elements.

At its very simplest, a given fracture type may consist of a single microstructural unit reflected symmetrically in the fracture plane. In more complicated settings, it may consist of two different microstructural units featuring differentiated fracture mineral coatings and non-symmetrical alteration. Deformation zones may consist of several microstructural units spread across multiple, closely spaced flow-bearing fractures. If there are significant stagnant zones flanking flow channels of high aspect-ratio, the inclusion of additional microstructural units may be justified. In highly

channelised flow situations, such as in flow channels potentially forming at enlarged intersections of open fractures, the standard linear model of matrix diffusive uptake underestimates retardation and models of radial diffusive uptake to the rock matrix may be more appropriate (Neretnieks 2023).

When evaluating borehole maps and associated data, consideration should be given to possible deviations from the previous fracture type definitions established in Byegård et al. (2008). The premise of using fracture mineral identity as the main determinant of fracture type classification should be re-examined in the context of the analysis in Crawford and Löfgren (2019) and updated data concerning microstructural and material properties of the undisturbed wall rock and alteration layers which overprint it.

Based on the spatial distribution of fracture types and deformation zone structures in the geosphere, consideration should be given to the need for defining separate transport domains and whether such partitions are statistically justified. Consideration should also be given to which quantitative measures should be used to describe frequencies of fracture types, occurrence of different fracture minerals, etc. given that borehole intersections represent point samples of a continuously variable property set.

In the final step of retardation model abstraction, parameter values are linked to the retardation model components while acknowledging and allowing for potential material property correlations between different microstructural units. Here, further consideration will need to be given concerning in what form model parameters will be delivered, remaining issues of upscaling, and how gaps in the quantitative database are managed. Depending on the outcomes of the lab and field program, this may require iteration between the specification of low-level retardation model components, and how microstructural units are defined and organised in the context of identified fracture types and deformation zone structures.

For geosphere transport calculations, it is envisaged that various predefined fracture types can be assigned to different flowpath segments to capture the spatial variability of transport properties related to both local variations in the background geology, hydrothermal alteration, and deposits of fracture minerals. The retardation model is the resultant sequence of segmented fracture types representing the spatially variable transport properties of the aggregate flowpath.

The building blocks of the proposed retardation model are both large-scale and small-scale. Large-scale building blocks represent significant volumes of the host rock, through which flowpaths intersect on their way from the engineered barrier to the surface system, or vice versa. In this report, the term "transport domains" is used to denote these large-scale building blocks. Transport domains are in turn comprised of different proportions of fracture types that are statistically representative for the rock volume under consideration. The fracture types themselves are composed in turn of "retardation components" which are defined separately and have material properties corresponding to those measured for identified microstructural elements in the rock (e.g. a specified rock type, rock with a specified alteration type, fracture mineralisation, sealed fracture networks, crush, breccia, etc.).

4.3.1 Transport domains

In the proposed retardation model, the geosphere is partitioned into transport domains where different fracture types are combined in a statistically representative manner to describe the retardation properties of the rock for transport of groundwater solutes including radionuclides. Figure 4-5 gives an overview of potential transport domains which could be included in the retardation model. These are briefly described in the following sub-sections.

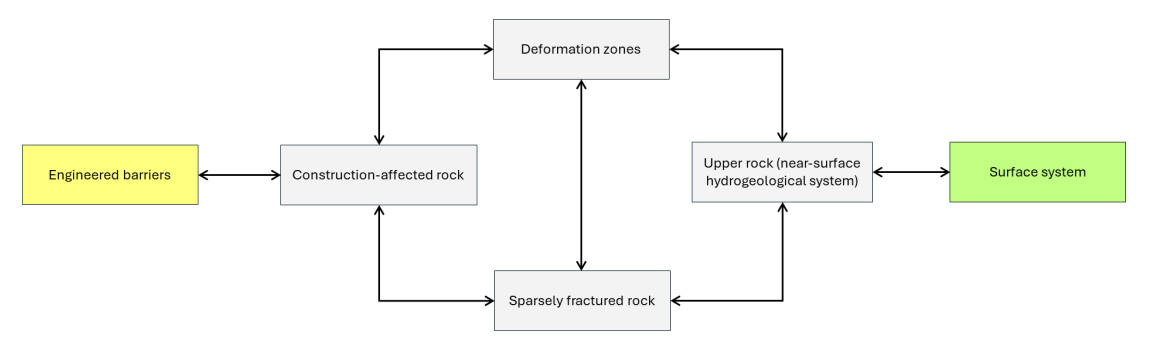


Figure 4-5. Overview of possible transport domains of the retardation model. In the present concept, the engineered barriers and surface system are not considered to be part of the retardation model. The arrows represent a case of solute transport along a discharge path. The bi-directional arrows indicate the possibility of solute transport along both discharge and recharge paths.

Deposition hole and other construction affected rock

This is the rock volume immediately surrounding the deposition holes and is the first to encounter radionuclides emanating from a canister breach. It also includes the rock volume immediately surrounding excavated tunnels and other engineered barriers and is representative of the rock surrounding the excavated vaults comprising the SFR and SFL repositories.

For deposition holes, this rock volume is on the same scale as the deposition hole and occasionally connects to the wider network of sparsely fractured rock. Owing to the design criteria for deposition hole acceptance, it is deemed unlikely for this rock to be directly connected to larger deformation zones. The acceptance criteria, however, do permit the partial intersection of deposition holes with fractures featuring low flow rates (e.g. SKB R-07-33, SKB TR-09-22). The deposition hole wall rock may be associated with mechanical damage in the form of a limited zone of increased small-scale fracturing (the so-called excavation damaged zone, EDZ) and minor spalling which differentiates it from undisturbed rock.

It is clear from the acceptance criteria that there may be deposition hole intersecting fractures which could reasonably be classed as being part of the sparsely fracture rock transport domain. These fractures, however, are a subset of those in the sparsely fractured rock since only fractures of very low transmissivity are permitted. If there are differences in retardation properties of fractures dependent on transmissivity, then these may need to be handled separately to the sparsely fractured rock domain. The EDZ surrounding excavated tunnels and rock vaults comprising the SFR and SFL repositories shares many similarities to the deposition hole rock, although the extent and intensity of excavation damage as well as the size and transmissivity of intersecting pre-existing fractures will differ due to differing acceptance criteria.

In general, it is expected that the EDZ should have material properties approximately representative of fresh rock since the excavation primarily occurs in fresh rock. Here, it is expected that alteration rims and fracture coatings will be mostly absent as most fractures will be newly formed. Due to the increased intensity of fracturing, however, the expected depth of matrix penetration may be very short depending on the frequency of flow bearing fractures (reflected in the increased permeability of the rock). If there is a very high intensity of diffusive microcracks in the rock and the matrix penetration depth is short, it may be permissible to model radionuclide transport using an equilibrium retardation approximation. How this is to be handled in the safety assessment modelling will need to be discussed in the context of how the EDZ is modelled in the hydrogeology site description so that the handling is consistent between disciplines.

Sparsely fractured rock

In this transport domain the rock matrix is intersected by discrete open, or partly open fractures. The sparsely fractured rock is characterised by a low intensity of transmissive fractures and, overall, a very low groundwater flow. This assures that flowpaths that transect this domain have large transport resistances relative to path length (see Section 3.2.2). It is envisaged that the rock matrix surrounding these flowpaths would have a low degree of hydrothermal alteration and brittle deformation. The sparsely fractured rock domain is presumed to be occasionally intersected by deformation zones and situated beneath the upper rock volume. Sparsely fractured rock also surrounds the backfilled underground openings of the repository.

Deformation zones

The host rock is intersected by deformation zones of different sizes. This is illustrated in Figure 4-6 where zones transecting the horizontal plane at repository depth at Forsmark are shown. From a hydrogeological point of view, it is the part of the deformation zone that has undergone brittle deformation that is of the greatest importance. In brittle deformation zones there is an increased intensity of open, or partly open fracture planes with greater transmissivity relative to the sparsely fractured rock. For many deformation zones, the core has been subjected to ductile deformation while brittle fracturing frequently has a higher intensity at their outer margins.

Rock that has undergone significant ductile deformation, although with little brittle deformation, is not necessarily part of this transport domain and may instead be considered as part of the sparsely fractured rock. Larger fracture zones may also be associated with crush zones in addition to discrete fractures. In crush zones, the fracturing is sufficiently intense that water flow can be envisioned to occur in a continuous porous medium that resembles very closely packed gravel. For discrete fractures in this transport domain, the surrounding rock matrix has often a higher degree of chemical alteration and is often subjected to a higher degree of brittle micro fracturing than the sparsely fractured rock.

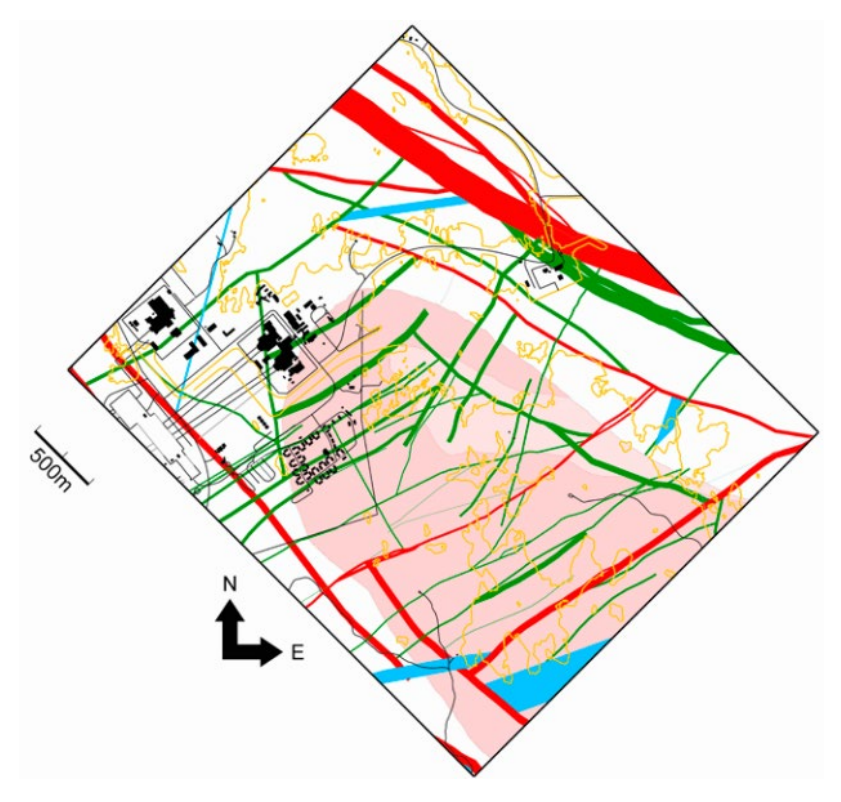


Figure 4-6. Two-dimensional model for deformation zones at -470 m elevation inside the local block model of the Forsmark site. Zones marked in red are vertical or steeply dipping and have a trace length at the surface longer than 3,000 m. Zones marked in green are vertical or steeply dipping and are less than 3,000 m in length. Zones marked in blue are gently dipping to the south and southeast. The shaded pinkish areas indicate rock domains. Reproduced from (Stephens and Simeonov 2015, Figure 5-3).

Upper rock

At the local Forsmark site, the uppermost part of the bedrock is heterogeneously intersected by horizontal sheet joints in addition to fractures and fracture zones. These are essentially giant horizontal flow-bearing features characterised by high transmissivity and large transport apertures. The report by Follin et al. (2007) gives a tentative estimation for the maximum depth occurrence of these features to be in the range of 100–150 m. More recent work described in Hartley et al. (2021) generally confirms the previous work, although constrains the depth occurrence of the main conductive features to be in the upper 30 m of the bedrock with a sparser occurrence of highly transmissive features at greater depths.

The sheet joints have a high intensity of horizontal or sub-horizontal fractures originating from the loading and unloading of ice sheets during repeated glaciations. The transmissivity of the sheet joints is high compared to fractures and fracture zones at greater depth, a difference that is very evident within the tectonic lens at Forsmark. Due to their geologically recent formation, the sheet joints either lack substantial fracture coatings or predominantly contain generation 4 minerals (clay minerals and calcite). The sheet joints are also considered to contain relatively large amounts of glacial sediments which partly accounts for their large hydraulic apertures.

4.3.2 Retardation components comprising microstructural units

Within a transport domain, the flowpath and its surroundings can be modelled to consist of different small-scale building blocks. As discussed previously, the flowpath is modelled in a segmented fashion where each segment is assigned individualised hydrodynamic transport properties and is associated with storage compartments that can be accessed only diffusively. In the present proposal six types of storage compartments are defined as the small-scale building blocks of the retardation model as shown in Figure 4-7. In the present work, these small-scale building blocks are referred to as "components" of the retardation model. The retardation components are summarised below.

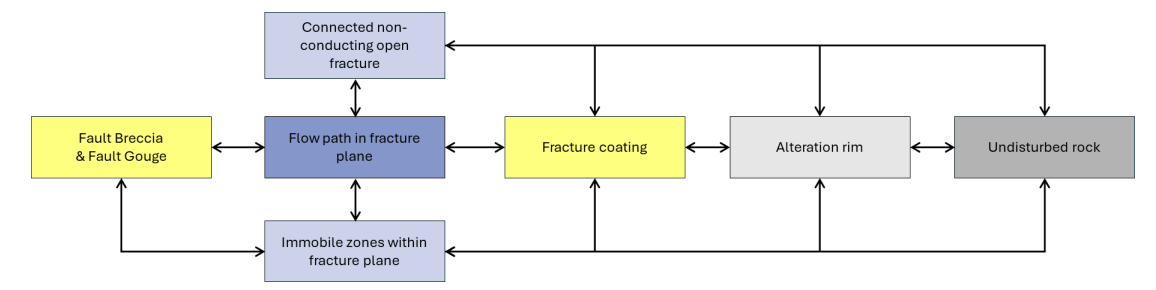


Figure 4-7. Overview of retardation components of the retardation model. Arrows indicate mass transfer connectivity via diffusive exchange.

Immobile zones within the fracture plane

The fracture plane may feature zones of effectively stagnant water which are accessible predominantly by diffusion. Here, it is acknowledged that open parts of transmissive fractures can never be truly stagnant if there is a hydraulic gradient however small this may be. Examples of effectively stagnant zones might be where the fracture aperture is locally very small, or where the fracture plane features a dead-end branch.

A non-negligible fraction of surface area contact is expected for most non-dilating fracture types due to the need to counteract the normal pressure across the fracture surface (e.g. Ogilvie et al. 2006). Contacting asperities are deformed, or more usually crushed until stress equilibrium is reached and contacting surfaces may even become welded due to pressure solution formation of secondary minerals. Depending on the fraction of contacting surface, substantial parts of the remaining open flow-wetted surface may be effectively inaccessible to flow due to poor hydraulic connectivity with flow entry and exit points in the fracture, as well as low hydraulic gradients associated with surface concave areas of significant aperture in the case of flanking dead-end zones (see, e.g. Crawford 2008, Appendix B).

Fault gouge and breccia

The fracture that hosts the flowpath may contain porous fracture infill such as fault gouge materials and larger breccia pieces. Here, we consider incohesive materials that are physically separate from mineral coatings associated with fracture surfaces. These non-cohesive materials may feature sufficient intraparticle porosity that they may be more accurately described as a porous bed in transport modelling. Small gouge particles and loose clay minerals may be modelled as equilibrium storage capacity similarly to fracture coatings while larger cm to dm-sized breccia pieces in flowpaths featuring low range F-factors may be more accurately modelled using a matrix diffusive description (i.e. an altered rock matrix of limited extent). If sufficiently large, the flow spaces surrounding such pieces might be considered separate sub-parallel flowpaths with explicitly defined hydrogeological properties. In most cases, however, it might be reasonably assumed that breccia pieces can be treated as equilibrium storage capacities.

Connected non-conducting open fractures

The fracture hosting the flowpath may be intersected by numerous open fractures that contain stagnant or near-stagnant groundwater (see Figure 4-8). In fact, the tectonic continuum hypothesis where fracture intensity versus size is described by a single power law implies the existence of a great number of such fractures below the minimum length of flow bearing fracture considered in hydrogeological DFN models (e.g. Follin 2008). Dissolved solutes, colloids, and macromolecules advectively transported in the flowpath may access these intersecting fractures by diffusion where they may subsequently sorb on mineral surfaces of the intersecting fractures.

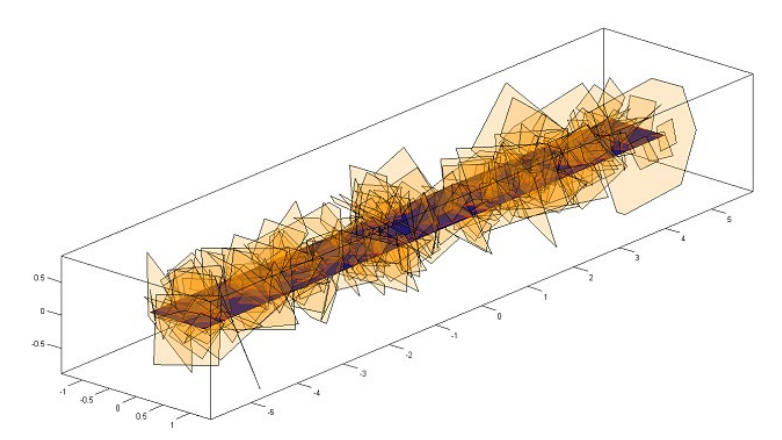


Figure 4-8. Visualisation of potential non-conducting open fractures (orange polygons) that intersect a rectangular flow channel hosted in a fracture assuming an isotropic intensity of open fractures below the minimum fracture size included in the SDM-Site hydrogeological DFN (dark blue rectangular polygon). Reproduced from Crawford (2008, Appendix I).

Small solutes might also access the adjacent wall rock. In the DarcyTools code, mass transfer processes involving such features are referred to as "subgrid" processes (Svensson et al. 2010). This additional diffusively accessible wetted surface was conservatively neglected in SR-Site for radionuclide transport calculations since it is difficult to avoid double counting matrix storage capacity where matrix diffusion simultaneously occurs from the main advective flow channel into the wall rock. The presence of such fractures, however, was used to justify the use of a higher effective diffusivity of salt² used in hydrogeological modelling (SKB TR-10-52, Appendix A).

Fracture coating

This is the retardation component directly adjacent to the fracture plane that consists of a very thin layer, or multiple thin layers of fracture minerals deposited in different generations. It has been observed in drill core mapping studies (exemplified in Figure 4-9) that fracture mineral layers do not generally coat the fracture surface to a uniform thickness (e.g. Eklund and Mattsson 2009). More typically, the fracture coating is made up of a patchwork of different generations of fracture minerals of varying thickness and a significant part of the fracture surface is observed to remain uncoated. Non-cohesive fracture infill and fault gouge materials are not included in the statistics of fracture coatings (e.g. Löfgren and Sidborn 2010) although are considered separately as part of the storage capacity within flow bearing and stagnant-water fractures typically found in deformation zones (see, previous description of fault gouge and breccia).

SKB R-20-17 68

٠

² The Na⁺/Cl⁻ ion pair which is used as a calculation basis for density dependent flow in hydrogeological modelling.

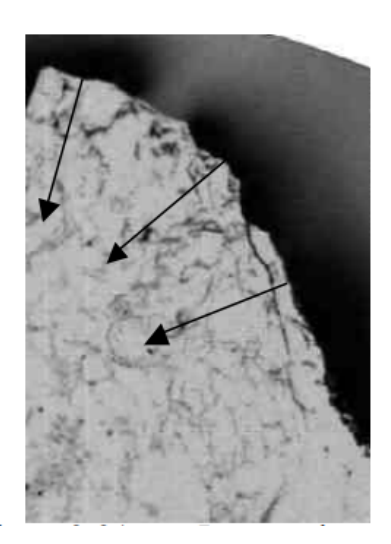


Figure 4-9. Left: Drill core sample from Laxemar intersecting an open fracture with a visible patch of calcite. Right: The patch of calcite is highlighted after image segmentation analysis. Reproduced from Eklund and Mattsson (2008, Figure 4-1).

Alteration rim

Adjacent to the fracture coating, the rock matrix is often affected by hydrothermal alteration, chemical weathering, and brittle microfracturing. Berglund and Selroos (2004) referred to this zone as altered wall rock. The alteration intensity typically decreases, terminating at some distance from the fracture surface where the rock may be considered relatively undisturbed. As one moves closer to the fracture surface, the transport properties of the rock matrix increasingly deviate from the undisturbed rock. Microfracture intensity, for example, often increases near the fracture due to differential stresses at the fracture surfaces and stress release. The mineral composition also changes and primary minerals such as biotite may be altered to chlorite, while feldspar minerals may undergo sericitisation forming sericite mica minerals (muscovite and illite).

Dissolution, or alteration of primary minerals can increase local porosity (e.g. Möri et al. 2003, Penttinen et al. 2006), while precipitation of alteration products may decrease it or clog the microporous system (Siitari-Kauppi et al. 2010, Metcalfe et al. 2021). Oxidation of biotite producing Fe oxides may induce local differential strain which can lead to further microfracturing (Goodfellow et al. 2016). Microfractures may also heal, especially in quartz-rich rocks where fluid inclusion planes are observed (Anders et al. 2014). A small increase in porosity near the rock surface is shown in Figure 4-10, taken from the TRUE Block Scale site at the Äspö HRL (Kelokaski et al. 2001).



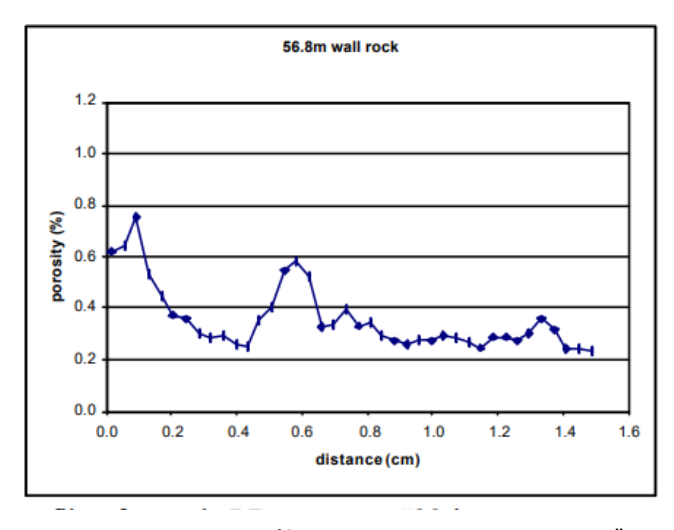


Figure 4-10. Left: Film autoradiograph of rock sample impregnated with ¹⁴C-PMMA from the TRUE site at Äspö HRL. Right: Porosity profile along the direction of the arrows in the autoradiograph, showing a slight increase in porosity in the proximity of the rock sample surface. Reproduced from Kelokaski et al. (2001, Figure 3-31).

Included in the definition of altered rock in the alteration rim adjacent to fractures are cataclasite and mylonite. Cataclasite consists of crushed and fragmented rock formed during brittle deformation which has subsequently become cemented in a matrix of smaller rock grains and secondary mineralisation to form a cohesive material. Mylonite, on the other hand, is formed at much greater depths at higher pressures and temperatures where the rock has deformed plastically during fault shear. Mylonite typically exhibits extensive foliation and anisotropy due to the alignment of elongated minerals. The grain size is typically very small, and the rock has a smooth, banded appearance relative to the more random structure of cataclasite.

Fresh rock

Beyond the alteration rim, the rock matrix is said to be undisturbed and referred to in SKB reports as fresh rock. In the context of the retardation model, the term fresh rock should be understood as unaffected by hydrothermal or weathering alteration from extant or previously flow bearing fractures. In the retardation model, this zone extends orthogonally from the fracture surface to a distance assumed to be equal to half the average distance to nearby flow bearing features.

If the rock is sparsely fractured, the average spacing between flow bearing fractures may be tens of metres. In more intensely fractured regions such as within deformation zones, flow bearing fractures may be only decimetres apart. Some transmissive fracture clusters may be so closely spaced that they may be modelled as a single transmissive feature. More pervasive ductile deformation and metamorphic alteration may affect the bulk rock, although it is considered fresh relative to fracture-associated alteration types.

The fresh rock is found both within deformation zones and outside deformation zones, although if fractures are sufficiently closely spaced, the rock in between may be solely comprised of altered rock. Considering how the retardation model will be used in subsequent transport modelling, it is practical to allow for local alteration associated with sealed fractures embedded in the undisturbed rock.

Some alteration types such as albitised and episyenitic rock (vuggy granite) may be sufficiently pervasive in parts of the geosphere that it makes sense to include them in the definition of fresh rock for transport modelling purposes. The dominant rock types at the Forsmark site are tabulated in Table 4-1. The table also gives the approximate volumetric proportions of each rock type for the most important rock domains at Forsmark. Importantly, a single rock type often spans over a broad range of mineralogical compositions. This can be exemplified with one of the most common rock types at Forsmark, "metamorphic, medium-grained granite to granodiorite" (101057). For this rock type the observed quartz content ranges from about 19 to 46 vol-% and the biotite content ranges from about 2 to 12 vol-% (Sandström and Stephens 2009, Table 3-7).

4.4 Parameterisation of building blocks

As discussed in Section 4.3.1, the geosphere can be divided into different transport domains that represent different rock volumes. Suggested domains, as visualised in Figure 4-5 are:

- Deposition hole and other excavation damaged rock, which constitutes the local volume of rock surrounding canister deposition holes, tunnels, shafts and other parts of the rock affected by excavation as well as rock vaults for the SFR/SFL repositories.
- *Upper rock*, which constitutes the upper bedrock volume.
- *Deformation zones*, which constitutes the volume of rock occupied by deterministically modelled deformation zones (cf. Figure 4-6).
- Sparsely fractured rock, which constitutes the entire host rock volume minus the above volumes.

The transport domain labelled sparsely fractured rock may be comprised of multiple volumes in the geosphere (i.e. geological rock domains) each composed of different volume fractions of the undisturbed ("fresh") rock types as defined in Table 4-1. These geological rock domains may be further subdivided into fracture domains (see Olofsson et al. 2007) and used as a basis for defining the hydrogeological model domains (e.g. Follin 2008).

Here, it is assumed that the various geological rock and fracture domains retain their identity in transport modelling and inherit material properties that are statistically representative of the rock and fracture domain subdivision being considered. Proportions of different transport classes defined in Chapter 7 then should reflect the local population of fracture types and their constituent microstructural units deemed to be present in each geological, hydrogeological and/or fracture domain.

4.4.1 Demarcation of transport domains

To achieve consistency amongst various sub-disciplines in site descriptive modelling, it is proposed that the boundaries of transport domains are defined in the same way that rock and fracture domains are defined and used in the geological and hydrogeological modelling. Transport flowpaths derived from particle tracking, however, are defined as one-dimensional pathline segments that traverse the transport domains.

In the following paragraphs, particular aspects of the hydrogeological modelling that are of relevance for how the retardation model is structured are highlighted. These considerations may be considered as general organising principles and separate to flowpaths and hydrodynamic properties that might be calculated later in site characterisation studies or in safety assessments.

The one-dimensional transport path segments are allocated to fractures resident in the hydrogeological modelling (cf. Section 3.2.2). Each flowpath segment has a start and an end point in the local model coordinate system and inherits hydrodynamic transport properties from the hydrogeological model. In the present modelling structure, inherited parameters include the "flow triplets" of equivalent flow rate, advective travel time, and F-factor (SKB TR-10-50, Joyce et al. 2010). If the entire segment cuts through the same transport domain, it can simply be allocated to that domain and take on material properties representative of that domain. If not, the segment can be proportionally divided into subsegments depending on the location of the segment relative to the defined boundaries of the transport domains that are intersected. At present it is assumed that the flow triplets can be simply proportioned between each subsegment in the same fashion.

4.4.2 Assigning retardation data to transport domains

After designating membership of individual flowpath segments to different transport domains it remains to assign retardation data to the rock comprising the retardation components used in transport modelling. Data exported from hydrogeological modelling already contains information concerning transport domain, rock-type, etc. and the task here is simply to ensure that the retardation model is compatible with these specifications. In the present discussion it is assumed that the wall rock flanking each flowpath segment is associated with three diffusive compartments corresponding to a three-layer representation of the rock matrix.

Each of the retardation components comprising the three-layer rock matrix are to be assigned point values for each of the primary transport retardation parameters. For each layer, j in the three-layer representation, this includes a quantitative estimate of the layer thickness (δ_j), transport porosity ($\phi_{\text{m}(j)}$), effective diffusivity ($D_{\text{e}(j)}$), and linear sorption partitioning coefficient ($K_{\text{d}(j)}$). Although not directly used in numerical models of transport, other supporting data associated with these parameters may be included in the site descriptive model. Such supporting data may include BET surface area, cation exchange capacity (CEC), mineralogy (volume fractions of constituent minerals), and redox properties (Mössbauer Fe(II)/Fe(III) ratios). These data are used to estimate and harmonise sorption properties in cases where quantitative K_d measurements are not available for specific elements and redox states.

The increased degree of complexity over the single layer rock matrix previously assumed in historical safety assessments does not only impact the safety assessment itself, but also the planning of complementary site investigations, and the way data should be supplied within the site descriptive modelling. In principle, the transport parameters can be assigned either deterministically for each retardation component or stochastically from pre-defined probability density functions depending on the statistical support for such a modelling decision.

Relationships between adjoining retardation components

There are several different organising principles that can be used in assigning retardation components to transport domains. The first approach is to use pre-defined microstructural units where the retardation components in each unit are fixed as illustrated in the upper image of Figure 4-11. Here, the microstructural units A, B, and C have fixed definitions although they may have material properties assigned from stochastic distributions. This means that fracture coating A, alteration rim A, and undisturbed rock type A always appear together in the definition of microstructural unit A. Likewise fracture coating B and C are always associated with the same alteration rim and undisturbed rock type. This may be considered a fully coupled approach as the properties of all three layers are fully specified in the definition of the named microstructural unit.

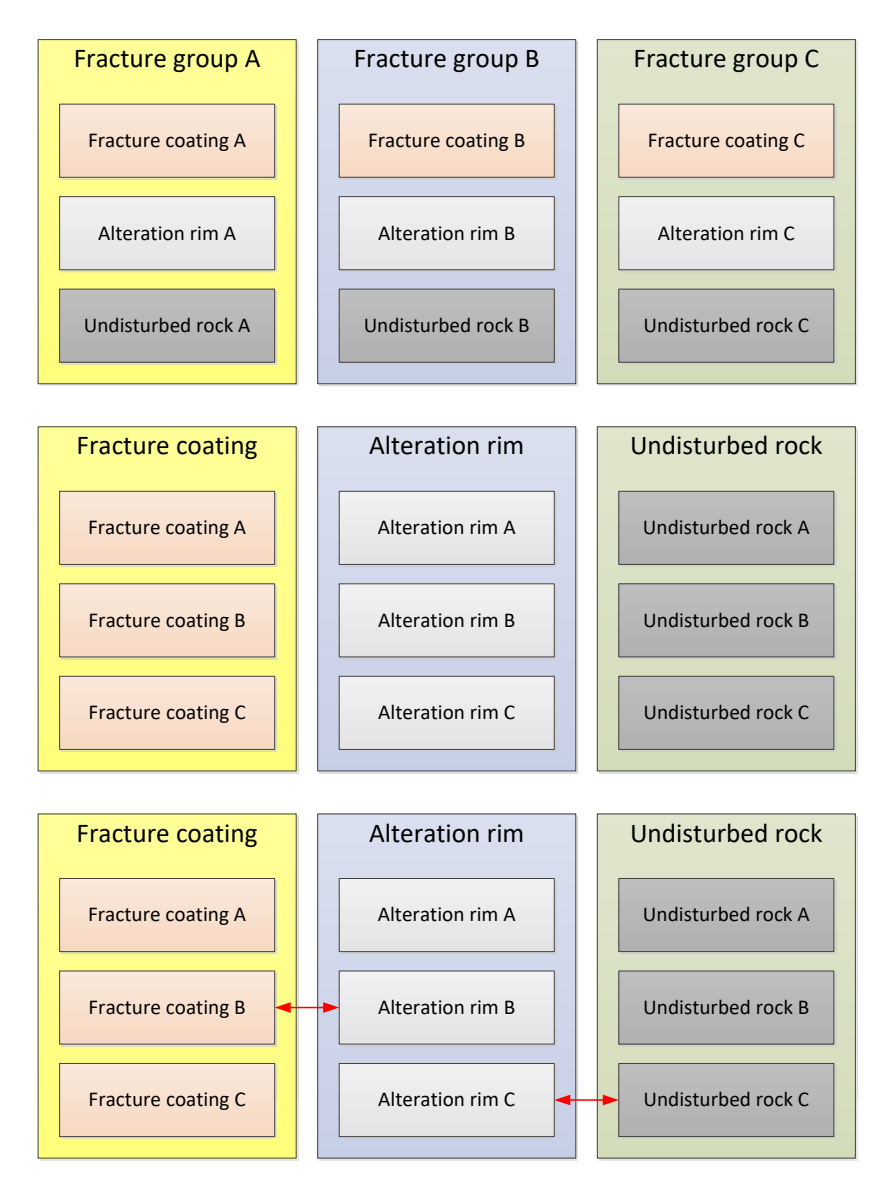


Figure 4-11. Organising principles for retardation components contained within microstructural units (termed "fracture groups" in the figure). Upper: fully coupled retardation components within microstructural units. Middle: fully decoupled retardation components. Lower: partly decoupled retardation components.

The second organising principle is to forgo named microstructural units and specify retardation components independently without specific relationships with other adjacent components. This is illustrated in the middle image of Figure 4-11. In this approach, microstructural units may be assembled by randomly combined fracture coating, alteration rim, and undisturbed rock type. This decoupled approach has more degrees of freedom than the fully coupled version since there are 27 different ways of combining the retardation components A, B and C.

A third possibility is the intermediate variant as shown in the lower image of Figure 4-11. Here the retardation components are partly decoupled as there may be associations between the different layers. In the case illustrated, fracture coating B and alteration layer B are related and always occur together while alteration layer C always coexists with undisturbed rock type C. There is some geological evidence from the site investigations that suggest that this is a reasonable assumption, particularly for associations between the altered rock and undisturbed rock. This is because the altered rock is, by definition, an altered form of the underlying undisturbed rock type.

In the site descriptive modelling work (Byegård et al. 2008) considerable effort was made to identify the defined fracture types A-H of Figure 4-1 and their relative frequency in different parts of the geosphere. Each fracture type was given a qualitative specification of the presence or absence of alteration and most likely range for its thickness. No correlation was specified between the identity of the fresh rock and the alteration layer.

Although material properties were only vaguely specified, this approach is in keeping with a fully coupled description for the fracture coating and altered rock components, while the relation between the undisturbed host rock and other retardation components was fully decoupled. Although guidance was not given in the site description, the available data at the time suggested only minor differences between the transport properties of the main rock types implying that the identified combinations of fracture coatings and altered rock could be combined freely with any undisturbed rock type. The available data in SDM-Site (Byegård et al. 2008) was sparse and heavily weighted towards samples of the volumetrically dominant metagranite rock type (101057), however, so it was difficult to motivate couplings between the alteration rim and undisturbed rock.

Based on the previous work, a partially decoupled modelling approach is proposed as a working hypothesis for developing a retardation model. This would consider:

- The possibility of correlated parameters across the three layers adjacent to the fracture. For example, if unaltered rock rich in biotite corresponds to an alteration rim rich in chloritized biotite, both layers might exhibit high K_d values for cation exchangers. Such correlations should be identified and studied through spatially matched sampling.
- The possibility that the three layers of the fracture adjacent rock may not have correlated parameters or have only weak couplings. If the retardation data appears to be randomly distributed, organising retardation components into fracture types may not be necessary.
- The usefulness of making á priori assumptions about fracture types to guide future site investigations. This can aid sampling strategies, especially when sample sizes are small and where a random sampling is impractical. On the other hand, if the á priori assumption is incorrect, this will introduce a systematic error in the retardation data.

In situations where data is scarce, relying on expert opinions for defining and parameterising fracture types may be the most straightforward approach. The decisions can be supported from experience and a wide range of qualitative and quantitative information derived from the previous site descriptive modelling work (Byegård et al. 2008). Furthermore, fracture types can serve as useful pedagogical tools to explain key features of the site's fracture network and surrounding rock.

Correlations between retardation parameters

Different retardation parameters may not always be numerically correlated which is important to consider in developing the retardation model. For example, two different alteration rims might have varying proportions of a mineral which has a large impact on the sorptive properties (e.g. hematite). This mineral, however, might not be correlated with diffusive properties in any meaningful manner. Even for a specific transport parameter such as K_d , the correlation between mineral volume fraction and sorptivity may be different for solutes that sorb by different mechanisms.

Provided deviations in the retardation properties of the altered zone relative to the undisturbed rock matrix can be quantitatively established, the impact of possible correlations between properties should be investigated by way of sensitivity analyses. If positive or negative correlations between $K_{\rm d}$ and $D_{\rm e}$ can be shown to have more than trivial importance for the safety assessment, then this should be considered to the extent feasible given the available data.

If investigations support complete decoupling of retardation components, then the model might feature a single fracture coating, alteration rim, and undisturbed rock component per transport domain, each with its own statistical distribution of retardation parameters where individual transport parameters (e.g. K_d and D_e as discussed above) are also decoupled from one-another. Here, it is envisaged that parameter values in each layer might be assigned independently from a probability distribution.

Assigning probabilistic distributions for transport parameters in this fashion should preserve mechanistic couplings even where properties are not strongly correlated. The procedure for assigning transport properties should therefore consider parameter covariance and whether certain combinations are inadmissible, or at least improbable. As an example, when assigning a parameter such as $D_{\rm e}$ from overlapping probability distributions, a proportion of stochastic realisations will have larger values assigned to the undisturbed rock than for the alteration layer. This will be the case even when the alteration layer on average has a higher effective diffusivity than the undisturbed rock. This implies an increased diffusive transport resistance in the alteration layer which might be contrary to the underlying process understanding as it relates to the altered layer.

It is noted that the probabilistic approach is not incompatible with the definition of fracture types, since the parameters for each retardation component of a given fracture type could also be specified in terms of probability distributions rather than single best estimate values.

Matched sampling of rock layers adjacent to hydraulically conductive features in the site investigations is particularly important to capture covariance between parameter values describing transport properties in adjacent layers. The transport parameters derived from the resulting stochastic model could be specified in several ways including:

- Probability distributions capturing both spatial (microstructure) and temporal variability (impact of groundwater composition).
- Tabulated single-point values with different occurrence probabilities.
- Single-point values if variability is low, or inconsequential.

It is also feasible to develop multiple independent retardation model parameterisations as deliverables within the site descriptive modelling. For example, one based on deterministic best estimate parameter values, and one with parameter values assigned from stochastic distributions with an aim to improve realism.

4.4.3 Proposal for specification of sorption properties for retardation components in the updated model

Specification of K_d values for the different retardation components is more complex than for porosity and effective diffusivity since measurement data may not be available for all radioelements and geological material types represented in the model. Furthermore, K_d values are strongly dependent on the composition of contacting groundwater which can be expected to vary considerably within the geosphere and will evolve over time. In the framework for recommendation of sorption properties discussed in Section 5.3, it is proposed that K_d values are provided for a set of reference conditions to which a correction factor is then applied to account for deviations of groundwater composition from the reference conditions. In the present proposal, the reference groundwater compositions are taken to be the synthetic groundwaters as defined for the laboratory programme.

In this treatment, it is implicitly assumed that the chemistry correction factors may be defined and applied independently of rock type in line with the underlying assumption of sorption linearity and a relatively dominant sorbing mineral (or mineral group with broadly similar sorptive properties) that is represented in all rock types. This may need to be revised, however, if there is significant sorptive variability which can be related to the mineralogical composition of rock types. A more detailed account of the definition of reference conditions and the extrapolation procedure for deviating groundwater composition is given in Section 5.3.

For radioelements where measurement data is lacking, it will be necessary to derive numerical values based on extrapolation from literature data or natural analogues. A basic outline of a procedure for incorporating generic literature data into the retardation model is described in

Section 5.2. A concept is also outlined in Section 5.3.5 for estimating K_d values for radioelements where there is a possibility to invoke geochemical analogies. It is presumed that extrapolated values are derived for the same reference groundwater compositions as for radioelements where site-specific measurement data are available from laboratory measurements. A specific proposal for estimation of K_d values for fracture minerals is given in Section 5.3.6 which might incorporate a mixture of measurement data for site-specific materials, literature data, and estimations derived from thermodynamic models documented in the literature.

In the case of retardation components defined in the context of microstructural units, it may be necessary to additionally consider covariance of K_d values in alteration layers relative to the adjacent undisturbed rock. It should be possible to handle this using surface area and mineralogical correction factors as outlined in Section 5.2 provided suitable proxy data are available in the form of quantitative mineralogical determinations, cation exchange capacities (CEC), and BET surface area measurements.

4.5 Basis for identification of fracture types

In this section, a brief outline is given for how fracture types might be identified for inclusion in the retardation model. It also considers how various features and processes in the geosphere might have an impact on transport properties and thereby influence the types and definitions of fracture types. Deformation zones are generally composed of clusters of interconnected and very closely spaced flowing features. In the transport model, these are conceptualised to be derived from the basic fracture types, although with transport properties that may deviate significantly from those typically encountered in sparsely fractured rock. A concept for how such features might be included in the retardation model is also given in this section.

4.5.1 Overview of basic requirements and issues related to the retardation model

It is acknowledged that there are different ways in which a retardation model can be organised representing different underlying notions of how site-specific information is to be structured. One way of doing this is to base descriptions on physically observable features in the rock. The previous retardation model developed with SDM-Site belongs within this category as the basic organising principle was classification according to groups of fracture minerals commonly observed occurring together. Another possibility is to organise data purely according to quantitative variations in transport properties identified in the lab and field programme. Such an approach may be less prescriptive concerning the types of minerals present in the fracture coatings as the focus is instead on sorptive and diffusive properties. Both approaches have their own advantages and disadvantages. The latter approach, however, might allow for a simpler description of retardation properties as less necessary details can be excluded if they do not have a meaningful impact on the modelled transport of solutes.

Any proposed retardation model for transport, however, should be compatible with descriptions used in geological, hydrogeological and DFN modelling to simplify interpretation and transfer of data between different models and sub-disciplines. This has already been discussed in Section 4.4.1. To a large extent this can be achieved by specifying domain specific proportions of fracture types based on the same geometric confines used by other modelling disciplines. Inter-disciplinary aspects of fracture definitions are discussed in the DFN modelling methodology report (Selroos et al. 2022). Consideration might also need to be given to the local *in-situ* stress situation as it affects diffusivity and anion exclusion effects. This implies additional exchange of data with the rock mechanics sub-discipline.

Deformation zones present a challenge, however, as the limited detail with which such features can be modelled in hydrogeological models may differ from requirements of the Transport discipline. As an example, in previous hydrogeological modelling (e.g. Selroos and Follin 2010) the F-factor for incremental path segments along a pathline was calculated as the advective travel time (calculated by particle tracking) divided by half the local transport aperture. For individual deformation zones, the transmissivity was approximately calculated assuming a generic exponentially decreasing trend as a function of depth. For some of the deterministic zones that were intersected by measurement boreholes, the transmissivity model could be roughly conditioned on measurement data. The estimated transport aperture, on the other hand, was based upon a simple universal quadratic relation with transmissivity reported in previous work by (Dershowitz et al. 2003) and applied to sparsely fractured rock and deformation zones alike.

Since the estimation of transport aperture does not give any additional information concerning intensities of connected flow bearing fractures in deformation zones, there was little scope to relate hydrodynamic properties to microstructure in a very detailed fashion. Understandably, the hydrodynamic transport resistance (F-factor) and advective travel time in deformation zones could only be very coarsely determined in this previous work. To properly model transport retardation in deformation zones, the hydrologic description of deformation zones and its relation to microstructure should be considered in greater detail in future work.

The above descriptions suggest that it may be difficult to tie together a detailed account of hydrodynamic transport properties with an equally detailed description of deformation zone microstructure in a convincing manner. If the hydrogeological description remains coarse then the best option might be to develop a retardation model for deformation zones that only seeks to identify an average transport class that captures the overall variation of microstructure as a function of depth. This is because the hydrogeological model for deformation zones in the previous site description essentially only captures the depth variation of transmissivity properties. Such a model may need to be partially generic for all deformation zones since there are not sufficiently many intersects of boreholes with named deterministic zones at different depths to treat them statistically.

4.5.2 Conceptualisation based on identified retardation components

In the present proposal, the three-layer representation of the rock matrix is a key construct underlying the retardation model. All the proposed sub-structures of the retardation model are derived from this basic representation and consist of a fracture coating, alteration rim, and undisturbed rock. In addition, the retardation components also include immobile zones and non-conducting fractures (see Figure 4-7). The immobile zones may include non-cohesive fault gouge or breccia within flow channels as a physically separate storage capacity to the fracture coating. Within deformation zones, alteration may be sufficiently pervasive that it occupies the entire region sandwiched between flowing fractures.

As noted in previous sections, more complex microstructures can be conceptualised and modelled as combinations of the basic three-layer configuration weighted in a suitable fashion over the flowpath segment under consideration. This is mostly of relevance for the modelling of deformation zones. The sparsely fractured rock comprising the bulk of the geosphere, on the other hand, is expected to be characterised by flow channels hosted in fractures where the surrounding host rock may have been subjected to limited episodes of metasomatism which only affects the rock within centimetre to decimetre distances from flowing features. For the sparsely fractured rock, fracture types are likely to have a more direct 1:1 correspondence to transport classes used in modelling.

The concept of fracture types is proposed as the main structure of interest. A fracture type is a group of fractures with common characteristics, i.e. the same microstructural model, and may consist of one or more microstructural units. The microstructural properties may include surface coverage, mineral composition, and thickness of fracture coating minerals, mineral composition and thickness of the alteration rim, and the rock matrix (rock type). Transport parameters for the different layers including ϕ , $D_{\rm e}$ and $K_{\rm d}$ are related to the underlying microstructural properties, although may be different for different solutes.

The other building blocks referred to in Section 4.3.2, namely connected non-conducting open fractures and immobile zones within the fracture plane are considered independently although they are not expected to result in additional fracture type definitions. One reason for considering immobile zones in fracture planes independently is that if they are to be considered in transport modelling, then the handling must be consistent with underlying assumptions implicit in the hydrogeological modelling (i.e. with regard to calculation of advective travel times and F-factors). For non-conducting open fractures that intersect flowpaths, on the other hand, the frequency of open fractures must be consistent with the cut-off limit for fractures considered in the underlying DFN model and assumptions concerning the existence of a continuum of fractures below the cut-off limit.

Another reason for handling non-conducting open fractures separately is that they are difficult to include explicitly in transport modelling without double counting matrix storage capacity. In cases where there is potential for enhanced matrix uptake due to a high frequency of stagnant fractures intersecting the flowpath, it may be easier to handle them by invoking an increased effective diffusivity near the main flowpath rather than attempting to model them explicitly as stagnant features.

In the context of deformation zones, fault gouge of small particle size might be reasonably considered to be an equilibrium storage capacity for transported solutes and can be lumped together with fracture coatings if they are treated similarly in transport modelling (i.e. as equilibrium storage capacities). On the other hand, if the fracture coatings are modelled explicitly as a diffusive barrier to matrix diffusion, then non-cohesive fault gouge should be considered separately to the fracture coatings. For larger pieces of breccia there may be justification to treat the material as a diffusively accessible immobile zone similar to the rock matrix although with a limited diffusion depth equal to half the effective particle diameter. A spheric diffusion geometry could also be considered.

Despite possible changes in the modelling approach, it is likely that at least one of the eight fracture types in the former analysis will be retained; this is group H, consisting of fractures in unaltered rock without any mineral coating. In the previous work this fracture type was found to constitute 5 % of open fractures and 13 % of flow-bearing fractures (Byegård et al. 2008). In the previous retardation model these fractures were not thought to be associated with an alteration rim, although this might be revised in the updated retardation model if stress release is found to be an important factor increasing the intensity of microfracturing and effective diffusivity in proximity of the fracture surface. This might be a relevant consideration even in the absence of recognisable alteration.

As a starting point, the approach of coupled retardation components as discussed in Section 4.3.1 results in a possible division into several fracture types comprising up to three retardation components and their variants:

- Fracture coating, alteration rim and undisturbed rock.
- Alteration rim and undisturbed rock only.
- Alteration rim only (e.g. large breccia pieces or closely spaced fractures).
- Fracture coating and alteration rim only (e.g. large breccia pieces or closely spaced fractures).
- Fracture coating and undisturbed rock only.
- Undisturbed rock only.

Although the three-layer concept is thought to be representative of a large proportion of flow bearing fractures encountered in the geosphere, consideration should be given to the possibility of more complex microstructures, their frequency of occurrence, and whether they can be subsumed into simpler categories using suitable modelling assumptions.

4.5.3 Proposed workflow for defining fracture types and deformation zone structures

A suggested iterative workflow for defining fracture types is given in Figure 4-12, starting with statistical analysis of existing and new collected data. The first aim of this analysis is to identify groups of retardation components which commonly occur together and then define fracture types based on these patterns. Such an analysis could use the existing fracture type definitions from Byegård et al. (2008) as a starting point. As already noted, however, these definitions overestimate the importance of mineral coating and do not consider undisturbed rock at all, so their relevance in the present context might be limited.

It is therefore proposed that a statistical analysis is applied to the data (noting that the data is comprised of a mix of categorical and numerical variables) to determine retardation components which may be sorted into fracture types. Methods and results presented in Crawford and Löfgren (2019) should provide valuable inputs to this work. The results of this analysis should be corroborated with input from experts in relevant disciplines, and the analysis iterated as necessary, before a definitive set of fracture types are defined.

Correlations should be sought between the fracture types defined from retardation components or combinations thereof and the different large-scale drivers (e.g. elevation, *in-situ* stress, strike/dip, etc.) which are thought to be most common for a given transport domain. If fracture types are appropriately defined, they can be assigned to each fracture in a drillhole log in the database using a set of criteria applied to small-scale fracture data such as mineral coating and alteration. Appropriate statistical tests can then be applied to the database to determine which (if any) of these large-scale drivers show a correlation with fracture types, and the strength of these correlations (see Section 7.4). Those which do not correlate to any type can be discarded as large-scale drivers in the rest of the analysis.

This approach would investigate flow-bearing and non-flow-bearing fractures separately. Non-flow-bearing fractures are of interest since they potentially belong to the retardation component "connected non-conductive open fractures". It may also be worthwhile to consider sealed fractures as they may influence how alteration layers are conceptualised and modelled.

The following questions will be investigated:

- Are there differences in the dominant large-scale drivers in different transport domains?
- Do the couplings between large-scale drivers and retardation components support a division into additional transport subdomains?
- Are there occurrences of combinations of different retardation components that are common enough to motivate the establishment of fracture types?

In the case that the data support classification in distinctive fracture types, we then have the additional questions:

- How are identified fracture types distributed between the transport domains?
- How are identified fracture types correlated to large-scale drivers?

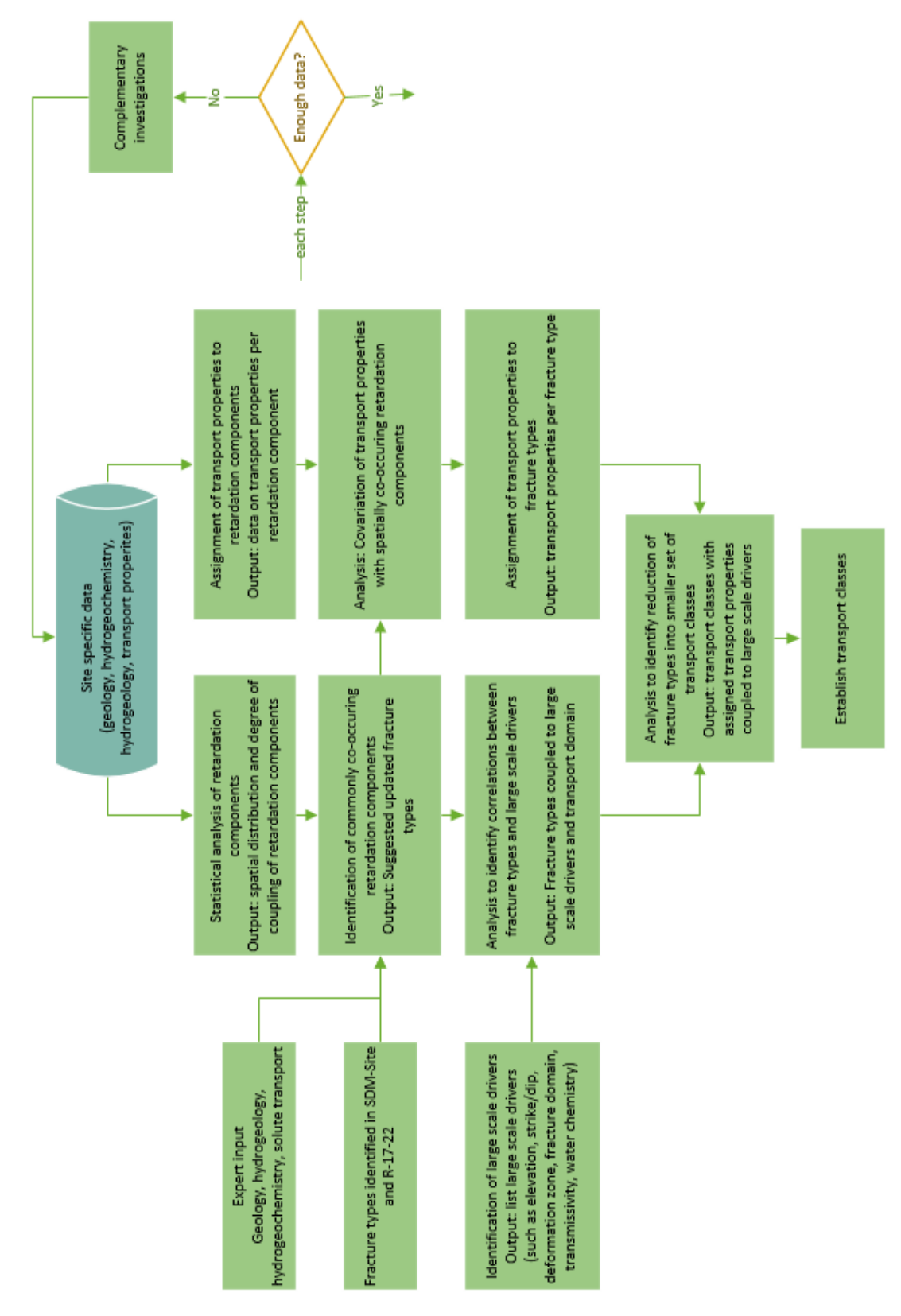


Figure 4-12. Workflow for identifying fracture types, comprising the retardation components fracture coating, alteration rim and undisturbed rock, and allocating them to the respective transport domains. At each step an evaluation is made if there is enough data or a need of complementary investigations. Finally, the concept of transport classes is tentatively reached, as further developed in Chapter 7.

The outcome will provide a basis for deciding which approach to the concept of fracture types is most advantageous, according to the discussion in Section 4.4.2 (i.e. what degree of coupling between retardation components should be assumed). Most probably, there will be a proportion of fractures that cannot be easily categorised within the defined group of fracture types. Depending on the frequency of such occurrences there may be some support for the concept of partly coupled or even non-coupled (i.e. randomly permuted) retardation components.

Following the identification of fracture types, the parameterisation of the different retardation components might lead to a set of fracture types with broadly similar properties which might be further reduced to a smaller set of transport classes. This concept is developed further in Section 7.4. As discussed in Section 4.4.2, diffusion and sorption parameters are not necessarily correlated in any simple fashion and might need separate handling when defining transport classes. Such a situation might arise, for example, where numerical values of D_e in adjacent layers are strongly coupled, although K_d may exhibit only weak or non-existent coupling.

4.6 Summary

In the preceding sections, a methodological proposal for development of an updated retardation model is suggested. The foundational principle of this model is the description of identified fracture types and deformation zone structures through the use of building blocks referred to as microstructural units. Microstructural units contain retardation components that are frequently found adjacent to each other in the rock, typically in a layered structure extending into the rock matrix from flow bearing fractures. The retardation components themselves are geological materials belonging to distinct classes which may include, although is not restricted to, fracture coatings, hydrothermally altered and oxidised rock, cohesive materials formed during ductile and brittle deformation such as cataclasite and mylonite, non-cohesive materials such as fault gouge/breccia, as well as undisturbed "fresh" rock. Individual retardation components have material properties that are variable although statistically quantified, while covariance between material property parameters in adjacent retardation components is described on the level of microstructural units.

The retardation model has a focus on material properties related to diffusive exchange, free storage, and adsorption processes while other classes of geochemical reactions are mostly excluded. The site-specific retardation model serves as a framework that integrates fractures and deformation zones into a coherent description of transport properties used to model and understand the migration of solutes in the geosphere. It is envisioned that the updated model will organise diverse geological material types into cohesive microstructural units within identified fracture types and deformation zone structures. Each of the microstructural units is characterised by unique features relating to the nature of the host rock, the extent of its fracturing and deformation and previous episodes of metasomatism.

It is proposed that the model will differentiate the geosphere into distinct transport domains, each with characteristic fracture types and domain-specific material properties. In this context, deformation zones may be considered as a class of transport domain containing subordinate structures and fracture types. This modular description is intended to facilitate a more detailed understanding of each transport domain's geological intricacies and properties affecting solute transport.

The possible covariance of material property parameters requires a sampling approach based on matched sampling of adjacent materials in bore cores. Parameters which are expected to exhibit small-scale spatial covariance include porosity (ϕ), effective diffusivity (D_e), and sorption partitioning coefficients (K_d) for specific solutes and well-defined reference groundwater composition. Proxy parameters associated with these processes such as mineralogy, BET-surface area, cation exchange capacity, Fe(II)/Fe(III) ratios, and other geochemical variables might be used to estimate the variation of transport property parameters on a detailed scale that is difficult to achieve solely using laboratory measurements of the primary transport parameters.

However, also a method/concept is needed that describes how these parameters can be obtained under *in-situ* conditions, either by direct *in-situ* measurements or by use of developed correlations. If salient correlations can be established between primary transport parameters and proxy variables, then data can be estimated for rock domains subjected to less detailed characterisation. This is likely to be particularly important for sorption properties where it may not be possible to perform detailed measurements for all radioelements of interest in safety assessments, especially considering the dependence on the varying groundwater compositions.

5 Derivation of retardation parameters

This chapter contains a summary of the key retardation parameters of interest in radionuclide transport modelling and their estimation. An overview and summary of the parameters is provided in Section 5.4 (see also Section 3.6). The proposed approach for estimation of retardation parameters is different for sorption (K_d) and diffusion (D_e), although both are combined with the transport porosity of the rock matrix (denoted as ϕ_p) to form a material properties group, κ_{MPG} :

$$\kappa_{MPG} = \sqrt{D_e(\phi_p + K_d \rho_b)} = \phi_p \sqrt{D_p R_p}$$
 (5-1)

where R_p is the retardation factor (see Equation 3-14), ρ_b is the bulk density and D_p is the pore diffusivity. The material properties group is the central parameter of importance for transport retardation where diffusion and sorption on rock matrix pore surfaces is invoked as the primary retardation mechanism for solute transport. For a single layer rock matrix of infinite extent, the material properties group κ_{MPG} is the key parameter governing solute retardation. For a given value of κ_{MPG} it makes no difference whether it is composed from a numerically low valued effective diffusivity, D_e and high-valued pore storage parameter, $R_p\phi_p$ or vice versa. This is not strictly true for a rock matrix of limited extent unless the rock matrix is "effectively infinite" on the timescale of solute transport (i.e. low solute penetration depth relative to the matrix layer thickness). More generally, in a layered rock matrix, where the altered layers have different κ_{MPG} relative to the unaltered rock, the residence time distribution for migrating tracers is not identically altered for different combinations of D_e and $R_p\phi_p$ with the same κ_{MPG} (Crawford 2008).

For diffusive properties of intact rock several different characterisation methods are used including electrical resistivity measurements (lab and *in-situ*), through-diffusion, and electromigration experiments. Each of these methods have strengths and weaknesses and may give differing results depending on the underlying physics of the method being employed, sampled volume, and modelling interpretation.

The porosity of the rock matrix establishes a lower limit for the influence of sorptivity in matrix diffusion-based migration below which sorption may be considered negligible. This lower limit is defined by the ratio of the connected porosity divided by bulk density which for most unaltered rock types gives a lower K_d limit on the order of $\sim 10^{-6}$ m³/kg below which the storage porosity of the pore fluid dominates over the surface-sorbed storage capacity. For altered rock types, the lower effective K_d limit is typically higher and commensurate with the greater porosity of the alteration type. The porosity can be used together with modified Archie's law type expressions to make rough estimates of D_e for materials where diffusivity measurement data are unavailable, although the accuracy of these estimates is much lower and subject to large stochastic uncertainty.

The transport porosity enters the material properties group via the definition of effective diffusivity. In modelling, the storage porosity of the rock matrix is typically assumed to be the same as the transport porosity, although this may not necessarily be the case if there is substantial secondary storage due to dead end pores and poor network connectivity of the rock matrix pore spaces. The storage porosity is always higher than the transport porosity since it includes all connected pore spaces, whereas the transport porosity only considers the principal network of pores that directly contribute to longer range diffusive transport. Although the transport porosity can be reasonably assumed identical to storage porosity on safety assessment timescales, such differentiation may be useful for interpretation of short-term laboratory measurements where the diffusive equilibration time of the storage porosity may be non-negligible.

For sorption, laboratory measurements of solute uptake on either monolithic and/or crushed materials are used for the estimation of K_d values, although data obtained from through electromigration experiments can also be used for certain solutes. K_d values are derived for reference rock types with a specified mineralogy and sorptive surface area in contact with groundwater of a specified composition. The reference rock types are typically intact rock types comprising the unaltered rock matrix, although altered materials are also included where feasible to do so.

The K_d values for the reference rock types are modified for use in the multilayer retardation model by applying a series of transfer factors to account for sorptive surface area, mineralogy, and groundwater compositions deviating from those used in laboratory investigations.

In the proposed methodology for quantification of sorption processes, K_d data is obtained from experiments involving both crushed rock and monolithic core samples. Although there are different methodological issues and biases associated with the use of both material types, a slight preference is given to data obtained from experiments involving monolithic materials. This is because these experiments most closely approximate the physics of solute uptake under *in-situ* conditions. In ongoing work possible improvements to an updated methodology for K_d estimation from laboratory data are suggested including a Bayesian approach to combine data of varying quality from different sources, aiming to provide more robust estimates of uncertainty.

In cases where the cohesiveness of samples is such that monolithic samples cannot be used, experiments involving crushed materials are presumed as the main basis for data acquisition. This, however, applies mostly to strongly altered materials and fracture coatings where the connected porosity of the materials is such that the problems associated with the use of crushed samples is likely to be less critical for derivation of reference K_d values.

In general, recommended K_d values for reference materials can be taken to be average values for site-specific rocks and well-defined alteration subtypes of those rocks for a specified reference groundwater composition. The transfer factors for surface area effects (including mechanical damage) and mineralogy should therefore be seen as a means to correct for the statistical representativity of samples used in laboratory investigations relative to volumetrically averaged values appropriate for deployment in the retardation model.

In some situations, K_d corrections relating to variable groundwater compositions might be assumed to be independent of rock and alteration type. This should be an acceptable approximation provided mineralogical differences between rock types are small. Depending on the feasibility of building a comprehensive component additive thermodynamic model of sorption, it may be necessary to specify relative sorptive properties of altered rock using a fixed multiplicative factor relative to the reference K_d for unaltered rock (i.e. implying either proportionally stronger or weaker sorption relative to unaltered rock). This is a simplification that might reduce unnecessary complexity for the specification of K_d values for different retardation components. K_d values for fracture minerals are treated separately regarding groundwater compositional variation where feasible to do so (principally calcite, barite, and other non-phyllosilicate minerals).

The simplest assumption in transport modelling is that the rock that surrounds water conducting fractures is homogenous and, accordingly, can be represented as a single layer with uniform material properties. This assumption was used previously in SR-Site (i.e. SKB TR-10-50) where all flowpaths were assumed to have identically uniform properties. This assumption does not mean that we really believe that material properties are uniform, but rather that we represent the small-scale spatial variation of material properties as statistically averaged values for modelling purposes. In this framework it is also feasible to define longitudinally segmented transport paths where different rock volumes are associated with different retardation properties. In the extended multilayer representation of rock matrix material properties, it is assumed that the rock surrounding water fractures features discrete layers with piecewise constant material properties to represent zones of metasomatic alteration associated with fracture fluid-rock reactions.

5.1 Strategy for estimating effective diffusivity and porosity

In this section we discuss the strategy for estimating effective diffusivity, D_e and porosity, ϕ_p in the rock matrix. This section also touches on the quantification of different transport classes, a concept that was used in the TURVA-2012 safety assessment within the Finnish waste management programme (Posiva 2013b, Section 7.8). While the concept of transport classes is discussed in Chapter 7, it is intended that this section should provide input to their parameterisation. Accordingly, different choices in the definition and use of transport classes puts different requirements on the data quantification.

The diffusive properties of the rock are assessed by multiple independent methods including resistivity measurements, through-diffusion and electromigration experiments, and modelling of out-diffusion of pore water solutes (concentration vs. time) profiles. The principal flows of

information for the assignment of D_e are shown in Figure 5-1. The *in-situ* method is based on interpretation of borehole resistivity logs, although this requires additional information about the porewater salinity which needs to be obtained from independent laboratory measurements of porewater composition. Porewater compositions for interval matched core samples can be derived from interpretation of salt out-diffusion experiments (e.g. Meier et al. 2015, Waber and Smellie 2008, Waber et al. 2011).

Comparison of laboratory and in-situ resistivity measurements allows the estimation of lab-to-field transfer factors to account for pore compression in-situ to extrapolate effective diffusivities obtained from through-diffusion experiments to in-situ stress conditions. The laboratory resistivity and through-diffusion measurements are also important as they are used to assign D_e values for interpretation of sorption experiments using the same monolithic samples (see Section 5.2.1). The laboratory-based through-diffusion and out-diffusion methods (after correction for pore compression) also provide independent corroborating estimates of the effective diffusivity obtained via the in-situ resistivity method.

For the connected porosity in the rock matrix, there are different complementary methods that can be used: In addition to the water saturation method, independent estimates of the open porosity have been obtained from interpretation of tracer breakthrough in through-diffusion measurements using HTO. In this case, the storage capacity of the rock, α_s is fitted by modelling of the solute breakthrough using the model described by Crank (1975), or equivalent frequency domain solutions for more complex descriptions of matrix diffusion.

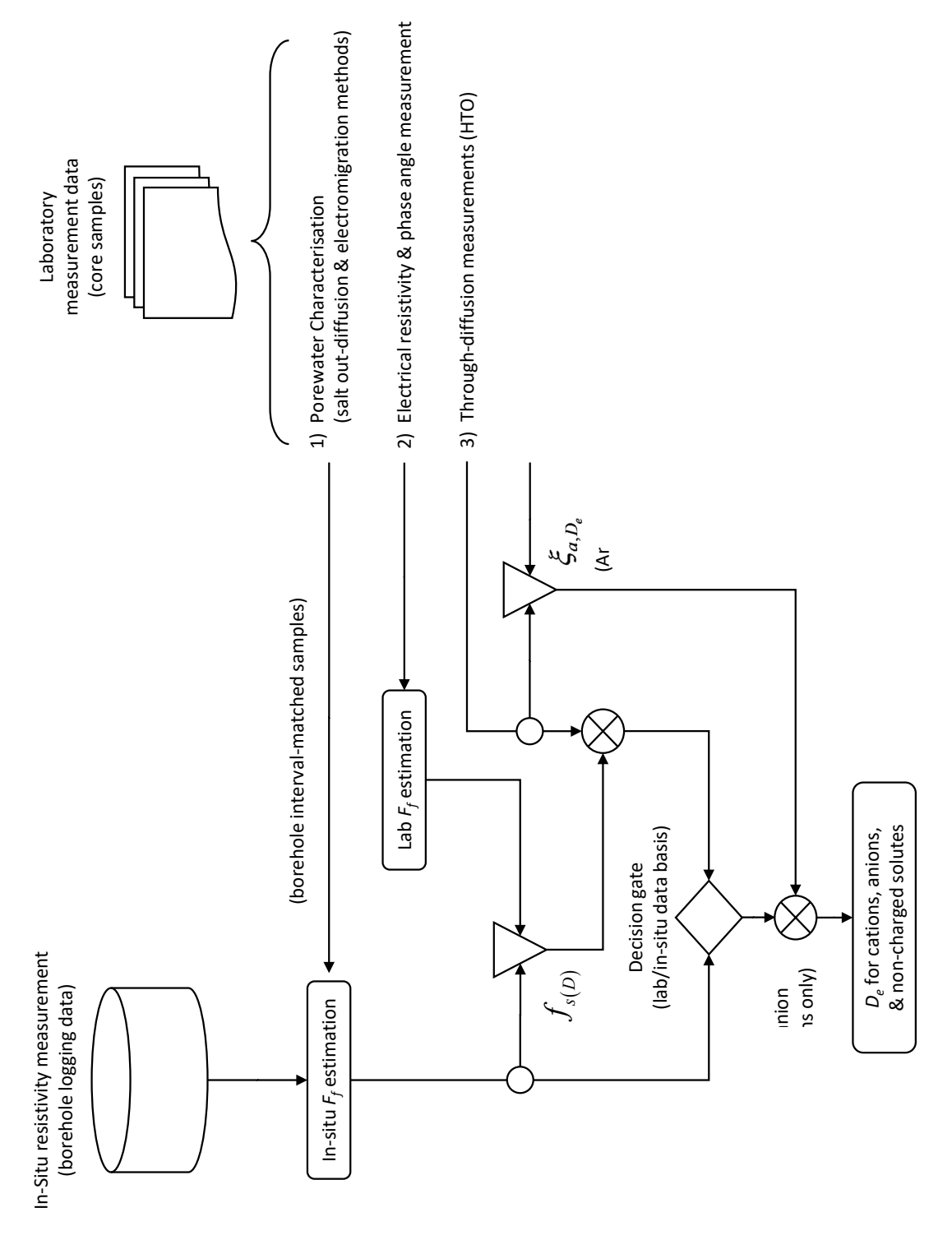


Figure 5-1. Procedural flowchart showing treatment of site-specific data obtained for effective diffusivity deriving from in-situ measurements (borehole resistivity logging) and monolithic core samples (laboratory resistivity and through-diffusion). Comparison of lab and in-situ resistivity data allow the estimation of lab-to-field transfer factor for pore compression under in-situ conditions. Laboratory through-diffusion measurements using HTO and I⁻ (destressed and re-stressed conditions) permit the estimation of anion exclusion effects. Effective diffusivities for cations and uncharged solutes can be obtained directly from in-situ resistivity data or laboratory data after correction for in-situ pore compression and are thus complementary methods. For anions, anion exclusion must be additionally considered.

Assuming that HTO is non-interacting, the storage capacity should be numerically identical to the porosity determined by the water saturation method. However, discrepancies have been noted in the SDM-Site laboratory programme. This could be interpreted as weak sorption of HTO, see Kaukonen et al. (1997). Other methods based on interpretation of gas adsorption isotherms (e.g. Lavonen et al. 2014), ¹⁴C- PMMA impregnation (Penttinen et al. 2006), and mercury intrusion porosimetry are used although more typically in a supporting role due to their additional complexity. The PMMA method is well suited for characterising fracture coatings and alteration rims which feature significant spatial variability.

5.1.1 Overview of pore-scale solute retardation properties

In previous SKB safety assessments it has been assumed that grain boundary porosity and microfracturing persists over significant distances into the rock matrix from fracture surfaces. There are multiple lines of reasoning that support this view. The ability to propagate electric current over many metres through the rock matrix at a resistivity level consistent with electrolytic conduction in the porewater is taken to be particularly strong evidence for a pervasive connectivity of grain boundary porosity.

The existence of brackish and saline water in matrix porewater many metres distant from the nearest identifiable fracture is also taken to be strong evidence for slow diffusive exchange with paleogroundwater in flow-bearing fractures (Waber et al. 2009). Mechanistically, it is expected that the differential expansion and contraction of mineral grains due to varying thermal expansion coefficients and bulk moduli of expansion creates voids around individual grains and intragranular microfracturing during cooling and uplift of rock after formation.

In general, the resistance of the principal matrix forming minerals are about four or more orders of magnitude higher than the measured *in-situ* resistivity suggesting that electronic conduction in mineral grains is negligible (Löfgren 2015). Furthermore, phenomena related to dielectric effects have been shown to have only a minor impact on resistivity measurements made using AC current (Löfgren 2015). Additional supporting evidence comes from PMMA impregnation measurements of core samples (Penttinen et al. 2006), although these are limited to cm scale connectivity and may be influenced by decompaction of the mineral grains due to stress release after bore core retrieval.

Although long range connectivity of the rock matrix porosity is deemed to be a reasonable assumption for Forsmark site-specific rock, this does not rule out occasional narrowing of pore spaces adjacent to fracture surfaces and armouring of fractures featuring thick secondary mineral coatings. Such pore narrowing processes might conceivably lead to significantly lower effective diffusivities in a rim zone (sub-mm to mm spatial scale) at fracture surfaces.

In Forsmark an increased connected porosity has been observed in the red-stained hydrothermally altered rock compared to fresh rock (Sandström et al. 2008). The connected porosity increases in the altered rock and is mainly due to microfractures and an increase in inter-granular porosity due to chloritisation of biotite.

In Penttinen et al. (2006) PMMA has been used to measure porosity. In this study the highest porosities were found in rock adjacent to water bearing fractures where intragranular microfracturing is dominant. In the lower porosity samples, on the other hand, grain boundaries are the dominant form of porosity. In some core samples featuring alteration halos surrounding sealed fractures there are some indications of reduced porosity as measured by the PMMA technique (Penttinen et al. 2006). It bears repeating, however, that the samples that have been studied are associated with sealed fractures and may not be representative of modern flow bearing fractures at the Forsmark site. Therefore, the representativity of these for describing the geosphere at Forsmark requires further investigation.

Here, it is relevant to note that alteration associated with sealed fractures, ancient hydrothermal alteration zones, cataclasites, etc. are not necessarily oriented in parallel with extant open fractures as identified in the drill cores. Modern flow bearing fractures may therefore have completely different orientation or be offset relative to the direction of material property zonation associated with paleo alteration. Based on how common this is it might need to be considered in the formulation of multilayer transport classes which, otherwise are presumed to have zones of alteration normal to their associated flow bearing fractures.

Furthermore, for non-porous coatings and fracture rim zones with reduced porosity and effective diffusivity to be important requires them to populate non-trivial fractions of the flow-wetted surface in the geosphere. Although isolated samples with low porosity rim zones have been identified in the PMMA studies, these appear to be the exception rather than the rule at the Forsmark site as most open fractures appear to be associated with weak alteration that is often barely perceptible to the naked eye.

5.1.2 Small-scale laboratory results

The data quantification in SR-Site relied partly on laboratory results for D_e and almost exclusively on laboratory results for ϕ_p . Experiments were generally made on drill core samples with the diameter of 50 mm and length ranging from 5 to 50 mm.

Effective diffusivity

Numerous through-diffusion measurements using HTO as the tracer were carried out, both for the Forsmark (Selnert et al. 2008) and Laxemar-Simpevarp site (Selnert et al. 2009b). Figure 5-2 shows a histogram and the fitted log-normal distribution of D_e obtained for the Forsmark site using this method. The median value of these data is $2.5 \cdot 10^{-13}$ m²/s, which applies for non-charged species under de-stressed conditions. Moreover, the standard deviation is almost half an order of magnitude, or roughly a factor of 3 in arithmetic terms. Given the careful measurements, most of the variance can be reasonably attributed to sample variability. It is not clear, however, whether this is dominated by between-sample variability (i.e. for largely identical materials sampled at the same location), or spatial variability reflecting differing properties in terms of mineralogy, grain size distribution, degree of alteration, etc. at different locations in the host rock.

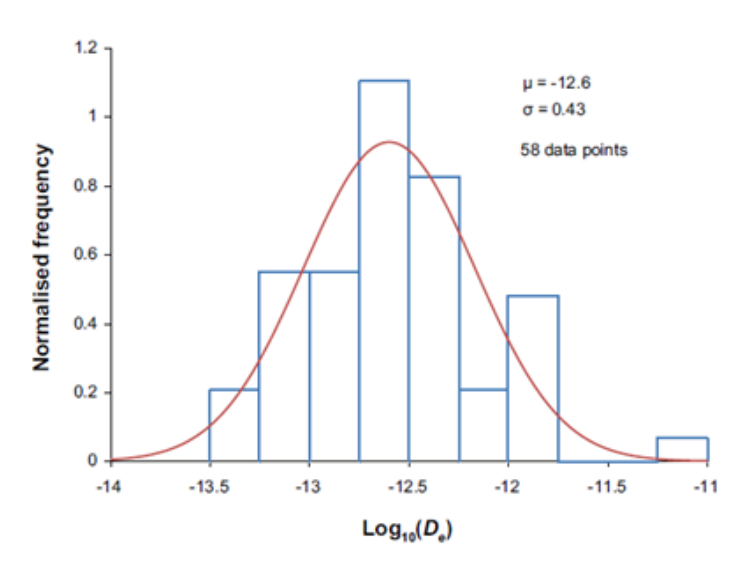


Figure 5-2. Histogram and fitted log_{10} -normal distribution of all effective diffusivities from laboratory through-diffusion measurements, excluding data from anomalous samples with porosities over 10 %. Reproduced from SKB TR-10-52 (Figure 6-79).

The formation factor F_f of drill core samples was also measured by using electrical methods (Selnert et al. 2008, 2009b). In these measurements an electrical current is propagated through the rock by solutes in the pore water. If the rock samples are saturated by an electrolyte of high ionic strength, the resistivity of the rock sample is inversely proportional to its formation factor. This is expressed in Equation 5-2 in terms of the measured electrical conductivity of the rock κ_r (S/m) and the average electrical conductivity of the pore water $\bar{\kappa}_w$ (S/m):

$$F_f = \frac{\kappa_r}{\kappa_w} \tag{5-2}$$

For the laboratory measurement campaign in the site investigations, a high ionic strength pore water was used (~1 M), so that the electrolytic conduction in the EDL is significantly outweighed by that in the bulk pore water. In SR-site a surface conductivity term, κ_s (S/m), was introduced to include the effect of the EDL:

$$F_f = \frac{\kappa_r - \kappa_s}{\kappa_w} \tag{5-3}$$

The surface conductivity and formation factor can be quantified in the laboratory on the same samples in independent measurements saturated firstly by an electrolyte of very low ionic strength (deionised water), and subsequently by a high ionic strength solution (1 M). Such measurements have been made by (Ohlsson 2001, Löfgren 2001). Under very low ionic strength conditions, the electrolytic current that is propagated through the rock sample is dominated by cations in the EDL and the conductivity of the sample is then roughly the same as the surface conductivity ($\kappa_r \approx \kappa_s$).

In SR-Site, the impact of anion exclusion on the electrical measurements was not explicitly considered. If there is very moderate anion exclusion, Equation 5-3 likely suffices when estimating the formation factor from electrical methods for application in SA. If not, more complex expressions which include the effect of anion exclusion need to be considered.

By using the simplified expression given by Equation 5-3 in SR-Site, a cumulative density function of formation factors obtained by laboratory electrical measurements was obtained for the Forsmark site. This is shown by the red solid curve in Figure 5-3. The dotted line in the figure shows the log_{10} -normal distribution fitted to the data. The blue curves are not discussed here although in subsequent sections. The dotted red line that can be compared to the fitted distribution for D_e data from through-diffusion measurements in Figure 5-2.

In SR-Site, the data supporting Figure 5-2 and Figure 5-3 were pooled together without dividing them into subpopulations based on rock type, mineralogy, grain size, etc. In SDM-Site, however, the data were sorted into subsets based on rock type (Crawford 2008, Table 4-9, Crawford and Sidborn 2009, Table 4-9). An additional subdivision was made based on if the drill core sample was taken from within or from outside a deterministic deformation zone. This, however, does not necessarily correlate with the degree of alteration that the sample had been subjected to.

Generally speaking, little difference was seen between rock types in Forsmark, while for Laxemar the differences were larger. It is difficult to draw specific conclusions, however, since measurements for several of the rock types are based on too few samples to be statistically informative. Samples taken from within deformation zones did not have significantly higher effective diffusivities than those taken from outside deformation zones, except for samples taken from specific deformation zone locations in Forsmark with significant quartz dissolution (i.e. episyenitic alteration).

Formation factors obtained by electrical methods

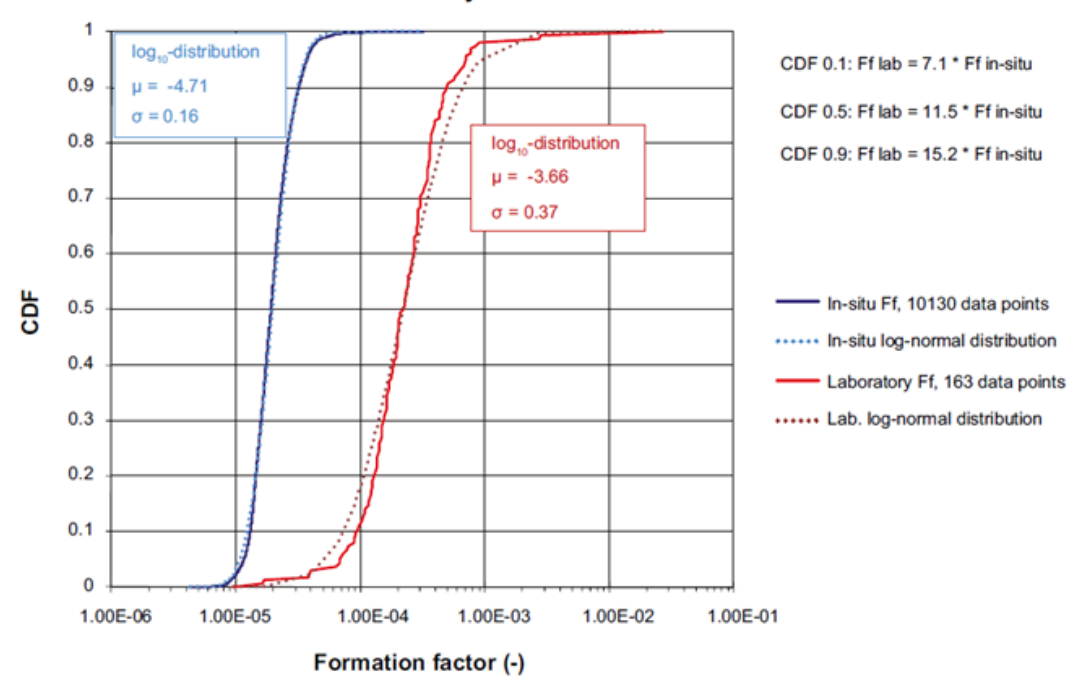


Figure 5-3. Red curves: CDF and best fit log-normal distribution of laboratory formation factors obtained by the electrical resistivity method. Blue curves: CDF and best fit log-normal distribution of in-situ formation factors for borehole KFM01D, KFM06A, and KFM08C. Reproduced from SKB TR-10-52 (Figure 6-80).

To aid quantification, it would be useful to revisit the previously studied samples to characterise their rock type, mineralogy, grain size distribution, degree of alteration and porosity measurements. Further sorting and statistical analysis of subpopulation data could provide useful insights into rock characteristics that significantly impact effective diffusivity, and those that have minimal or no effect. This could validate the use of rock types (Chapter 4) and possibly transport classes (Chapter 7), especially regarding effective diffusivity. It is also important to examine if systematic errors, such as those associated with stress release could obscure true data differences between subpopulation samples in the laboratory.

Diffusion available porosity

Connected porosity was measured using the water saturation method. In SR-Site, diffusion-available porosity was considered equal to water saturation porosity for all species. The average diffusion available porosity in Forsmark site was estimated at 0.23 % for intact rock taken from outside deformation zones, whereas it was 0.24 % at the Laxemar site.

In through-diffusion experiments using non-charged tracers, the capacity factor α is assumed equal to the diffusion accessible porosity. In the site investigations, HTO was typically used as tracer and as a result a larger number of capacity factors have been obtained assuming that HTO does not sorb on the surface³. When pooling relevant capacity factors from both Forsmark and Laxemar-Simpevarp site investigations through-diffusion experiments, the average value is 0.76 %⁴. This includes all capacity factors below 4 % (104 out of 117 available values), assuming that values above this represent samples strongly altered from within deformation zones. This assumption could be further verified in subsequent data quantification.

 $^{^3}$ Hydrogen exchange with hydroxyl surface groups is typically measured with titrations and the exchange of tritium with the surface groups of the mineral groups should be considered. K_d values for HTO of 0.01 to 0.1 ml/g (1× 10⁻⁵ to 1 × 10⁻⁴ m³/kg) are reported for granites in the scientific literature, see e.g. Kaukonen et al. (1997). That is within the range that can be calculated based on the expected surface charge amounts.

⁴ A K_d on the order of 2 × 10⁻⁶ m³/kg would be enough to give a capacity of 0.75 % with a porosity of 0.25 %. (α = ϕ_p + K_d ρ_b = 0.0025 + 1.8 × 10⁻⁶ × 2700 = 0.0075).

The cumulative density function of all 104 capacity factors under 4 % is shown in Figure 5-4. The median value of the data is $5.3 \cdot 10^{-3}$, while the arithmetic mean is $7.6 \cdot 10^{-3}$. Provided there is a sufficient number of data points, samples subjected to capacity factor or water saturation measurements should be sorted based on rock type, mineralogy, grain size distribution, and degree of alteration to facilitate statistical analysis on data subpopulations. The discrepancy between the estimated capacity factor and water saturation porosity should be further investigated. If methodological issues leading to systematic errors are suspected, affected data points should be excluded when quantifying ϕ_0 for use in SA, as far as possible.

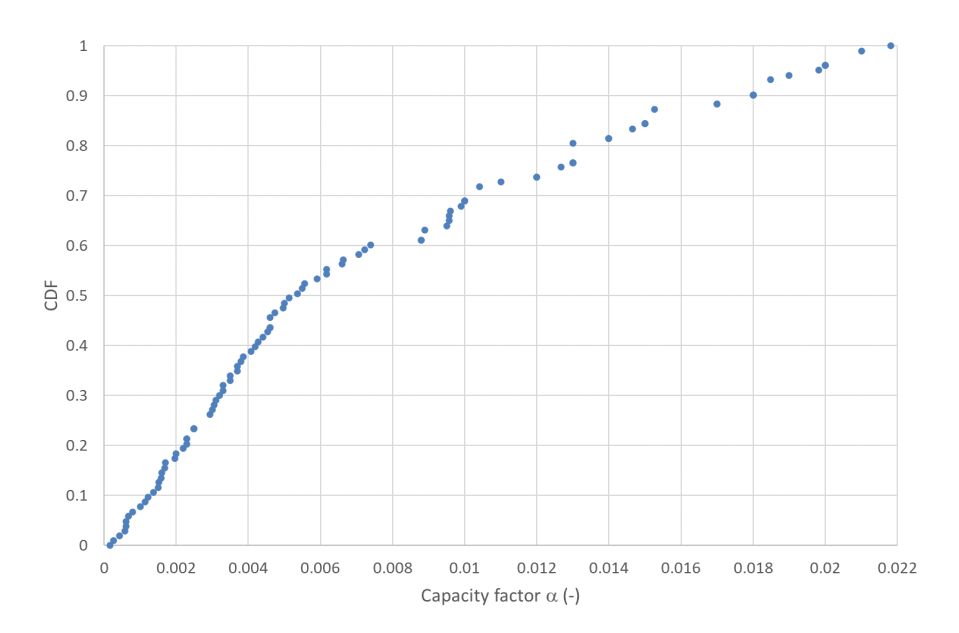


Figure 5-4. CDF of capacity factors obtained in through-diffusion experiments using HTO as tracer (Selnert et al. 2008, 2009b).

5.1.3 Correlation between parameters

Possible correlations between ϕ_p and D_e , and between K_d and D_e , should be investigated further. This is probably of greatest importance for multilayer rock matrix representations of the rock, since neglecting correlation between these properties would likely give different statistical distributions of κ_{MPG} for stochastic modelling than if correlations were to be included. For moderately to strongly sorbing radioelements, correlation between K_d and D_e would likely have the largest impact on the calculation of κ_{MPG} as the free storage capacity is negligible in such cases (i.e. $\kappa_{MPG} \approx \sqrt{D_e K_d \rho_b}$). The bulk density, ρ_b of the site-specific rocks is relatively well constrained and is not likely to have a large impact on κ_{MPG} .

Correlation between ϕ_p and D_e is well known for sedimentary rocks, commonly expressed in terms of the Archie's power-law expression (e.g. Glover 2016). The accuracy of the correlation is generally less good for igneous rocks of low porosity (< 4 %) which limits its usefulness for granitic rocks. To a lesser extent, correlations between variables may have an impact on the quantification of uncertainty associated with Equation 5-1.

Based on laboratory measurements, the correlation between the effective diffusivity and capacity factor has been studied in the site investigations. A plot of these parameters is shown for Forsmark samples in Figure 5-5. A similar plot is shown for the Laxemar site in Figure 5-6, although there the formation factor is plotted versus the water-saturation porosity. These previous studies show a weak correlation between D_e and α , and between F_f and ϕ_p , even when sorting the data based on rock type. Note that the encircled data points labelled "Episyenites" in the figure relate to small but highly altered rock volumes at the Forsmark site, which have been subjected to quartz dissolution (i.e. so-called "vuggy" granite).

For higher porosity altered rocks, and surface coatings, use of the Archie expression relating porosity and formation factor may be more useful, particularly given the fact that through-diffusion and resistivity measurements may be more difficult to perform on such samples. In this case, the amount of unexplained variation must be considered as part of the overall uncertainty of the porosity parameter that is propagated in the calculations. For transport modelling purposes, however, this uncertainty is likely to be significantly less than that shown in Figure 5-5 and Figure 5-6 due to the effects of flowpath averaging. In this case, the relevant uncertainty to propagate in calculations would be the confidence interval of the regression estimate rather than the prediction interval of the sampled population.

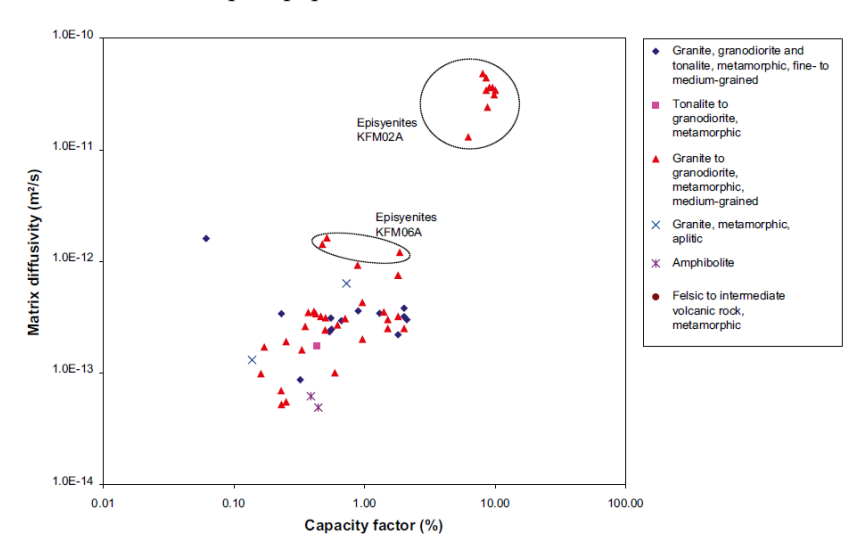


Figure 5-5. Effective diffusivity D_e plotted vs. capacity factor α , from through-diffusion experiments on Forsmark rock using HTO as the tracer. Reproduced from Selnert et al. (2008, Figure 4-17).

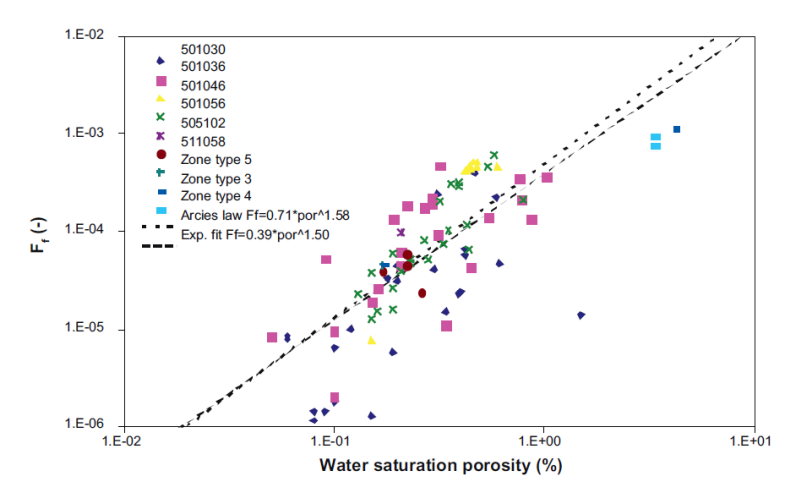


Figure 5-6. Formation factor F_f plotted vs. water saturation porosity, with formation factor determined from throughdiffusion experiments on Laxemar rock using HTO as the tracer. Reproduced from Selnert et al. (2009b, Figure 4-16).

Possible correlations between K_d and D_e are difficult to deduce. When interpreting laboratory data, one typically finds a range of K_d and D_e values that give the same κ_{MPG} (cf. Figure 5-12). Although this might lead one to believe that K_d and D_e should be anticorrelated, this is more of an artefact of data interpretation rather than a true mechanistic process. Intuitively, one might expect that K_d should not be correlated with D_e since the former is proportionally related to pore surface area whereas the latter is more closely related to pore cross-sectional area. However, it should be noted that for altered rock both porosity and BET surface are typically larger than for intact rock (Byegård et al. 2008)

Altered rock is expected to have greater BET surface area due to increased microfracturing and stress release near fracture surfaces as well as a greater proportion of secondary sheet silicate minerals than fresh rock. Since K_d is strongly correlated with BET surface area, it might be possible to establish correlations with D_e by way of surface conductivity and zeta potential measurements on larger (> 3-5 cm) core samples at low ionic strength. There is a great strength in measurements of BET surface area and porosity on the same samples to be able to establish degrees of correlations.

5.1.4 Medium-scale and large-scale spatial variability

Fracture coating and alteration rim

In most cases, fracture coatings at Forsmark are expected to be a fraction of a millimetre thick, whereas the alteration rim may extend from the cm- to dm-scale. For fracture coatings there is no need for upscaling on account of their limited thickness. In radionuclide transport calculations, they are typically modelled using an equilibrium retardation factor where the storage capacity is assumed to be instantaneously equilibrated on the time scale of advective transport.

In cases where fracture coatings comprise a significant diffusion barrier to the uptake of radionuclides, a matrix diffusive description of the fracture coating can be used where the $D_{\rm e}$ and effective $K_{\rm d}$ value for the fracture coating is simply flowpath-averaged over the specific flowpath segment (taking into consideration that the impermeable coating only partly covers the fracture surface). Another possibility is to simply reduce the F-factor for the flowpath segment in proportion to the surface area coverage of minerals that block diffusive uptake to the rock matrix.

In a multilayer rock matrix representation, the relative impact of the different layers on radionuclide transport is more complicated than for the single layer case which is fully described using a single material properties group, κ_{MPG} . Attribution of retardation to the different rock matrix layers for a migrating radionuclide is dependent on the hydrodynamic transport resistance (F-factor), thickness of the layers, and transport parameters K_d , D_e , and to a lesser extent ϕ_p . It is also dependent on whether the focus is on early or late arriving breakthrough since the travel time of early arriving solute is mostly associated with retardation in the rim zone, whereas the travel time of later arriving solute is more strongly associated with retardation in deeper lying rock matrix layers.

In the single layer case, it is possible to calculate a flowpath average κ_{MPG} for the entire migration path where the average is calculated by weighting relative to the F-factor (flow-wetted surface to flow ration) along the flowpath. For a multilayer rock matrix this is not strictly possible, although it is still reasonable to calculate averaged individual property values (i.e. D_e and K_d) for a segmented flowpath featuring different transport classes. Here, each transport class assumes averaged properties for the different layers of the rock matrix both normal to the fracture surface and laterally along the flowpath.

In general, flowpaths with alteration rims featuring higher κ_{MPG} values in proximity to fracture surfaces will exhibit greater transport retardation than those without. The extent to which this will impact far-field fluxes, however, depends on the F-factor and the individualised K_d and D_e values for the alteration layer relative to the deeper lying rock matrix layer (as well as the half-life of the migrating radionuclide). It can be shown that an alteration rim with larger κ_{MPG} relative to the deeper rock layer will have a larger effect if the increase is K_d -related rather than due to enhanced D_e (e.g. Crawford 2008, Appendix J).

Results from previous site investigations suggest that fracture coatings of hydraulically conductive fractures are very thin, on the order of 0.1 mm distributed in a patch wise manner for those fractures where fracture coatings have been identified (Löfgren and Sidborn 2010). Based on the data compiled by Löfgren and Sidborn (2010, 2016), one can estimate that flow-bearing fractures at the Forsmark site host on average 15–30 g/m² calcite, 25–50 g/m² chlorite, and 8–14 g/m² of mixed layer clays (i.e. per square metre of flow-wetted surface). The retardation effect of these mineral coatings may be large for strongly sorbing solutes, although this will mostly have an impact for flowpaths featuring low F-factors. The enhanced retardation of weakly to moderately sorbing solutes, on the other hand, may be only minor relative to that in the alteration rim and possibly insignificant.

For flowpaths featuring high F-factors, the enhanced retardation effect of fracture coatings is likely to be inconsequential for most radionuclides. Based on the few observations that exist, from e.g. PMMA-impregnation studies, the fracture coating is seemingly not impervious, but instead often more porous than the underlying alteration rim. Furthermore, the observed patch-wise coverage of the fracture coatings, where much of the wall rock remains uncoated, (see Section 4.3.2), strongly suggests that this layer does not hinder diffusive uptake.

In previous safety assessments, the alteration rim was thought to be less consequential for radionuclide transport modelling since it mostly enhances the host rock retardation capacity and neglecting it can be shown to be a conservative assumption. The underlying assumption here is that the alteration rim has increased ϕ_p , D_e and K_d values relative to the underlying rock. This, however, may not always be true around all segments of hydraulically conductivity fractures, as there is likely significant spatial variability. Given the lack of systematic knowledge on the alteration rim and its material properties, one suggested way forward is to perform new measurements in upcoming site investigations. If the retardation properties of the alteration rim only differ marginally from those of the underlying rock, one may choose to assume the identical properties for the alteration rim and underlying undisturbed rock (i.e. a one-layer rock matrix model as used in SR-Site), in which case flowpath-averaged values of κ_{MPG} can be used for the entire flowpath (or flowpath segment within a transport domain).

When using a multilayer rock matrix representation, an additional parameter to include is the thickness of the alteration rim. It may be difficult to assume a uniform thickness since different transport properties may vary differently with the distance from the fracture. This can be exemplified by the storage capacity in the right-hand term of Equation 5-1. The fracture adjacent wall rock often shows elevated porosities within a few mm to about 1 cm, or so from the fracture surface following a decreasing intensity trend asymptotically approaching the background porosity. For the diffusive properties of the rock this may suggest an alteration rim on the order of a centimetre thick. In Sandström and Tullborg (2006) it is argued that the connected porosity increases in the altered rock are mainly due to an increased intensity of micro-fracturing and, to a lesser extent, due to increases in inter-granular porosity resulting from chloritisation of biotite. For non-sorbing radionuclides, this will be the depth of alteration associated with enhanced retardation. On the other hand, hematite red staining, chloritisation or other alteration may extend several cm, or more from the fracture surface (Sandström and Tullborg 2006).

Wider zones are generally associated with penetrative networks of minor fractures, many of which may have subsequently undergone annealing. There is also evidence that chloritisation persists over greater distances into the rock than the red staining associated with saussuritisation of plagioclase (visible red staining due to the presence of sub-microscopic grains of hematite in altered plagioclase grains, along microfractures, and grain boundaries). Similar characteristic features of alteration have also been identified in other SKB investigation areas (e.g. Landström et al. 2001, Drake and Tullborg 2006a, b) so it is not specific to the Forsmark site.

This may suggest an effective alteration rim thickness of as much as a decimetre for sorbing species, where radionuclides that sorb by different mechanisms may experience different alteration depths. This is not problematic if additional layers are defined to properly reflect the trend of material properties variation for each variable of interest. If the multilayer rock matrix representation is confined to a single alteration rim around flowpath segments, however, the description of sorption may need to be simplified using flowpath averaging approaches.

Additionally, it can be noted that the assignment of a fixed thickness of an alteration layer is a simplification of what is likely to be a continuous variation of a given material property. The question of where different layers start and finish is not a trivial one and can have consequences in modelling. Generally, one might use a heuristic rule such as the alteration layer finishes where the difference between the value of a given material property in the layer and the succeeding layer is less than a given threshold value.

For alteration types where the deviation diminishes in a roughly exponential fashion with distance, as might be the case for hydrothermal alteration, the threshold is arbitrary and relatively large differences in layer thickness may be calculated depending on the assumed threshold levels. This impacts transport modelling since it is generally infeasible to model a continuously variable rock

matrix in safety assessment codes based on analytical solutions. The calculated average property value for the alteration layer is dependent on the thickness of the layer since the material property variation must be integrated over the assumed thickness. These, however, are minor issues and can be reasonably handled by sensitivity analysis when defining the transport classes comprising the retardation model.

For a material property that diminishes continuously from the fracture surface, the average value calculated for the alteration rim will be lower for increasing layer thicknesses assumed in the calculation. This will be particularly noticeable if the studied property varies over multiple orders of magnitude. In cases where the bulk of solute retardation is associated with the alteration layer, a thinner layer may then give a greater retardation effect than if a thicker layer was assumed in the calculation. Since the effective penetration depth (Crawford and Löfgren 2019) associated with retardation varies proportionally with the F-factor for the flowpath segment, this is potentially problematic since the retardation effect for different flowpaths will vary in a way that may not be exactly captured in a mechanistically correct manner. One way around this is to use a more finely discretised multilayer representation to capture the material property variation more accurately, although at the expense of more complex rock matrix description.

For the parameters comprising the material properties group $(D_e, K_d, and \phi_p)$ an appropriate upscaling procedure is to assume the central tendency (i.e. "expected value") of each parameter in transport calculations. In practice, where probability distributions are estimated based on laboratory studies for a finite number of samples, this implies calculation of the arithmetic average and its normally distributed standard error. This applies even if the parameter itself is lognormally distributed due to the central limit theorem. The underlying assumption, however, is that the variance of laboratory values is representative of spatial variability *in-situ*.

This is likely reasonable for effective diffusivity where uncertainty of data interpretation is relatively well-constrained (*in-situ* pore compression effects notwithstanding). Effective diffusivities derived from *in-situ* resistivity measurements, on the other hand, are thought to be approximately representative of *in-situ* pore compression and averaged over the appropriate volumetric support scale already at the point of measurement. These data are not thought to require special upscaling techniques after correction for known biases. Spatial variation is also relatively well described in the boreholes (principally, KFM01D and KFM08C) where porewater chemistry is documented in relatively high resolution from porewater leaching studies.

In cases where uncertainty of data interpretation is a dominant effect, it is difficult to demonstrate that an arithmetic average is the most appropriate measure for the upscaled parameter. This is likely to be the case for K_d derived from interpretation of time series data for solute uptake to crushed or monolithic rock. The application of f_m and f_q transfer factors, however, should be understood as an upscaling process since appropriate values need to be calculated to reflect the average properties of the *in-situ* rock described as "fresh".

When parameter uncertainty dominates, it is usually more appropriate to use the full uncertainty distribution in stochastic simulations. For a variable with a lognormally distributed uncertainty, this implies use of the geometric mean (median). Use of the full uncertainty distribution in probabilistic simulations, rather than the sampling distribution of the mean ensures that the full uncertainty of the parameter, given the observed data, is propagated into calculations which should result in more accurate predictions.

In keeping with this underlying principle, the best estimate for K_d was given as the geometric mean in SR-Site with a recommendation for random sampling within the 97.5 % confidence interval for probabilistic calculations.

As discussed previously, for alteration rims there is the additional problem of averaging material properties over the layer thickness assumed in the modelling. For a material property such as K_d or ϕ_p , upscaled values can be calculated by integration over the alteration layer thickness if a suitable model for the parameter variation normal to the fracture surface exists. For an alteration rim of thickness, d_L the upscaled K_d value would be calculated as:

$$\overline{K}_{d} = \frac{1}{d_L} \int_0^{d_L} K_{d}(x) dx \tag{5-4}$$

In principle, the same handling is recommended for diffusive properties, although here the integration must be made for the inverse of D_e (Crank 1975):

$$\frac{1}{\bar{D}_{e}} = \frac{1}{d_{L}} \int_{0}^{d_{L}} \frac{1}{D_{e}(x)} dx \tag{5-5}$$

As can be seen from the above equations, the upscaled value depends on the threshold at which point the altered layer is deemed to finish and can have a significant impact on the upscaled value if the parameter varies over multiple orders of magnitude.

Undisturbed rock

In SR-Site, the mean value and spatial variability of the effective diffusivity were estimated for undisturbed (intact) rock on two scales. On the scale of laboratory drill core samples, a standard deviation was observed for the effective diffusivity, or formation factor, of about 0.4 log₁₀-units (see Figure 5-2 and Figure 5-3). The formation factor was also measured *in-situ* by electrical methods in SDM-Site. In this method, a focused electrical current is emitted from a probe into the rock surrounding the borehole where the support volume of the measurement can be assumed to be on the scale of a cubic metre, or greater. Figure 5-7 shows the normal distribution fitted to *in-situ* formation factors (logarithmised data) from the three boreholes judged to provide the most reliable data in SR-Site. The distribution includes over 10,000 data points which provides a good basis for statistical analysis. As is shown in the figure, the observed standard deviation is only 0.16 log₁₀-units for the *in-situ* values.

The lower statistical dispersion relative to laboratory scale is most likely due to averaging effects given the larger support volume of the *in-situ* measurements relative to lab values. This would appear to corroborate the idea that small-scale variance averages out over increasingly large scales. In a supporting semi-variogram analysis carried out within SDM-Site (Crawford 2008, Appendix I) it was noted that at least 20 % of the depth-detrended variation of $\log_{10}F_f$ in borehole KFM01D appeared to be associated with a length scale of less than 1 m with around 80 % associated with a length scale on the order of 5-7 m based on visual curve matching.

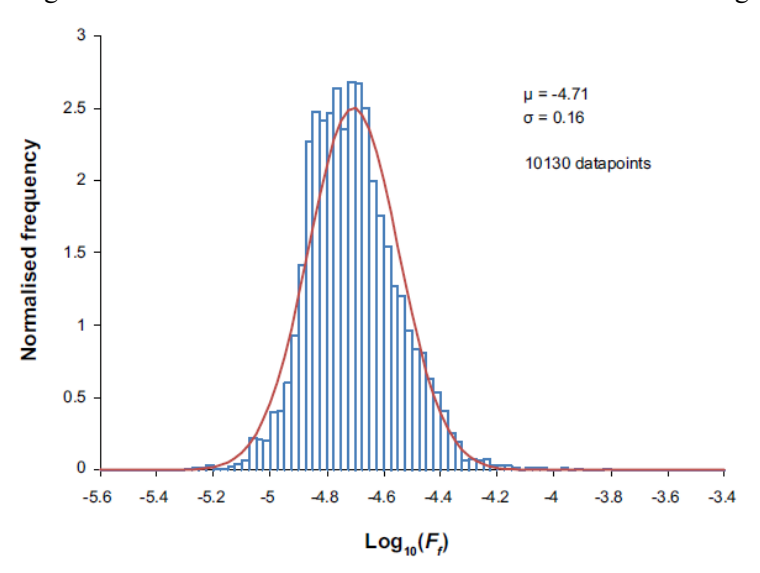


Figure 5-7. Histogram of all in-situ formation factor data from boreholes KFM01D, KFM06A, and KFM08C, together with best fit (log₁₀)-normal distribution. Reproduced from SKB TR-10-52 (Figure 6-78).

As a single-layer rock matrix was assumed in SR-Site, and different flowpaths were not assigned different retardation properties, the arithmetic mean $D_{\rm e}$ (or, equivalently F_f) was used as the flowpath averaged value for the entire host rock. As detailed in SKB TR-10-52 (Section 6.8) the effective diffusivity was derived by two different methods, which are not completely independent. In the primary method, the arithmetic mean F_f of the fitted probability distribution in Figure 5-7 was used, which is $2.1 \cdot 10^{-5}$. This value was multiplied with an assumed D_w of $1 \cdot 10^{-9}$ m²/s for cations and non-charged species, giving a resulting best estimate effective diffusivity of $2.1 \cdot 10^{-14}$ m²/s (SKB TR-10-52, Table 6-91). As the data are obtained *in-situ*, no lab-to-field transfer factor needs to be applied.

In the supporting method, a uniform lab-to-field transfer factor of 11.5 was applied to reduce the effective diffusivities obtained in the laboratory through-diffusion experiments. The derivation of the lab-to-field transfer factor is further discussed in Section 5.1.5. By applying this uniform reduction factor, the laboratory $D_{\rm e}$ -distribution (cf. Figure 5-3) was shifted downward and its central part matches the distribution of $D_{\rm e}$ derived from *in-situ* measurements reasonably well (SKB TR-10-52, Figure 6-81).

Importantly, no statistical analysis was performed for different subpopulations of *in-situ* formation factors in SR-Site regarding, e.g. rock type, deformation zone or non-deformation zone origin, or depth. Such an analysis was however made in SDM-Site (Crawford 2008). Results for Forsmark are shown in Figure 5-8 where the data are filtered by rock type, however, these data have not been corrected for surface conductivity bias (cf. Equation 5-3) and are associated with different levels of statistical support. Furthermore, sorting was also made based on unaltered/altered rock, samples taken from within/outside deformation zones, and combinations thereof.

The empirical distributions are broadly similar if allowance is made for sampling bias amongst the less well represented rock types. The conclusion was that no large systematic differences could be seen in the data based on these subpopulations. This presented a compelling argument for using a single parameterisation representing all rock types at the Forsmark site. The analysis, however, also included data from boreholes that were judged to be of lesser quality than those included in Figure 5-7.

This conclusion should be considered provisional, however, as the sorting is based on variables assigned in the Boremap methodology based on lithological and structural core logging and BIPS camera logging of the borehole wall (e.g. Stephens et al. 2007). The Boremap data may not be fully representative of the *in-situ* measurements since it is unknown how far out into the rock volume that Boremap variables can be considered accurately determined.

This is mostly problematic for locations where mapped rock and alteration types vary significantly over a decimetre to sub-metre scale. In an updated analysis it may be possible to assign local uncertainty to different parts of the Boremap results depending on the length scale over which parameter variation occurs.

It is proposed that the analysis from Crawford (2008) could be updated while keeping track of which data are of better or lesser quality. In doing this, it would be possible to include data from more recent (and upcoming) measurements. There may also be scope to expand the sorting criteria to include additional or updated parameters assigned in the Boremap system, particularly regarding association of rock alteration with identified flow bearing fractures. This would be in line with the detailed characterisation of the host rock suggested in Chapter 4. Even so, the available data suggest that a highly granular subdivision of the host rock into transport domains may not be warranted from an effective diffusivity point of view.

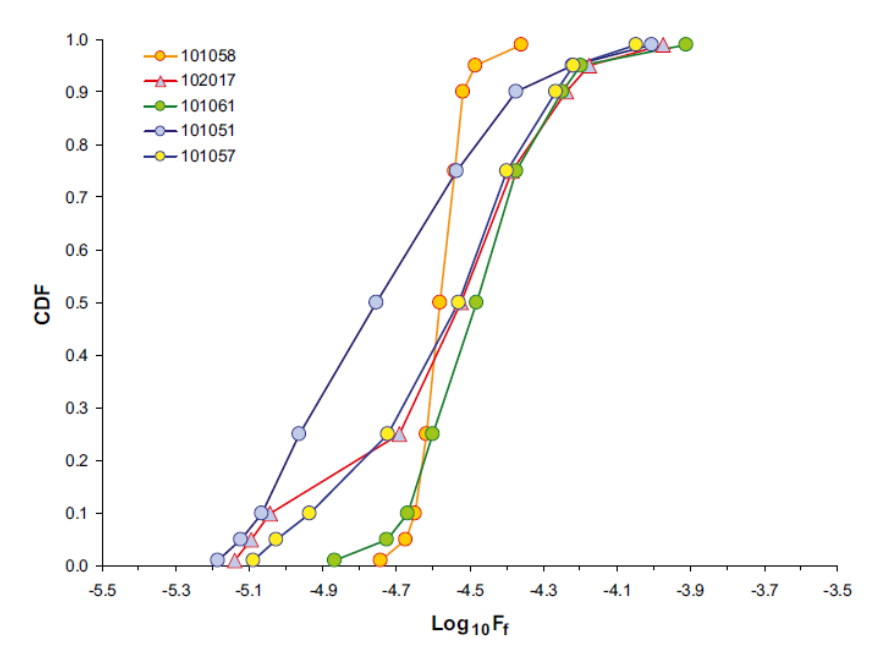


Figure 5-8. Empirical percentiles for in-situ matrix formation factors, specified according to rock type within rock domain RFM029 (fracture domains FFM01–03) and plotted as a cumulative distribution function, CDF. Data are plotted for (unaltered) rock types 101057 (~34,000 data points), 101051 (3,591 data points), 101061 (1,353 data points), 102017 (567 data points), and 101058 (382 data points). Reproduced from Crawford (2008, Figure H-10).

Concerning the diffusion available porosity of the undisturbed rock, its quantification was based on data obtained in the laboratory on small-scale rock samples. Based on flowpath averaging principles, the arithmetic means of the most volumetrically important Forsmark rock types (for samples taken from outside deformation zones) were used (Crawford 2008, Table 4-6). As a result, a best estimate porosity value of 0.23 % was suggested for de-stressed rock in the laboratory. For the porosity, it is likely that only small errors would be introduced by flowpath averaging, even if using a multilayer representation, since the pore retardation is typically dominated by sorption for most sorbing solutes (i.e. $K_{\rm d}\rho_b\gg\phi_p$). For this reason, it may suffice to use a single value in safety assessment, at least within transport domains.

In SR-Site, the diffusion available porosity was not assigned an uncertainty based on arguments related to flowpath averaging. In SR-Site, the same diffusion available porosity was assumed for cations, non-charged species, and anions. This is further discussed in relation to anion exclusion in Section 5.1.6.

For the effective diffusivity, the best estimate value for D_e was assigned an uncertainty range of $\pm 0.25 \log_{10}$ -units, where the uncertainty was primarily attributed to possible systematic errors in measurement and evaluation. It is recognised that this may be an underestimate and in Löfgren (2015) the most well-known sources of systematic error are described. Several proposals are made in the report for verification and methodological improvement which range from checking the calibration of the geophysical tool to investigating complex current propagation mechanisms that have previously been neglected.

5.1.5 Lab-to-field transfer factor

Laboratory measurements are typically made at atmospheric pressure. Under *in-situ* conditions, on the other hand, the hydrostatic pressure and mechanical rock stresses will result in a compressed porous system. It is generally assumed that this compression reduces both the connected porosity of the rock matrix and the effective diffusivity (by an even greater margin). This behaviour has also been clearly observed by performing through-diffusion and electrical formation factor measurements on core samples confined in a hydraulic pressure cell pumped to different pressures corresponding to *in-situ* stress levels (Skagius and Neretnieks 1986).

In SR-Site, the lab-to-field transfer factor $f_{s(D)}$ for the effective diffusivity was based on a comparison of formation factors obtained by electrical resistivity-based methods in the laboratory and *in-situ*. When comparing data from individual boreholes, one can see a broad trend where laboratory formation factors based on the electrical resistivity method are about one order of magnitude larger than those obtained *in-situ*. This is illustrated for borehole KFM01A in Figure 5-9, although the plot in fact displays apparent formation factors where no compensation has been made for surface conduction. When correcting for surface conduction bias the difference is slightly larger than this. For the borehole KFM01D, which is the only borehole where corrections have been made thus far, the formation factors are reduced by, on average, a factor of two relative to the uncorrected apparent values.

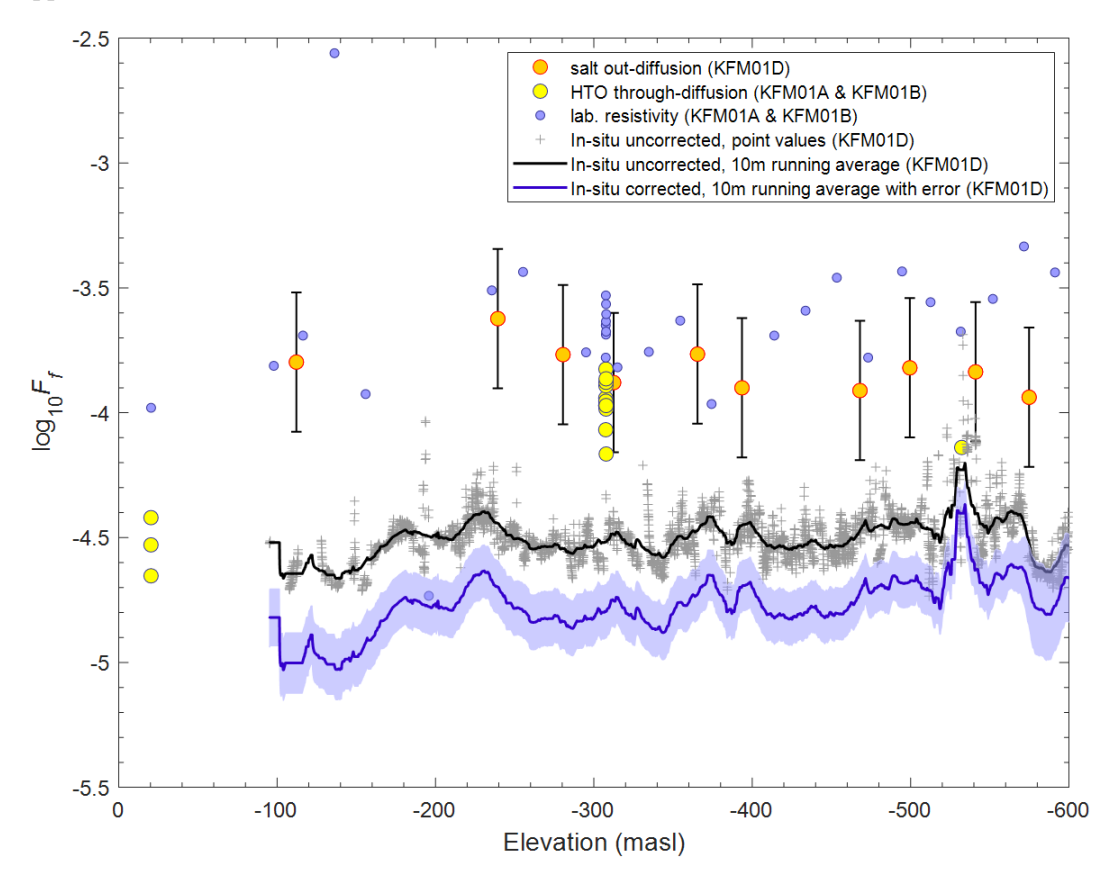


Figure 5-9. Plot of apparent formation factors from electrical measurements in-situ and in the laboratory, as well as results from through-diffusion and salt out-diffusion.

The sample volume used in laboratory measurements (20-100 cm³) is much smaller than the support volume of *in-situ* measurements which is at least a cubic metre, or likely more. For this reason, and for issues concerning mechanical damage discussed above, it was chosen not to make direct comparisons based on drill core sample locations in SR-Site. Instead, the empirical cumulative distribution of laboratory data was compared directly with the corresponding distribution of *in-situ* data (red and blue curves in Figure 5-3). From the ratio of median values of the empirical data, a factor of 11.5 was estimated as a uniform lab-to-field transfer factor for transport modelling in SR-Site. Deviations from this value when comparing the upper and lower tails of the laboratory data distribution are presumed to be due to sampling bias.

When the lab-to-field transfer factor is updated with new data in upcoming investigations, it is recommended not to pool all data from the site, but to filter the data using appropriate sorting criteria. In this manner, one may estimate different lab-to-field transfer factors for different depth ranges, and possibly rock and alteration types if the sample size is sufficiently large to avoid significant sampling bias. In doing this, however, data known to be affected by mechanical damage arising from the early drilling technique should be removed.

It should be highlighted that any systematic errors in the rock resistivity measurements made in the geophysical logging campaigns would also give a systematic error in the estimated *in-situ* effective diffusivities. The downhole tool used by SKB has been calibrated towards another similar tool with good results (Nielsen and Ringgaard 2004, Löfgren and Neretnieks 2005, Probst et al. 2005), although there are remaining unknowns. An independent means of quantifying the lab-to-field transfer factor would be to repeat the experiments of (Skagius and Neretnieks 1986) on site-specific rock samples from Forsmark and Laxemar-Simpevarp following a modernised measurement protocol⁵. This would imply measuring the rock formation factor in the laboratory under different confining pressures up to that of the *in-situ* rock stresses at the sites.

It is hypothesised that anionic transport is more sensitive to compression of the porous system, as such compression would likely first affect already constricted pore-throats. Increasing compression would presumably increase the population of very narrow pore throats prior to significant compression of the grain boundary porosity itself due to the need for grain boundaries to be in contact to transmit stress. This would result in an increased average constrictivity of the rock and increased effective tortuosity for anionic solutes which then need to find alternative diffusive pathways through the rock matrix.

As discussed in (Löfgren 2015) for alternating current, an electrolytic current can be propagated through rock samples even in the hypothetical case of total anion exclusion at pore throats where the rock is effectively a leaky cation selective membrane. For this reason, the procedure for estimating lab-to-field transfer factors in SR-Site is not applicable for anions in cases where anion exclusion is prominent. Consequently, an updated strategy for estimating lab-to-field transfer factors for anions needs to be developed within the upcoming site investigations. This is discussed further in Section 5.1.6.

A separate lab-to-field transfer factor, $f_{s(\phi)}$ was also introduced for the connected porosity in SR-Site. This was based on changes in the rock volume of drill core samples as they were subjected to triaxial compression tests (Jacobsson 2007). The uniform value chosen in SR-Site was $f_{s(\phi)} \sim 0.8$ for all rock types and all depths. In the SR-Site treatment, the transfer factor was intended to account primarily for mechanical damage leading to microcrack formation during core drilling and extraction. Although a constant site average value was assumed in SR-Site, the existence of a depth trend of increasing formation factor in the resistivity-based measurements for KFM01A (see Figure 5-9) suggests that the mechanical damage effect for samples retrieved from that borehole was nonconstant and likely related to the increased force needed for core drilling at increasing depths.

The transfer factor used in SR-Site was not intended to account for elastic compression of existing pore spaces due to confining *in-situ* stresses as this depends on the prevailing *in-situ* stress situation and will vary with location in the geosphere. The impact of stress-release as it relates to *in-situ* anion exclusion requires additional information concerning the *in-situ* stress field which was not feasible to incorporate into the lab-to-field transfer factor for SR-Site. It is intended, however, that this should be considered in greater detail in the continued site investigations. This will require greater integration with modelling and data provided by the Rock mechanics discipline.

5.1.6 Anion exclusion

Impact on storage porosity

The anion exclusion factor for the porosity $\xi_{a,\phi}(-)$ can be used to estimate the diffusion available porosity for anions. Here, we are mostly concerned with pore sizes in the mesoporous (2–50 nm) range as defined by the IUPAC standard (IUPAC 1976). In the present conceptualisation, individual hydrated anions are assumed to have access to virtually the entire porewater volume of the micropore although due to electrostatic repulsion of the negatively charged mineral surface the anion concentration decreases in proximity to the pore wall. At the same time, cations become more concentrated in proximity to the pore wall. The increased concentration of cations near the pore surface is then said to "shield" the bulk pore water from the negative charge of the surface.

⁵ It is presumed that earlier experiments may have used core samples subject to less gentle drilling techniques. There are also remaining questions concerning sealing techniques used to prevent current short circuiting in earlier studies that might need to be reviewed.

For a given storage porosity, ϕ_p (-) and BET surface area, A_s (m²/kg) within the rock matrix, an anion exclusion factor for the porosity, $\xi_{a,\phi}$, can be expressed as:

$$\xi_{a,\phi} = \frac{\phi_p - \lambda_a A_S \rho_b}{\phi_p} \tag{5-6}$$

where λ_a (m) is the effective distance from the pore surface from which anions are excluded. Although there is no true exclusion distance (in the strictest sense of the term) since anionic concentration varies continuously within the EDL, the exclusion distance must be interpreted as an effective parameter calculated by integration of the concentration profile across the pore aperture. Although inexact for very narrow pore spaces with overlapping EDL, λ_a can be approximated using the Debye length, λ_D (m). From the Debye-Hückel approximation, the Debye length is calculated as:

$$\lambda_D = \sqrt{\frac{\varepsilon \varepsilon_0 RT}{2F^2 I_S}} \tag{5-7}$$

where ε (–) is the relative permittivity of the pore water, ε_0 (F/m) is the permittivity of vacuum, R (J/mol·K) is the universal gas constant, T (K) is the temperature, F is the Faraday constant (A/mol) and I_s the ionic strength (mol/m³). At ambient temperature and assuming a simple 1:1 NaCl electrolyte, the Debye length (nm) can be approximately given by the formula (Stumm and Morgan 1996):

$$\lambda_D(\text{nm}) \approx 0.309 / \sqrt{I_s}$$
 (5-8)

where the ionic strength, I_s is specified in mol/l. For the range of typical groundwater ionic strengths found at the Forsmark site, λ_D typically ranges from about 2-4 nm and clearly will likely not affect the storage capacity for anions to a large extent. Assuming $\lambda_a \approx \lambda_D$ is a rough approximation, however, although is likely sufficient for scoping calculations concerning the impact of anion exclusion for a given average pore aperture. For very narrow pore apertures less than 5-10 nm, such as might be found in pore throats, more accurate numerical calculation of the concentration profile is necessary using the Poisson-Nernst-Boltzmann theory to estimate λ_a even at relatively high porewater ionic strengths.

Impact on effective diffusivity

It is not straight forward to estimate the anion exclusion factor for the effective diffusivity because the EDL may occupy a much larger fraction of the aperture (and possibly even overlap) at narrow pore throats relative to the bulk of the pore space where apertures are much larger. Based on the previous discussion of porosity, however, the aperture of such pore throats would need to be on the order of 10 nm or less to bring about a significant anion exclusion effect. Furthermore, scoping calculations suggest that the population of narrow pore throats featuring near total anion exclusion must approach the theoretical percolation threshold to have a large impact on the effective diffusivity.

As diffusion experiments are typically performed on rock samples that have been dried and then resaturated with synthetic groundwater, it seems possible that re-saturation might be incomplete if such narrow pore throats are numerous. On the other hand, it is not uncommon that behaviour consistent with an anion exclusion process is observed laboratory diffusion experiments. There are also indications from Finnish porewater chemistry studies (e.g. Eichinger et al. 2015) and *in-situ* tracer experiments that anion exclusion may be a significant process for geosphere matrix diffusive processes (Poteri et al. 2018a, b).

If the anion exclusion factor for effective diffusivity, ξ_{a,D_e} is to be quantified based strictly on empirical observations, such observations must be made under relevant conditions. This means preferably observations under *in-situ* conditions in rock volumes that have not undergone significant stress-release due to the presence of the exploratory borehole. This could be achieved by *in-situ* diffusion experiments, although such experiments would require unreasonably long contact times.

Although the anion exclusion factor cannot be deduced from electrical resistivity-based measurements, an electrical potential gradient can be used to drive anionic tracers over relatively long distances through the rock matrix in an electromigration based experiment. Such experiments would allow one to probe the rock matrix significantly beyond the stress-released zone.

Although there is risk of additional mechanical damage occurring during core drilling and sample preparation, it is also possible to re-stress drill core samples in the laboratory using a similar procedure as Skagius and Neretnieks (1986). The anion exclusion effect could then be studied using anionic tracers and either using a concentration gradient in a standard through-diffusion test, or an electrical potential gradient as the driving force. Another advantage of using re-stressed samples in the laboratory is that it allows one to study the effect over a range of different confining stresses. Other potential future studies could involve modelling the water saturation process, or resin impregnation experiments using radiocarbon-labelled MMA. The feasibility of preforming such an experiment *in-situ* has been previously demonstrated in Möri et al. (2003).

5.2 Interpretation of sorption properties from site-specific data

Site-specific data on sorption properties are typically obtained in laboratory experiments using rock samples taken from drill cores. As far as possible, samples are chosen to be statistically representative of different rock types and alteration classes. The samples selected for laboratory study are, however, limited in volume and thus sample-size related variations in mineralogy and sorptive surface area are expected to dominate uncertainty when extrapolations are made to *in-situ* reference conditions.

Measurements made using small particulate materials are thought to be more affected by these issues than monolithic samples. This is due to the smaller volumes of rock and contact solutions used in small particulate experiments, as well as biases introduced by the crushing procedure. The uncertainties in interpreting solute uptake kinetics for crushed rock also appear to be less pronounced for monolithic samples since solute uptake to monolithic samples more closely resembles the physics involved in field-scale retardation processes. In the present proposal data from both crushed rock and monolithic samples (including both in-diffusion and electromigration experiments) are suggested to be combined using a Bayesian updating approach to give recommended K_d estimates for reference rock types and groundwater compositions.

Much of the existing K_d data obtained in the SDM-Site investigations (Selnert et al. 2008, 2009b) were obtained in experiments using crushed rock. There were, however, some radionuclides that were studied in both crush and monolith experiments as well as a smaller number of through-diffusion experiments using 3 cm thick core slices in the LTDE-SD project (Widestrand et al. 2010a). Due to the long contact times required to obtain solute breakthrough in through-diffusion cells, only activity changes in the source compartments could be measured in LTDE-SD, which means they are effectively in-diffusion experiments. K_d values were also evaluated from penetration profiles (Widestrand et al. 2007). Although there is a large emphasis on crushed rock in the previous laboratory campaigns, there is scope for further analysis of these historical data sets to obtain more precise estimates of K_d that can be used in a supporting role for future laboratory campaigns investigating sorption properties of the rock.

The main problem associated with the use of crushed rock is that the crushing process increases the surface area by up to an order of magnitude depending on size fraction and might also increase accessibility to sorbing mineral surfaces that might otherwise be obstructed by adjoining matrix minerals in intact core samples. As sorption is a surface-related process, the sorption data needs to be corrected for the increased surface area. To account for this, normalisation with respect to surface area is required to extrapolate data from crushed rock to values appropriate for intact rock in the geosphere.

Furthermore, since sorption often occurs preferentially on different mineral surfaces, additional corrections may be needed if the mineralogy of the lab sample or the accessibility of these minerals differs from the *in-situ* rock. After making these corrections, the K_d value can be specified for a reference rock type and the groundwater composition used in the laboratory experiments. Large particles and monolithic samples are less influenced by surface area effects but can be difficult to work with in the laboratory because a representative penetration depth in the rock may be difficult to achieve in the limited time frame of a laboratory experiment.

The procedure for interpretation of sorption properties from site-specific data is similar for crushed rock and monolithic samples, although the corrections for surface area effects are modest and possibly negligible for monolithic samples. The necessary corrections are incorporated in the lab-to-

field transfer factors f_m and f_q for surface area and mineralogy effects, respectively. A modelling approach that accounts for diffusive disequilibrium and other kinetic processes may be needed to interpret the equilibrium state from tracer uptake time series data. This type of modelling introduces additional uncertainties and biases that are not always straight-forward to account for, although are necessary to avoid underestimation of K_d values. If the data do not exhibit a mechanistically relevant temporal trend or are excessively noisy, an alternative is to take a simple weighted average of the measurement data and neglect possible diffusive disequilibrium.

A process flowchart showing the principal flows of information and procedure for estimating K_d values for the *in-situ* rock is given in Figure 5-10. In the proposed framework for data evaluation, the symbol R_d^0 is used to indicate estimated equilibrium sorption partitioning coefficients for the crushed or monolithic rock prior to correction for surface area and mineralogical effects. The R_d^0 value is sample-specific for the characteristic sorptive surface area and mineralogy of the sample being studied. The symbol K_d^0 is used to represent the *in-situ* sorption partitioning coefficient derived for a specified reference groundwater composition after application of the lab-to-field transfer factors.

There are some differences in the way in which equilibrium $R_{\rm d}^0$ estimates are derived from solute uptake time series in the crush and monolith cases, although these are discussed in more detail in Section 5.2.1. Essentially, the transfer factor approach attempts to relate properties of the rock samples used in experiments to average properties of *in-situ* rocks. It is possible, at least in principle, to estimate sorptive properties for geosphere rock and alteration types that have not been studied by quantitative consideration of their mineralogy and microstructural characteristics relative to rocks that have been included in laboratory investigations. This hypothesis was used previously to import data from the Laxemar-Simpevarp site investigations to augment sorption data from Forsmark in the recommendation of $K_{\rm d}$ values for SR-Site (Crawford 2010) and SR-PSU (Crawford 2013) and is discussed in more detail in Section 5.2.2.

In cases where it is not feasible to perform laboratory experiments to obtain data on site-specific materials, an analogous although simplified procedure is used to estimate $K_{\rm d}^0$ values from literature data sources. This is illustrated in the flowchart given in Figure 5-11 which follows the same overall procedure as for site-specific data. Typically, literature data consists of single-point values measured after 7–28 days, often requiring digitisation from low-resolution graphics. In these instances, process-based modelling is usually impractical. Instead, a simple weighted average, may be used together with appropriately estimated lab-to-field transfer factors wherever possible.

When combining data from multiple literature sources, an approach based on Bayesian updating may be useful (see Section 5.2.5) provided the data are for sufficiently similar contact water compositions. This requirement may need to be relaxed and considered together with chemistry correction transfer factors using the methods described in Section 5.3 if the literature data are sparse. This approach for literature data, although ambitious given the data quality, may vary depending on the number of samples, relevant metadata, and reported uncertainties.

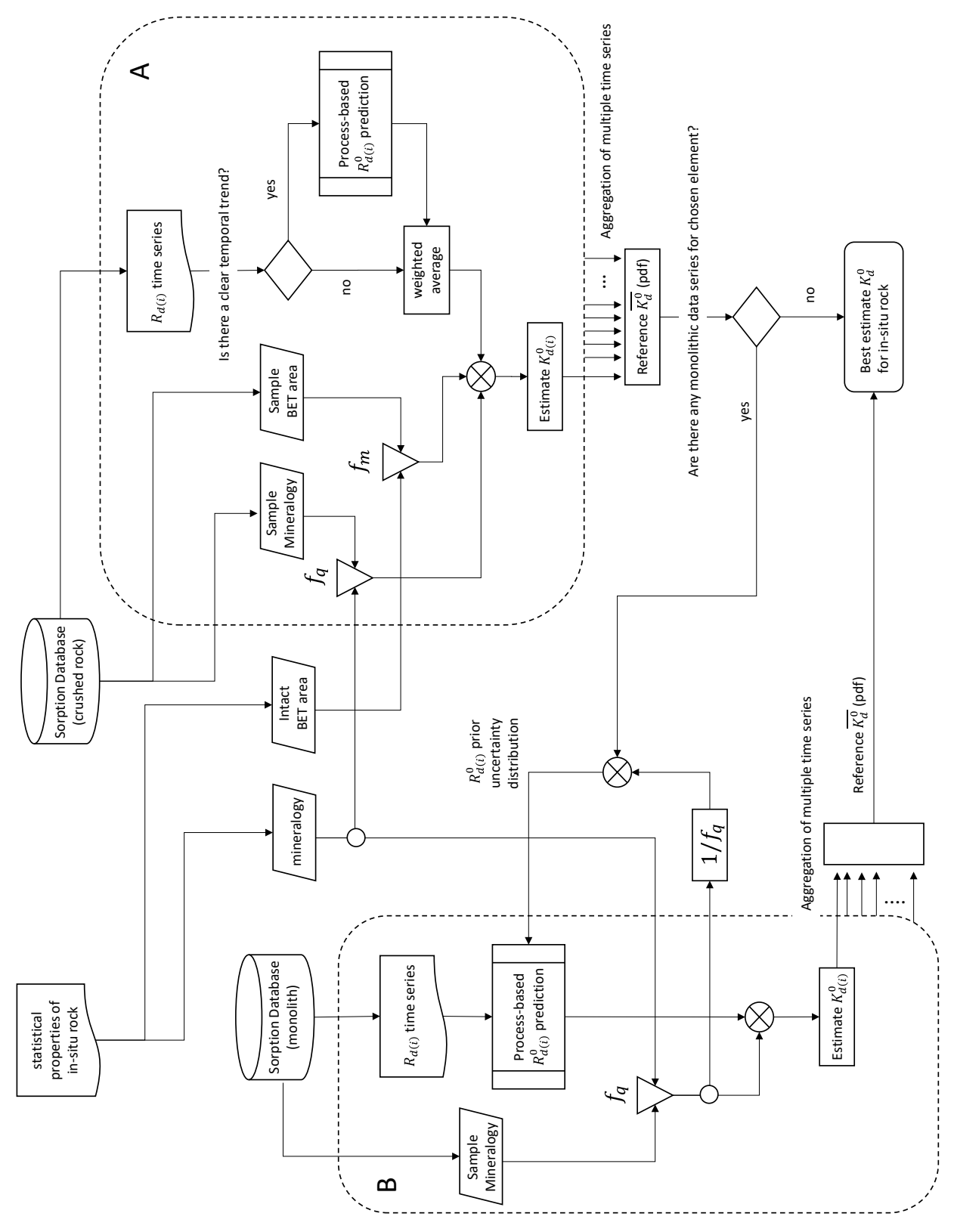


Figure 5-10. Procedural flowchart showing treatment of site-specific data obtained for A) crushed or otherwise non-cohesive materials (including strongly altered rock), and B) monolithic core samples. Finely divided fracture coating materials are excluded from this flowchart owing to a lesser relevance of diffusive uptake kinetics and surface area transfer factors for such materials.

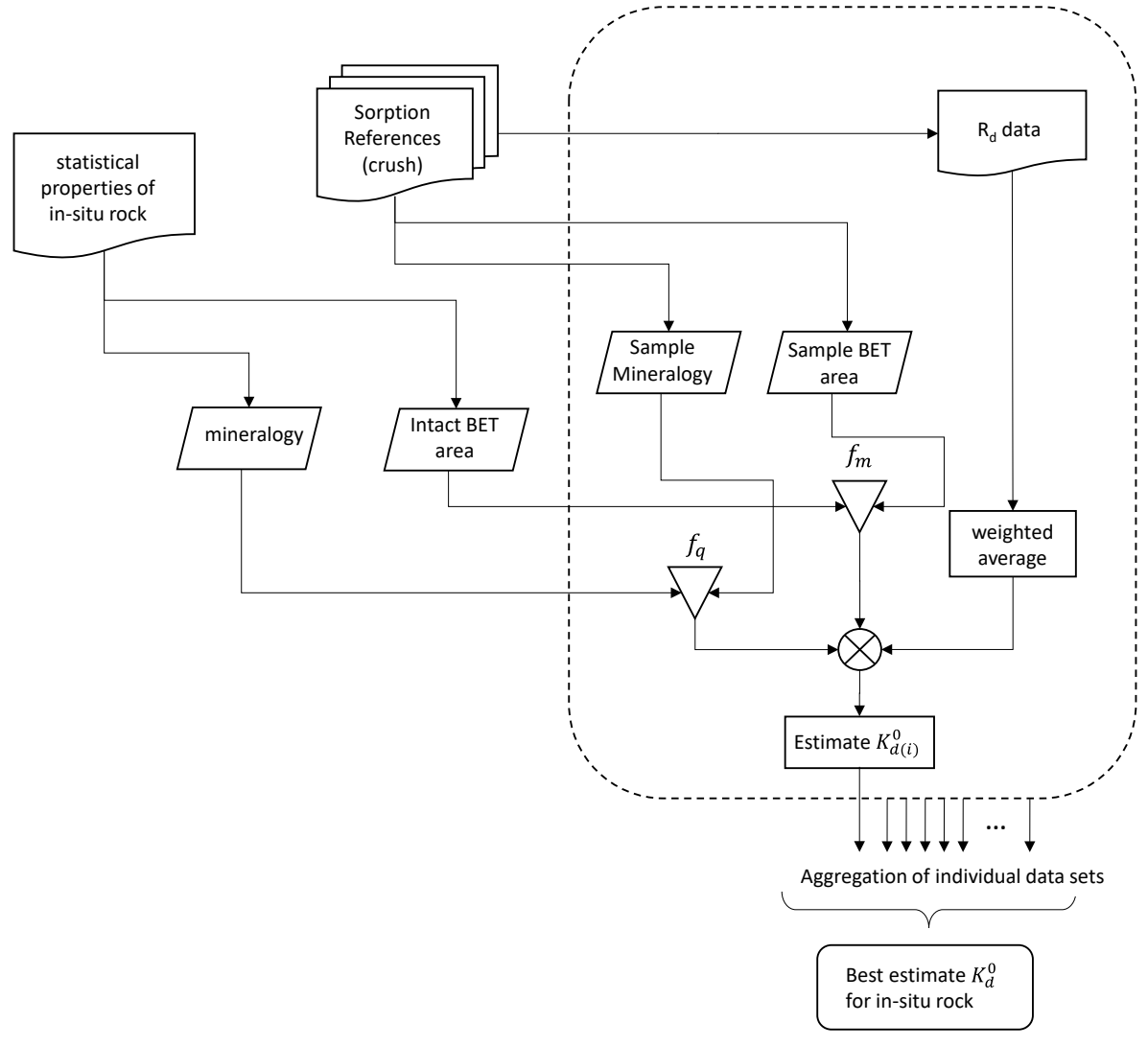


Figure 5-11. Procedural flowchart showing treatment of literature data (principally crushed rock). The same procedure is followed as for site-specific laboratory data as far as it is possible to do so. The feasibility of calculating f_m and f_q lab-to-field transfer factors, however, is dependent on the quality of documentation of the literature data and must be handled on a case-by-case basis. Similarly, the bulk of data available in the open literature are typically based on single measurements made after short contact times of 7-28 days. Since this strongly curtails the possibility of correcting for diffusive disequilibrium and other kinetic effects, it is assumed in the flowchart that process-based modelling is not feasible and simple weighted averages are used instead.

Recommended K_d values for application conditions are obtained by applying chemistry correction factors, f_{chem} to the reference K_d^0 values. This is not shown in Figure 5-10 although is discussed in depth in Section 5.3. Here, the application conditions may refer to statistics of groundwater composition for the present-day situation (site descriptive modelling), or projected compositions for some future state (safety assessment). Since it is only feasible to study a small number of representative groundwater types in laboratory studies, it is presumed that the chemical composition of the groundwater under application conditions may be subject to spatial and temporal variation and differ significantly from the reference compositions used in laboratory investigations.

5.2.1 Estimation of equilibrium R_{d}^{0} values from laboratory experiments

In upcoming laboratory campaigns, it is proposed that measurements using monolithic samples should be favoured, at least for those radionuclides where such experiments are deemed feasible. It is expected that monolithic samples should be less disturbed relative to the *in-situ* rock than crushed rock and therefore provide more accurate estimates of *in-situ* sorptivity than crushed rock, provided sufficiently detailed time series of solute concentrations can be acquired. The interpretation is not as clear for crushed materials where clear indications of equilibrium onset are absent as is the case

with most of the SDM-Site and LTDE-SD data. A key motivation for this preference is that the surface area corrections for monolithic samples are smaller and associated with less uncertainty than that required for the lab-to-field extrapolation of data derived from crushed rock samples.

Sorption measurements on thin sections can be used as a complementary method to discriminate the contributions made by different minerals toward the sorption magnitude measured in experiments using crushed and monolithic samples. Although relative sorptive surface areas of minerals imaged in thin section experiments may not be fully representative of proportions of reactive surfaces in contact with the rock matrix porosity, it is nevertheless a useful tool. It is envisaged that data obtained from such measurements might help inform corrections necessary to account for differing mineralogy and to disentangle their connection to groundwater chemistry.

Measurement time-series data can be interpreted by numerical fitting of diffusive uptake from a stirred vessel of limited volume using optimisation tools and Monte-Carlo modelling methods. Although additional features and processes including heterogeneous diffusion within a secondary porosity, kinetics, polydisperse particle size distributions, and impact of carrier colloids can be readily included in the modelling flow, the present demonstration calculations shown as an example in Figure 5-12 only consider single rate uptake to a monoporous matrix. In the case of heterogeneity (bi-porosity), it can be shown that the assumption of a single rate monoporous diffusion-sorption model cautiously underestimates equilibrium R_d^0 values when used to interpret time series data derived from laboratory experiments.

Issues related to stress release and mechanical damage at sample surfaces need to be considered in the interpretation of data from experiments using monoliths. This is because the effective diffusivity of core samples measured using through-diffusion experiments with tritiated water may not be fully representative of the pore system sampled by sorbing tracers which achieve a much more limited penetration depth during experiments of short duration (i.e. 6-12 months). The impact of this is suggested to be studied in more detail through the use of sensitivity studies in the data evaluation.

It is suggested that a mix of approaches is used since it is not straightforward to assess the relative merits of performing a small number of experiments using monoliths versus a larger number of less expensive measurements using crushed rock. Instead, different methods should complement each other and other methods such as using desorption and sorption to thin sections may provide additional valuable input.

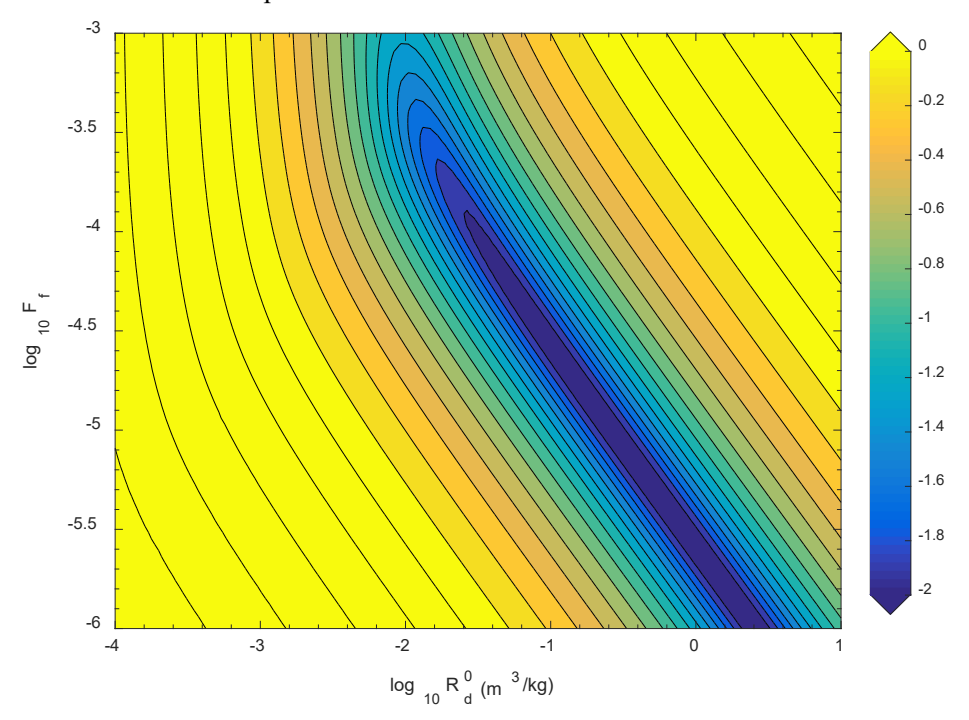


Figure 5-12. Least squares objective function for diffusive uptake of Ni(II) to crushed Forsmark metagranite (2-4 mm size fraction) sampled from borehole KFM07A (387.47 m) in contact with Forsmark saline groundwater. The diagonal ridge shown by dark blue shading of the plot indicates optimal combinations of R_d^0 and F_f that are equally consistent with the measurement data.

For the estimation of R_d^0 values from monolithic samples, the results are highly dependent on the precision with which the effective diffusivity of the sample can be determined. This is because it is not possible to uniquely separate the contributions of diffusion and sorption towards the observed uptake kinetics in the absence of independent information concerning the effective diffusivity. This is also an issue for experiments using crushed rock where onset of equilibrium conditions cannot be confirmed.

Although it is theoretically feasible to separate sorptive and diffusive properties by simultaneous analysis of aqueous phase time series and sorption depth profiles in monolithic samples, experience from the LTDE-SD project (Nilsson et al. 2010) suggests that this is difficult to achieve in practice. This is partly due to small penetration depths, limited resolution, high detection limits, and heterogeneity effects which do not conform to a simple matrix diffusion interpretation.

Independent assessment of diffusive properties of monolithic samples can, however, be achieved using electrical resistivity measurements or through-diffusion experiments performed using non-sorbing tracers for the same core samples. Since independent evaluation of effective diffusivity is subject to its own uncertainties, an efficient means of incorporating these uncertainties in the estimation of conditional $R_{\rm d}^0$ values is required. One way of doing this is using Bayesian estimation methods which quantify uncertainty ranges by direct sampling of underlying uncertainty distributions.

The optimisation problem for matching solute uptake data essentially involves fitting the product of sorption and diffusion parameters in the form of the material properties group, κ_{MPG} (Equation 5-1). Some care needs to be taken if R_d^0 and D_e (or, equivalently F_f) are estimated simultaneously in numerical evaluations since they are anti-correlated by way of the fitted material properties group. The impact of this can be visualised best by plotting the least squares objective function for the optimisation problem as a function of the two fitting parameters R_d^0 and F_f as in Figure 5-12. Although the plot indicates an upper limit of F_f and lower limit of R_d^0 that are mutually consistent with the measurement data, the entire ridgeline of dark blue values represents equally optimal parameter combinations.

While most optimisation methods will find viable local solutions to the problem, there is typically sensitivity of the result to initial conditions which can be easily confirmed by choosing different starting guesses for the optimisation problem. Furthermore, the location of the ridgeline defining the optimum κ_{MPG} and the accuracy with which it can be estimated is highly dependent on the precision of the underlying measurement data. Measurement time series characterised by small numbers of noisy measurements are often difficult to fit convincingly which degrades the overall quality of the evaluation if the ranges of statistical uncertainty are characterised by broad tails.

Since the data do not fully constrain the model, it is obviously important to have some way of fixing one, or the other parameter independently to derive useful results. For in-diffusion experiments using a monolithic sample, the effective diffusivity can be assessed with acceptable accuracy using either electrical resistivity measurements, by including a suitable non-sorbing tracer as part of the tracer spike cocktail, or even by subjecting the same core sample to a separate non-sorbing tracer experiment in a through-diffusion configuration.

If the penetration depth achieved in the experiment is very low, then the appropriate formation factor may be higher than that estimated from independent measurements. This is because the effective tortuosity of the rock matrix may not be fully representative of the bulk rock very close to the surface of the rock. Near the surface of the rock, it is expected to approach a limiting value of $\tau_D \approx 1$ whereas in the bulk rock matrix it can be as much as an order of magnitude larger. The porosity of the rock matrix may also be greater very close to the surface of the rock due to mechanical damage effects. These uncertainties can be expected to affect the interpretation of both monolithic and crushed rock experiments. The potential deviation for monolithic samples, however, may be easier to bound. The impact of these uncertainties will need to be considered in the data evaluation.

In the case of crushed rock, there is no simple way at present of assessing intraparticle effective diffusivity, so a broad range of assumed values typically needs to be considered. One way of inferring a fixed diffusivity is to run the experiment to such a time that equilibrium or near-equilibrium conditions can be inferred. For most of the radioelements studied in SDM-Site contact times longer than six months appear to be required to obtain an approach to equilibrium. In many cases, however, measurement noise makes the approach to equilibrium difficult to identify even if it might occur within the timeframe of the experiment.

5.2.2 Estimation of reference K_d^0 values for geosphere sorption

Below is an updated proposal for the estimation of K_d values for the *in-situ* rock under safety assessment conditions. The basic premise for assigning K_d values is similar to that adopted previously in SR-Site (Crawford 2010) and is based on applying a series of lab-to-field transfer factors to correct for various biases in the underlying measurement data derived from laboratory experiments. A theoretical derivation of the transfer factors together with a discussion of the various underlying assumptions is given in Appendix A. Assuming that the magnitude of sorption is both proportional to total sorptive surface area and the relative sorptive affinity of mineral surfaces, a reference K_d^0 value for intact *in-situ* rock can be estimated from the proportional rescaling formula:

$$K_{\rm d}^0 = R_{\rm d}^0 \cdot f_m \cdot f_q \tag{5-9}$$

The variables in Equation 5-9 are defined as:

- R_d Best estimate partitioning coefficient (m³/kg) for equilibrium adsorptive uptake on crushed or monolithic material corresponding to a specific rock type and mineralogical composition in contact with a specified reference synthetic groundwater used in a laboratory experiment.
- $K_{\rm d}^0$ Recommended partitioning coefficient (m³/kg) for equilibrium adsorption on intact *insitu* rock in contact with groundwater of identical composition to that used in laboratory experiments. The *in-situ* rock may or may not have different mineralogical composition and reactive surface area to that used in laboratory experiments.
- f_m A correction factor that accounts for differences in the total diffusion-accessible adsorptive surface area of geological materials used in the laboratory experiments relative to the *in-situ* rock.
- A correction factor to account for differences in mineralogy between the *in-situ* rock and that used in laboratory experiments which have an impact on the intensity of sorption on the micro-surfaces of the bulk rock matrix. The factor is related to the relative reactive surface areas of the minerals contributing towards the sorption. However, as a simplification it can often be quantified in terms of the volumetric fraction of sorption dominating minerals in the rock used in experiments relative to the *in-situ* rock. This is further described below and in Appendix A.

Although f_m and f_q are operationally defined in a simplified fashion in this work, their underlying mechanistic basis can be derived from first principles based on the thermodynamic description of surface complexation and cation exchange. Since the transfer factors are defined as ratios of variables with relatively large uncertainty bounds, they are treated as log-normally distributed variables. This implies that the Equation 5-9 can be expressed as a summation in the logarithmic domain:

$$\log_{10} K_{\rm d}^0 = \log_{10} R_{\rm d}^0 + \log_{10} f_m + \log_{10} f_q \tag{5-10}$$

In previous work the f_m transfer factor was referred to as a "mechanical damage" transfer factor to reflect the fact that the corrections are typically made to account for the damage incurred during crushing of rock to small particle sizes used in batch experiments. This, however, is not the only situation in which the correction factor might be used, and the concept is expanded in the present work to additionally account for sorptive surface area differences between different rock types *in-situ*. It might be used, for example, to estimate K_d values for altered rock to enable multilayer rock matrix representations in transport classes where measurement data are sparse. The feasibility of this, however, depends on our ability to quantify the sorptive surface area of altered rock possibly using independent proxy measures for surface area (e.g. using geophysical methods such as spectral induced polarisation or NMR). This is a possible area for future development within site descriptive modelling.

Reference $K_{\rm d}^0$ values need to be estimated for all rock and alteration types used in the retardation model. In cases where there are actual measurement data for the rock and alteration type under consideration, the task of extrapolation to *in-situ* conditions is less uncertain than the case where reference values must be extrapolated from data for other rock types. Equation 5-10 is formulated to be generalisable to other rock and alteration types that need to be assigned material properties in the

retardation model. The main difference is that material-specific values need to be calculated for the $f_{\rm m}$ and $f_{\rm q}$ transfer factors that reflect the microstructural and mineralogical properties of each material component in the retardation model.

Fracture coating materials consisting of one or more secondary mineral types will need to be dealt with on a case-by-case basis. It is presumed that fracture coatings can be handled similarly to intact rock by applying f_m and f_q transfer factors to reflect *in-situ* properties (and variability) relative to samples studied in the laboratory. It is expected that diffusive disequilibrium effects may be less important for sorption experiments involving fracture coatings relative to rock due to their higher porosity and friability. Care needs to be taken, however, in the interpretation of laboratory data if the *in-situ* fracture coatings are well-cemented relative to crushed samples used in laboratory investigations. For fracture coatings that are mineralogically well-defined or consist of a single dominant mineral type it might be possible to use thermodynamic sorption models taken from the literature to estimate their properties. This may be the case for ferric oxides, calcite, illite and clay minerals, although calibration of component additivity models against site-specific measurement data may be useful.

In SR-Site, the f_q transfer factor was only used to rescale data derived from Laxemar site-specific samples to K_d values appropriate for Forsmark rock types. The rock volumes that comprise the Laxemar-Simpevarp site investigation area have, on average, a biotite content that is roughly twice that of the corresponding rock volume at Forsmark although crushed samples have similar measured BET surface areas. For the same surface area of crushed rock, it was assumed in Crawford (2010) that the higher biotite content of Laxemar rock should sorb proportionally more strongly than if the surface area was comprised of less strongly sorbing minerals.

Preferential sorption of some fission products and actinides on mafic minerals and iron oxides in granitic rock has been widely acknowledged for many years based on autoradiographic studies that have been influential in radioactive waste management literature (e.g. Allard and Beall 1979, Beall et al. 1980, Allard 1982, Torstenfelt et al. 1982, Vandergraaf and Abry 1982, Pinnioja et al. 1983, Allard et al. 1985, Ittner et al. 1988a, b). The key mafic minerals in granitic rocks principally include biotite and its alteration product chlorite, as well as amphibole (hornblende). Although not a mafic mineral, muscovite mica is also included since it has very similar crystallographic properties to biotite.

More recent studies, although confirming the importance of mafic minerals, suggest a more prominent role for feldspar minerals, and to a lesser extent quartz than was previously inferred. This is at least partly because quantification of sorbed activity in film autoradiography requires microphotodensitometric evaluation calibrated with suitable reference standards which is a relatively coarse and low sensitivity approach (e.g. Pinnioja et al. 1983). Modern digital autoradiographic techniques with improved sensitivity, however, enable the quantification of sorbed activity in association with individual mineral grains in thin-section sorption experiments at a level of detail that was simply not possible previously (e.g. Delayre et al. 2020, Fabritius et al. 2024).

Although the more recent studies suggest a nuanced view on the role of mafic minerals, the sorptive contribution of feldspar minerals and quartz is at least partly related to surface roughness effects where the greatest sorption is associated with grain boundaries, cracks, surface pits, and structural features such as edge/kink and defect sites (e.g. Demnitz et al. 2022a, b). Since the polished surfaces of thin sections used in autoradiographic studies are clearly not representative of the matrix porosity itself (i.e. being a polished cross-section of the rock) this presents complications if the data is to be used to assist in the parameterisation of a component additivity sorption model for intact rock. The relationship between sorptive surface area sampled in autoradiographic studies and surface roughness of minerals, however, can be accounted for if it is quantified using a technique such as vertical scanning interferometry (Demnitz et al. 2022a, b). This might allow the estimation of more accurate surface area-normalised, K_a values for minerals contributing towards sorptivity in the bulk rock.

In the K_d data compilation used by Posiva in the TURVA-2012 safety assessment (Hakanen et al. 2014), it was assumed that all diffusion accessible surface areas should have the same sorption site density and sorptive affinity. It was furthermore assumed that sorptive surface area was dominated by mica minerals (principally biotite and chlorite) so that *in-situ* reactive surface area for sorption could be estimated directly from the volumetric proportion of mica in the rock and the BET surface area measured for crushed samples of pure biotite. For some rock types, an additional empirically determined factor was included to account for the accessibility of the surface area for matrix diffusive processes.

In the present SKB proposal, the f_m transfer factor is defined in terms of the measured BET surface area of the rock used in laboratory experiments and the corresponding intact rock *in-situ*. As shown in Appendix A, the transfer factor correction for bulk surface area can be applied separately to the mineralogy transfer factor. The mineralogy transfer factor, f_q is defined as a weighted sum of contributions from individual minerals contributing towards the measured magnitude of sorption in laboratory experiments. This is quantified in terms of the surface area fraction, $f_{q(j)}$ of each solution-facing mineral in the rock used in sorption experiments relative to the reference rock type, and the fraction of total activity sorbed by the mineral surface, $f_{r(1,j)}$ as assessed by, for example, thin section autoradiographs for the same contact water composition:

$$f_q = \sum_{j=1}^n f_{q(j)} \cdot f_{r(1,j)} \tag{5-11}$$

Since the true reactive surface area contributed by each mineral in the rock matrix is difficult to assess quantitatively, it is necessary to introduce simplifying assumptions. For the estimation of f_q it is assumed that the component-wise surface area fractions of each mineral are approximately proportional to the mineral volume fraction over a small range of mineralogical variability. In the limiting case of a single mineral or mineral group (e.g. mica) dominating sorption, then Equation 5-11 simplifies to the ratio of mineral fractions for the dominant contributor in the rock used in laboratory experiments relative to the reference *in-situ* rock type.

For radioelements where thin-section autoradiography measurements are unavailable for the estimation of the $f_{r(1,j)}$ weights, then it might be possible to calculate these based on extrapolation from available data for a near geochemical analogue. Failing this, it may be necessary to calculate the weights from first principles using a component additivity modelling approach. A more detailed explanation of the calculation of the mineralogical transfer factor, f_q and its uncertainty may be found in Appendix A.

Although not based on site-specific materials or water compositions, the quantitative autoradiographic measurements reported by Pinnioja et al. (1983) give some broad hints on the relative contribution of different primary mineral phases for several radioelements of interest. For Cs(I), it was found that the K_d ratio for biotite was about 1500 relative to quartz and on the order of 250 relative to K-feldspar. For Am(III), on the other hand, the ratio was 16 for sorption on biotite relative to quartz, and roughly 30 relative to K-feldspar. For Co(II), the ratio was 24 for sorption on biotite relative to quartz, and roughly 17 relative to K-feldspar.

Since the mica content of the main Forsmark rock types is relatively low, the non-mica minerals likely contribute a greater share of sorption than might be expected based purely on the relative K_d ratios estimated for the non-mica minerals where biotite is clearly dominant. For the volumetrically important metamorphic granite to granodiorite rock type (101057), for example, the average biotite content is only about 5 %, meaning that the non-biotite minerals may contribute as much as 20 times the reactive surface area of biotite (assuming that reactive surface areas are roughly proportional to mineralogical volume fraction which is uncertain).

Here, it is probably reasonable to assume that the sorption of Cs(I) is dominated by biotite in which case a simplified calculation of f_q is possible in accordance with the discussions above. For Am(III) and Co(II), however, the non-mica minerals might contribute roughly in parity with biotite to the overall sorption. This would imply a reduced sensitivity to mica content at least for small variations of the volumetric content of this mineral group. A further aspect that might be important to consider is the specific surface area of the mica minerals relative to the quartz and plagioclase/alkali-feldspar content since the present discussion assumes a division of reactive surface area in proportion to volumetric mineral content.

If the specific surface area of mica minerals in the rock contributes a greater share of reactive surface area than the mineralogical volume fraction suggests, then this would likely reduce the importance of non-mica minerals towards the measured bulk sorptivity. Studies such as Dubois (2011) suggest that specific surface areas of biotite and chlorite are as much as an order of magnitude higher than those of quartz, plagioclase and alkali feldspar minerals for crushed samples in the same size range.

The issue is further complicated by the fact that different surfaces of phyllosilicate minerals feature different reactivity for surface complexation and cation exchange reactions which might be important to consider when assessing the overall contribution of these minerals to sorption.

Whether or not the mineralogical transfer factor can be neglected in the case of Am(III) and Co(II) also depends on how chemistry transfer factors are calculated. If a generalised composite model of sorption is adopted and a suitably calibrated model exists, then it may be feasible to omit the mineralogical transfer factor altogether for Am(III), Co(II), and their geochemical analogues if it can be shown that the different mineral phases contribute equally towards the overall sorptivity. If a component additivity approach is used, on the other hand, the relative contributions of each mineral component would likely still need to be modelled for the chemistry extrapolation.

Presently, the quantitative evidence for variation of K_d with mineralogy is weak for Forsmark site-specific rock with the possible exception of Cs(I) sorption. This is at least partly due to the low mineralogical variability between samples studied in the laboratory programme and the small number of drill core sections sampled. Since the relative variation of BET surface area between the different crushed size fractions was larger, the impact of surface area on the magnitude of measured K_d is much clearer.

For extrapolation to *in-situ* conditions, the uncertainty surrounding the impact of mineralogy is exacerbated by issues of representativity where there are not insignificant differences between samples used for mineralogical point counting and those used in laboratory sorption studies. The uncertainty of the point counting method for the typically low volume fractions of mafic minerals in the rock is also an issue that needs to be considered. An alternative procedure using quantitative XRD measurements on the same crushed rock samples used in laboratory sorption measurement may be preferable, although this remains to be investigated. Modelling using a component additivity approach may be used as to disentangle the effects of surface area and mineralogy on macroscopic K_d estimates. In this case variability arising from differing mineralogy would be included as part of the overall envelope of uncertainty for estimated K_d^0 values. In some cases, a lab-to-field transfer factor based on cation exchange capacity (CEC) measurements may be preferable to separate surface area and mineralogical transfer factors, at least for cation exchanging solutes, Cs(I) in particular.

5.2.3 Sorptive surface areas, CEC, and mafic mineral content of site-specific rocks

In general, it is not possible to directly measure sorptive surface area of rock and it is necessary to use a proxy measure such as the BET surface area derived from measurement of adsorption of gaseous probe molecules (typically N_2 or Kr) on pore surfaces. In SDM-Site, N_2 -BET surface areas of rock samples used in laboratory experiments were measured although only for the smallest (0.063–0.125 mm) and largest (2–4 mm) sieve size fractions, whereas sorption experiments were carried out on the 0.063–0.125 mm, 0.25–0.5 mm, and 1–2 mm size fractions. To not introduce any unnecessary uncertainties, it is suggested that the specific surface area of all fractions used for sorption studies are measured.

Cation exchange capacities were previously measured on site-specific geological materials including crushed rock in SR-Site using the ISO 13536 method for batch CEC determination using $BaCl_2/MgSO_4$ (Byegård et al. 2008). It was found, however, that due to the low CEC of the rock, the measurement uncertainty was very high and roughly the same order of magnitude as the central estimate for the smallest size fraction (0.063–0.125 mm). For larger size fractions quantification was not feasible and the CEC could only be estimated as being less than a specified value, on the order of ~ 1 cmol/kg

In the previous work (Crawford 2010, 2013), it was assumed that biotite would dominate the sorptive properties of the rock and contributions from other minerals were neglected. In the updated methodology, sorptive contributions from other minerals are to be considered to the extent that this is possible to quantify. The feasibility of doing this is to be investigated during the continuing site investigations. The following paragraphs therefore are specific to the previous handling in SR-Site and assume that variations in the volumetric content of mafic minerals fully determine the mineralogy transfer factor.

Since the mineralogy correction factor was only used to extrapolate R_d values from the Laxemar site to Forsmark rock types in SR-Site, the estimated Fe content of the rock was proposed in Crawford (2010) as an alternative proxy measure to calculate f_q . Here, it was assumed that the mafic minerals (principally biotite and chlorite) mostly dominate both the Fe(II) content and the CEC of the main rock types at Forsmark and Laxemar. For this a detailed statistical analysis of Fe-content was available (Sidborn et al. 2010) at the time of the K_d report preparation (Crawford 2010) and therefore this was used to calculate the site-average f_q .

In SR-Site, the mineralogical correction was applied to site-specific R_d data for Cs, Sr, Ni, Ra, Np, and U, whereas data for Am and Eu were not adjusted. Am and Eu were not adjusted since studies in the literature (e.g. Kienzler et al. 2009) suggested that unlike for other elements studied there may not be a strong sorptive association of trivalent radionuclides with dark minerals including biotite. The calculated f_q value was treated as a site average and no attempt was made to discriminate between the much smaller number of measurements that were made with other rock types. Since the estimated transfer factor was only considered order-of-magnitude accurate and because the bulk of site-specific sorption data for Laxemar was obtained on Ävrö granite, this was considered sufficiently accurate for purpose.

It can also be noted that in the Finnish safety assessment TURVA-2012 (Hakanen et al. 2014), the measured BET surface area of gneissic rocks is wholly attributed to their mica content for the purpose of calculating lab-to-field transfer factors for K_d estimation. This is probably a much better assumption for the Olkiluoto site given the substantially higher biotite content of the Finnish rock (10 to 30 %) relative to the Swedish rock types.

5.2.4 Relations between surface area, mineralogy, and sorptivity

In the proposed methodology, the underlying concept of rescaling R_d values to *in-situ* conditions using lab-to-field transfer factors is based on the premise that sorptivity is proportional to both sorptive surface area and relative proportion of minerals with high sorptive affinity. This is central for the applicability of the lab-to-field transfer factor approach (Equation 5-9), and for calculation of the overall uncertainty of extrapolated K_d values. Although a correlation between equilibrium R_d and BET surface area is expected for surface complexation processes, the role of mineralogy is less clear at present. The absence of a clear correlation between equilibrium R_d and mafic mineral content for a given solute would lend weight to the prospect of neglecting the f_q transfer factor in such cases.

It is envisaged that a range of different approaches be brought to bear on this problem including statistical analysis of extant data from SDM-Site, newly acquired data from the detailed site investigations (including quantitative autoradiographic studies where possible), as well as additional modelling and sensitivity analyses based on thermodynamic data published in the scientific literature.

From the site-specific data obtained during SDM-Site (Selnert et al. 2008, 2009b) a moderate degree of support exists for a correlation between R_d of some radionuclides with both BET-surface area and mica/mafic mineral content, although the correlation is significantly stronger for BET-surface area. The most convincing correlation is found for the cation exchanging solute, Cs(I) as might be expected based on its known preferential sorption on biotite. The covariance of R_d with mica content for Ni(II) and Ra(II), on the other hand, is weak although cannot be entirely ruled out. For Am(III) and Eu(III), however, the effect appears to be below the level of stochastic noise associated with the measurements and unquantifiable. For these elements, attribution of sorptive variation between different mineral surfaces might be necessary in order to extrapolate to differing groundwater compositions, even if f_q might be reasonably neglected for the reference groundwater compositions where K_d measurement data are available.

5.2.5 Aggregation of sorption data and extrapolation to geosphere reference conditions

There are multiple available options for aggregation of sorption data and extrapolation to the reference *in-situ* rock type for each specified reference groundwater. The basic idea, however, is that the aggregation procedure should be robust to combining data from different sources with varying degrees of uncertainty, e.g. data derived from crushed rock measurements, in-diffusion experiments on monolithic samples, and literature data values. In the case that only data for crushed rock are available, then an aggregation procedure based on calculating the weighted average (sample number and variance) of the uncertainty distributions calculated for each time series individually is suggested.

The calculation of a weighted average of individual estimates assumes a sufficient sample size that it is a reasonable approximation of the true sampling distribution. On the other hand, when combining data from various sources such as crush and monolith experiments, or when dealing with a limited sample number, a Bayesian updating-based data aggregation approach may be more suitable. However, data from different experiment types may not be equally accurate or of the same quality. This issue often arises when there are many measurement time series for crushed rock but only a few, presumably more representative, monolith-type measurements.

In such cases, the crushed rock data can be assigned a different weight depending on the degree of subjective uncertainty attributed to the underlying modelling interpretation. The crushed rock data can then serve as a prior uncertainty distribution for the reference $K_{\rm d}^0$ value. In some cases, we might have good prior information and can assign a well-bounded uncertainty distribution. In other cases, we might not have very good prior knowledge and then need to use a very broad or "non-informative" uncertainty distribution for the prior.

Figure 5-13 shows an example for Cs(I) sorption studied in the supporting lab programme of the LTDE-SD experiment (Widestrand et al. 2010a). The plots show the impact of combining data for crushed rock and monolithic in-diffusion experiments using a Bayesian updating approach based on (Gelman et al 2004). The posterior predictive sampling distribution for $\log_{10} K_d^0$ is plotted as a normal fit to the numerically sampled data (solid blue curve) together with a numerically calculated kernel density estimate (orange broken curve). Results for the non-informative prior case (red curve) and the convex combination case (green curve) are also shown. The prior uncertainty distribution for $\log_{10} K_d^0$ based on interpretation of crushed rock data is shown as the broken light-blue curve. The individual data estimates from a preliminary modelling interpretation of monolithic uptake data are plotted for reference purposes as staggered circular markers with error bars corresponding to the posterior predictive estimates calculated for each time series.

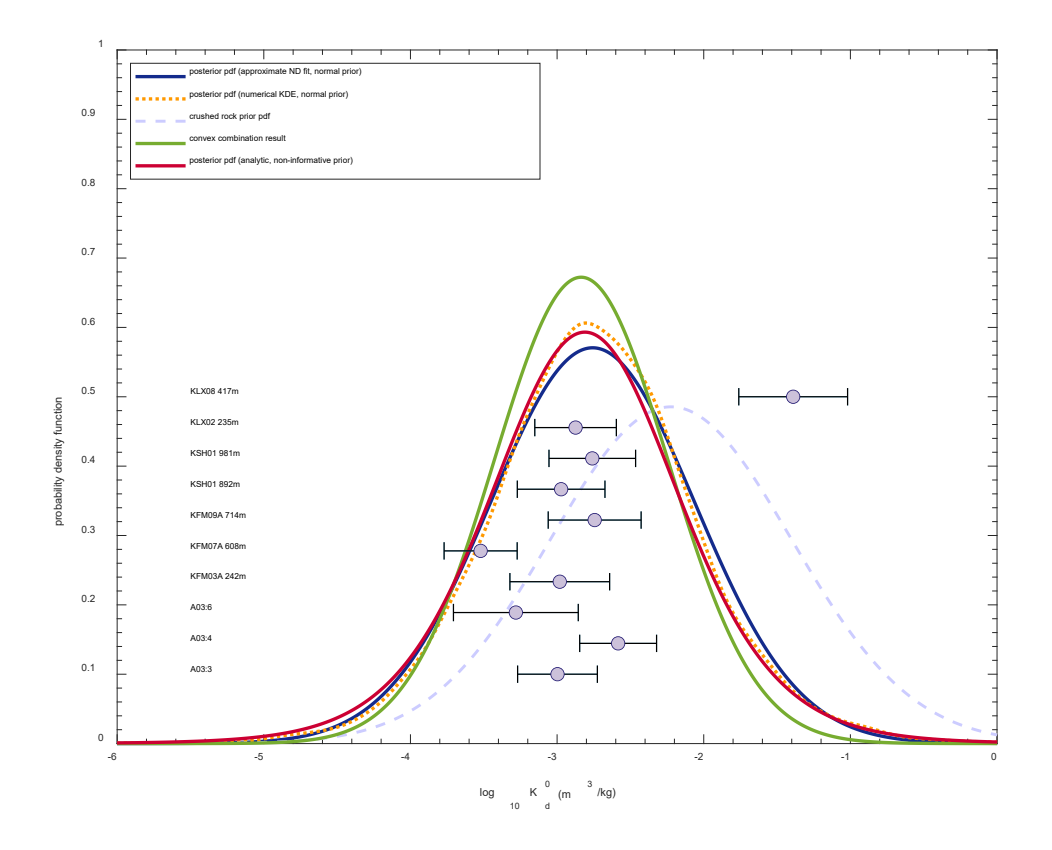


Figure 5-13. Comparison of results from Bayesian updating calculations for Cs(I) sorption in LTDE-SD synthetic groundwater. The broken orange curve shows the kernel density estimate of the posterior distribution while the unbroken blue curve shows a normal fit to the same sampled data. The prior pdf for crushed rock is plotted as the light blue broken curve. The unbroken red curve shows the posterior pdf distribution for the non-informative prior. For comparison, the uncertainty distribution calculated using a simple convex combination procedure is shown as a green unbroken curve. The estimated data for the available monolith experiments are overlaid as circular markers with error bars for reference.

As can be seen from Figure 5-13, the prior (6 time series for crushed rock) has only a small impact on the posterior sampling distribution when assigned a weight of unity together with 10 monolithic data sets. If a larger weight were to be assigned to the crushed data set, however, the posterior would be shifted closer to the prior. An additional example is shown for Se sorption in Figure 5-14. In this case, the prior (6 time series for crushed rock) has a larger impact when combined with 4 monolithic data sets, although the effect is still limited when the crushed rock is assigned a weight of unity. In both examples, only the f_m transfer factor is considered in calculations since the effect of mineralogy is insufficiently well characterised for all data sets for the f_q transfer factor to be applied consistently throughout. It is interesting to note that the spread of data for the monolithic experiments is relatively small even though they represent a mix of Forsmark, Laxemar, and Äspö site-specific rock types without correction for mineralogical differences.

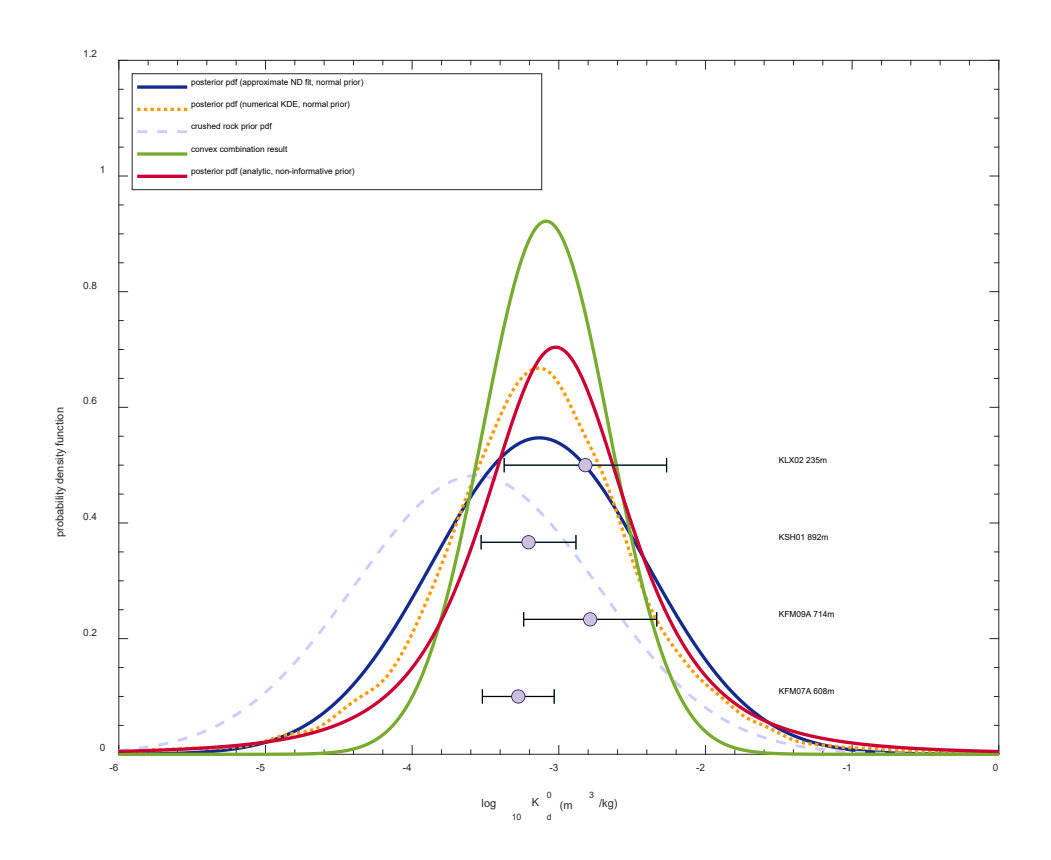


Figure 5-14. Comparison of results from Bayesian updating calculations for presumed Se(IV) sorption in LTDE-SD synthetic groundwater. The broken orange curve shows the kernel density estimate of the posterior distribution while the unbroken blue curve shows a normal fit to the same sampled data. The prior pdf for crushed rock is plotted as the light blue broken curve. The unbroken red curve shows the posterior pdf distribution for the non-informative prior. For comparison, the uncertainty distribution calculated using a simple convex combination procedure is shown as a green unbroken curve. The estimated data for the available monolith experiments are overlaid as circular markers with error bars for reference.

5.3 Extrapolation of K_d values to application conditions

In the methodological framework established in SR-Site (Crawford 2010) and further developed in Section 5.2, the mechanical damage and mineralogical transfer factors are used to estimate K_d^0 values for an intact reference rock type and for a specified porewater composition. In this framework, it is also tacitly assumed that K_d values for hydrothermally altered or otherwise mechanically damaged rock close to fracture surfaces can be estimated by choosing f_m and f_q transfer factors appropriate for the geological microstructure under consideration regardless of whether there are laboratory measurements (anchor values) underpinning the data for altered rock. In the cases where there are empirical measurement data (K_d) for altered rock, these should therefore be directly relatable to the corresponding values obtained in fresh rock if the use of surface area and mineralogical transfer factors is to be defensible.

Since groundwater chemistry has by far the largest impact on sorptivity, however, additional consideration must be given to how the groundwater composition under application conditions differs from that used in laboratory experiments. Here, "application conditions" can be taken to mean either the existing groundwater chemistry profile (i.e. reference state) prior to repository construction and operation, or projected safety assessment conditions.

In SR-Site, an additional transfer factor, f_{chem} was defined to account for deviations of groundwater chemistry from the reference compositions used in the laboratory experiments. Although the reference compositions were chosen to reflect typical groundwater types, they were also perturbed relative to the originally specified compositions. This was deemed to be most likely due to readjustment of pH and carbonate concentration in response to the low pCO₂ in the headspace of the

glove boxes used for sorption experiments. The chemistry correction transfer factor, f_{chem} was conceptualised in a similar fashion to the previously defined lab-to-field transfer factors:

$$K_{\rm d} = K_{\rm d}^0 \cdot f_{\rm chem} \tag{5-12}$$

Here, f_{chem} is defined in terms of the theoretically calculated ratio of K_{d} values for the application groundwater condition, K_{d} relative to the reference (laboratory) composition, K_{d}^{0} :

$$f_{\text{chem}} = \frac{\kappa_{\text{d}}}{\kappa_{\text{d}}^{2}} \tag{5-13}$$

A key difference between this transfer factor and the f_m and f_q transfer factors discussed previously is that f_{chem} is not necessarily a lognormally distributed uncertainty when considering more than a single groundwater composition. This is because it can incorporate features of spatial-temporal variability that are flowpath-specific or related to groundwater compositional statistics that do not need to be lognormally distributed. In this conceptualisation we seek to distinguish between physical properties that are uncertain although mostly temporally invariant (e.g. sorptive surface area and mineralogy) and properties that have significant temporal variability (groundwater composition).

The distinction here is arbitrary and relates more to how data are typically used in modelling rather than a specific underlying feature of chemistry versus the physical properties of the rock. As an example, each rock and alteration type in the multilayer retardation model has reference properties that are extrapolated from laboratory measurements using f_m and f_q transfer factors. As outlined in Section 5.2.2, these are formally defined as having approximately lognormally distributed uncertainties. In transport calculations one may seek to calculate a flowpath average for a larger volume of rock or a flowpath featuring multiple transport classes. The flowpath average will have an uncertainty that is inherited from the properties of the underlying geological materials. This may be associated with a normal or lognormally distributed uncertainty depending upon how the mean property is calculated. The calculated uncertainty, however, is defined for a reference groundwater composition that is fixed.

For extrapolation to variable groundwater composition, the uncertainty distribution of f_{chem} can incorporate a range of different sources of variability (e.g. groundwater statistical variation) and uncertainty (i.e. thermodynamic model parameters, etc.). In the general case of multiple minerals that contribute towards sorptivity, it is not possible to separate f_q and f_{chem} in a simple fashion and a more complex mathematical treatment is required in order to compute f_{chem} (see Appendix A). For each groundwater compositional vector, i (amongst possibly many), the chemistry transfer factor is defined as:

$$f_{\text{chem}(i)} = \frac{\sum_{j=1}^{n} f_{q(j)} \cdot f_{r(1,j)} \cdot f_{c(i,j)}}{\sum_{j=1}^{n} f_{q(j)} \cdot f_{r(1,j)}}$$
(5-14)

Here, the $f_{q(j)}$ and $f_{r(1,j)}$ variables are the same as defined previously in Equation 5-11, and the $f_{c(i,j)}$ factors are mineral-specific for those minerals that contribute to the overall sorption:

$$f_{c(i,j)} = \frac{K_{d(i,j)}}{K_{d(j)}^0}$$
 (5-15)

If the probability density function describing the distribution of f_{chem} over all considered groundwater compositions is not lognormal, then it cannot be added in log-space analogously to Equation 5-10 and should be calculated by convolution of the probability functions describing K_d^0 and f_{chem} instead. The resulting conditional distribution is then the marginal probability distribution of K_d integrated over all feasible groundwater chemistries, i specified in the calculation of f_{chem} .

The uncertainty distribution calculated using Equation 5-12 should be understood as being context dependent. The f_{chem} transfer factor, for example, could represent the chemistry at a single point in space and time that is obtained from hydrochemical modelling. In this case it might be a single value, or possibly a central value with an associated uncertainty distribution. In the context of a larger spatial volume (e.g. a portion of the geosphere), however, the uncertainty distribution computed for K_d could represent the likelihood of K_d being in a specified range for any random location in that volume, or even a flowpath averaged value. The context in which the f_{chem} factor is derived and the resulting probability distribution for K_d therefore must take into consideration both how the K_d value is going to be used in modelling and the physical interpretation of that use if it is to be meaningful.

The extrapolation of reference K_d^0 values to *in-situ* conditions using chemistry transfer factors based on mechanistic modelling is, for all practical purposes, a procedure for "Smart K_d " calculation as it is informally referred to in the literature (e.g. Kulik 2002). The proposed use of thermodynamic sorption models in combination with statistics of measured (or modelled) groundwater compositions to predict probability distributions of site-specific K_d values is also broadly similar to other proposals found in the literature (e.g. Turner and Pabalan 1999, Stockmann et al. 2017). It is also similar to the handling of K_d values for bentonite in SKB safety assessments (e.g. Ochs and Talerico 2004).

The workflow for extrapolation of K_d^0 values to application conditions is shown in Figure 5-15. Here, the reference groundwater compositions are the synthetic contact waters used in laboratory experiments studying sorption. In SDM-Site, there were four different compositions used to represent type groundwaters present at Forsmark (saline, marine, fresh, and brine). For the Laxemar site an additional groundwater of brackish non-marine origin was also used. The reference saline composition for Forsmark and Laxemar differed slightly, although the fresh, marine, and brine compositions were identical for both sites.

The application groundwater compositions may be defined for a specified groundwater type not studied in the laboratory, statistics of sampled present day groundwaters, or modelled compositions intended to represent some future groundwater state. Modelled compositions may be derived from large scale 3D hydrogeochemical simulations, or simplified descriptions of reactive transport processes of interest (e.g. mixing-reaction models).

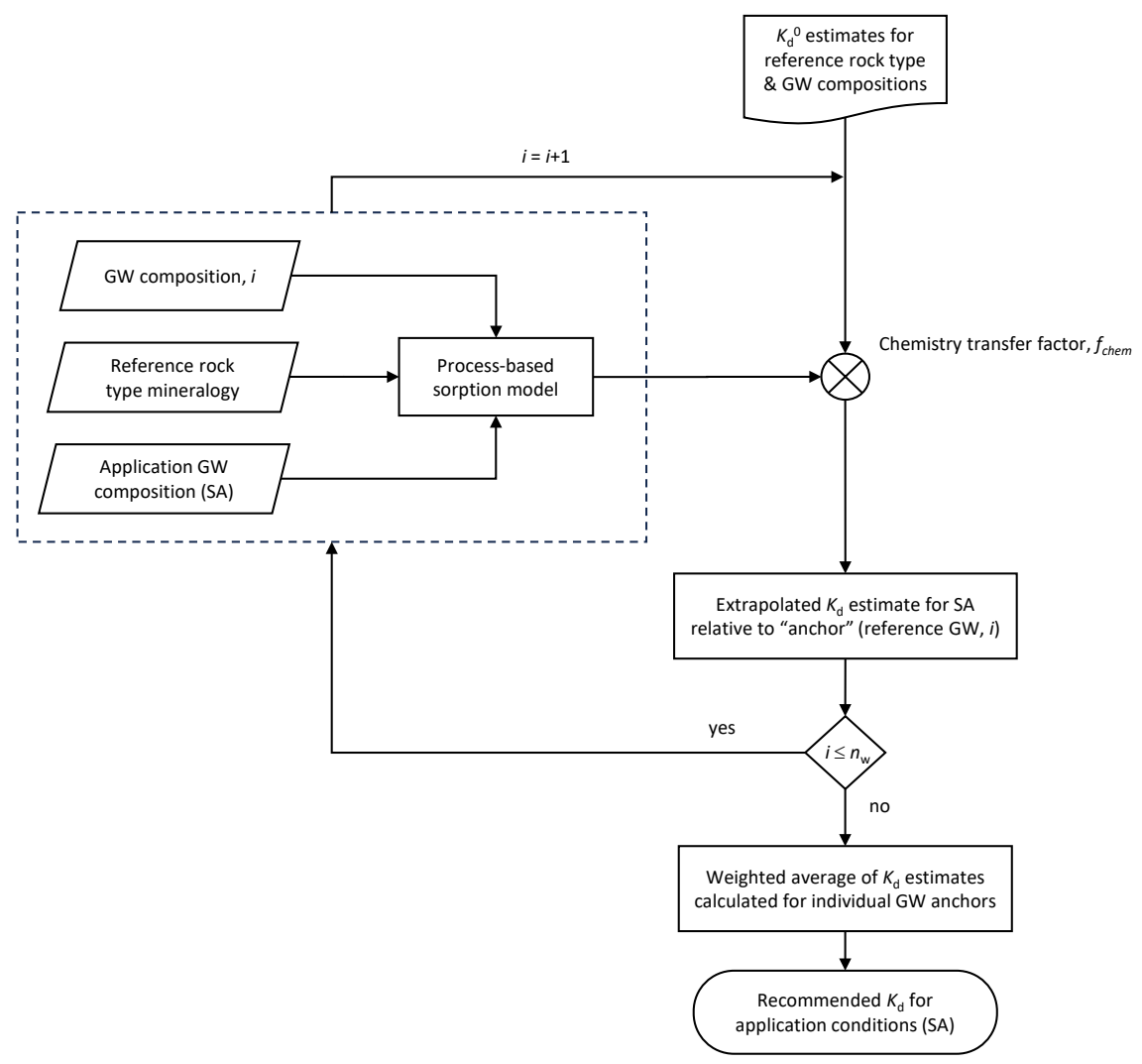


Figure 5-15. Procedural flowchart showing the proposed procedure for extrapolation of K_d^0 values for reference rock types and n_w groundwater anchors to in-situ, application conditions with deviating groundwater composition.

Using mechanistic sorption models (i.e. surface complexation and cation exchange), chemistry transfer factors, f_{chem} can be defined using Equation 5-13 which are then used to extrapolate reference $K_{\rm d}^0$ "anchor" values to the application groundwater composition. It is possible to separate variability and parametric uncertainty in the calculation of $f_{\rm chem}$ using the approach described by Ciffroy (2020). This is similar to the approach in Crawford (2010) where the uncertainty of cation exchange selectivity constants was propagated in calculations together with statistics of groundwater compositional variability for the cation exchanging elements Cs, Sr, and Ra.

Given that mechanistic models typically incorporate a simplified description of sorption, it is reasonable to expect that K_d values extrapolated from different reference states might not always be in full agreement. This is particularly relevant for redox sensitive solutes where the sorptivity of oxidised and reduced forms may vary over many orders of magnitude. For this reason, it is proposed in the present strategy that extrapolated K_d values corresponding to different anchors should be averaged using an appropriate weighting scheme. Here, differences in predicted K_d values associated with different anchors will need to be included as part of the envelope of uncertainty for the specified application conditions.

In the final recommendation of data for modelling purposes, it is envisaged that different K_d data sets will be defined for different application conditions. Generic probability density functions for average K_d may be defined for the statistics of groundwater composition at various elevation intervals in the geosphere. It may also be feasible to calculate a simplified set of response surface equations for the K_d of some solutes as a function of a small subset of groundwater chemical variables (e.g. ionic strength, pH, Eh, DIC, etc.).

5.3.1 Overview of modelling approach

The original motivation for using a chemistry correction factor approach over direct estimation of $in\text{-}situ\ K_d$ values through thermodynamic sorption modelling is based on the premiss that K_d values estimated from laboratory measurements should take precedence in the data recommendation process. Despite significant advancements in modelling surface complexation and ion-exchange processes, the produced models remain rough approximations of reality, although they may adequately fit the data in a mechanistically reasonable manner (e.g. Westall 1994, Wang et al. 1997, Davis et al. 1998, Kaplan 2021).

The main reason put forward in this work for the use of chemistry transfer factors rather than calculation of K_d values directly from mechanistic models is that it is usually not possible to specify key parameters of mechanistic models to the degree of accuracy necessary to give a sufficiently reliable estimate of the K_d value in an absolute sense, although such models still might provide a mechanistically plausible account of relative sorptive variation that is defensible given underlying uncertainties.

The central hypothesis is that multiple uncertain parameters should be normalisable (i.e. the unknown quantity proportionally affects both the numerator and denominator of Equation 5-13 and therefore cancels out when calculating the ratio). Such parameters include sorptive surface area, binding site densities, and cation exchange capacity of mineral phases in the site-specific rock. As demonstrated in Appendix A, the principle of normalisability can be derived from first principles for an arbitrary number of minerals and surface reactions contributing towards the overall sorptivity of the rock for a given radioelement.

Since the chemistry transfer factor is treated as a separate entity to the reference $K_{\rm d}^0$ anchor value for the rock, there is considerable freedom available to the modeller as to how $f_{\rm chem}$ is calculated and its quantification is not necessarily restricted to a particular sub-class of Thermodynamic Sorption Model (TSM) or modelling approach. In this context, even a response surface conditioned on empirical data might find use for calculation of $f_{\rm chem}$ values in a limited range. This flexibility is considered a strength of the approach since the validity of underlying assumptions can be evaluated independently of the overall conceptual framework and different TSMs can be readily substituted into the workflow without overturning the underlying premise of a transfer factor-based approach.

In this work, we assume that the bulk K_d value of the rock can be defined as the sum of linear contributions from multiple binding site types (i.e. a component additivity description). These are implicitly assumed to correspond to n_m separate mineral phases. If independent measurements are

made using rock thin sections, then digital autoradiography could potentially be used to quantify the relative contribution of each mineral phase to the $K_{\rm d}^0$ at the reference groundwater composition (e.g. Fabritius et al. 2024). Using this data, the $f_{q(j)}$ and $f_{r(1,j)}$ components of the overall mineralogy transfer factor, f_q can be estimated.

With this information it is possible, at least in principle, to calculate $f_{\rm chem}$ for a surface complexing solute while only knowing the reference and application groundwater compositions, binding constants for surface complexation reactions on each mineral, and the corresponding protonation-deprotonation pK_a values for each site type. The binding site density and relative accessible surface area for each mineral phase considered separately, are normalisable parameters and thus should not have a large impact on the outcome of the calculation, provided the target solute sorbs at trace levels below the concentration required for site saturation. The net sorption also depends on the accuracy with which the $f_{r(1,j)}$ components for each contributing mineral phase can be determined from independent measurements or estimated from literature data. This is a relatively large uncertainty for the computation of $f_{\rm chem}$.

If the relative contribution of each mineral to the K_d^0 value at the reference groundwater composition cannot be quantified, then simplifications must be made. One simplification adopted previously in Crawford (2013) is to assume that a single mineral such as biotite dominates sorption in the rock. For cation exchanging solutes, Cs(I) in particular, the assumption of biotite as a dominant sorbing phase is likely a good assumption. This is because it is typically the highest CEC bearing mineral in granitic rock. The assumption may be less good for surface complexing solutes such as transition metals and trivalent/tetravalent actinides, however, and may not give as accurate predictions if other mineral phases contribute in a non-negligible way (if those minerals exhibit pH dependent trends in reactivity that differ significantly from biotite).

Due to the scarcity of published TSMs for biotite, the phyllosilicate mineral illite was proposed as an approximate geochemical analogue in Crawford (2013). The reason for this is that (unlike montmorillonite) it is a non-expanding clay with an analogous crystal structure to biotite, consisting of repeating silica tetrahedra (T) units interspersed with octahedral (O) alumina units in a so-called TOT structure. The non-expanding nature of illite is also a key property of relevance since the interlayer of similar, although expanding clay minerals such as montmorillonite and other related smectite minerals have differing sorption properties due to the accessibility of the interlayer for hydrated cations.

As with most TSM-based calculations, the largest uncertainty is the assumption of specific reaction mechanisms for sorption of surface complexing solutes. In the absence of spectroscopic measurements to confirm the existence of hypothesised surface species, the assumed stoichiometries of sorption reactions are, at best, a guess calibrated on measurement data for a very narrow set of experimental conditions and simplified background electrolyte compositions. Extrapolation of K_d values very far outside the region of model calibration is thus subject to considerable uncertainty and can lead to very large errors (multiple orders of magnitude) if the reaction mechanism is incorrectly inferred. This is why it is important to have a good set of well-chosen anchor points within which f_{chem} values and K_d can be interpolated. This is considered a non-normalisable uncertainty. This and other uncertainties related to relative proportions of multiple binding site types can be investigated by sensitivity studies and variation analysis.

5.3.2 Mechanistic models for calculation of chemistry correction factors

In the current proposal for handling of application groundwater compositional variability, a simplified approach is taken whereby a theoretical model for surface complexation on a small number of contributing mineral phases is developed using the component additivity approach. One possibility would be to assume quartz, feldspar (encompassing both plagioclase and alkali feldspar), and mica minerals as a group (i.e. biotite, chlorite, and muscovite) with the possible inclusion of a ferric oxide component for oxidised rocks. If one or more of these mineral phases can be shown to only have a minor influence, they might be neglected without introducing large uncertainties. In the case that the mica content of the rock overwhelmingly dominates sorptivity, it may be sufficient to consider this mineral group only.

Here, illite is used as a geochemical analogue for biotite and other mica minerals (considered as a group). For radioelements that sorb by way of a surface complexation mechanism, we have adopted the model described by Bradbury and Baeyens (2009a, b) for the illite-biotite geochemical analogy. For brevity this model is referred to in the present report as the BB09 model.

For quartz, feldspar, and the various ferric oxide polymorphs there are several models described in the literature which might be used as a basis for a component additivity modelling set. A useful resource for identifying candidate models and data for TSMs is the RES³T database (Brendler et al. 2003) which is freely accessible via internet. In the continued modelling work, extensive use will be made of this database to screen for suitable data sets and modelling studies that might be adopted for the calculation of chemistry transfer factors using the component additivity approach.

Although it may be theoretically possible to create a relatively detailed component additivity Surface Complexation Model (SCM), it is acknowledged that this may not be feasible for all radioelements.

The BB09 model is the same as used in Crawford (2013) for estimation of f_{chem} values for surface complexing solutes. Although the BB09 model contains a simplified description of cation exchange for sorption of specific solutes at low pH, this is not used in the present work for radioelements whose sorption is predominantly governed by cation exchange (i.e. Cs(I), Sr(II), Ra(II)) as there are better alternatives (e.g. the three-site cation exchange model for biotite described by Söderlund et al. 2018, 2019).

The principle of parameter normalisation implies that it should be sufficient to assume an arbitrary sorptive surface area and binding site density consistent with the pK_a values for the binding sites to calculate f_{chem} at an acceptable level of accuracy for the sorbing mineral (electrostatic corrections notwithstanding). The main restriction is that reactions with the surface should not significantly perturb the contact solution from its initially defined composition and that the radioelement is modelled at a trace concentration level such that sorption is approximately linear.

One of the advantages of the BB09 model is that a linear free energy relation (LFER) with very good data support is available which can be used to estimate K_d for surface complexing radioelements not studied in the original reference. With the exception of the ferric oxides, appropriate LFERs are sparse in the literature for minerals and those that exist are relatively uncertain. LFERs established for diffuse layer model (DLM) implementations may also not be directly comparable with binding constants determined for triple layer (TLM) and constant capacitance (CCM) models due to underlying differences in the treatment of surface reactions and electrostatic corrections.

As outlined previously, the modelling approach is modular in the sense that different thermodynamic sorption models can be readily substituted in the workflow to give independent estimates of f_{chem} . This modularity permits model specific sensitivity analyses to be made in a straightforward fashion and allows the inclusion of more advanced models that cannot, at present, be foreseen.

5.3.3 Anchoring of modelled data to reference K_d values for studied groundwater types

A significant limitation to the use of thermodynamic sorption modelling for the prediction of sorption is the need to calibrate models against appropriately detailed measurement data for the system in question. It should be feasible to create a component additivity model from suitably chosen literature sources and first compare with measurement data obtained in the site descriptive modelling to initially ascertain the deviation of measurement data from first principles calculation of the K_d .

In this modelling step, binding constants and protonation-deprotonation constants consistent with the site densities as assumed in the original literature sources can be used. If these parameters are taken to be constant and approximately valid for the simulated water composition, the main adjustable variables are the relative reactive surface area contributions of constituent minerals, $f_{r(1,j)}$ comprising the rock matrix relative to the total BET surface area of the rock. This is identical the proposal for the calculation of f_{chem} , the only difference being that the modelled K_d value for a

specific groundwater composition is given as an absolute value and not normalised relative to the corresponding estimate for a reference groundwater composition (cf. equations 5-13 and 5-15).

As noted previously, for a rock matrix consisting of more than two surface area contributing minerals, there are multiple parameters that cannot be fixed in the absence of additional measurement data points (i.e. measured K_d values for different contact water compositions) or quantitative autoradiographic data. As a first approximation it is possible to use literature values for surface areas of crushed minerals in a given size interval together with volumetric proportions of each constituent mineral to ascertain the relative surface area contributions. In the case of a rock matrix assumed to be comprised of quartz, feldspar, biotite, and a smaller amount of ferric oxide (e.g. goethite), it may be necessary to perform a variation analysis to ascertain reasonable ranges of the first principles K_d estimate for the reference composition. It is acknowledged that it may not be possible to create a detailed component additivity model for all radionuclides of interest and the feasibility of this must be investigated on a case-by-case basis.

The use of a transfer factor-based approach to correct for groundwater chemistry deviations assumes the existence of at least one, or more reference K_d values for calibration of the model (i.e. K_d^0 in Equation 5-12 and its model calculated counterpart in Equation 5-13). In the present work, the empirically measured K_d^0 values are referred to as "anchor" values. The existence of multiple anchors is valuable since it permits a basic quantification of model extrapolation error if each measurement anchor is presumed to be an equally accurate representation of the true sorptivity. If anchor values for site-specific materials are unavailable, then it is necessary to invoke geochemical analogues or import literature data. If there are no suitable geochemical analogues or if the literature data is highly uncertain it may be necessary to make conservative assumptions concerning the anchor values.

A consistency issue naturally arises if the anchors are not mutually consistent with the modelled trends in the parametric response surface describing f_{chem} . This, however, should probably be regarded as the norm for data sets representing very different groundwater compositions. This is because TSMs used to calculate sorption are typically calibrated on much simpler electrolyte compositions that may not fully capture the mechanistic details of the sorption processes in a more complex groundwater. As noted previously in Section 5.3.1, an additional issue influencing the accuracy of the extrapolation is the fact that postulated sorption mechanisms are rarely confirmed using spectroscopic data (which is not always possible anyway, particularly at trace concentrations).

Multiple prototype modelling examples are given in Appendix C. In these examples, calculations of stepwise increasing complexity are considered to demonstrate the various possibilities for extrapolation of measurement data to application groundwater compositions. In the original concept for K_d extrapolation using chemistry correction factors as described in Crawford (2010), the justification for using the Forsmark saline groundwater as a main reference anchor was twofold.

Firstly, the Forsmark saline groundwater was deemed to be most like the expected composition at repository depth during much of the temperate time period when radionuclide release would have greatest dose impact for surface communities (Avila et al. 2010). The use of the saline groundwater data as an anchor point would therefore imply smaller extrapolations for this period and consequently, reduced error if used as an anchor rather than the other groundwater compositions.

Secondly, for most of the SDM-Site data sets there were significantly more measurements made for the saline groundwater than other groundwater types. The reference K_d^0 value estimated for the saline groundwater might therefore be reasonably expected to be more statistically representative than K_d^0 values derived for the other groundwater types. This was not applied uniformly for all data sets, however, and in the case of Sr(II) the measured R_d values for the saline groundwater were sufficiently close to the quantification limit that the fresh groundwater type was deemed a more appropriate reference anchor.

Given that R_d measurement data for sorption often exhibit a range of variation that differs from predictions made using an assumed thermodynamic sorption model, there is a reasonable expectation that the use of multiple anchors representing several different synthetic groundwaters might give a better overall view of uncertainty than the use of a single anchor value.

One way of approaching the problem of harmonising predictions for multiple (possibly conflicting) anchors would be to calculate a simple logarithmic mean and standard deviation taken over all predictions. This would give some indication of potential model uncertainty and preserve the shape of the response surface, thus honouring the underlying model constrained covariance of key variables.

If there is greater confidence in data for certain anchors and lesser confidence in others, then the calculation could be modified to give greater weight to those which are deemed more accurate. For inaccuracies related to small sample sizes and standard errors associated with each $K_{\rm d}^{\,0}$ anchor, a simple weighting function based on the uncertainty of individual anchor values might be used to give greater emphasis to extrapolations from more reliable anchors. Other, more sophisticated interpolation techniques are feasible, although whether this reduces overall extrapolation uncertainty is not clear.

The calculations shown in Appendix C are a demonstration of a methodology for estimation of Smart K_d values using chemistry correction factors. It is acknowledged that the use of a very simple non-electrostatic model of sorption for a single surface complexation binding site type, as is the case with the BB09 model, is likely not an accurate assumption outside its range of calibration. It is likely to be even more inaccurate for prediction of sorption where multiple mineral surfaces might contribute in a non-negligible fashion towards measured K_d values in laboratory measurements.

It is intended that a more detailed component additivity-based model will be produced and tested during the detailed site investigations for those radioelements where non-mica minerals make significant contributions towards the overall sorptivity of the rock. It is envisaged that this modelling work will be informed by quantitative measurements of sorption on thin sections using digital autoradiographic techniques. This should result in a more precise description of sorptive variability than can be otherwise achieved using first principles assumptions concerning the distribution of reactive surface areas.

Despite this, the modelling results are useful since they clearly indicate an impact of speciation giving very low K_d values in some parts of the geosphere and much higher values in other parts. Since the multimodal probability density describing K_d variation reflects considerable spatial variability, it therefore would not be recommended to simply sample from the probability density directly without consideration of the trend of groundwater chemistry along individual migration paths. This represents a major shift in thinking relative to the previous limited handling of Smart K_d within SR-Site (i.e. for the cation exchanging solutes Cs, Sr, Ra). In transport calculations using codes such as MARFA (Painter and Mancillas 2013, Painter et al. 2022), Smart K_d values could be supplied for individual migration paths for sensitivity analysis.

5.3.4 Estimation of Smart K_d for colloids

Carrier colloids present in the geosphere are present both as natural colloids and bentonite colloids released from the buffer and/or backfill. Intrinsic colloids, i.e. microprecipitation of hydrolysed solute species in suspension, are also present (Crawford 2008). The levels of natural colloids at the Forsmark site are not expected to exceed a maximum of 180 µg/l (SKB TR-21-06) during temperate and submerged marine climate regimes. This colloid concentration ceiling is based on previous investigations by Hallbeck and Pedersen (2008), Hedqvist and Degueldre (2008) and Nilsson and Degueldre (2007), and is considered relatively cautious. As a comparison, the bentonite colloid concentration is estimated to be present up to 20 mg/l in groundwaters with low ionic strength (Wold 2010), such as may be encountered during glacial conditions (although mostly during glacial advance and retreat). Transport by bentonite carrier colloids is therefore thought to have the greatest potential to influence transport retardation during periods where bentonite erosion is significant.

Radionuclides that have a strong affinity for bentonite will sorb onto bentonite colloids and may be transported through the geosphere and potentially reduce interactions with the rock matrix. Sorption to mobile clay colloids is an uncertain process that is handled pessimistically in SR-Site by neglecting a range of potential mitigating processes. The maximum impact of reversible colloid sorption on matrix interaction was approximately quantified by the apparent reduction in matrix diffusive uptake using the equation (Crawford 2008):

$$f_{rc} = \frac{F_{app}}{F} = \frac{1}{1 + m_c K_c} \tag{5-16}$$

Where F (y/m) is the F-factor (flow-wetted surface to flow ratio) for a flowpath, F_{app} (y/m) is the apparent F-factor in the presence of a groundwater colloid loading of m_c (kg/m³), for a colloid sorption partitioning coefficient, K_c (m³/kg). In general, if the dimensionless product $m_c K_c$ is much less than unity, the impact of colloids will be insignificant. Under normal groundwater conditions, the colloid loading is sufficiently low that K_c values significantly exceeding 1000 m³/kg would be necessary to have any effect on radionuclide retardation which rules out natural carrier colloids as a meaningful transport mechanism.

When buffer erosion is included, on the other hand, the retardation in the geosphere may be significantly reduced for the periods in which high colloid concentrations are possible. These periods are very brief, however, and the small near-field release rates are sufficient to keep dose-equivalent releases below the dose corresponding to the risk limit (SKB TR-10-50).

Sorption on bentonite colloids is assumed to occur on suspended montmorillonite platelets where radionuclides can sorb both by inner and outer sphere surface complexation on variable charge edge sites and cation exchange on basal planes and interlayers. The sorption onto the carrier colloids is thereby dependent on the type of radionuclide and groundwater composition (i.e. ionic strength, pH, dissolved organic carbon, etc.) in a similar fashion to sorption on fracture minerals and the rock matrix. The sorption process is assumed to be reversible over the characteristic transport times.

The partitioning coefficient for sorption onto bentonite colloids K_c (m³/kg) may be related to the corresponding K_d (m³/kg) for sorption onto bentonite buffer material as $K_c = \gamma K_d$ where γ is a ratio of specific surface areas for colloidal and bulk bentonite (SKB TR-10-50). SKB has incorporated the effective transport parameters regarding colloids in the MARFA code (SKB TR-10-50).

 K_c values for montmorillonite colloids can be predicted directly from published thermodynamic sorption models and statistics of groundwater compositional data for projected groundwater conditions. This can be done in a broadly similar fashion to the procedure outlined for estimation of K_d values for fracture minerals. The 2-site non-electrostatic model by Bradbury and Baeyens is suggested as the most likely candidate for Smart K_d estimation (e.g. Bradbury and Baeyens 2005a, 2006) as a linear free energy relation exists which might be used to estimate sorption of radioelements that have not been studied experimentally.

Sorption irreversibility for tetravalent and some other radionuclides has been observed in experiments (Shelton et al. 2018). At the colloid concentrations likely to be found in the bedrock, a significant increase in risk could arise if a meaningful proportion of the radionuclides associated with colloids are irreversibly sorbed. Several processes help mitigate the potential effects of irreversible sorption to colloids. These mitigating processes include permanent filtration of the colloids, colloid surface attachment and retardation. It is acknowledged that irreversible sorption onto bentonite would dramatically reduce near-field release and limit the availability of sorption sites on bentonite colloids (SKB TR-10-50). Experiments have confirmed that there is strong retention of colloids in the rock. Colloid retention has been observed even at conditions where high mobility was expected (i.e. under unfavourable electrostatic conditions) (Shelton et al. 2018). However, the mechanisms that contribute to colloid retention are not yet fully understood (Shelton et al. 2018) and need further investigation.

5.3.5 Estimation of Smart K_d for radioelements lacking measurement data

In site investigations, it is generally infeasible to quantify K_d values for all radionuclides of relevance to safety assessment including all relevant geological materials and contact water compositions. For this reason, the focus in SDM-Site was on quantifying the sorption of radioelements representing specific classes of sorptivity (Widestrand et al. 2003) with the aim of invoking geochemical analogies to assign K_d values for radioelements that were not studied.

Sorption classes investigated in the SDM-Site laboratory campaign included monovalent cations (Cs^+) , hard divalent cations $(Sr^{2+}$ and $Ra^{2+})$, divalent cations of intermediate hardness (Ni^{2+}) , trivalent cations $(Am^{3+}$ and $Eu^{3+})$, tetravalent cations (Th^{4+}) , as well as the redox sensitive classes $(Np(V)O_2^+)$ and $U(VI)O_2^{2+})$. Due to difficulties in the evaluation of the blank measurements the Th data were not included in the data evaluation.

In the context of the presently proposed strategy, this allows one to use reference K_d values for a geochemical analogue where data is available together with a chemistry transfer factor to calculate the Smart K_d value for a target radioelement for which there is no measurement data. The correction is similar, although differs subtly to that used previously to extrapolate reference K_d^0 values to differing groundwater composition since it is necessary to also account for chemical differences between the target radioelement and the analogue for which experimental data is available. In principle, this can be incorporated directly in the computation of f_{chem} values without further complication.

An example calculation is shown in Appendix C showing how the K_d value for Pb(II) sorption might be estimated from that derived for Ni(II) where the latter has a K_d value measured in the site investigation lab program. The example calculation uses the BB09 model assuming a dominant effect of biotite sorption in the rock. As shown in the calculation example there are significant variations in the K_d calculated for Pb(II) sorption relative to that for Ni(II) for different synthetic groundwaters over the range of pH values studied. This suggests that a correction for the differing chemistry of Pb(II) relative to Ni(II) is justified rather than simply assuming that they have the same K_d as was done previously in SR-Site (Crawford 2010).

Some radioelements of lesser importance may not have suitable analogues among those studied in the laboratory programme. Furthermore, it is possible that not all of these will have well quantified thermodynamic constants to enable predictive modelling. For these radioelements, literature data sources will form the main input for estimation of K_d values. In a similar fashion to the handling of literature data sources in SR-Site (e.g. Crawford 2010), K_d values should be harmonised with the intact site-specific rock by applying surface area corrections wherever possible. Consideration should also be given to differences in speciation that might affect sorptivity in the application specific groundwater relative to that used in the literature.

If the K_d estimate derived from a literature source is only known from a very small number of measurements, then the quantifiable uncertainty may be much narrower than what is realistic. In some cases, this may require estimation of an expanded range of uncertainty, particularly if there are no suitable thermodynamic sorption models for calculation of chemistry correction factors. This should be dealt with on a case-by-case basis depending on the importance of the radionuclide in the safety assessment, the quality of the data source, and existence of sufficiently detailed supporting data given in the reference.

5.3.6 Estimation of Smart K_d for fracture coatings

In transport calculations, it is customary to model sorption on fracture coatings as an instantaneous equilibrium process since the equilibration time is typically short relative to advective travel times. The equilibrium retardation factor for the fracture coating can be defined for a given flowpath segment as (SKB TR-10-50, Appendix B):

$$R_f = 1 + \frac{d_s}{2b}\phi_s + \frac{1}{2b}\sum_{k=1}^n f_{eq(k)}K_{ds(k)}m_{s(k)} \approx 1 + \frac{1}{2b}\sum_{k=1}^n f_{eq(k)}K_{ds(k)}m_{s(k)}$$
(5-17)

where, d_s (m) is the average thickness of the mineral coating summed over both surfaces of the fracture, b (m) is the transport half-aperture of the fracture, ϕ_s (–) is the porosity of the coating, $K_{ds(k)}$ (m³/kg) is the average partitioning coefficient for fracture mineral k, $f_{eq(k)}$ is an equilibration fraction, and $m_{s(k)}$ (kg/m²) is the average mass of fracture mineral k per square metre of the flowwetted surface (i.e. mass summed over opposing fracture surfaces).

The $f_{eq(k)}$ parameter is an additional factor which quantifies the fraction of mineral mass that is equilibrated on the timescale of transport. This concept was introduced in (Crawford 2013) and is useful in situations where a transported radionuclide undergoes an exchange process with a mineral such as calcite. Retardation of specific radionuclides by formation of solid solutions may also be modelled if the radionuclide concentrations are sufficiently dilute that the sorption is approximately linear. The sorption of Ra on radiobarite, RaxBa(1-x)SO₄ can be included provided the average abundance of barite can be estimated for the fracture minerals. Recent work by (Weber 2017) suggests that full equilibration of radiobarite with mobile Ra groundwater concentrations (i.e. $f_{eq} \approx 1$) may be a reasonable assumption for safety assessment modelling.

Exchange of some radionuclides with the outer few molecular layers of calcite crystals in fracture coatings may also be modelled as an approximately linear sorption process that can be characterised by a K_d value. In these cases, however, the equilibration factor is not well known, and it may be necessary to adopt a conservative view that only the first few dozens of monolayers are exchangeable on the timescale of transport. A similar assumption was invoked to estimate exchange of C-14 as dissolved carbonate on fracture calcites in SR-PSU (Crawford 2013). It might also be possible to use a surface-complexation based TSM to describe sorption on calcite (e.g. Zavarin et al. 2005, Heberling et al. 2011, Belova et al. 2014) assuming sorption occurs at the surface-active monolayer only.

In Bradbury et al. (2010) it was speculated that approximately the first 30 or so, monolayers ($\sim 10^{-8}$ m) at the calcite surface should be readily accessible over safety assessment timescales based on consideration of earlier work by Stipp et al. (1994, 1996). A BET surface area of 2.2 m²/g is reported by Byegård et al. (2008) for calcite dominated fracture coatings at the Forsmark site. Based on a volumetric balance and assuming that the reported BET surface area is approximately representative of calcite crystals hosted in fracture coatings, this would imply a calcite equilibration fraction of:

$$f_{\rm eq} = A_s \rho_s \eta \approx 2200 \, \frac{\rm m^2}{\rm kg} \times 2710 \, \frac{\rm kg}{\rm m^3} \times 10^{-8} \, \rm m \approx 6 \, \%$$
 (5-18)

This is a rough approximation, however, as different solutes likely penetrate to different depths in the calcite surface depending on their similarity to the Ca²⁺ or CO₃²⁻ ion that is being replaced in the calcite crystal.

The definition given in Equation 5-17 assumes that the contributions of individual minerals can be summed in a component additivity fashion and armouring effects can be neglected. This may overestimate contributions of individual minerals if there is significant cementation of the fracture coating, although is a reasonable approximation for relatively porous fracture coatings. This might be accounted for by using sorption measurements on actual fracture coating samples as anchor values to rescale $K_{ds(k)}$ values to effective values for multi-mineral coatings. In this case, the $f_{eq(k)}$ for each mineral can be adjusted proportionally to give an approximate match to the anchor value.

The use of sorption measurement data for site-specific fracture coatings as anchor values also enables a Smart K_d treatment in a similar fashion to that described in previous sections for the rock matrix. K_d values for fracture mineral coatings can also be estimated using Equation 5-17 and thermodynamic models taken directly from the literature for the individual minerals comprising the fracture coating. An average K_d value for the fracture coating can be defined as:

$$\bar{K}_{ds} = \frac{\sum_{k=1}^{n} f_{eq(k)} K_{ds(k)} m_{s(k)}}{\sum_{k=1}^{n} m_{s(k)}}$$
(5-19)

Owing to the thinness of the fracture coatings, K_d estimates may not need to be as accurate as for the rock matrix as, in most cases, they will only give marginally increased retardation for most radionuclides. For some radionuclides that sorb only weakly within the rock matrix, although associate strongly with fracture calcite, the effect could be important.

5.4 Summary and overview of transport property parameter specification for safety assessment

In the preceding sections, a detailed strategy for the estimation of retardation properties of the rock has been presented. Effective diffusivity and diffusion accessible porosity are dealt with in Section 5.1 and the main recommendations are summarised in the following Section 5.4.1. Since the diffusive properties and porosity of the rock are expected to be relatively constant over the time scale of safety assessment (excluding impacts of glaciation on *in-situ* stresses), it should be sufficient to define tables of D_e and ϕ_p for the retardation model where these parameters are treated as constants in the multilayer rock matrix representation. It is acknowledged that changing *in-situ* stress levels and groundwater salinity during a glaciation cycle may impact these transport properties, although the extent to which this can, or should, be accounted for in transport modelling remains to be determined by a combination of experimental investigations and microstructural models.

The sorptive properties of the rock, quantified through the K_d parameter, are explored in sections 5.2 and 5.3. In parameterising sorption, both the physical and microstructural properties of the geological material as well as the porewater chemistry need to be taken into account. While the physical/microstructural properties of the geological material remain relatively constant over safety assessment timescales, groundwater chemistry is subject to significant spatial and temporal variation.

Therefore, in the development of the retardation model, we aim to distinguish between the constant sorption features specific to a given geological material (such as BET surface area scaling and sorptive mineral surface area fraction) and variable features (porewater/groundwater composition). A preliminary proposal for packaging K_d values for use in site descriptive modelling and safety assessment is provided in Section 5.4.2. The focus is defining the characteristics of data deliveries suitable for various types of analysis and transport modelling scenarios. The methodology suggested includes an iterative approach where adjustments are made with respect to the needs of end-users and to make use of additional information gathered from investigations of transport properties and from other disciplines.

5.4.1 Effective diffusivity and diffusion accessible porosity

Measurements based on the *in-situ* resistivity method together with direct laboratory measurements of effective diffusivity (through-diffusion method) and laboratory-based resistivity measurements are proposed as primary methods for assignment of effective diffusivity, D_e for the volumetrically dominant rock types. At present the most accurate data are thought to be for boreholes KFM01D and KFM08C, although the statistical coverage for different rock types varies considerably. The granite-to-granodiorite, metamorphic, medium-grained rock type (SKB rock code 101057) is the most well represented followed by pegmatite, pegmatitic granite (SKB rock code 101061).

Measurements for other rock types are only known from a very small number of in-situ measurements and may not be statistically representative owing to much smaller sample sizes than the main rock types. For less common rock types and altered materials, D_e values derived from laboratory through-diffusion measurements are recommended to be used after correction for compression of the grain boundary porosity due to in-situ stresses.

An additional correction needs to be applied to account for anion exclusion effects which reduces the D_e for anionic solutes. The impact of anion exclusion has been observed in, for example, through-diffusion measurements for HTO and I⁻ made by Vilks et al. (2005) on core samples from Äspö HRL, and samples from Finland (Olin et al. 1997, Kaukonen et al. 1997, Voutilainen et al. 2018, 2022, Eichinger et al. 2023). Updated estimates for site-specific materials based on a range of confining pressures to estimate the magnitude of the effect at *in-situ* stress levels are suggested.

Comparison of formation factor measurements obtained using the laboratory resistivity-based method with *in-situ* resistivity measurements permits evaluation of the lab-to-field transfer factor, $f_{s(D)}$ accounting for stress release in the laboratory samples. This is thought to provide a reasonable estimate of the impact of *in-situ* pore compression on D_e for cations and non-charged solutes for the main rock types where there is good data coverage. At present an estimate is made through side-by-side comparison of empirical distribution data. More accurate estimates, however, are suggested to be made by matching data for individual core samples with the corresponding *in-situ* measurement data.

Small scale variation of $D_{\rm e}$ in the alteration zone surrounding flow bearing fractures is difficult to quantify using customary methods based on through-diffusion experiments and resistivity measurement. For these materials, estimates based on Archie's law might be used as a first approximation for parameterisation of alteration layers in the retardation model in the absence of more accurate measurement data.

More detailed studies are suggested of the porosity variation in intact fracture coatings and the adjoining alteration zones near fracture surfaces to support the quantification of the diffusive properties of these materials in the retardation model. This could be particularly of interest to ascertain whether sealed fractures filled with fracture minerals constitute significant low-permeability barriers in the rock matrix. Since sub-parallel sealed fractures are commonly found in close proximity to flow bearing features, this is important to establish connectivity of the rock matrix since impermeable structures of this kind may not be directly identifiable from borehole resistivity logs.

5.4.2 Sorption properties

In the retardation model, K_d values will need to be supplied for each of the alteration layers of the rock matrix including fracture coatings. In the case of a multilayer rock matrix including one or more alteration rims, it is assumed that the alteration rims are modified forms of the underlying host rock (see discussion in Section 4.4.2). Here it is also acknowledged that the deep rock matrix itself may also be an altered form (hydrothermal or metamorphic) of an original rock type, although of an older generation than the alteration rim flanking modern flow-bearing fractures. In the case that the alteration rim can be treated as a modified form of the host rock type, it may be simpler in some cases (i.e. where there is sparse measurement data) to define radioelement specific K_d values for the host rock and specify a net transfer factor to scale the K_d for the alteration layer relative to the (reference) host rock.

The overall transfer factor is equal to the product of surface area and mineralogical transfer factors (f_m and f_q) as defined in Section 5.2.2 for the alteration rim relative to the host rock. If more than one constituent mineral in the rock contributes towards sorption in a non-negligible fashion, f_{chem} values for the impact of groundwater chemistry may need to be estimated separately for the host rock and the alteration layer. This might be the case if mineralogy in the alteration rim differs considerably from the host rock. Depending on the radioelement under consideration, the differences might not always be very large, in which case the same or an averaged f_{chem} transfer factor might be appropriate.

When defining tables of recommended values for transport calculations in safety assessment and other applications, care must be taken to understand how the recommended data are going to be used. Depending on the application of K_d , data deliveries can be adjusted. Below is a list with different possible deliveries and their intended use. It should be noted that different deliveries are suited for different modelling purposes and codes. Not all of the possible deliveries may be of interest in the modelling, but the list provides an overview of different concepts and degrees of complexity.

- 1. K_d anchor values (mean and standard error) for defined synthetic groundwater compositions used in laboratory investigations. This dataset is the basis for all subsequent K_d calculations as it defines the reference conditions for all subsequent extrapolations.
- 2. K_d uncertainty distributions for broadly defined groundwater compositional types where consideration is given to covariance of chemistry parameter ranges within the designated water type (e.g. extant water types in the geosphere and projected future groundwater types). This is the basic data package that might be used in radionuclide transport modelling where a given groundwater compositional type is assumed to dominate large parts of the geosphere, or for specific depth zonation. It corresponds to the generalised application conditions for which data are requested in safety assessment.
- 3. K_d values (mean and standard error) for coordinate-indexed locations in the geosphere derived from hydrogeochemical modelling. This is the most detailed data package and is meant to facilitate calculation of migration path specific sorption properties. As an example, if local groundwater compositions are mapped to the coordinates of static migration paths, then flowpath averaged K_d values might be pre-calculated for migration path segments featuring groundwater compositional trends deviating from typical water types.
- 4. Simplified K_d parametric response surfaces for individual radioelements derived from statistical analysis of groundwater chemistry parameter covariance. This is mostly a tool that may be used for simplified analyses, sensitivity studies, and as a pedagogical device to assist mechanistic understanding and explanations.

In each of the proposals given above, element and groundwater specific K_d values are to be supplied for each rock type represented in the site descriptive geological model and for major alteration types comprising different layers in each fracture type. At the most basic level it is envisaged that tables of K_d values should be provided for the reference synthetic groundwater compositions used in laboratory investigations (Byegård et al. 2008). This constitutes data package (1) in the above list. These data consist of empirically measured anchor values to be used for all subsequent Smart K_d calculations and are defined for specified reference groundwater compositions (fresh, marine, saline, brine, etc.). The anchor values are specified as mean values with a calculated standard error as described in Section 5.2.5.

It is also envisaged that Smart K_d tables (2) should be produced that consider the statistical distribution of different chemistry parameters for more broadly defined groundwater compositional types. This is similar to the data request that was made in SR-PSU for K_d values consistent with groundwater compositions defined for use in the safety assessment of the SFR repository (see Crawford 2013). In the Hydrogeochemistry programme there are now at least 9 different groundwater types based on statistics of modern groundwater measurement data at the Forsmark site. Smart K_d values for these groundwater compositional types can be derived from anchor values given in (1). Here, additional consideration is given to contributions to the overall K_d uncertainty from anchor value uncertainty (extrapolations from different anchors), modelling uncertainty (impact of uncertain model parameters and assumptions in calculation of f_{chem}), and compositional variability of the groundwater type. It is expected that the statistical dispersion of K_d probability density functions for groundwater types should be greater than that of the anchor values owing to these propagated uncertainties.

As part of the envelope of uncertainty calculated for extrapolated groundwater compositions, it is intended that alternative sorption reaction mechanisms and thermodynamic sorption models can be substituted in the workflow to test the impact of underlying assumptions (depending on the availability of relevant models described in the literature). This naturally also extends to the choice of thermodynamic database used for such calculations as predictions made by thermodynamic sorption models are not only sensitive to the aleatory uncertainty of parameters used in modelled reactions, but also more generally to specific aqueous ligand reactions included or excluded from the database used in the calculations as well as differences relative to those used in the original literature references.

 K_d values calculated in (1) are extrapolated to a coordinate indexed database in data package (3) using the f_{chem} transfer factor methodology. The data would be supplied as a database of K_d values associated with spatial co-ordinates output by the model to facilitate mapping to particle tracking data in transport modelling. As discussed in Section 5.3.3, this would permit more precise calculations of radionuclide transport as it specifically excludes non-relevant groundwater compositions belonging to regions of the geosphere that are not visited by migrating radionuclides.

Data package (4) is a simplified parametric description of radioelement-specific Smart K_d vales for generic groundwater types. The response surface would presumably be defined as a polynomial with terms for different groundwater compositional parameters affecting the K_d value (e.g. pH, Eh, ionic strength, pCO₂, complexing ligand concentration, etc.). This data package might be useful for exploratory scoping calculations examining, for example, the sensitivity of transport modelling results for uncertainties in each chemistry parameter. It is envisaged that response surfaces can be calculated for different radioelements by statistical analysis of data previously generated in data package (3).

5.4.3 Verifying in-situ experiments

Many of the supporting analyses used to parameterise the retardation model are based on laboratory measurements using materials that may be considered disturbed, or otherwise not fully representative of the *in-situ* rock. There is consequently a need for verification of underlying modelling assumptions and transport properties of the intact rock that is best addressed through *in-situ* experiments in the rock volume where the repository will be located. To enable verifying *in-situ* transport experiments within the continued site investigations for the SFK repository, it is proposed that an experimental niche is established at an appropriate depth adjacent to the access ramp of the repository during the early construction phase.

Although the exact number and types of *in-situ* experiments that will be performed is yet to be decided, candidate proposals may include a simplified version of the long-term sorption-diffusion experiment at Äspö (LTDE-SD, Widestrand et al. 2010b) with focus on confirmation of diffusive-sorptive properties of the matrix rock, monitoring of out-diffusion natural analogue radionuclides in a packed-off borehole section, a between-boreholes electromigration experiment to confirm long-range rock matrix connectivity using physical tracers, SWIW tests, and possibly more traditional tracer experiments in a pumped dipole flow field. Although a laboratory-based study, there may even be the possibility to extract drill cores during exploratory drilling of the main tunnel to obtain more detailed information on rock material properties in the actual repository volume (e.g. using through diffusion tests) to improve the understanding of the variations in site-specific material properties at depth.

6 Derivation of flow-related parameters

6.1 Introduction

As explained in the parameter overview in Section 3.6, the flow-related transport parameters quantify properties of the advective transport along flowpaths in the fracture network and the conditions for mass exchange between the flowing groundwater and immobile water in the pore system of the rock matrix. The main flow-related parameters are the water travel or residence time (denoted as t_w) and the hydrodynamic transport resistance or F-parameter (denoted F, also called F-factor).

Whereas t_w has a straight-forward interpretation as the time spent by a particle or "water parcel" along a flowpath in the fracture network or a single fracture plane, F depends on both advective transport and the conditions for mass transfer conditions along the flowpath. What these "mass transfer conditions" are and how they are represented and quantified depends on the conceptualisation of transport (e.g. Berglund and Selroos 2004, Appendix A, Andersson et al. 1998). Essentially, F depends on a geometric feature such as the flow-wetted surface area or fracture aperture in combination with groundwater flow features, i.e. the flow rate and advective travel time, respectively. For the present discussion, it is sufficient to state that a high value of F corresponds to more favourable conditions for mass transfer and hence to comparatively larger retardation due to interactions with the rock matrix than a low F value.

The handling of the flow-related parameters can be viewed as a collaborative effort between the Hydrogeology and Transport modelling disciplines, insofar that the parameters are calculated by Hydrogeology in groundwater flow models and then utilised by Transport in safety assessment radionuclide transport simulations (which means that "Transport" here is the safety assessment modelling team). Thus, Hydrogeology is responsible for the calculation of these parameters, including model development and any supporting studies required to substantiate assumptions related to, for instance, the handling of spatial variability.

However, communication between "suppliers" and "users" of flow-related parameters is necessary and should take place when planning the modelling activities producing the parameters (e.g. in connection with development of internal task descriptions). The demarcation between Hydrogeology and Transport when it comes to transport processes in the fracture plane is not obvious, mainly because retardation could occur also in other immobile zones than the rock matrix, and cooperation is therefore needed. Whether this cooperation is best handled "on the fly" or within some kind of established activity or group remains to be decided.

Flow-related transport parameters will be produced in the safety assessment stages of future modelling only. If site-specific flow-related parameters are needed to further develop site understanding in forthcoming site descriptive modelling, e.g. to perform sensitivity studies of coupled transport processes like those in Crawford (2008, Chapter 5), relevant input can most likely be obtained from earlier modelling results (i.e. SR-Site or SR-PSU).

6.2 Overview of processes and scales

As discussed in Chapter 3, transport in fractured media implies a coupling between in-plane hydrodynamic processes, i.e. groundwater flow in the fracture plane, and diffusion-controlled processes in the rock matrix. This coupling is quantified by means of the so-called flow-related parameters. For radionuclide transport, as already discussed in Section 3.2.2, the key flow-related parameter is the hydrodynamic transport resistance, usually referred to as the F-parameter (or simply as F) in the SKB radionuclide transport modelling context.

The transport resistance is a groundwater-related quantity and thus should be evaluated using groundwater flow modelling only. However, cumulative transport resistance is typically defined and integrated along transport pathways, which, in turn, are delineated by means of particle tracking simulations. Special treatment is required by Equivalent Continuous Porous Media (ECPM) models since the F-factor here needs to be quantitatively described at the representative scale of the continuum model. This implies accounting for all the local hydraulically active intersecting fracture surface area relative to the local available volume of flowing water.

A second flow-related parameter is needed if diffusion into in-plane stagnant water is to be considered, a parameter that depends on the width of the flowing channel. In natural applications, the parameterisation of in-plane flowing channels and stagnant water zones is difficult for the simple reason that natural fractures display a significant range of in-plane groundwater velocities, which makes it difficult to draw a line delimitating the so-called flow channel from the stagnant water zones. In this context, the efforts are focused on defining equivalent parameters; this is further discussed below.

The high degree of heterogeneity of granitic rocks, which is observed over a range of very different scales, results in groundwater flow being organised according to complex and unevenly distributed patterns, which might be concentrated to a limited part of the fracture plane. This phenomenon is known as channelling. Quantitative direct information of in-plane flow and transport processes can only be obtained under very specific and controlled conditions in the laboratory and for scales from a few millimetres up to a centimetre.

When the scale of the investigated rock mass is larger (e.g. on the order of a few decimetres), flow and tracer tests performed on a single fracture might provide lumped information on the underlying heterogeneity, while direct measurements of aperture can only be performed on the external fracture trace. Post-mortem analysis is still possible at this scale but poses great challenges due to material loss. At the field scale (metre to decametre scale), single fractures might be isolated and tested providing lumped information that is affected by a high level of epistemic uncertainty due to, for example, the influence of the background flow field. At even larger scales (hundreds of meters to a kilometre) channelling can only be assessed by mapping flowing points in outcrops or in drifts, and the gathered information has limited relevance due to the influence of network topology.

In summary, the characterisation of in-plane flow processes is subject to the "tyranny of scales", as illustrated in the sketch of Figure 6-1. It turns out that when building large-scale transport models, appropriate abstractions of internal fracture heterogeneity are needed, which must in turn be anchored to existing information, if any, obtained from laboratory experiments. Alternatively, neglecting internal variability requires supporting numerical analyses that clearly and unambiguously show that most of the variability of transport processes at larger scales is accounted for by the network heterogeneity (Makedonska et al. 2016), or evidence that it constitutes a conservative assumption for the application at hand.

Although the present discussion is focused on in-plane and network-scale channelling, it should be noted that there are additional channelling phenomena that might deserve to be addressed in forthcoming site investigations. Crawford (2008) provides a discussion that could be taken as a starting point for such an extended analysis; in addition to network-scale and in-plane channelling, Crawford (2008, Section 2.1.3) considers the following channelling phenomena: flow channelling at fracture intersections, flow channelling at geological interfaces, flow channelling within foliations, and flow channelling within fault stepovers, shears and fracture jogs.

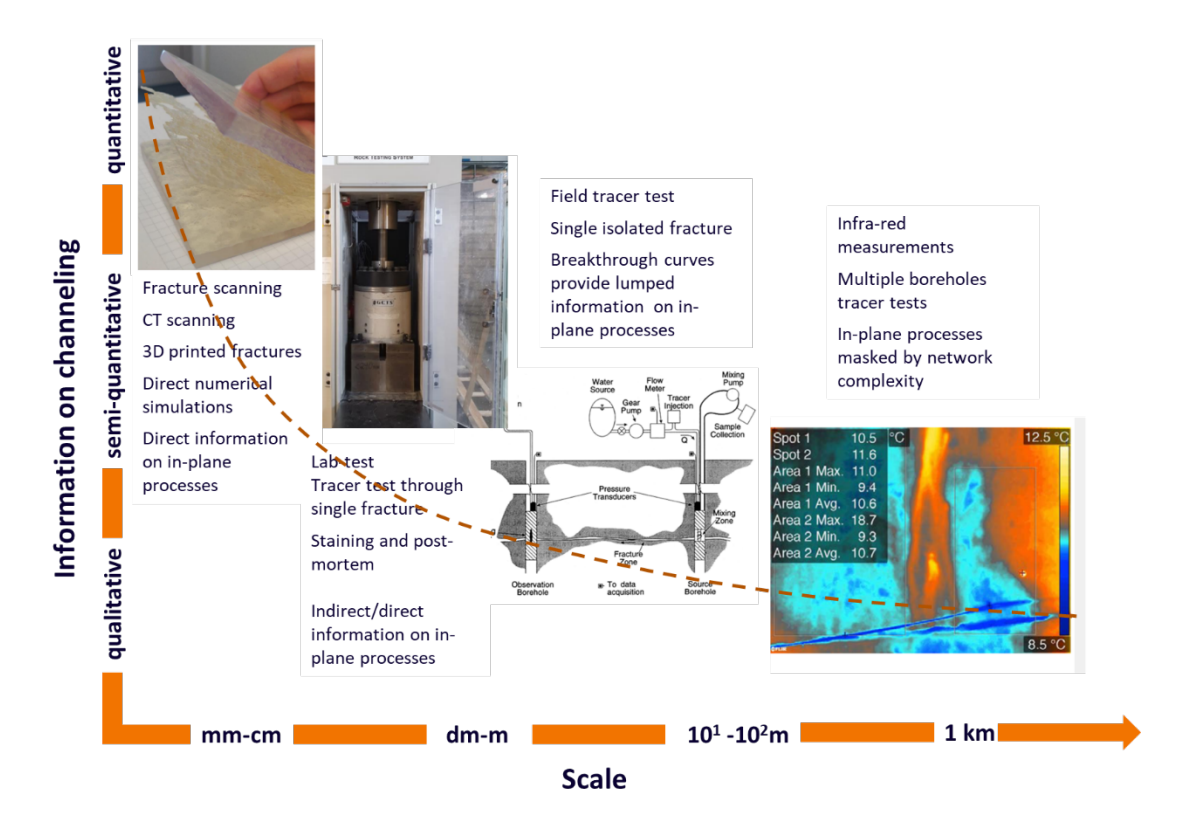


Figure 6-1. Sketch summarising the "tyranny of scales": information of in-plane groundwater flow processes degrades rapidly with increasing scale. The figure uses illustrations from Neretnieks et al. (2018), Bodin et al. (2003) and internal SKB presentations.

6.3 Flow-related parameters and pathway tracing

6.3.1 Methodology for quantification of parameters

Flow-related parameters are dependent on fracture characteristics, primarily fracture aperture or specific flow-wetted surface area, but also fracture intensity for models based on continuum representations. As such, they are strictly related to the site characterisation of the fractured medium and are typically obtained from Discrete Fracture Network (DFN) modelling combined with groundwater flow models and particle tracing (Figure 6-2). Notice that groundwater flow models might in turn be based on either an explicit DFN representation or an ECPM approach, or a combination of these. When an ECPM approach is used, flow-related parameters need to be properly upscaled.

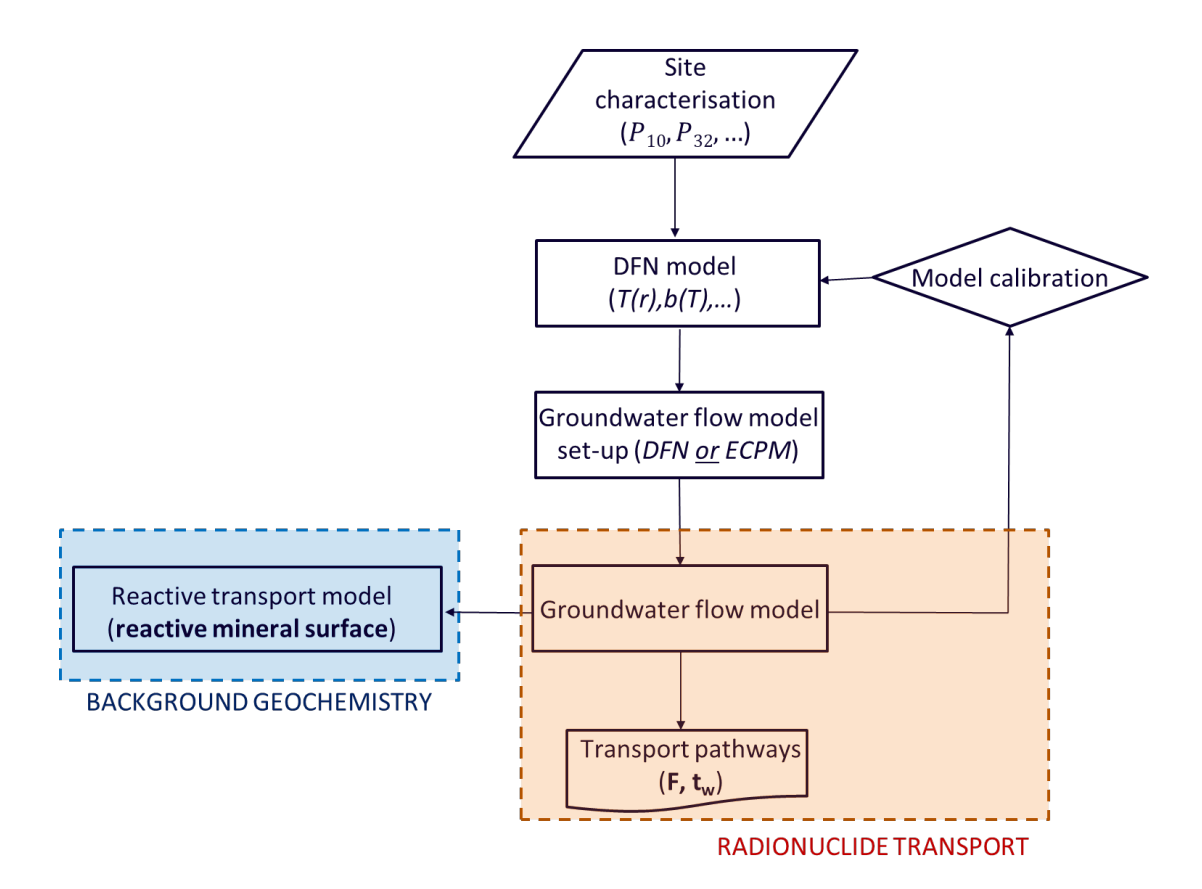


Figure 6-2. Flowchart showing the transport modelling procedure with emphasis on the derivation and/or parameterisation of flow-related parameters (F and t_w). The methodology for groundwater flow model calibration is described in Odén et al. (2025).

A stepwise methodology for the calculation of flow-related parameters is shown in Figure 6-3. The first step of this methodology consists in the construction of a DFN model of the site under investigation. The construction of a such a DFN model entails the integration of several field observations, such as data from outcrops and core logging. Besides reliably describing the geological conditions of the site, in terms of e.g. fracture intensity, the DFN model must be able to reproduce the general hydraulic behaviour of the medium. More information on the construction of DFN models is provided in the DFN modelling methodology report (Selroos et al. 2022).

Groundwater flow conditions at depth are strongly influenced by external drivers, which have a direct effect on boundary conditions. Thus, the definition of flow boundary conditions needs to be substantiated by supporting data and models, including climate models and landscape models (e.g. models describing topography and bathymetry). External drivers could also affect domain discretisation. The subsequent part of the flowchart in Figure 6-3 is conditioned on the methodology to be used to simulate groundwater flow and to subsequently delineate transport pathways.

Explicit DFN modelling implies that the level of detail of transport pathways is the single fracture. This in turn implies that channelling effects can be considered either explicitly (i.e. describing the fracture internal variability) or using simplified representations. The former option is probably computationally infeasible given the large size of models used in safety assessment calculations. Possible simplifications include the population of tessellated fractures in a "chequerboard" fashion using relatively large patches (Figure 6-4). However, it should be noted that although internal aperture variability could be important in some cases, the main contributor to channelling likely often is the network effect.

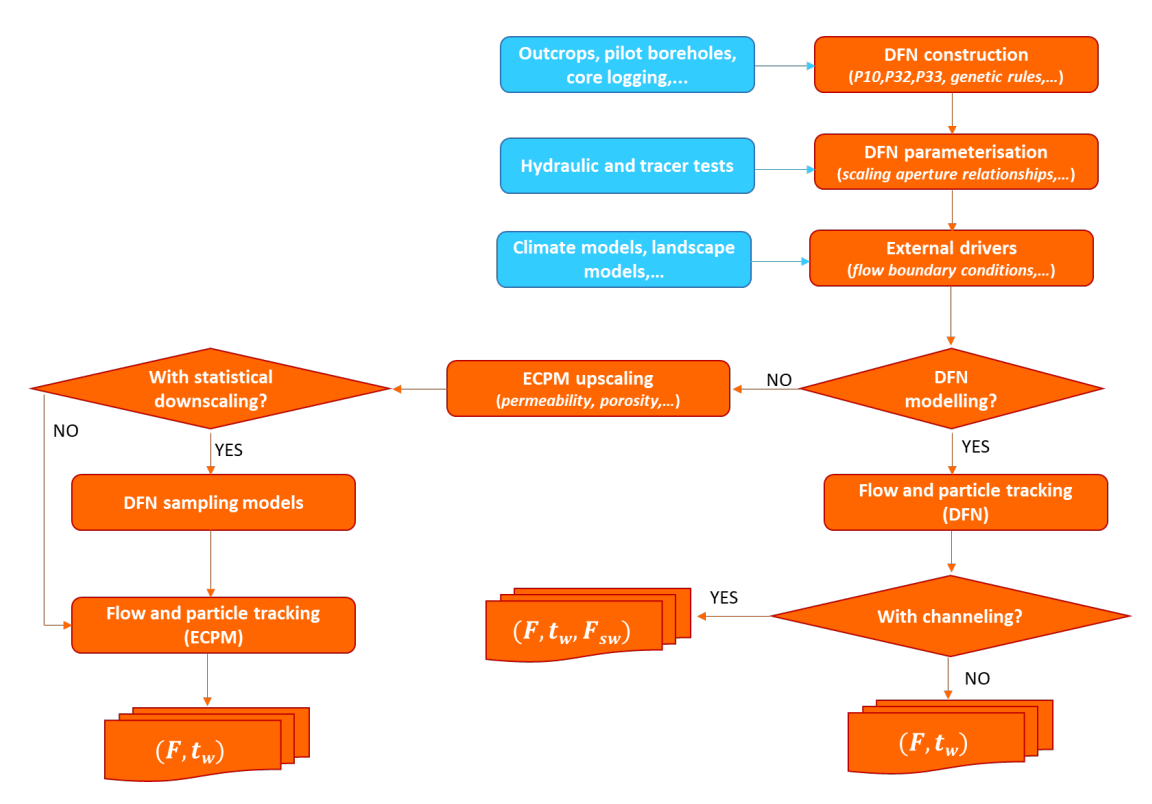


Figure 6-3. Flowchart showing the steps and alternative approaches for the calculation of flow-related parameters. Dependencies on supporting data and models are indicated by the blue boxes. The parameter F_{sw} is an "F-factor" for the stagnant water zones, cf. Mahmoudzadeh et al. (2013).

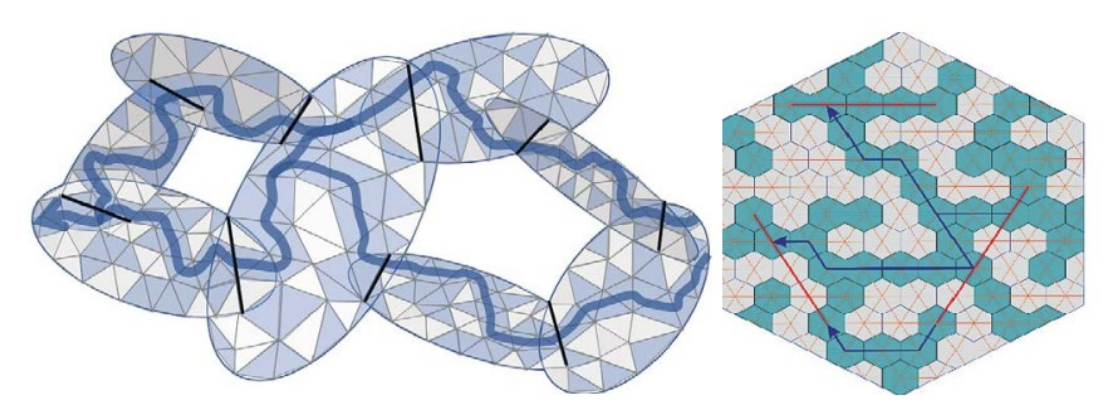


Figure 6-4. Chequerboard representation of openings distributed randomly over a tessellated fracture (implemented on triangles on the left and on a hexagonal Voronoi mesh on the right) creating channelised flow as indicated by the arrows. Figure taken from Selroos et al. (2022).

6.3.2 Pathway delineation in different codes

In the process and parameter overview chapter of this report (e.g. Section 3.2.2), it is discussed that radionuclide transport simulations are typically carried out using a fixed pathway representation and that radionuclide retention depends on the transport resistance (the F-factor). Pathway tracing is typically done using particle tracking calculations and the underlying groundwater velocity field is taken from existing hydrogeological models. These models are either based on a DFN representation of the fractured medium or upscaled in a continuum grid using the so-called Equivalent Continuous Porous Medium (ECPM) approach.

In DFN models, fluid flow along fractures is explicitly resolved and fracture features, such as aperture, are retained and explicitly used to quantify the transport resistance. Transport pathway delineation carried out in DFN models samples single fracture segments and thus transport

resistance is defined on a segment basis using the computed groundwater travel time and the assigned fracture half-aperture (*b*), as discussed in Section 3.2.2.

In ECPM formulations, the F-factor is computed based on contributions from multiple intersecting fractures. Upscaling methods are required in ECPM models. It turns out that an important condition for a proper parameterisation in ECPM-based radionuclide transport calculations is that the ECPM model honours the observed fracture statistical properties of fracture intensity and fracture volume fraction. Notice that models based on the pathway simplification could include also flowpath segments in the near-surface unconsolidated Quaternary deposits, as was done for instance in Selroos and Painter (2012).

The preferred method for tracing pathlines in ConnectFlow since ODFN3 (Olkiluoto DFN model version 3, Hartley et al. 2018) is the "mass-conserving method", which is based on the formulation presented by Cordes and Kinzelbach (1992). The mass-conserving method performs well if the flow solution is accurate. The same mass-conserving method applies to ECPM-based calculations.

DarcyTools particle tracking can be used in two different modes of operation. The first is the traditional way of moving the particle along the local velocity vector (similar to what is done in the "standard method" of ConnectFlow), while the second method uses the so-called "cell-jump" approach. In the second approach, a particle stays in a cell for a time equal to the free volume of the cell divided by the flow rate through the cell and then jumps to a neighbouring cell that has an outgoing flow direction. The choice of neighbouring cell is made with a likelihood that is proportional to the flow rates, which means that complete mixing in a cell is assumed.

DarcyTools uses an ECPM representation of the fractured system, which implies that transport resistance needs to be properly represented in the underlying DFN. The equivalent transport resistance *F* (Chapter 3, Section 6.1) of the *i*-th particle jump is computed as follows (Ferry 2019):

$$F = \int_{0}^{\tau} \frac{FWS}{V_{v}} d\varepsilon \tag{6-1}$$

where V_{ν} is the local free volume along the particle trajectory and FWS [L²] is the local flow-wetted surface area. For stochastically generated fractures, the flow-wetted surface area is computed using the following power-law relationship:

$$fws_i = fws_0 \cdot T_i^{-\lambda} \tag{6-2}$$

where fws_0 is a scaling factor, T_i [L²T⁻¹] is the fracture transmissivity and λ is an empirical exponent. The subscript here indicates that the value applies to the single *i*-th fracture. The local flow-wetted surface area of the *j*-th grid cell is computed as a size weighted sum of contributions:

$$FWS_j = L_j \sum_{i=1}^n \frac{fwS_i}{l_i^*} \tag{6-3}$$

where L_i [m] is the grid cell size and

$$\begin{cases}
l_i^* = l_i & \text{if } l_i \le L_j \\
l_i^* = L_j & \text{if } l_i > L_j
\end{cases}$$
(6-4)

As discussed in Section 3.2.2, the fixed transport pathway simplification has several advantages, especially related to computational efficiency and the absence of numerical dispersion. However, the formulation also has important limitations concerning the handling of transient groundwater flow conditions, which only can be considered in the form of a uniform scaling of groundwater travel time and transport resistance for the whole set of flowpaths (see Selroos et al. 2013).

It should be noted that transient flow conditions could affect also flow directions and locations of flowpaths, which might have further implications for the effects of retardation processes (i.e. both flow magnitudes and flowpath locations affect retardation). Detailed analysis of such cases requires other modelling approaches than the fixed transport pathway representation.

6.4 Examples of supporting analyses

Fracture internal heterogeneity as well as network-scale connectivity might lead to flow channelling, which is the situation when groundwater flow is restricted to a limited part of the fracture surface. Flow channelling could have a significant impact on radionuclide transport and retention but also on the potential buffering capacity of the fractured medium against potential geochemical perturbations. Evidence of flow channelling has been observed in several laboratory and field experiments. A review of experimental observations was produced by Tsang and Neretnieks (1998).

Watanabe et al. (2009) performed integrated experimental-numerical analyses on flow through shear fractures and quantified the channels and proportions of contact and noncontact areas (Figure 6-5). Despite the still largely unresolved challenges related to model parameterisation, these studies emphasise the significant influence of flow channelling on transport and retention. Further efforts are required to derive robust effective parameters for use in segment-based time-domain random walk simulations.

In a recent work, Trinchero et al. (2021) analysed the combined effect of variable fracture aperture (Figure 6-6a) and fracture-filling mineral patches (Figure 6-6b) on the fracture hydrodynamic retention properties. The model was built using a Darcy-Brinkman-Stokes formulation (Molins et al. 2021), which was implemented into the computational fluid dynamic code OpenFOAM (Jasak et al. 2007) and includes geochemical reactions, namely the dissolution of the mineral patches. The results of the modelling show that mineral patches act as throats and lead to channelling forcing some of the particles through parts of the fracture with smaller aperture (Figure 6-6c). Thus, the related observed distribution of F shows a significant tail. Once mineral patches have been dissolved the variance of F decreases and the distribution shows much less tailing (Figure 6-6d).

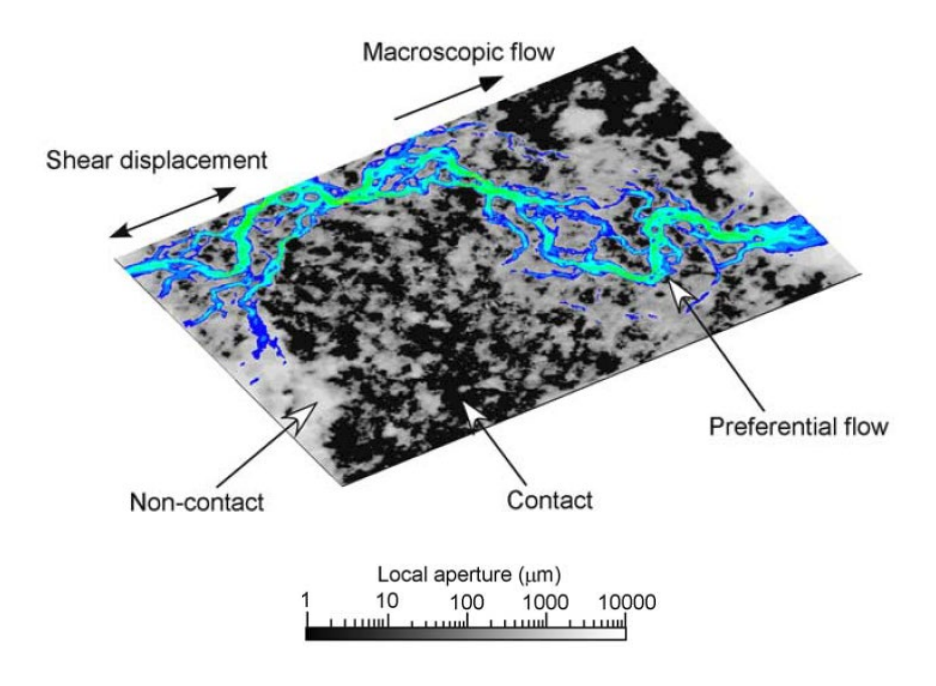


Figure 6-5. Composite image showing fracture aperture and the development of preferential flowpaths from Watanabe et al. (2009) in a core sample of dimensions 95 mm by 150 mm.

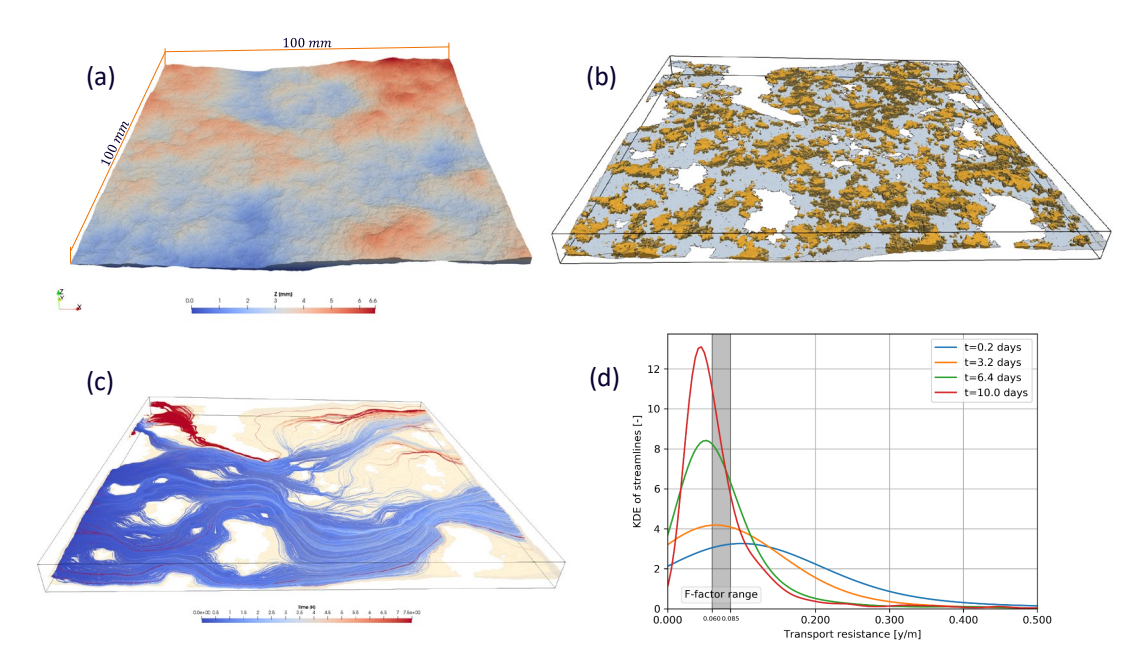


Figure 6-6. (a) Fracture aperture, (b) distribution of calcite mineral patches, (c) streamline delineation and (d) distribution of transport resistance at different times. Note that after 10 days most of the mineral patches have been dissolved. Figures from research reported in Trinchero et al. (2021).

Flow channelling has potential implications for both the parameterisation of radionuclide transport models with flow-related parameters and for the modelling of radionuclide retardation. In a fracture plane characterised by strongly channelised flow, only parts of the fracture surfaces are in contact with flowing groundwater, which means that the fracture surface area taking part in mass transfer and radionuclide retardation is reduced. This implies that flow-related parameters quantified using the whole fracture surface areas need to be modified to adequately reflect the prevailing conditions. Reductions of F-values have been made in some of the earlier Posiva and SKB safety assessments. No such reduction was applied in SR-Site and PSAR SFK, see discussion in SKB TR-21-07 (Section 2.1.1).

The other main effect of channelling is that parts of the water volume in the fracture plane are immobile (stagnant) and therefore may contribute to radionuclide retardation in essentially two ways: (1) retardation in the stagnant water itself following diffusion from the flowing water, and (2) retardation in the matrix following diffusive transport through the stagnant water to the matrix with the stagnant water providing access to additional fracture surface area compared to that in directly contact with the flowing water.

The second mechanism implies that the effect of channelling on retardation under certain conditions could be compensated by diffusive transport through the stagnant water. The effects of stagnant water on solute transport were investigated in a recent modelling study, which concluded that the impact of stagnant water on solute retardation was modest (Sanglas et al. 2024). It may be noted that SKB is carrying out a research programme in this area that will improve the knowledge on transport in heterogeneous fractures, especially regarding coupled processes.

As indicated by the examples summarised above, extensive experimental and modelling studies could be performed to investigate the basis for in-plane transport processes and simplifying assumptions related to calculations of flow-related transport parameters in the relatively large-scale groundwater flow models that are used for this purpose. This is not to say that site-specific versions of this kind of studies should be carried out in connection with all forthcoming site descriptions and/or safety assessments. Most likely, estimates based on less detailed information, possibly from supporting DFN modelling in combination with expert judgement, will be sufficient in most cases.

For the purposes of the present report, it is sufficient to emphasise that the effects of channelling on flow-related parameters should be assessed. Whereas no specific methodology for this assessment is devised, it should be noted that an example and possible starting point is provided by the modelling study of channelling performed for SR-Site, which was used also in the PSAR SFK reporting, from which Figure 6-7 is taken (SKB TR-21-07, Appendix A). The effects of stagnant water on radionuclide retardation are probably best addressed through sensitivity calculations using already available SKB modelling tools. Any supporting modelling associated with flow-related parameters or retardation related to stagnant water zones could be organised within the framework of the inter-disciplinary cooperation proposed in Section 6.1.

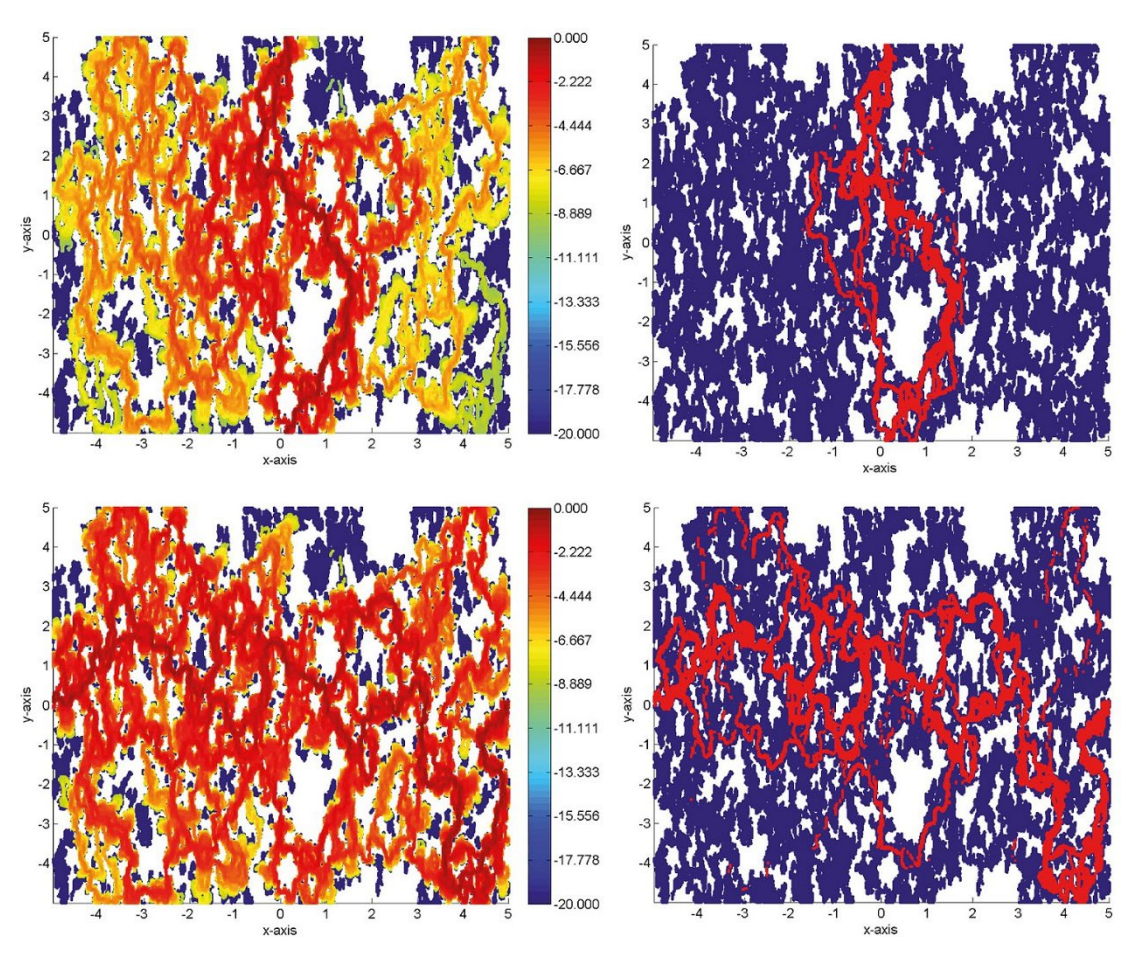


Figure 6-7. Example results from SR-Site/PSAR SFK channelling analysis (SKB TR-21-07, Appendix A) showing typical dynamic flow channels arising in a variable aperture fracture with a surface asperity contact fraction of 40 % and hydraulic gradient applied vertically (top) and horizontally (bottom) for a simple line source/sink dipole boundary condition of limited extent. Hydraulically inaccessible regions of the fracture are non-coloured. The left-hand images indicate the flow magnitude normalised with respect to the maximum flow rate (\log_{10} units). The right-hand images show flow channels featuring flow > 1 % (arithmetic units) of the maximum flowrate highlighted in red.

7 Transport simulations

As discussed in the introductory chapters, the present report provides methodology for two main groups of activities, i.e. derivation (including data interpretation) of transport parameters and development (including parameterisation) of transport models. Whereas the parameters are discussed in chapters 5 and 6, Chapter 4 describes the first step in the model development, the establishment of a site-specific retardation model. The present chapter describes the continued model development, with focus on the radionuclide transport simulations performed in safety assessments.

The aim of this chapter is not to present methodology covering all aspects of the radionuclide transport modelling to be performed in future safety assessments. Much of this methodology will be developed and described within the planning of forthcoming safety assessment projects. Furthermore, the methodology for safety assessments is continuously being further developed and tested as part of the preparations for the upcoming license applications.

Instead, the main purpose of the present chapter is to describe how the retardation model (Chapter 4) and the retardation parameters (Chapter 5) are taken further in the modelling process, especially how they are applied in the identification of "transport classes" and the parameterisation of radionuclide transport models (Section 7.4). However, this requires some background and context, which is why the chapter also contains descriptions of the overall radionuclide transport modelling (Section 7.1), numerical modelling approaches (Section 7.2), and modelling tools (Sections 7.3).

In addition, the present chapter briefly discusses the planned future use of modelling tools (also included in Section 7.3), transport by gas and colloids (Section 7.5) and transport modelling to be performed by other modelling disciplines (Section 7.6). These other disciplines are Hydrogeology and Hydrogeochemistry, where processes similar to those influencing radionuclide retardation are modelled. Other transport simulations, such as those that might be performed for the environmental impact assessment, are not considered here.

7.1 Overview of radionuclide transport modelling

7.1.1 Model domains and modelling methodology

Figure 7-1 shows a generic conceptual model of radionuclide transport from a nuclear waste repository in the bedrock up to the surface and further within and between different types of surface ecosystems where humans and non-human biota (NHB) could potentially be exposed to radionuclides. A hypothetical flowpath, along which dissolved radionuclides could be transported, is shown as a red dotted line. The figure illustrates/indicates the three main types of transport domains that are considered in the radionuclide transport modelling:

- The repository and its engineered (man-made) barriers that are represented using so-called nearfield transport models describing the source term (inventory) and release of radionuclides from canisters (SFK), waste vaults (SFR), and other repository components.
- The bedrock or geosphere (often referred to as the far-field in safety assessments) where radionuclide transport takes place in fractures and larger deformation zones, as described in geosphere/far-field transport models representing radionuclide transport from the repository to (usually) the bedrock surface.
- The surface system or biosphere where radionuclides arriving with discharging deep groundwater are further transported by near-surface groundwater and surface water systems, as described in biosphere transport models which also include the quantification of consequences in terms of doses to humans and NHB.

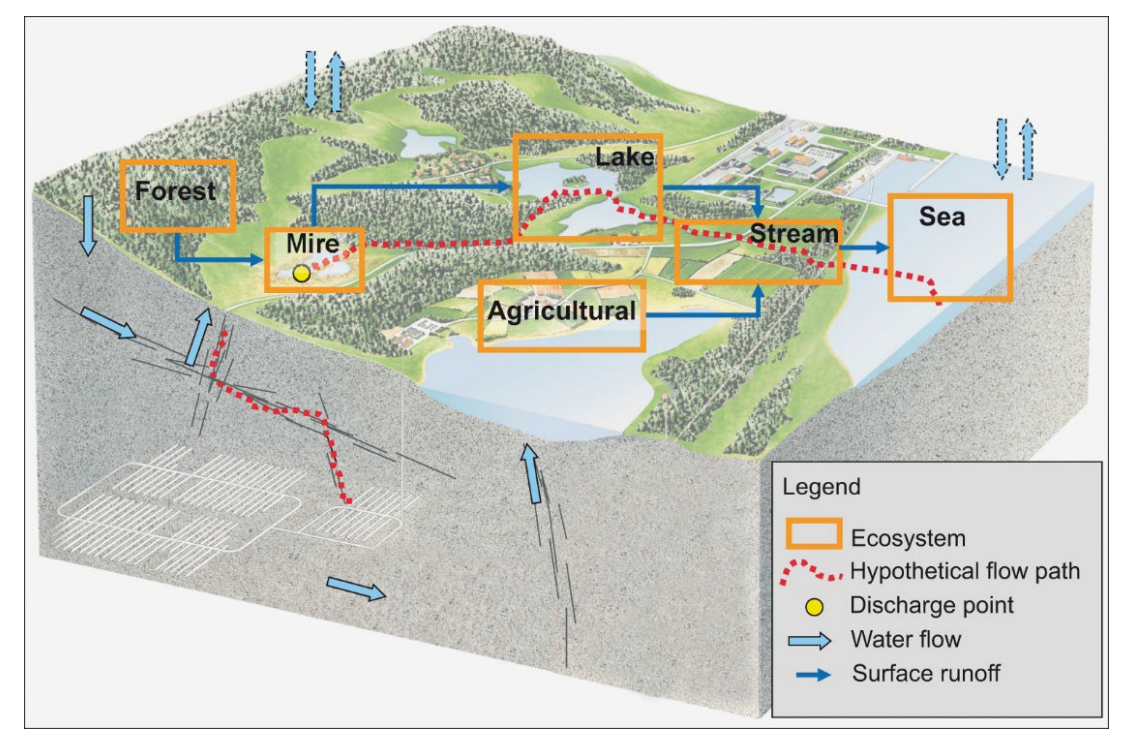


Figure 7-1. Conceptual model of radionuclide transport along a hypothetical flowpath from a nuclear waste repository, which is indicated by the white lines in the grey bedrock part of the model, up to a discharge point (the yellow dot in the box marked "Mire"), and further through different types of surface ecosystems to the sea. Figure from Lindborg (2010).

It follows that whereas the present modelling methodology is focused on transport in the bedrock, also other systems need to be involved in site descriptive and safety assessment transport modelling to provide a complete account of transport properties relevant for site description and safety assessment. Essentially, these systems include man-made repository components and the surface systems above the bedrock surface.

In the safety assessment, the transport modelling is divided into near-field models, representing the radionuclide sources and engineered barriers in the repository, far-field models, describing transport in the geosphere (bedrock), and biosphere transport models for calculating radionuclide transport and doses in the surface systems. The following sub-sections give overviews of the SFK (Section 7.1.2) and SFR (Section 7.1.3), with emphasis on overall modelling procedures and near-field models, whereas the biosphere modelling is outlined in Section 7.1.4. Some additional comments and suggestions are given in Section 7.1.5.

Figure 7-2 gives an overview of safety assessment models and data flows using SR-PSU (SKB TR-14-09) as an example. Most of the input data are represented by the ovals to the left in the figure. However, the inputs of geosphere transport parameters come from the "Migration and material data for rock" (retardation parameters) and "Far-field flow" (flow-related parameters from the hydrogeological modelling) ovals. The main radionuclide transport models are linked through the "Release" arrows, i.e. the near-field model release provides input to the far-field/geosphere model which processes the input to a far-field release to the biosphere model. This is the "radionuclide transport modelling chain" applied in slightly different variants in all safety assessments.

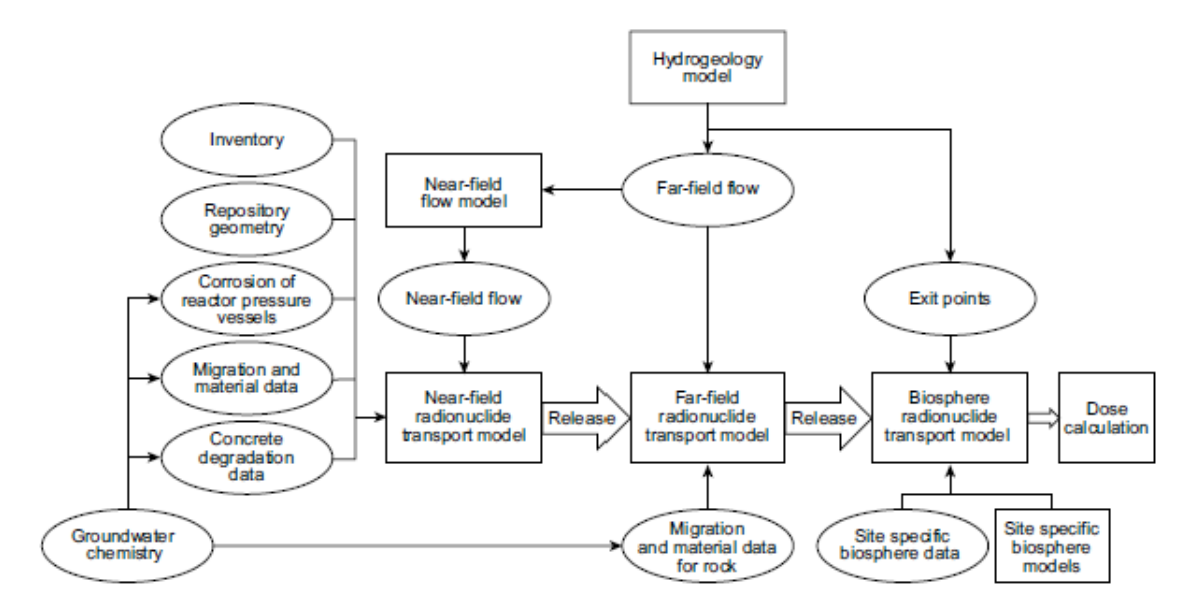


Figure 7-2. Models and data for the radionuclide transport and dose calculations in SR-PSU. Boxes represent modelling activities and ovals represent data. Figure from SKB TR-14-09 (Figure 2-3).

7.1.2 The spent fuel repository (SR-Site and PSAR SFK)

In the radionuclide transport simulations for the SFK safety assessments SR-Site and PSAR SFK, there is a division into three main model domains in the modelling chain. As indicated in Figure 7-3, there is a separate/off-line biosphere transport model which is providing "LDF values" (landscape dose conversion factors) that represent the biosphere in the calculations of radionuclide transport and doses. Thus, these LDFs are used to convert release rates from the geosphere to annual doses (e.g. SKB TR-21-01).

Calculations of radionuclide release and transport for the SFK near-field are performed using the computer code COMP23 (Romero 1995, Cliffe and Kelly 2006, Kelly and Cliffe 2006). This is a multiple-path compartment model used for transient radionuclide transport calculations in the near-field of a KBS-3 repository system, i.e. the canister and the other engineered system components (Figure 7-4). In analogy with an electrical circuit network, the model uses a network of coupled resistances and capacitances.

Instead of using fine discretisations of sensitive zones, i.e. at the exit point of the canister hole and at the entrance to fractures, analytical solutions are embedded to enhance calculation speed. An implementation of the COMP23 model written in Matlab/Simulink is used for the near-field transport calculations. This implementation of COMP23 is also called Compulink (Vahlund and Hermansson 2006). As further explained below, both these near-field codes require information derived from groundwater velocity fields calculated with groundwater flow modelling codes (ConnectFlow and DarcyTools).

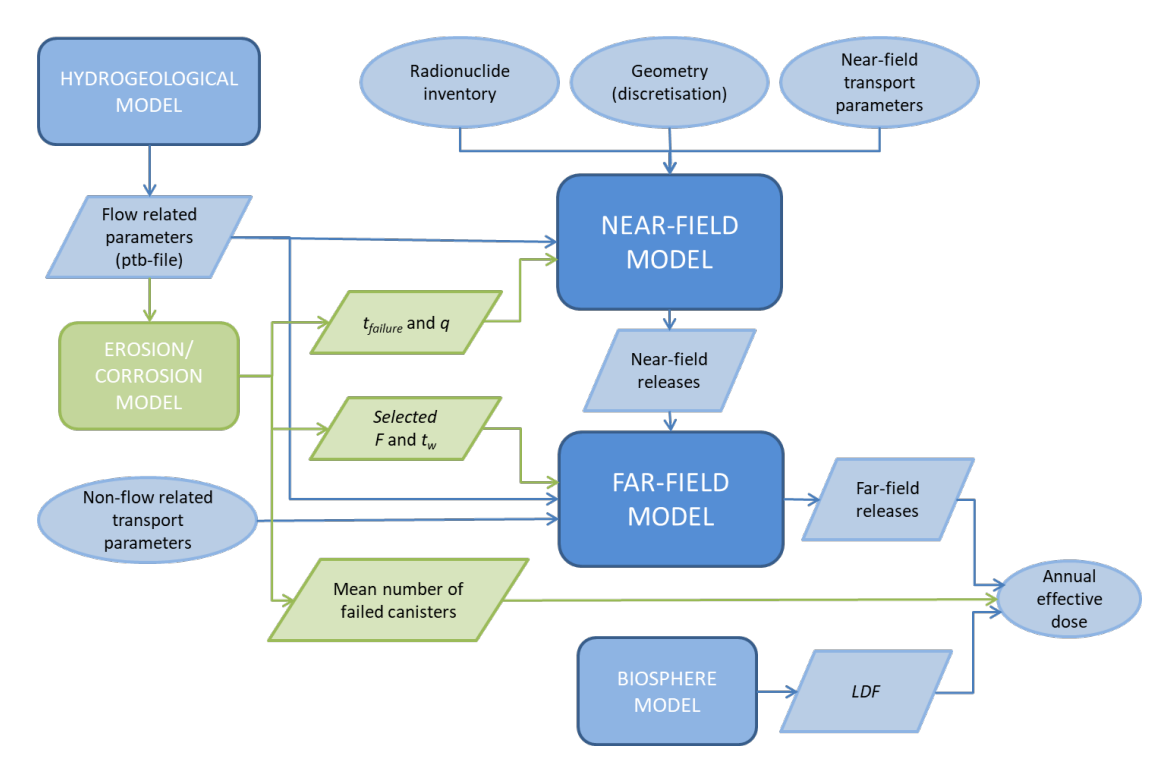


Figure 7-3. Model linkages and data flows in the radionuclide transport simulations carried out for SR-Site and PSAR SFK. Models are indicated by rectangles, data transferred between models by parallelograms and other input/output data by ovals. The erosion/corrosion model and related output, failure time ($t_{failure}$), flow in deposition hole (q), flow-related transport resistance (F), advective travel time (t_{w}) and the mean number of failed canister are shown in a divergent colour (green) as this model is only used in the scenario with canister failure due to corrosion. Note that the erosion-corrosion model does not actually calculate the F and t_{w} values, rather a selection of values from the ptb-file is propagated based on the results from the erosion-corrosion calculations.

Figure 7-4 shows the canister, deposition hole and deposition tunnel backfill and how these are modelled by COMP23 in the growing pinhole scenario, which is one of several scenarios modelled in the safety assessments for SFK. The near-field model includes processes related to radionuclide release and transport in the canister interior, the buffer and the deposition tunnel backfill. These incorporate the processes radioactive decay, metal corrosion (modelled as a constant metal corrosion rate), fuel dissolution, dissolution of gap inventory (modelled as an instantaneous release; "gap" refers to the gap between fuel and cladding), speciation of radionuclides (i.e. dissolution/precipitation of nuclides with shared elemental solubilities), diffusion and sorption in the buffer and advection, and diffusion and sorption in the deposition tunnel backfill.

As illustrated in Figure 7-4, the near-field model also handles the release of radionuclides to up to three different release paths from the near-field, depending on scenario: a fracture intersecting the deposition hole at the vertical position of the canister lid, denoted Q1, an excavation damaged zone, EDZ, in the floor of the deposition tunnel (if such a zone is assumed to exist), Q2, and a fracture intersecting the deposition tunnel, Q3. The advective flow rates (derived from the Darcy flux, U_0) as well as the equivalent flow rates, Q_{eq} , at all three release paths Q1, Q2 and Q3 are calculated as an integral part of the hydrogeological modelling and transferred to COMP23.

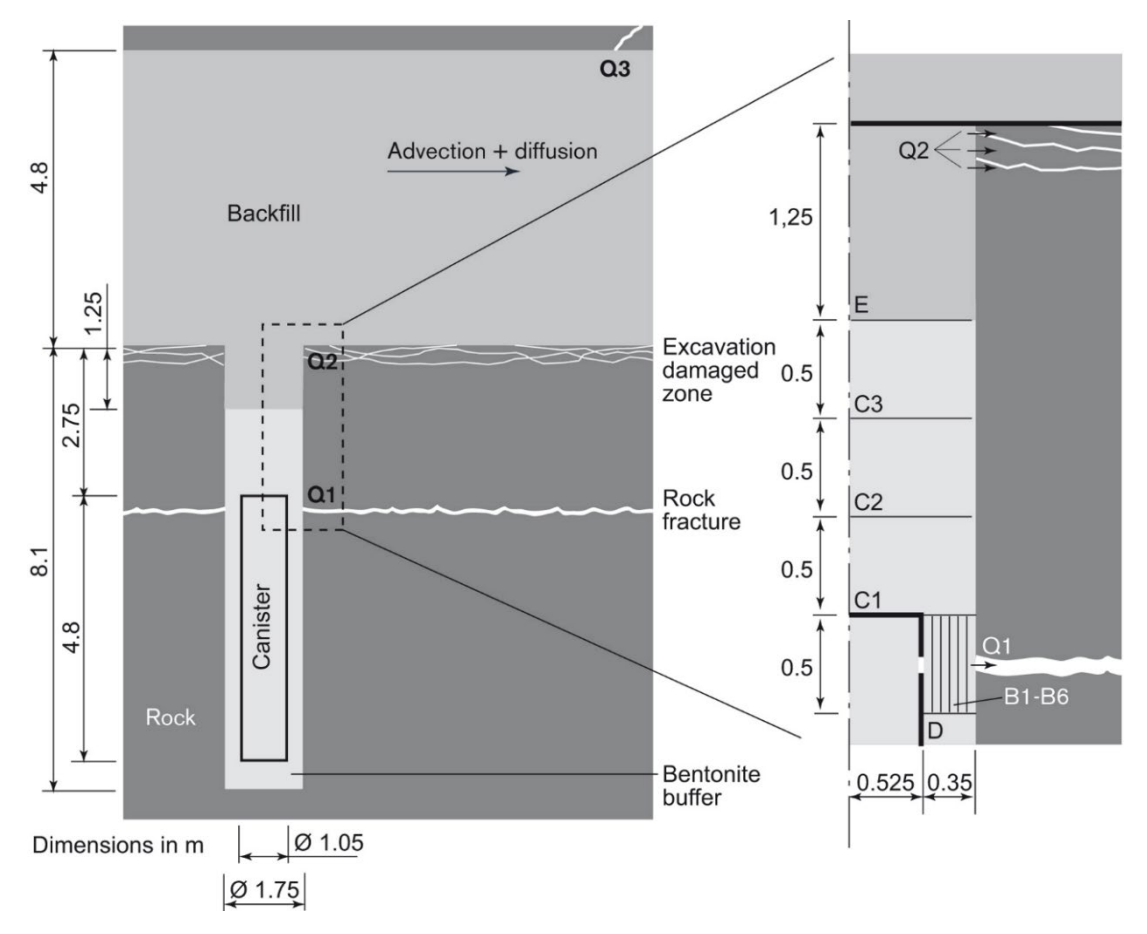


Figure 7-4. COMP23 model for the growing pinhole scenario, with details of its model representation as compartments B1–B6, C1–C3, D and E. The release paths Q1, Q2 and Q3 to a fracture intersecting the deposition hole, to the excavation damaged zone, and to a fracture intersecting the deposition tunnel, respectively, are also shown. Figure from SKB TR-21-07 (Appendix G).

The radionuclide transport is assumed to occur by diffusion in the buffer and backfill in the deposition hole and by diffusion and advection in the deposition tunnel. The nuclides are sorbed with varying efficiency in the buffer and backfill. The water flow, the diffusion and sorption properties in the backfill determine the time for advection and diffusion through the buffer and backfill to the rock at the three release paths Q1, Q2 and Q3.

Advective conditions in the buffer, as in the corrosion scenario, are simply treated by equating the outflux from the canister interior compartment with the release to Q1. The release paths Q2 and Q3 are not modelled when advective conditions are assumed in the buffer since releases to Q1 completely dominate over those to Q2 and Q3 in such cases. COMP23 calculates the radionuclide release rates in terms of moles of radionuclides per unit time and realisation. More details on the discretisation, parameterisation, diffusion resistances and boundary conditions used in the different scenarios are provided in SKB TR-21-07 (Appendix G).

7.1.3 The SFR repository (SR-PSU and PSAR SFR)

In SR-PSU (Figure 7-2), all calculations were performed with models implemented in the ECOLEGO modelling tool, which is a tool for creating compartment models and performing deterministic and probabilistic simulations (SKB TR-14-09). Thus, in SR-PSU the geosphere transport was represented as compartments using similar modelling concepts as the near-field and biosphere models. The geosphere part was integrated and attached to the near-field models for each waste vault. In principle, compartment models of the same type were used in PSAR SFR, although with some differences in the specific tools employed. In the following the PSAR SFR modelling is summarised based on the description in the main report of that safety assessment (SKB TR-23-01, Section 7.3).

The model chain starts with the near-field model that describes the transport, retardation and release of radionuclides in and from the waste domain and the surrounding engineered barriers in a vault (Figure 7-5). The radionuclide release to the geosphere at the waste vault-bedrock interface is also calculated. The geosphere model describes the subsequent transport and retention of radionuclides through and in the fractured bedrock towards the surface. The biosphere model describes transport and accumulation of radionuclides in aquatic and terrestrial ecosystems (Section 7.1.4).

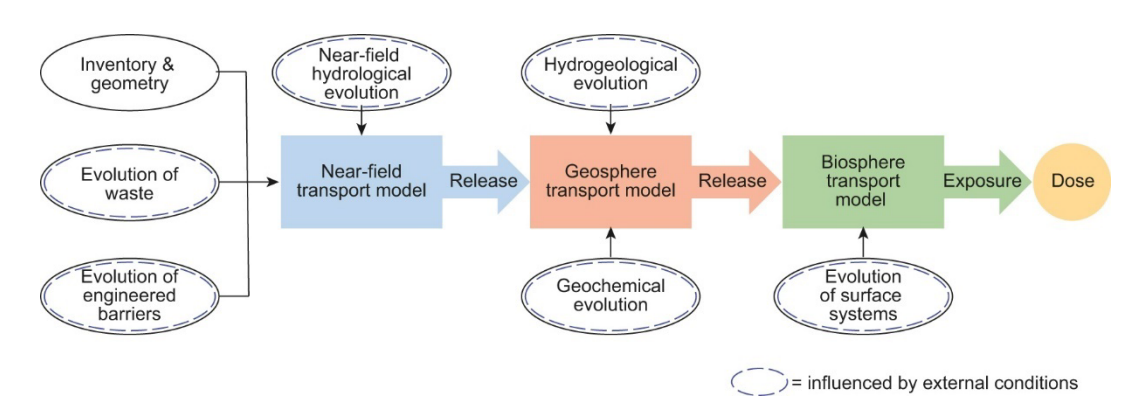


Figure 7-5. Models and data used for the radionuclide transport and dose calculations in PSAR SFR. Boxes represent modelling activities and ovals represent data. Dashed ovals indicate that the data are influenced, directly or indirectly, by external conditions. Figure from SKB TR-23-01 (Figure 7-1).

All models are implemented as compartment models. This approach assumes that the system can be adequately represented by discretisation into a limited number of model compartments, each of which is internally homogeneous and connected to other compartments. In PSAR SFR, the near-field and biosphere models are implemented in the ECOLEGO compartment modelling software, and the geosphere model is implemented in Matlab (SKB TR-19-06, Appendix B "FARFCOMP – an implementation of a geosphere modelling tool in Matlab"). Thus, off-line biosphere modelling and landscape dose conversion factors (LDFs) were not used in the SFR radionuclide transport modelling.

The radionuclide transport calculations are carried out as dynamic simulations, where the output from one model, in terms of the annual activity release for each radionuclide, is used as input to the next. The modelling tools are coupled indirectly, i.e. the model chain has been executed for one entity at a time followed by a semi-automatic transfer of results to the calculation tool for the subsequent model. To ensure functional coupling between the three models, the models have been designed to use compatible definitions of the parameters. Calculations are performed both deterministically and probabilistically for most calculation cases.

The near-field models describe the transport and retention of radionuclides in the waste domain and the surrounding engineered barriers as well as releases of radionuclides from the waste vaults to the geosphere. To account for different barrier designs and waste types, separate models have been developed for each waste vault in the extended SFR.

The engineered concrete barriers and bentonite barriers (only for the silo) limit the release of radionuclides from the near-field by reducing the groundwater flow through the waste and by providing sorption capacity for many radionuclides. These barriers are explicitly represented by several model compartments in the near-field models.

The transport in the macadam backfill is dominated by advection. Thus, the release of radionuclides from the near-field, for all vaults except the silo, is calculated as the sum of the advective transfers from the backfill compartments to the geosphere. As bentonite constitutes the main hydraulic barrier in the silo, the transport of radionuclides to the geosphere from this vault is predominantly diffusive rather than advective. Therefore, transport from the silo to the geosphere is represented by an equivalent water flow, $Q_{\rm eq}$, which depends both on the diffusivity of radionuclides in water and the flow-related migration properties of the geosphere.

7.1.4 Biosphere models and interface to the geosphere

In addition to the calculations of flow-related parameters, a second important transport-related output from the particle tracking simulations in bedrock groundwater flow models is that they provide discharge points (also called exit points) in the biosphere. These discharge points indicate where flowpaths from release locations in the studied repository reach the biosphere, and hence also where radionuclides hypothetically travelling along these flowpaths would enter the biosphere where humans and the environment could be exposed to the contamination.

In the radionuclide transport modelling for the SFR repository, both the time and starting location for which the release is assumed to start are relatively well-defined. However, for the SFK repository, both the release location and the timing of the releases are considerably more uncertain. Depending on the considered scenario, none, one, or several canisters may potentially fail, with failure times that may span several glacial periods. Consequently, the time and location for the releases to the surface system are more delimited for SFR and could vary much more for SFK depending on which canister(s) that fail and when. The use of the LDF concept served as a means to ensure that all potential times and locations were covered by determining the maximum potential contribution for each nuclide for realistic future biosphere objects. Since the time and location for the release from SFR are more precisely defined, it is easier to directly couple the transport from the geosphere to the biosphere for that repository.

Figure 7-6 shows discharge points calculated using DarcyTools for the existing SFR repository and its planned extension. The calculations are performed in steady-state velocity fields representing different times in the future. For SR-PSU and PSAR SFR, these results from Odén et al. (2014) and Öhman and Odén (2018) indicate that, for most calculation cases, it is sufficient to use one so-called biosphere object (the object denoted as 157_2) as the primary discharge area for examining the effects of a geosphere release, i.e. the entire geosphere release is discharged to this object.

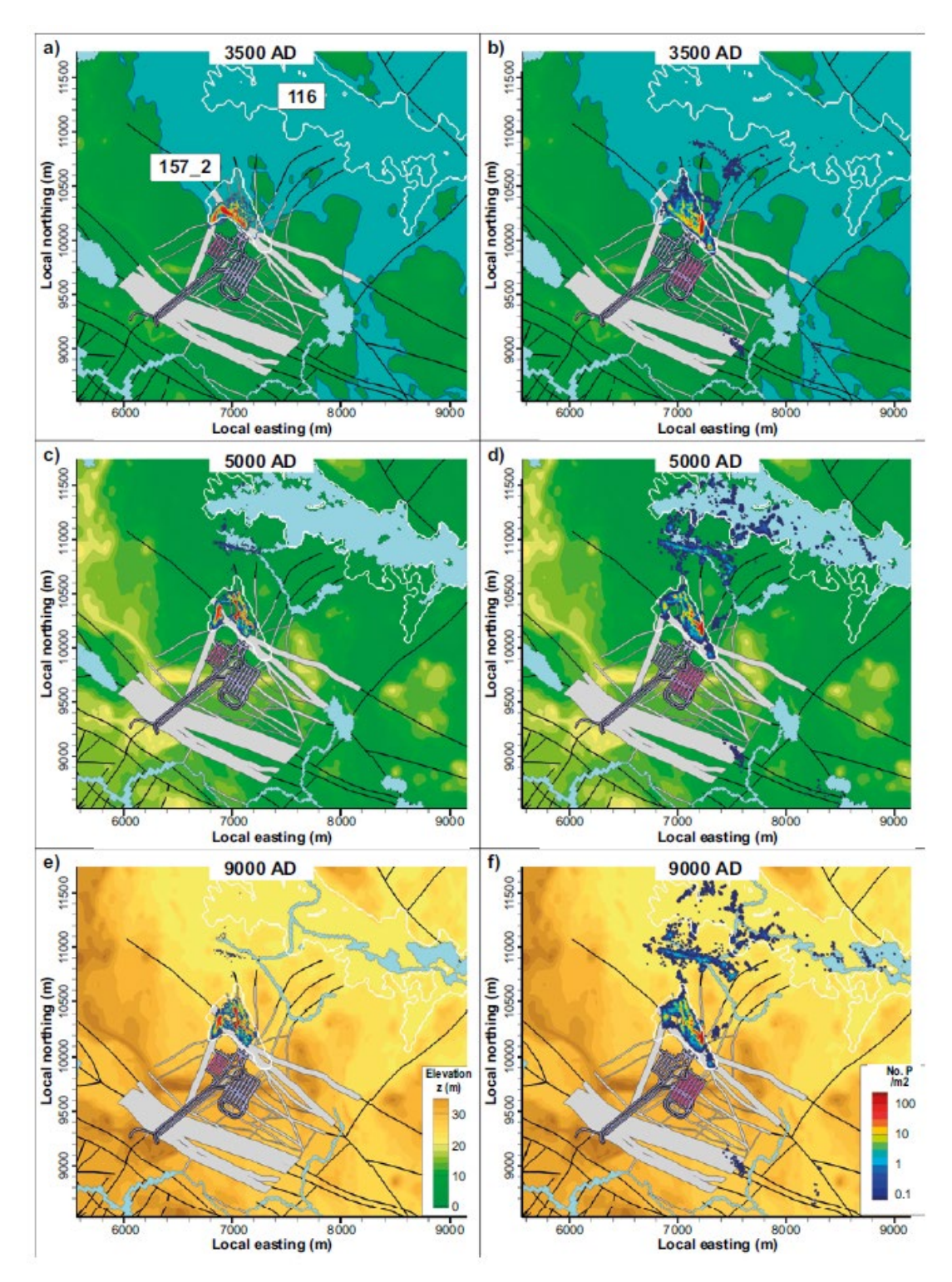


Figure 7-6. Maps of the locations where particles from the existing SFR repository (left) and the planned SFR extension (right) discharge into the regolith from the bedrock surface according to the DarcyTools simulations conducted in Odén et al. (2014). Discharge locations are presented in units of "particles per square meter" (No. P/m²). Results are presented for simulations representing 3500, 5000, and 9000 AD along with the delineation of biosphere objects 157_2 and 116 (white contours). Elevations are presented relative to the estimated sea-level at the time considered in the simulation.

This exemplifies how the geosphere particle tracking simulations direct the biosphere analyses by identifying the geosphere release locations that constitute the starting points of biosphere model development. Specifically, the discharge points are used to define biosphere objects for which compartment models used in transport and dose modelling are developed. The corresponding modelling procedure for SR-Site, including discharge points and description of modelling methodology, is presented in some detail in Lindborg (2010).

Radionuclide transport in the biosphere is described using the BioTEx model (Figure 7-7) which calculates radionuclide transport and accumulation in the near-surface environment and ecosystems as well as potential doses to humans and dose rates to non-human biota (NHB). The BioTEx model is based on earlier SKB biosphere models, especially the model developed for the SR-PSU assessment (Saetre et al. 2013). Two main types of ecosystems are simulated, namely aquatic ecosystems (including sea basins, lakes and streams) and terrestrial ecosystems (including mires and agricultural land).

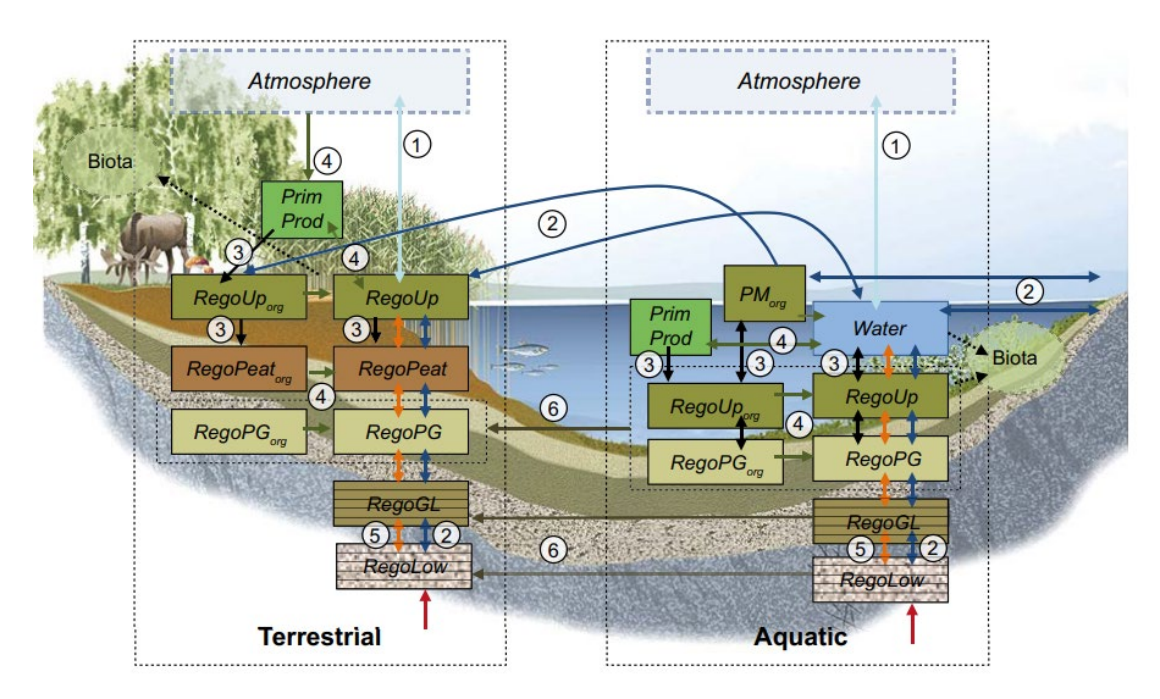


Figure 7-7. Conceptual model corresponding to the BioTEx model used to simulate transport and accumulation in a discharge area with coupled terrestrial and aquatic ecosystems (delimited by thin dotted black lines). Each box within the ecosystems corresponds to a radionuclide inventory associated with a physical or biological compartment. Sub-discretisation of radionuclide inventories is indicated by a solid black line within the box. Arrows represent flows of radionuclides between compartments and flows into and out of the system. Radionuclide flows are linked to mass flows of gas (1, light blue), water (2, dark blue) and solid matter (3, black), transformation between inorganic and organic forms of radionuclides (4, green), diffusion in soil pore water (5, orange), and ingrowth of wetland vegetation (6). The red arrows indicate that the geosphere release enters the biosphere via groundwater discharge to the till layer (compartments RegoLow). Dotted boxes (atmosphere and biota) are assumed to be in equilibrium with the corresponding environmental media, and the uptake of radionuclides into biota (dotted arrow) is not included in the mass balance of the BioTEx model. Figure from SKB TR-19-05 (Figure 8-1).

In BioTEx (Figure 7-7), radionuclides released from the geosphere enter the surface system through deep groundwater discharge into the lower layers of the model and then reach the soil, sediments, water and air. The distribution of radionuclides in aquatic ecosystems is represented by six compartments associated with several regolith layers, two compartments associated with the water, and one compartment associated with aquatic primary producers. Correspondingly, the distribution of radionuclides in mire ecosystems is represented by eight compartments associated with several regolith layers and one compartment associated with the mire vegetation. In addition, a garden plot is used to evaluate consequences of irrigation with water from a drilled well in the bedrock.

7.1.5 Future directions and implications for modelling methodology

Recent developments of the radionuclide transport modelling chain have been in the direction of model integration into one tool that includes the models for all three domains. Furthermore, the domain models have been developed towards more similar modelling approaches and representations, i.e. numerical compartment models and, if practicable, a uniform platform. Thus, the aim is to have an integrated fully numerical model chain, where the use of a compartment approach for the geosphere offers improved flexibility in terms of features and processes that can be represented and a faster solution method that enables more extensive "production calculations" of radionuclide transport.

For example, there is ongoing work to replace previously used codes and to port existing codes into Python. This affects the near-field code COMP23/Compulink, currently implemented in Matlab/Simulink, and will have several positive effects such as improved integration, readability and simplified maintenance. In addition, the far-field code FARF31 will be replaced by the recently developed far-field transport code FARFCOMP, also ported into Python. These modifications will provide a Python package well suited for further integration with the biosphere transport model, originally developed in Python.

However, the choice of code does not affect the data needed for each code or what is propagated from one code to another. This means that there will be interfaces between the domain models also in the future. To further facilitate the integration of codes and simplify the procedure of changing codes, a standardised file format (e.g. HDF5) will be adopted.

In forthcoming site descriptive and safety assessment modelling, these enhanced model capabilities can be used to represent and analyse additional processes, and features such as spatial (e.g. multi-layer matrix systems) and temporal variability in the transport parameters, see also the discussion of geosphere modelling tools in Section 7.3.2. This could also motivate additional modelling studies along the lines of Crawford and Löfgren (2019) to investigate under which conditions explicit representation of heterogeneity is needed and possible.

Concerning developments in biosphere modelling for SFK, the plan is to use a biosphere object that can be directly coupled to the releases from the geosphere in a similar manner as for SFR, thereby eliminating the timing assumptions in the LDF-concept. This object will consider the uncertainties associated with the potential release area by varying its spatial and hydrological properties.

Irrespective of whether more integrated numerical tools or separate domain models are used, there will always be discussions about model (or sub-model) interfaces (such as in the SSM reviews of SR-Site, see Section 2.5). It is noted that the availability of numerical tools integrating several domains, e.g. surface and bedrock systems, enables further investigations of important domain interfaces and interface zones. Thus, the planning for forthcoming site descriptive and safety assessment modelling could consider more detailed modelling of, in particular, "geosphere-biosphere interface zones" to substantiate assumptions made in the model chain for production calculations. To this end, the modelling performed in connection with SR-Site and reported in Lindborg (2010, Chapter 6) could serve as a starting point.

7.2 Framework for geosphere numerical transport modelling

This section provides an overview of the concepts and methods used in numerical modelling of radionuclide transport and related modelling activities such as the groundwater flow modelling producing the flow-related transport parameters.

7.2.1 Introduction to DFN modelling

The hydraulic and transport behaviour of fractured media is often described using the Discrete Fracture Network (DFN) method, in which processes are described over a discrete number of connected fractures (e.g. Cacas et al. 1990). The spatial arrangement, intensity and connectivity of fractures can be simulated using different approaches, probably the most common being the statistical model, in which equiprobable realisations can be produced based on statistical distributions, which are in turn derived from field observations.

Alternative models account for the nucleation, growth and termination of fractures based on geomechanical rules (e.g. genetic models, Davy et al. 2010). An exhaustive discussion of these models, which might significantly differ in terms of connectivity, is out of the scope of this report. For such a discussion the reader is referred to the DFN modelling methodology report (Selroos et al. 2022).

Hydraulic properties of single fractures are typically defined by empirical laws that relate the fracture size or radius to its transmissivity. Although it is not strictly needed for the flow simulations, the hydraulic aperture can be related to the fracture transmissivity through the cubic law (Witherspoon et al. 1980):

$$T = \frac{2\rho g}{3\mu} b_h^3 \tag{7-1}$$

where ρ [kg/m³] is the water density, g [m/s²] is the gravity acceleration, μ [Pa·s] is the dynamic viscosity and b_h [m] is the hydraulic half-aperture. Note that flow and transport models of fractures are often simplified based on the assumption of symmetry and therefore the half-aperture is typically employed, see Section 3.2.3 for further discussion on fracture aperture definitions.

Transport in the DFN can be carried out using the advection-dispersion equation (Section 3.2.1), although for radionuclide transport the simplification based on fixed transport pathways is typically used (Section 3.2.2). This requires an integration along flow/transport paths in the velocity fields, which can be done using streamline tracing or particle tracking simulations. It has been discussed in chapters 3 and 6 that mass exchange between a flowing fracture and the adjacent rock matrix is controlled by the transport resistance or F-factor (sections 3.2.2 and 3.6), which in turn is a function of the inverse of the fracture half-aperture (i.e. the fracture specific surface area).

7.2.2 The continuum approximation

DFN models are routinely used to trace transport pathways for use in radionuclide transport simulations. However, their use for reactive transport modelling is still at a development stage and there are currently no operational frameworks available for that purpose. Therefore, DFN models are often up-scaled into continuum numerical grids, which are computationally much more tractable.

The use of DFN-derived continuum models is not restricted to the simulation of background geochemistry. In fact, hydrogeological models used in performance assessment studies are commonly based on nested ECPM/CPM and DFN representations. It turns out that flow-related parameters, such as the volumetric flow-wetted surface, need to be properly represented in the continuum grid. This is typically done by using the upscaled porosity and the upscaled P_{32} (a measure of fracture intensity), which are used to compute the upscaled fracture specific surface area. More details on the evaluation of the transport resistance in DarcyTools (Svensson et al. 2010) are provided in Section 6.3.2. The same approach is used in ConnectFlow.

Besides proper upscaling of DFN properties, pathway tracing in ECPM requires a careful choice of the particle tracking scheme as well as the particle time step. In fact, not all particle schemes are well suited to handle abrupt changes in properties (Salamon et al. 2006). Moreover, particle jump methods, i.e. methods where particles are routed along nodes of computational grids using time-domain approximations, are prone to numerical dispersion (Selroos et al. 2013).

7.2.3 The time domain random walk approach

Yamashita and Kimura (1990) and Delay and Bodin (2001) were the first to propose the time domain (TD) method for the simulation of radionuclide transport in fractured media. The method was later generalised by Painter and Cvetkovic (2005), who provided models for a broad range of retardation/retention processes. The important difference compared to "classical" random walk schemes, where the displacement is the random variable, is that here particles are moved from a fracture intersection to the following using a single "jump" and the time for the displacement is treated as a random variable. This approach is much more efficient in fractured media, where velocity might show variations of several orders of magnitude.

For each fracture segment, the mass discharge at the outlet can be written as a convolution of the time-dependent mass input to the segment and a travel (transit) time distribution. The TD algorithm implemented in the numerical code MARFA, together with a broad range of retention models, is outlined in Appendix D.

Recently, the TD method was used to simulate radionuclide transport through brittle fault zones (Williams et al. 2021). The motivation of this work was that recent updates of Discrete Fracture Network (DFN) modelling methodologies for the SKB and Posiva safety cases imply large computational efforts focused on the description of brittle fault zones (BFZ) as swarms of fractures (e.g. Hartley et al. 2018). Due to these high computational costs, it is probably not feasible to use the explicit swarm representation of deformation zones to carry out all the particle tracking transport calculations required in a typical safety assessment.

Thus, a study was initiated to assess a range of different upscaling and downscaling approaches to reduce the computational burden of the transport calculations while preserving the signature of the underlying small-scale heterogeneity structure. More specifically, the approach consists in first representing the BFZ into single collapsed planes. The small scale heterogeneity, which is lost in this upscaling step and is important for capturing underlying transport processes, is recovered using a downscaling algorithm originally developed by Painter and Cvetkovic (2005). The results of the project showed that the time-domain based downscaling approach provides a very accurate description of radionuclide breakthrough curves at compliance or outlet boundaries (Williams et al. 2021, Figure 6).

7.3 Toolbox for numerical modelling

This section describes transport modelling tools, i.e. codes used in geosphere radionuclide transport simulations and supporting modelling activities. The objective of this section is not to provide an exhaustive and complete description of all existing numerical codes for subsurface transport but rather to give a brief overview of codes that either were used in previous safety analyses or that are likely to be used in future safety assessments. The codes are divided into two main groups: software for radionuclide transport modelling (sections 7.3.1 and 7.3.2) and tools for reactive transport modelling (Section 7.3.3).

7.3.1 Radionuclide transport modelling

MARFA

The computer code Migration Analysis of Radionuclides in the Far Field (MARFA) (Painter et al. 2008, Painter and Mancillas 2013) uses a time-domain (TD) Monte Carlo method (see Section 7.2.3) to simulate the transport of radionuclides in a sparsely fractured geological medium. The algorithm uses non-interacting particles to represent packets of radionuclide mass. These particles are moved through the system according to rules that mimic the underlying physical transport and retention processes. The physical processes represented in MARFA include advection, longitudinal dispersion, Fickian diffusion into an infinite or finite rock matrix, equilibrium sorption, decay, and in-growth. Recently, the possibility to simulate diffusion into stagnant water has also been included (Trinchero et al. 2020).

Because the algorithm uses non-interacting particles, transport and retention processes are limited to those that depend linearly on radionuclide concentration. Multiple non-branching decay chains of arbitrary length are supported, as is full heterogeneity in the transport and retention properties. Two variants of the code are provided. These two versions differ in how particles are routed through the computational domain.

In the main version of MARFA (MARFA-SP), transport is assumed to occur along a set of trajectories or pathways that originate at radionuclide source locations. The trajectories are intended to represent the movement of hypothetical, advectively transported groundwater tracers and are typically calculated by pathline tracing in a discrete fracture network flow or ECPM code. The groundwater velocity and retention properties along each pathway may change in time, but the pathway trajectories are fixed. A new version of MARFA, called MARFA-DFN, is being developed. MARFA-DFN is integrated into the DFN simulator dfnWorks and thus allows a closer integration with a changing velocity field. Another important development effort is the integration of the newly developed MARFA library with DarcyTools.

FARF31

FARF31 (Norman and Kjellbert 1990, Lindgren et al. 2002, Elert et al. 2004) is a Fortran code used for radionuclide migration calculations in the far-field, i.e. the geosphere. The FARF31 code has been employed in several earlier assessments, e.g. SR 97 (Lindgren and Lindström 1999), SR-Can (SKB TR-06-09), SR-Site (SKB TR-11-01, SKB TR-10-50) and PSAR SFK (SKB TR-21-01, SKB TR-21-07).

FARF31 is based on a model with a one-dimensional advection-dispersion equation along a, possibly curved, streamtube coupled to a pure diffusion equation (matrix diffusion) in the direction perpendicular to the centroid of the streamtube, for a number of radionuclides. Linear equilibrium sorption, chain decay and in-growth are included in the model.

The governing equations are solved in the Laplace domain using the advective travel time in the longitudinal direction as the independent variable to obtain a unit response function, which is subsequently convoluted with the input function to obtain the output function. A detailed description of the solution method can be found in Norman and Kjellbert (1990). It is noted that the equations are expressed in terms of accumulated travel time rather than distance along the flowpath. This feature makes it easy to calculate travel times in a stand-alone groundwater flow model, and subsequently radionuclide transport in a decoupled fashion.

FARF31 was originally developed to be used with a groundwater flow model adopting a continuum representation of the rock. In more recent safety assessments, groundwater flow has primarily been modelled through a discrete fracture network (DFN) where individual fractures are represented explicitly. Here, the conceptualisation of a migration path is slightly different than in a continuum-based groundwater flow model. Rather than macroscopic streamtubes encompassing both rock and flowpaths, the equation now describes flowpaths through the actual open pore space, i.e. through the connected fracture network. However, the governing equations are identical for the two conceptualisations.

As discussed in Chapter 6, the entities calculated in the DFN-based groundwater flow models are the advective travel time (t_w) and flow-related transport resistance (F) along flowpaths. The input to FARF31 comprises both parameters that are possible to assign statistical distributions, constant parameters and input time series (i.e. the output function from the near-field model).

FARFCOMP

FARFCOMP (SKB TR-19-06, Appendix B) is a compartment model used for radionuclide transport calculations in fractured rock implemented in Matlab. It is the successor code of FARF31, which as described above is a radionuclide transport code based on a semi-analytical approach and developed using Fortran (Norman and Kjellbert 1990). The FARF31 code was later reformulated to include the relevant processes in a numerical compartment-based framework (Vahlund and Hermansson 2006). Based on those predecessor codes, FARFCOMP was developed to improve usability, flexibility and efficiency in radionuclide transport modelling. FARFCOMP was applied in the PSAR SFR project and developed, introduced and described within the SFL safety evaluation project SE-SFL (SKB TR-19-01).

Conceptually, the model uses one-dimensional transport in the direction of water flow along a trajectory within fractures (conceptualised as a streamtube) surrounded by porous rock and thus coupled with one-dimensional transport by diffusion into the immobile pore water in the rock matrix. The fracture is conceptually viewed as a flat, vertical slit with parallel walls surrounded by porous rock. The transport equations use a so-called dual porosity description with advection-dispersion in the mobile phase (transport by flowing water with a constant groundwater velocity along the rock fracture) and diffusion into immobile pore water in the rock matrix, where sorption is also considered. Sorption within the fracture and temporally variable water flow rate have been added to the code since its introduction.

The two coupled, one-dimensional equations (the dual-porosity model) are approximated using a compartment approach. A compartment model (also known as a box model) is a type of mathematical model used to describe the way materials are transferred between different compartments of a system. Each compartment is usually assumed to be a homogeneous entity within which the entities being modelled are uniformly distributed and equally available for transfer to other compartments.

The compartment model is defined as a system of ordinary differential equations with time as the independent variable and can therefore readily be solved using any ordinary differential equation solver. Hence, the partial differential equation needs to be discretised in space (into homogenous compartments) such that a system of ordinary differential equations representing an approximation to the system can be obtained. The discretised equations are derived using the finite volume approach with second-order central differences for the dispersion/diffusion terms and a first-order upwind scheme for the advective term and the interface term between the fracture and the rock matrix.

The main reason for developing the FARFCOMP code has been to get a transparent, more flexible, faster and more consistent solution method compared with existing codes for solving the transport equation in one flowpath. In terms of flexibility, FARFCOMP is designed to allow straightforward implementation of various features and processes that have not been considered in SKB's transport modelling code FARF31. Examples of processes that could be considered include cylindrical, rather than flat-slit, fracture shapes with radial diffusion, colloid-facilitated transport, and variation in time of various properties.

A detailed description of the mathematical theory behind the numerical implementation as well as a verification using a series of comparisons with other codes and analytical solutions is provided in the radionuclide transport report for the safety evaluation SE-SFL (SKB TR-19-06, Appendix B). In line with the idea of harmonising computer codes for "production calculations", FARFCOMP is also implemented using the Python programming language.

CHAN3D

The code CHAN3D (Gylling et al. 1999) is an implementation of the Channel Network Model (Moreno and Neretnieks 1993). The model assumes that fluid flow takes place in a network of interconnected flow channels in the rock. Each member of the channel network is assigned a hydraulic conductance. This is the only entity required to calculate the flow. Conductances together with boundary conditions determine the pressures/head field and the flows in the system. In CHAN3D, a cubic grid is used for illustration purposes. In reality, the channels can have orientations that are not aligned with the regular grid, and they can also have different lengths.

Not all channels must be hydraulically conductive. The transmissivity distribution, the channel density, and flow-wetted surface of the rock are chosen so that they agree with field observations. The model considers solute transport in a suite of single channels. Each channel has a rock matrix of a given thickness on each side, into which the radionuclides may diffuse and be adsorbed. The model includes advective flow in channels, linear sorption on the fracture surfaces, diffusion into the rock matrix and linear sorption onto micro-surfaces within the rock matrix. Radioactive chain decay is also included. The solution for each path is calculated in Laplace space. To obtain breakthrough curves, the solution is numerically inverted from Laplace to ordinary space, see Shahkarami (2017).

7.3.2 Development and future usage of radionuclide transport codes

The plan is to continue the development of both MARFA and codes based on FARF31 for radionuclide transport. MARFA can apply a dynamic K_d concept, where K_d is determined by mineral and groundwater compositions over time and space (Trinchero et al. 2016). This methodology has been further developed and used by Posiva. Furthermore, MARFA has been tested for time-varying flow conditions, allowing changes in flow magnitude and direction along flowpaths. This is useful for scenarios like glacial periods, where flow can be nearly stagnant under a stationary ice sheet but very high when the ice front passes over the repository. There is also an ongoing joint SKB-Posiva development effort that aims to link MARFA more effectively with the hydrogeological code DarcyTools and dfnWorks (see "MARFA" section above).

SKB intends to replace the semi-analytical geosphere code FARF31 with a fully discretised numerical variant. This new variant, used in safety evaluations for SFL and PSAR for SFR, offers flexibility in handling processes and can manage heterogeneous properties in the matrix. For the calculations related to radionuclide transport, two different code concepts are planned to be applied. The code FARF31 and its derivatives are characterised by computational efficiency, allowing many cases/variants to be run in probabilistic calculations.

With the compartmentalisation of FARF31 in the form of FARFCOMP, the ability to handle variable transport properties has increased. However, if all segments are to have different properties, the calculation speed would decrease significantly. It follows that the FARF31 and FARFCOMP codes will be used primarily for the following types of transport conditions and simulations:

- Stationary flow situations with calculations of distributions of performance measures (flow rates and flow-related transport parameters).
- Homogeneous matrix conditions (mean-valued transport properties).
- Probabilistic compliance simulations for dose and risk assessments.

MARFA, on the other hand, is designed to include processes such as alterations along the flowpaths and transient flow conditions. This code is therefore better suited for handling complex cases and scenarios involving conditions and processes such as:

- Transient flow situations.
- Heterogeneous matrix conditions (along flowpaths, e.g. different rock types, or in the matrix, e.g. multi-layer matrix).
- Transport by colloids.

7.3.3 Reactive transport modelling

Reactive transport modelling enables supporting analyses for specific questions relating to radionuclide transport. These may include questions related to the application of Smart- K_d (with focus on couplings between sorptivity and the groundwater evolution), potential effects on retention of processes such as co-precipitation, multicomponent diffusion coupled with sorption processes, impacts of anion exclusion, and modelling of natural analogues. Such modelling also enables direct testing of independently estimated Smart K_d values to properly account for the migratory behaviour of radionuclides subject to strong non-linear physico-chemical couplings when undergoing transport in fractured rock.

This sub-section gives a presentation of available reactive transport modelling codes with a related short description of capabilities and specific features of each code. The codes are summarised in Table 7-1.

Table 7-1. List of the main reactive transport modelling codes used in recent far-field/geosphere related applications at SKB. GIA: global implicit approach; SIA: sequential iterative approach; SNIA: sequential non-iterative approach. The asterisk indicates that the capability is in a development or testing stage. Notice that the geochemical engine of both ConnectFlow and iCP (i.e. PHREEQC) is freely distributed by the U.S. Geological Survey

Code	Approach	Solution method	Distribution
PFLOTRAN	Continuum	GIA	Open source
ConnectFlow-PHREEQC	Continuum/DFN	SIA	Proprietary
iCP (interface COMSOL- PHREEQC)	Continuum/DFN*	SNIA	Proprietary
FASTREACT	Travel-time based	-	SKB property

PFLOTRAN and iDP

PFLOTRAN (Hammond et al. 2014, Lichtner et al. 2015) is an open source, state-of-the-art massively parallel subsurface flow and reactive transport code. PFLOTRAN solves a system of generally nonlinear partial differential equations describing multiphase, multicomponent and multiscale reactive flow and transport in porous materials. The code is designed to run on massively parallelised computing architectures as well as workstations and laptops. Parallelisation is achieved through domain decomposition using the PETSc (Portable Extensible Toolkit for Scientific Computation) libraries.

PFLOTRAN has been developed from the ground up for parallel scalability and has been run on up to 2¹⁸ processor cores with problem sizes up to 2 billion degrees of freedom. PFLOTRAN is written in object oriented, free formatted Fortran 2003. The choice of Fortran over C/C++ was based primarily on the need to enlist and preserve tight collaboration with experienced domain scientists, without which PFLOTRAN's sophisticated process models would not exist. The reactive transport equations can be solved using either a fully implicit Newton-Raphson algorithm or the less robust operator splitting method.

Sometimes PFLOTRAN benefits from being one-way coupled with the groundwater code DarcyTools. To this end, a focused interface, called iDP, has been developed (Molinero et al. 2016). Both PFLOTRAN as stand-alone code and iDP have been used in several SKB applications (e.g. Román-Ross et al. 2014, Iraola et al. 2017, Trinchero et al. 2017).

ConnectFlow-PHREEQC

ConnectFlow (Amentum 2024) can simulate the transport of solutes in a number of ways such as the transport of total salinity, the transport of end-member waters and the transport of chemical components. In past safety assessment simulations of Forsmark and Olkiluoto carried out using ConnectFlow, the evolution of groundwater in regional-scale paleo-climate simulations was formalised in terms of the transport of reference waters (Follin 2008, Joyce et al. 2010, Hartley et al. 2013a, b), with each end-member water representing a specific groundwater type (e.g. meteoric or glacial, Littorina-type, etc.). Thus, the composition of the groundwater at any point was expressed in terms of the mixing of fractions of such reference waters. Subsequent batch simulations were carried out to simulate equilibrium of the computed mixture of waters with e.g. pH and redox controlling minerals, thereby yielding the concentrations of different chemical species (Salas et al. 2010).

This approach based on end-member waters is valid as long as controlling minerals are in equilibrium (De Simoni et al. 2007) but it breaks down when kinetic reactions need to be included or when cation exchange reactions need to be considered. Therefore, ConnectFlow was further extended to include multi-component reactive transport explicitly. This implementation was carried out in the form of an interface and using the external library iPhreeqc (Charlton and Parkhurst 2011) as speciation and reaction engine.

In this implementation, components (intended as the "master species" of PHREEQC) are transported by ConnectFlow and geochemical reactions (e.g. equilibration of aqueous solutions with minerals, ion exchanger materials, surface complexes, solid solutions and gases) are computed in PHREEQC using a split operator approach.

ConnectFlow-PHREEQC was used to simulate paleo-climate hydrogeochemical evolution at the Forsmark site based on continuum models (Joyce et al. 2015a, b, see example results in Figure 7-8). SKB publications describing development and applications of this tool include Joyce et al. (2015a, b, 2019), of which the 2019 report was produced within the SE-SFL project which mainly used data from the Laxemar site.

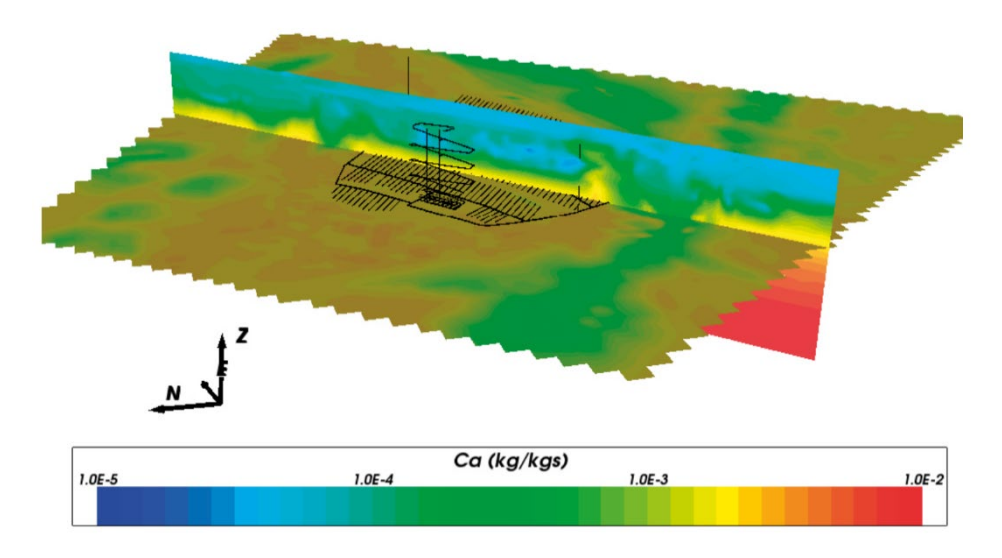


Figure 7-8. Vertical and horizontal slices, coloured by calcium mass fraction, taken through the repository volume of the Forsmark local area ECPM paleo-climate model at 2000 AD. Figure from Joyce et al. (2015a).

ConnectFlow-PHREEQC can also be used for reactive transport modelling in explicit DFNs. However, this implementation has required some simplifications, and transport and reactions are only computed in global nodes (i.e. nodes located at fracture intersections). It turns out that, for instance, internal variability cannot be included in the models (or can be included in a highly simplified fashion by chequerboarding the fractures). This might have an impact on the results since fracture internal variability could enhance groundwater mixing, thus affecting reaction rates (Dentz et al. 2011).

iCP

iCP stands for interface COMSOL-PHREEQC (Nardi et al. 2014). It is in fact an interface that couples two standalone simulation softwares: the general-purpose finite element framework COMSOL Multiphysics® and the geochemical simulator PHREEQC. The main goal of the interface is to maximise the synergies between the aforementioned codes, providing a numerical platform that can efficiently simulate a broad number of multi-physics problems coupled with geochemistry.

iCP inherits almost all the capabilities of both codes but also some of their limitations. The user cannot expect better convergence or performance than that obtained using the codes as standalone tools. Furthermore, the coupling scheme introduces some issues that should be accounted for:

- Sequential Non-Iterative Approach (SNIA) Operator Splitting (OS) scheme: So far, iCP uses the SNIA scheme. Compared to the Sequential Iterative Approach (SIA), the SNIA does not pose global convergence problems but a close control on the time step is required to minimise the operator-splitting errors (Barry et al. 1996).
- COMSOL start and stop run penalty: COMSOL must reconstruct the matrix system and the initialisation setup at every step, which causes some penalty time.

On the other hand, iCP has been optimised to reduce the computational time of the reactive step:

- The computation has been parallelised over multiple cores.
- iCP provides an option to prevent recalculation when chemical changes are below a given threshold.

iCP has been used extensively in applications related to near-field modelling (e.g. Idiart and Pękala 2016, Idiart et al. 2019). In far-field modelling, iCP has been used to assess radionuclide transport in the regolith for the SFL safety evaluation project (SKB TR-19-05, Chapter 15, Sáinz-García et al. 2022). Recently, iCP has been extended to include the possibility to simulate reactive transport in DFNs. However, this capability is still in a development stage.

FASTREACT

In order to circumvent the limitation of standard reactive transport codes, a numerical tool, denoted FASTREACT, was developed (Trinchero et al. 2014a, b). The tool, which relies on the theory of Stochastic-Convective models, decomposes complex three-dimensional geometries into a set of independent streamlines. Reactive transport processes are then solved over the whole set of streamlines using one single (or a few) reference simulations that incorporate explicitly all the relevant geochemical processes.

FASTREACT was developed for safety assessment calculations of radionuclide transport in fractured rock and thus provides efficient handling of the coupling between advection, reactions and matrix diffusion processes for large amounts of input and output data. In the original implementation of FASTREACT, the reference simulation was constructed using PHREEQC, which has limited capabilities to simulate matrix diffusion. However, the methodology can readily be modified to include alternative codes (e.g. PFLOTRAN) that can provide a better description of matrix diffusion processes.

7.4 Identification and application of transport classes

As described in Chapter 4, the retardation model consists of building blocks that are used to formulate fracture types and deformation zone structures. To implement the information contained in the retardation model in the numerical radionuclide transport models, the concept of transport classes will be used. The transport classes describe properties of the layered matrix in groups that are simplified descriptions based on the fracture types and available information on the transport properties. They are allocated to structural elements (flowpath segments) in the radionuclide transport model using drivers obtained from statistical analysis of a site-specific geospatial database.

Single fractures and their associated properties are the basis for the establishment of a site-specific structural framework for transport classes. The first step of such a framework is the definition of fracture types, which may subsequently be merged into transport classes if this is supported by fracture data. Thus, the development of the retardation model is the first step of the procedure described here, but for details on this part of the analysis the reader is referred to Chapter 4.

It should also be noted that there is no obvious demarcation between site descriptive and safety assessment modelling in the procedure presented below, except that the parameterisation of segments is part of the safety assessment. This means that the analysis could be divided between these two modelling activities depending on available time and other resources as well as other factors such as the status of the geospatial database and access to other inputs.

The main inputs to the approach outlined in the present section are the results and experiences gained from earlier SKB and Posiva work on conceptual and quantitative analyses of fractures for use in transport modelling. Concerning previous SKB work, it is noted that the modelling study presented in Crawford and Löfgren (2019) constitutes a step forward compared to the SDM-Site retardation model (Section 4.2), insofar that it to larger extent is based on quantitative data on fracture mineralogy in its definition of fracture types. Thus, it provides an adequate starting point for forthcoming analyses.

In recent safety assessment studies carried out by Posiva for Olkiluoto in Finland, fracture types and then transport classes were developed from an initial classification of fractures based on identified past hydro-alteration events (Hartley et al. 2018, Joyce et al. 2021). These "alteration classes" were developed into transport class definitions which could be determined for each observed fracture using simple criteria applied to small-scale fracture data such as mineral coating and alteration, stored in borehole logs in a geospatial database. Where alteration classes could not be readily distinguished according to these database criteria, they were merged, resulting in a final set of three transport classes.

Below is a description of the steps planned for the development of transport classes and their implementation in radionuclide transport models. A workflow for a generic structural framework for transport classes is shown in Figure 7-9. The analysis is explained in more detail in the text, in terms of seven steps where each step corresponds to a sub-section.

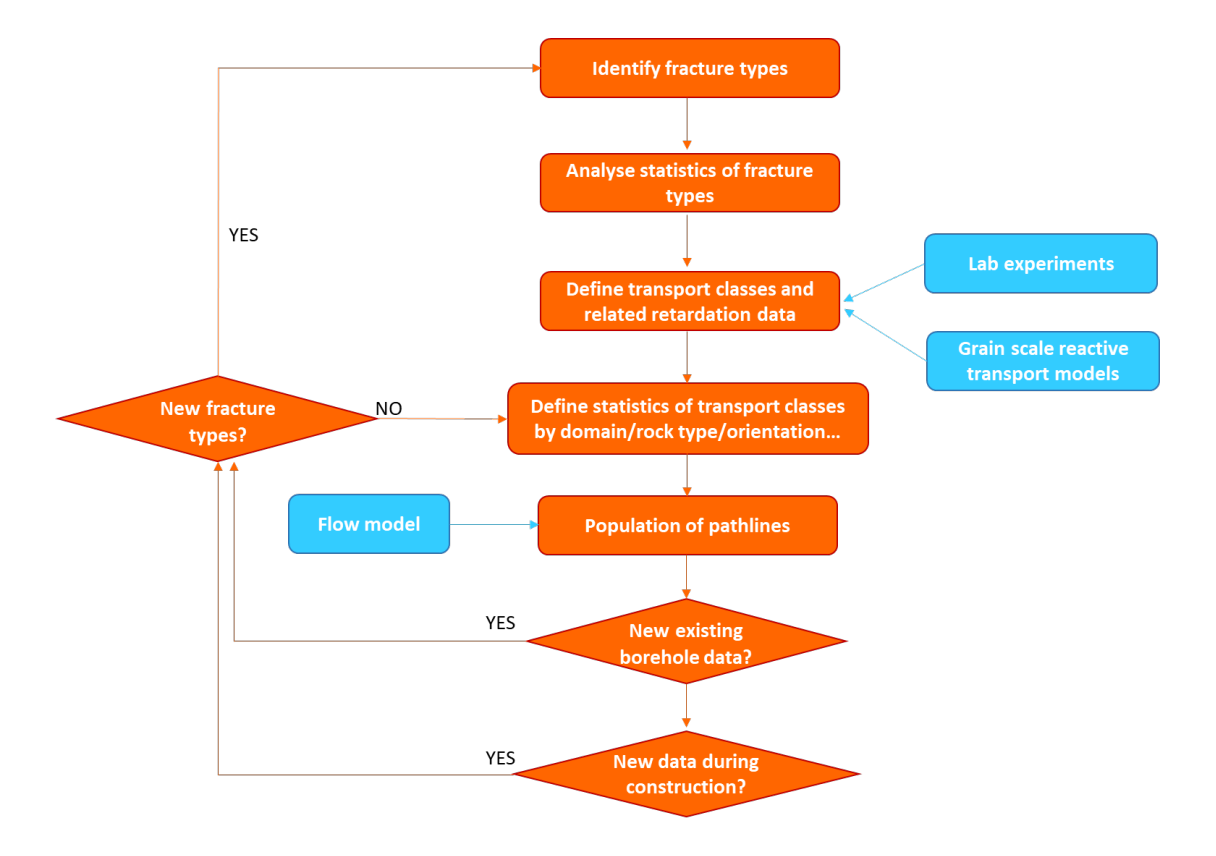


Figure 7-9. Workflow for the formulation of a generic structural framework for transport classes.

7.4.1 Step 1 – Identify fracture types

In Section 4.4.2, methods for assigning retardation components and associated data to transport domains are discussed for different approaches. These are based on whether the predefined microstructural units contain either fixed, fully independent, or partly decoupled retardation components (Figure 4-11). It is suggested that a partially decoupled approach is used to identify microstructural units, since this reflects the understanding of geological processes at the site.

As discussed in Section 4.5 (see Figure 4-12), the approach is an iterative process carried out in cooperation with the Geology (including DFN), Hydrogeology, Hydrogeochemistry disciplines, informed by a thorough statistical analysis of the relevant information present in a geospatial fracture database for both flowing and non-flowing fractures. The statistical analysis will begin by giving equal importance to the three selected retardation model components (fracture coating, alteration rim and undisturbed/fresh rock) and seeking common clusters of these properties which may form the basis of fracture types. These will then be iterated further after feedback from each discipline has been obtained.

7.4.2 Step 2 – Analyse the statistics of fracture types

The workflow shown in Figure 7-9 also includes a statistical analysis to derive patterns and correlations of predominance of the different fracture types conditioned to the geology of the underlying building block as well as to other possible drivers such as fracture orientation (which is related to underlying principal stress components), depth and deformation zones (Doolaeghe et al. 2023). These "large-scale" drivers are here denoted as *geological conditioning factors*, when considered in the context of transport classes.

7.4.3 Step 3 – Define transport classes and retardation data

As the next step of the structural framework for transport classes, once fracture types are determined, a check will be made as to whether the properties of each fracture type promote merging into fewer fracture types. If the available fracture data shows that diffusion and sorption

properties (e.g. diffusivity, porosity, anion exclusion factor, etc.) do not show significant differences between two fracture types, then the two may be combined into a single merged type (i.e. a transport class) for modelling purposes. Merging may also be carried out in cases similar to that described previously for the Posiva alteration classes, i.e. where there is not enough information available to make a distinction between different fracture types.

Each transport class should be abstracted to a related retention model, i.e. a layer structure with retardation parameters. The three-layer matrix model is typically used for this purpose (see Figure 7-10), although some transport classes can lack an alteration rim and/or a coating layer. (In Forsmark, the "fresh rock only" class will be important.) This conceptualisation can be supported by modelling such as that presented in Crawford and Löfgren (2019) and by micro-DFN models such as those described in Svensson et al. (2018).

An example of a suggested primary parameter table for hypothetical transport class α in a transport domain can be found below in Table 7-2. Due to the large data amount expected for sorption parameters, these will be presented in separate tables providing data for each radionuclide for different materials and water compositions. Additional secondary or ternary tables could be provided, presenting complementary data such as breakthrough curves from through electromigration (TEM) experiments, mineral content, and pore size distributions.

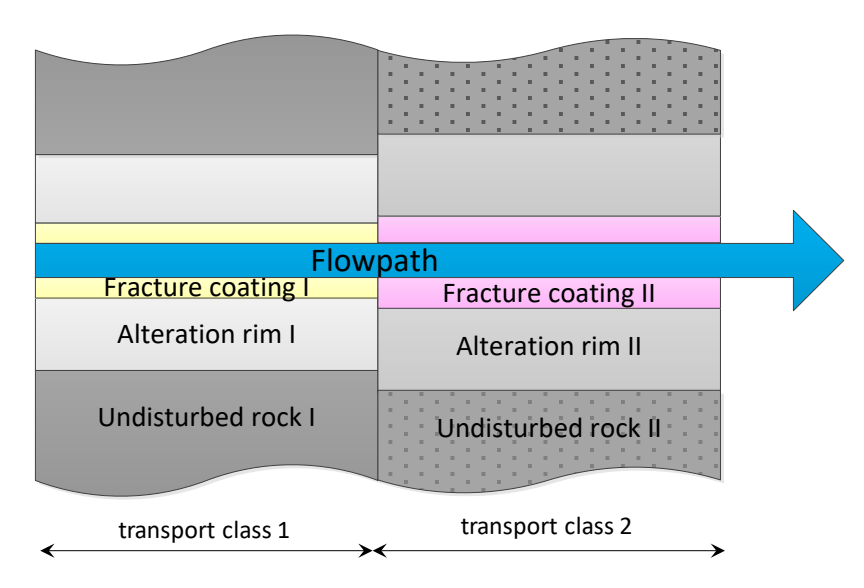


Figure 7-10. Sketch of a flowpath traversing two different transport classes. Figure modified from Crawford and Löfgren (2019).

Table 7-2. Example look-up table: Parameters for transport class α in one of the transport domains (tentative). The values do not refer to real data. In case the same values, within reasonable uncertainty limits, are obtained for other fracture types, these could be merged into one transport class. Sorption parameters should also be addressed, but in one or more separate tables due to a more complex data set

Parameter	Fracture coating		Alteration rim		Undisturbed rock	
Thickness (mm)	0.1 Probability distribution		15		Different at different depths	
Porosity (%)	Mean 1.0 ± 0.4	Median 1.2	Mean 0.8 ± 0.4	Median 0.6	Mean 0.2 ± 0.1	Median 0.2
	Porosity profile		Porosity profile			
Anion exclusion factor	-		-		0.3	
Diffusivity, D_e (m ² /s)	1.5 × 10 ⁻¹²		5 × 10 ⁻¹³		6 × 10 ⁻¹⁴	

7.4.4 Step 4 – Define statistics of transport classes by drivers

Once a set of merged types with distinct properties has been finalised and abstracted to retention properties, a transport class can be assigned to each observed fracture in a geospatial database and further analysis performed. This will provide, as an output, conditional probability functions of transport classes predominance, which are typically expressed in the form of look-up tables. Initially, appropriate statistical tests (e.g. chi-squared, Cramer's V) should be applied to the database in order to determine which geological conditioning factors show a correlation with transport classes, and the strength of these correlations.

Amongst those potential geological conditioning factors mentioned in Section 7.4.2, several should be considered in this case:

- Elevation
- Fracture orientation (strike/dip)
- Deformation zone (and its type)
- Fracture domain
- Rock domain
- Rock stress
- Other geospatial drivers as yet undefined.

Other geospatial drivers could include other-than-geological properties such as groundwater chemistry.

7.4.5 Step 5 – Basis for assigning transport classes to pathline segments

For these factors to be of use in assigning transport classes to simulated pathlines, it must be possible to determine them for a pathline segment at a given location within a DFN or ECPM groundwater flow model. For some factors (elevation, deformation zones) this is trivial, as they can be directly extracted from the pathline output of a groundwater flow and transport code such as ConnectFlow or DarcyTools in either model concept.

For others (fracture domain, rock domain), this information is only available in ECPM model output, and a look-up into the geospatial database containing these geological volumes must be made for pathlines within a DFN model; this should be handled using a Python scripting approach for postprocessing of pathline files, as was adopted by Posiva. Finally, orientation of individual fractures can only be determined for DFN models and does not exist in an ECPM model. In this case, a separate set of look-up tables should be generated in which transport class occurrence probability is averaged across all fracture orientations, for use in ECPM models.

Those factors which are not found to correlate with transport class occurrence can be discarded as geological conditioning factors in the rest of the analysis. If no significant correlations are found, this result indicates that the data does not support the association of transport classes with geological conditioning factors, and therefore the following analysis is not required. In these cases, either a simpler approach, in which transport class occurrences do not vary spatially, or an alternative concept in which for example transport domains are used to assign retardation properties to pathlines, should be adopted.

If a set of geological conditioning factors is found to correlate with transport classes, it is suggested that determining the relative occurrence of each transport class within each group of factors could then be treated using appropriate algorithms. The parameters of the classifier model, and the treatment of the input factors, can be adjusted iteratively until a sufficiently high performance is obtained. Look-up tables of probabilities that a given transport class will be observed for a given combination of geological conditioning factors can be produced directly from this model, allowing transport classes to be stochastically assigned to pathline segments, as discussed in the following subsection. Table 7-3 is an excerpt of such a look-up table presented in Hartley et al. (2018).

Table 7-3. Part of the look-up table used in Posiva ODFN3 to assign transport classes (Hartley et al. 2018, Table 5-7). Probabilities of the three transport classes (HT1, HT2/3 and NHT) are given for each combination of elevation, orientation set and geology ("Altered BFZ" etc.). Note that this is just a part of the original table showing probabilities for only one out of four fracture sets

Minerals	Altered BFZ	Other BFZ	PGR/MFGN	Other				
Above -200m								
EW/NW – HT1	36 %	31 %	18 %	18 %				
EW/NW – HT2/3	57 %	56 %	58 %	74 %				
EW/NW – NHT	7 %	13 %	24 %	8 %				
Below -200m								
EW/NW-HT1	74 %	62 %	13 %	15 %				
EW/NW-HT2/3	7 %	33 %	69 %	74 %				
EW/NW – NHT	19 %	5 %	18 %	11 %				

7.4.6 Step 6 – Handling new information

New information could include new data from surface boreholes, tunnel boreholes, and other data from detailed investigations performed in connection with repository construction. As more data are acquired, an iterative procedure is planned to be implemented in which an analysis is made at each data freeze of whether new fracture types have been identified. This will subsequently lead to a new analysis of the fracture types, as described in Step 1 above (Section 7.4.1).

7.4.7 Step 7 – Implementation in radionuclide transport models

The implementation of transport classes in the numerical radionuclide transport modelling is planned to be performed in two steps. First, modelling applying the transport classes is performed using MARFA. Based on the results an analysis is made for identification of which simplifications that can be made for the probabilistic calculations to be performed. It is foreseen that these may include modelling with divisions made in terms of domains instead of segments.

Two workflows for the implementation of a structural framework for transport classes are outlined/identified here. They are denoted as Option A and Option B. These workflows are generic and not specifically associated with the approach used to define the transport classes. Thus, they are valid operational approaches if a structural framework for transport classes is employed.

Option A works as follows:

- 1. Particle tracking simulations are carried out in the groundwater flow model and segmented transport pathways are traced.
- 2. Each segment is internally assigned geological conditioning factors (see previous sub-section) based on e.g. its spatial location and orientation.
- 3. Given the pre-computed look-up tables and the assigned geological drivers, a transport class is assigned to the segment and then the set of transport pathways is rewritten in the form of an ASCII file. This file contains information on transport classes.
- 4. The set of trajectories generated in the previous step are used in the MARFA simulations.

This workflow, which is very similar to that employed in the radionuclide transport simulations of the latest Posiva safety assessment (Hartley et al. 2018), implies that look-up tables are handled outside of MARFA (as a pre-processing step). This might not be optimal for model reproducibility. Moreover, each segment is the result of a single stochastic realisation of the transport classes, and this might have some implication in terms of statistical non-ergodicity – particularly when a geological group is crossed by very few pathway segments. On the other hand, the main advantage of Option A is that it does not require any modification of MARFA. Yet, the implementation of

Option A presumes the availability of a geospatial database that can be used to map transport segments into geological groups.

Option B works as follows:

- 1. Particle tracking simulations are carried out in the groundwater flow model and segmented transport pathways are traced.
- 2. Each segment is assigned geological conditioning factors based on, for example, its spatial location and orientation and the set of transport pathways is rewritten in the form of an ASCII file. This file contains information on geological conditioning factors.
- 3. MARFA simulations are carried out, in which each particle visiting a given segment samples the related look-up table on-the-fly.

The main difference compared to Option A is that look-up tables are handled in MARFA and sampled on-the-fly. This implies a better model reproducibility. Moreover, look-up tables are sampled many more times than in Option A, which ensures statistical ergodicity. Option B implies the implementation of additional capability to the current version of MARFA (MARFA version 5.0). As in Option A, a geospatial database is needed also for Option B.

7.5 Handling of other transport processes

This section contains brief descriptions of the handling of a few additional components and processes involved in the radionuclide transport modelling. The descriptions refer to the SFK and SFR PSAR-stage analyses, since these are the latest ones carried out and published.

7.5.1 Bedrock wells in transport modelling

Treatment of bedrock wells in PSAR SFK

As soon as a biosphere object has emerged from the sea it is assumed that the released radionuclides reach a hypothetical well drilled into the bedrock. The activity concentration in well water (Bq/m³) was calculated by dividing the total release rate to the biosphere (Bq/y) by the well capacity (m³/y). This implies complete capture of the radionuclide plume irrespective of the well abstraction rate and is thus a cautious assumption. The capacity of the well was selected to represent wells drilled in the central part of the site investigation area, where they potentially could receive radionuclides released from the repository (SKB TR-21-01).

Treatment of bedrock wells in PSAR SFR

Bedrock wells drilled outside of the repository footprint are considered in the analyses as water pumped from these wells could be contaminated by radionuclides. The likelihood of this water being contaminated by radionuclides is assessed based on the location of these wells relative to the location of a plume of radionuclide contaminated groundwater downstream of the repository. The area covered by this plume, combined with the area of influence of any potential well drilled around the plume, is deemed the well interaction area. The spatial coverage of the well interaction area in the PSAR assessment is the same as in SR-PSU. The probability of drilling a well into the well interaction area is not taken into account (SKB TR-23-09).

Future treatment of bedrock wells

The future handling of drilled wells is planned to include a well interaction area and the use of particle tracking to determine the proportion of a radionuclide release that may travel to the well. The effect of pumping in the well on the flux to the well will be evaluated.

7.5.2 Transport of radionuclides in the gas phase

Transport of radionuclides in the gas phase in PSAR SFK

Transport in the gas phase is treated pessimistically as a short circuit of the repository to the biosphere, i.e. transport through the geosphere is neglected. The gaseous radionuclides assessed in this way are C-14, presumed to be present as methane or carbon dioxide, and Rn-222. As long as this cautious approach shows that transport of gaseous radionuclides causes no significant risk, it is

not considered necessary to examine the details of the migration process (SKB TR-21-04). Transport via colloidal material that is transported with gas bubbles is not taken into account in the PSAR SFK safety assessment.

Transport of radionuclides in the gas phase in PSAR SFR

Radionuclide transport in the gas phase is not explicitly included in the radionuclide transport modelling in the barriers. Escape of radionuclides in the gas phase is neglected when modelling radionuclide transport in the aqueous phase; the whole radionuclide inventory is therefore modelled as being available for transport in the aqueous phase (SKB TR-23-09).

Future treatment of transport of radionuclides in the gas phase

The plan is to treat transport of radionuclides in the gas phase similarly as has been done previously. A cautious approach can be taken by assuming a bypass of the geosphere, as long as this leads to insignificant calculated risks.

7.5.3 Colloid facilitated transport

The contents of colloids and microbes in the groundwater are of great importance for radionuclide transport, since these particles can act as carriers of radionuclides. At high concentrations, strongly sorbing radionuclides will be able to adhere to colloids and microbes in competition with the retention on the fracture surfaces, and thereby they might be transported with the groundwater flow. In the investigated groundwaters, the concentrations of natural colloids have been so low that the associated transport mechanism is considered to be of no importance for the safety assessment (SKB TR-21-04).

Treatment of colloids in PSAR SFK

The presence of bentonite material in tunnel backfill and borehole buffer is expected to result in bentonite colloids in the groundwater near deposition holes and along the geosphere transport pathways. Radionuclides that have a strong affinity for bentonite will sorb onto bentonite colloids and may be transported through the geosphere with reduced interaction with the rock matrix, i.e. with a reduced retention.

Colloid facilitated transport involves a complicated combination of processes, many of which can mitigate the transport. Mitigating processes include colloid retardation in fractures, physical filtration (straining) of colloids in fractures, colloid flocculation and sedimentation, saturation of sorption sites on colloids, and competition for sites on colloids.

Rather than attempting to develop detailed process models for colloid-facilitated transport, potential mitigating processes are ignored so as to place an upper bound on the possible effect. Ignoring these potential mitigating processes and taking into consideration that sorption of radionuclides onto bentonite is understood to be a reversible process on the time scale of geosphere transport (SKB TR-21-03), the effect of colloids in facilitating transport may be modelled through the introduction of effective transport parameters for reversible sorption. The effective parameters depend on the colloid concentration and on the equilibrium partitioning coefficient for sorption onto colloids. This is further explained in Appendix I of SKB TR-21-07.

The potential role of bentonite colloids in facilitating transport of certain radionuclides is addressed in variant modelling cases using MARFA. In the colloid-facilitated transport variant the output from the near-field is processed to partition radionuclides between colloid-associated and dissolved states.

Treatment of colloids in PSAR SFR

PSAR SFR does not include transport with colloids. Based on the water chemistry and boundary conditions, it is judged in SKB TR-14-05 that colloids are expected to have a negligible influence on the transport of radionuclides in the geosphere. Colloids are thus not handled explicitly.

Future treatment of colloid facilitated transport

The plan is to treat colloids similarly to what has been done previously.

7.6 Interactions with other transport modelling

Transport parameters are needed also for other purposes than radionuclide transport modelling. Limiting the present discussion to retention/retardation parameters, it is noted parameters similar to those used in radionuclide transport models are needed in all modelling that considers mass exchanges between the flowing groundwater and the various immobile domains along the flowpaths and potentially also further transport in these immobile domains.

Models that consider such interactions and transport components are employed within both hydrogeological and hydrogeochemical modelling:

- Hydrogeology develops groundwater flow models that take density-dependent flow into account. This means that fracture-matrix exchanges of solutes that affect water density need to be included in the modelling. In this context, this is usually referred to as salt transport/exchange; see, for example, Follin et al. (2008, Section 3.5) for a description of the solute transport model in the SDM-Site ECPM groundwater flow model.
- The hydrogeochemical modelling uses transport models that involve mobile-immobile zone interactions for a variety of purposes, where the two main categories are simulations of the hydrogeochemical evolution of the site and safety-related simulations of the transport of hydrochemical components potentially affecting repository conditions.

Specifically, the hydrogeochemical transport applications include, but are not limited to, the following modelling tasks (see references for information on transport processes considered and how they are modelled):

- Modelling salinity and solute transport coupled with reactions for analyses of groundwater composition and its evolution. References describing this type of modelling in recent safety assessments are Salas et al. (2010) and Joyce et al. (2015a, b) for the SR-Site modelling, Roman-Ross et al. (2014) for SR-PSU, Roman-Ross et al. (2024) for SR-PSU/PSAR SFR and Joyce et al. (2019) for SE-SFL.
- Modelling the infiltration of diluted water into the bedrock. Relevant SKB references include Joyce et al. (2010) for the modelling in SR-Site and a recent report for PSAR SFK by Shahkarami (2024).
- Modelling the penetration of oxygen into the bedrock. References describing this form of modelling include Sidborn et al. (2010) that was produced for SR-Site and papers by Trinchero et al. (2017, 2018b, 2019).
- Modelling grout degradation and the formation of high-pH plumes. References presenting SKB modelling in this area include Sidborn et al. (2014) and Molinero et al. (2016).
- Modelling sulphate reduction and the associated sulphide concentrations at repository depth.
 This type of analysis requires the use of multicomponent reactive transport models, see the modelling study of the Olkiluoto site in Posiva (2021), and has recently been carried out also for Forsmark (to be reported).

Since the transport modelling performed by Hydrogeology and Hydrogeochemistry differs from the radionuclide transport modelling in several ways, parameter needs and even parameter values of seemingly the same parameters may also differ between different models and types of models. For example, Follin et al. (2008) discuss the parameterisation of the solute transport component of the SDM-Site groundwater flow model and how parameters were modified compared to original estimates.

There are several factors that affect the parameterisation of hydrogeological and hydrogeochemical models with transport parameters, such that the parameters supplied to the radionuclide transport modelling cannot be used by others. In addition to the obvious reasons, e.g. that chemical substances with different properties are modelled, differences between model types and model scales may require modifications of parameters and parameter values, e.g. through upscaling. In some cases, different mass transfer models are used, such that, for instance, rate coefficients rather than diffusivities are needed as input.

Many of the parameter- and model-related factors outlined above might require some kind of transport-related analysis, possibly including simulations, to be sorted out and to assure consistency in the treatment of transport processes by different modelling disciplines. Since details regarding future transport modelling and parameter needs are not known at this time, methodology for providing and analysing transport parameters in applications such as those discussed above cannot be presented in this report. However, it is clear that cooperation between Transport and others that perform transport simulations is important and needs to be considered in the planning of forthcoming site descriptive and safety assessment modelling.

References

SKB's (Svensk Kärnbränslehantering AB) publications can be found at www.skb.com/publications. SKBdoc documents and unpublished SKB reports will be submitted upon request to document@skb.se.

Allard B, 1982. Sorption of actinides in granitic rock. SKBF/KBS TR 82-21, Svensk Kärnbränslehantering AB.

Allard B, Beall G W, 1979. Sorption of americium on geologic media. Journal of Environmental Science and Health. Part A: Environmental Science and Engineering 14, 507–518. https://doi.org/10.1080/10934527909374895

Allard B, Karlsson M, Tullborg E-L, Larson S Å, 1983. Ion exchange capacities and surface areas of some major components and fracture filling materials of igneous rocks. SKBF/KBS TR 83-64, Svensk Kärnbränslehantering AB.

Allard B, Ittner T, Torstenfelt B, 1985. Migration of trace elements into water-exposed natural fissure surfaces of granitic rock. Chemical Geology 49, 31–42. https://doi.org/10.1016/0009-2541(85)90145-7

Amentum, 2024. ConnectFlow Technical Summary. Version 13.1 – 4 November 2024. Available at: https://www.connectflow.com/resources/docs/conflow_technical.pdf [31 March 2025].

Anders M H, Laubach S E, Scholz C H, 2014. Microfractures: A review. Journal of Structural Geology 69 Part B, 377–394. https://doi.org/10.1016/j.jsg.2014.05.011

Andersson J, Hermanson J, Elert M, Gylling B, Moreno L, Selroos J-O, 1998. Derivation and treatment of the flow wetted surface and other geosphere parameters in the transport models FARF31 and COMP23 for use in safety assessment. SKB R-98-60, Svensk Kärnbränslehantering AB.

Andersson P, Byegård J, Dershowitz B, Doe T, Hermanson J, Meier P, Tullborg E-L, Winberg A (ed), 2002. Final report of the TRUE Block Scale project. 1. Characterisation and model development. SKB TR-02-13, Svensk Kärnbränslehantering AB.

Andersson P, Gustafsson E, Wass E, 2019. Analysis and evaluation of groundwater flow measurements in permanently installed boreholes at Forsmark 2005–2017. SKB TR-18-16, Svensk Kärnbränslehantering AB.

Appelo C A J, Postma D, 2005. Geochemistry, groundwater and pollution. 2nd ed. Rotterdam: Balkema.

Avila R, Ekström P-A, Per-Gustav Åstrand P-G, 2010. Landscape dose conversion factors used in the safety assessment SR-Site. SKB TR-10-06, Svensk Kärnbränslehantering AB.

Barry D A, Miller C T, Culligan-Hensley P J, 1996. Temporal discretisation errors in non-iterative split-operator approaches to solving chemical reaction/groundwater transport models. Journal of Contaminant Hydrology 22, 1–17. https://doi.org/10.1016/0169-7722(95)00062-3

Beall G W, O'Kelley G D, Allard B, 1980. An autoradiographic study of actinide sorption on climax stock granite. ORNL-5617, Oak Ridge National Laboratory, United States.

Belova D A, Lakshtanov L Z, Carneiro J F, Stipp S L S, 2014. Nickel adsorption on chalk and calcite. Journal of Contaminant Hydrology 170, 1–9. https://doi.org/10.1016/j.jconhyd.2014.09.007

Berglund S, Lindborg T (eds), 2017. Monitoring Forsmark – evaluation and recommendations for programme update. SKB TR-15-01, Svensk Kärnbränslehantering AB.

Berglund S, Selroos J-O, 2004. Transport properties site descriptive model. Guidelines for evaluation and modelling. SKB R-03-09, Svensk Kärnbränslehantering AB.

Berglund S, Crawford J, Andersson P, Byegård J, 2020. Preparatory studies for update of the strategy for site descriptive modelling of bedrock transport properties. Summary of activities in the DETUM-1 project. SKBdoc 1452535 ver 2.0, Svensk Kärnbränslehantering AB.

Bertetti F P, 2014. Detailed assessment of radionuclide K_d -values for the geosphere. Main review phase. SSM Technical Note 2014:38, Strålsäkerhetsmyndigheten (Swedish Radiation Safety Authority).

Bickmore B R, Rosso K M, Mitchell S C, 2006. Chapter 9 – Is there hope for multi-site complexation (MUSIC) modeling? In Lützenkirchen J (ed). Surface complexation modeling. Interface science and technology, Volume 11. Amsterdam: Elsevier, 269–283.

Bodin J, Delay F, de Marsily G, 2003. Solute transport in a single fracture with negligible matrix permeability: 1. fundamental mechanisms. Hydrogeology Journal 11, 418–433. https://doi.org/10.1007/s10040-003-0268-2

Bolt G H, 1980. Soil Chemistry, Part B: Physico-Chemical Models. Soil Science 130, 110.

Bourg I C, Sposito G, Bourg A C M, 2007. Modeling the acid—base surface chemistry of montmorillonite. Journal of Colloid and Interface Science 312, 297–310. https://doi.org/10.1016/j.jcis.2007.03.062

Bradbury M H, Baeyens B, 2000. A generalised sorption model for the concentration dependent uptake of caesium by argillaceous rocks. Journal of Contaminant Hydrology 42, 141–163. https://doi.org/10.1016/S0169-7722(99)00094-7

Bradbury M H, Baeyens B, 2005a. Modelling the sorption of Mn(II), Co(II), Ni(II), Zn(II), Cd(II), Eu(III), Am(III), Sn(IV), Th(IV), Np(V) and U(VI) on montmorillonite: Linear free energy relationships and estimates of surface binding constants for some selected heavy metals and actinides. Geochimica et Cosmochimica Acta 69, 875–892. https://doi.org/10.1016/j.gca.2004.07.020

Bradbury M H, Baeyens B, 2005b. Experimental measurements and modeling of sorption competition on montmorillonite. Geochimica et Cosmochimica Acta 69, 4187–4197, and Erratum 69, 5863–5864. https://doi.org/10.1016/j.gca.2005.04.014

Bradbury M H, Baeyens B, 2006. Modelling sorption data for the actinides Am(III), Np(V) and Pa(V) on montmorillonite. Radiochimica Acta 94, 619–625. https://doi.org/10.1524/ract.2006.94.9-11.619

Bradbury M H, Baeyens B, 2009a. Sorption modelling on illite Part I: Titration measurements and the sorption of Ni, Co, Eu and Sn. Geochimica et Cosmochimica Acta 73, 990–1003. https://doi.org/10.1016/j.gca.2008.11.017

Bradbury M H, Baeyens B, 2009b. Sorption modelling on illite. Part II: Actinide sorption and linear free energy relationships. Geochimica et Cosmochimica Acta 73, 1004–1013. https://doi.org/10.1016/j.gca.2008.11.016

Bradbury M H, Baeyens B, Thoenen T, 2010. Sorption data bases for generic Swiss argillaceous rock systems. Nagra Technical Report NTB 09-03, Nagra, Switzerland.

Brendler V, Vahle A, Arnold T, Bernhard G, Fanghänel T, 2003. RES³T-Rossendorf expert system for surface and sorption thermodynamics. Journal of Contaminant Hydrology 61, 281–291. https://doi.org/10.1016/S0169-7722(02)00129-8

Brendler V, Arnold T, Richter A, Bernhard G, 2004. Capability of surface complexation models and databases for predicting radionuclide sorption. Paper WM-4070, Waste Management 2004 Symposium, Tucson, Arizona, February 29–March 4, 2004. Available at: https://archivedproceedings.econference.io/wmsym/2004/pdfs/4070.pdf [30 April 2025].

Britz S M, 2018. Europium sorption experiments with muscovite, orthoclase, and quartz. Modeling of surface complexation and reactive transport. PhD thesis. Technical University of Braunschweig, Germany.

Byegård J, Selnert E, Tullborg E-L, 2008. Bedrock transport properties. Data evaluation and retardation model. Site descriptive modelling SDM-Site Forsmark. SKB R-08-98, Svensk Kärnbränslehantering AB.

Cacas M C, Ledoux E, de Marsily G, Tillie B, Barbreau A, Durand E, Feuga B, Peaudecerf P, 1990. Modeling fracture flow with a stochastic discrete fracture network: calibration and validation: 1. The flow model. Water Resources Research 26, 479–489. https://doi.org/10.1029/WR026i003p00479

Carrera J, Sánchez-Vila X, Benet I, Medina A, Galarza G, Guimerà J, 1998. On matrix diffusion: formulations, solution methods and qualitative effects. Hydrogeology Journal 6, 178–190. https://doi.org/10.1007/s100400050143

Carslaw H S, Jaeger J C, 1959. Conduction of heat in solids. 2nd ed. Oxford: Clarendon Press.

Charlton S R, Parkhurst D L, 2011. Modules based on the geochemical model PHREEQC for use in scripting and programming languages. Computers & Geosciences 37, 1653–1663. https://doi.org/10.1016/j.cageo.2011.02.005

Ciffroy P, 2020. A comprehensive probabilistic approach for integrating and separating natural variability and parametric uncertainty in the prediction of distribution coefficient of radionuclides in rivers. Journal of Environmental Radioactivity 225, 106371. https://doi.org/10.1016/j.jenvrad.2020.106371

Cliffe K A, Kelly M, 2006. COMP23 version 1.2.2 user's manual. SKB R-04-64, Svensk Kärnbränslehantering AB.

Cordes C, Kinzelbach W, 1992. Continuous groundwater velocity fields and path lines in linear, bilinear, and trilinear finite elements. Water Resources Research 28, 2903–2911. https://doi.org/10.1029/92WR01686

Crank J, 1975. The mathematics of diffusion. 2nd ed. London: Oxford University Press.

Crawford J, 2008. Bedrock transport properties Forsmark. Site descriptive modelling. SDM-Site Forsmark. SKB R-08-48, Svensk Kärnbränslehantering AB.

Crawford J, 2010. Bedrock *K*_d data and uncertainty assessment for application in SR-Site geosphere transport calculations. SKB R-10-48, Svensk Kärnbränslehantering AB.

Crawford J, 2013. Quantification of rock matrix K_d data and uncertainties for SR-PSU. SKB R-13-38, Svensk Kärnbränslehantering AB.

Crawford J, 2022. Project NukPrio – Identification of elements with greatest sorption data needs for the KBS-3 repository. SKB R-20-06, Svensk Kärnbränslehantering AB.

Crawford J, Löfgren M, 2019. Modelling of radionuclide retention by matrix diffusion in a layered rock model. SKB R-17-22, Svensk Kärnbränslehantering AB.

Crawford J, Sidborn M, 2009. Bedrock transport properties Laxemar. Site descriptive modelling SDM-Site Laxemar. SKB R-08-94, Svensk Kärnbränslehantering AB.

Crow E L, Shimizu K, (eds), 1988. Lognormal distributions: theory and applications. New York: Dekker.

Cvetkovic V, 2010. Significance of fracture rim zone heterogeneity for tracer transport in crystalline rock. Water Resources Research 46, W03504. https://doi.org/10.1029/2009WR007755

Cvetkovic V, Dagan G, 1994. Transport of kinetically sorbing solute by steady random velocity in heterogeneous porous formations. Journal of Fluid Mechanics 265, 189–216. https://doi.org/10.1017/S0022112094000807

Cvetkovic V, Selroos J, Cheng H, 1999. Transport of reactive tracers in rock fractures. Journal of Fluid Mechanics 378, 335–356. https://doi.org/10.1017/S0022112098003450

Davis J A, Coston J A, Kent D B, Fuller C C, 1998. Application of the surface complexation concept to complex mineral assemblages. Environmental Science & Technology 32, 2820–2828. https://doi.org/10.1021/es980312q

Davy P, Le Goc R, Darcel C, Bour O, de Dreuzy J R, Munier R, 2010. A likely universal model of fracture scaling and its consequence for crustal hydromechanics. Journal of Geophysical Research 115, B10411. https://doi.org/10.1029/2009JB007043

Delay F, Bodin J, 2001. Time domain random walk method to simulate transport by advection-dispersion and matrix diffusion in fracture networks. Geophysical Research Letters 28, 4051–4054. https://doi.org/10.1029/2001GL013698

Delayre C, Sammaljärvi J, Billon S, Muuri E, Sardini P, Siitari-Kauppi M, 2020. Comparison of phosphor screen autoradiography and micro-pattern gas detector based autoradiography for the porosity of altered rocks. Scientific Reports 10, 9455. https://doi.org/10.1038/s41598-020-65791-7

Delhorme M, Labbez C, Caillet C, Thomas F, 2010. Acid-base properties of 2:1 clays. I. Modeling the role of electrostatics. Langmuir 26, 9240–9249. https://doi.org/10.1021/la100069g

Demnitz M, Schymura S, Neumann J, Schmidt M, Schäfer T, Stumpf T, Müller K, 2022a. Mechanistic understanding of Curium(III) sorption on natural K-feldspar surfaces. Science of The Total Environment 843, 156920. https://doi.org/10.1016/j.scitotenv.2022.156920

Demnitz M, Molodtsov K, Schymura S, Schierz A, Müller K, Jankovsky F, Havlova V, Stumpf T, Schmidt M, 2022b. Effects of surface roughness and mineralogy on the sorption of Cm(III) on crystalline rock. Journal of Hazardous Materials 423, 127006. https://doi.org/10.1016/j.jhazmat.2021.127006

Dentz M, Le Borgne T, Englert A, Bijeljic B, 2011. Mixing, spreading and reaction in heterogeneous media: A brief review. Journal of Contaminant Hydrology 120–121, 1–17. https://doi.org/10.1016/j.jconhyd.2010.05.002

Dershowitz W, Winberg A, Hermanson J, Byegård J, Tullborg E-L, Andersson P, Mazurek M, 2003. Äspö Hard Rock Laboratory. Äspö Task Force on modelling of groundwater flow and transport of solutes. Task 6c. A semi-synthetic model of block scale conductive structures at the Äspö HRL. SKB IPR-03-13, Svensk Kärnbränslehantering AB.

De Simoni M, Sanchez-Vila X, Carrera J, Saaltink M W, 2007. A mixing ratios-based formulation for multicomponent reactive transport. Water Resources Research 43, W07419. https://doi.org/10.1029/2006WR005256

Doolaeghe D, Darcel C, Selroos J-O, Mas Ivars D, Davy P, 2023. Controls on fracture openness and reactivation in Forsmark, Sweden. Scientific Reports 13, 6686. https://doi.org/10.1038/s41598-023-33619-9

Drake H, Tullborg E-L, 2006a. Oskarshamn site investigation. Mineralogical, chemical and redox features of red-staining adjacent to fractures. Results from drill cores KSH01A+B and KSH03A+B. SKB P-06-01, Svensk Kärnbränslehantering AB.

Drake H, Tullborg E-L, 2006b. Oskarshamn site investigation. Mineralogical, chemical and redox features of red-staining adjacent to fractures – Results from drill core KLX04. SKB P-06-02, Svensk Kärnbränslehantering AB.

Dubois I E, Holgersson S, Allard S, Malmström M E, 2011. Dependency of BET surface area on particle size for some granitic minerals. Proceedings in Radiochemistry 1, 75–82. https://doi.org/10.1524/rcpr.2011.0013

Dzombak D A, Morel F M M, 1990. Surface complexation modeling: hydrous ferric oxide. New York: John Wiley & Sons.

Eichinger F, Iannotta J, 2024. Characterisation of porewater of core samples from borehole KFR121. Chemical composition in out-diffusion experiment solutions and stable isotopes. SKB R-21-21, Svensk Kärnbränslehantering AB.

Eichinger F, Meier D, Waber H N, 2015. Matrix pore water in Olkiluoto bedrock from drilling OL-KR54 and OL-KR55 – Chemical and isotopic characterization and evaluation of contamination by drilling fluid. Posiva Working Report 2014-66, Posiva Oy, Finland.

Eichinger F, Voutilainen M, Siitari-Kauppi M, Sammaljärvi J, Ikonen J, Joutsen A, Van den Heuvel D, Versin P, 2023. Transport properties and petrography of rock samples from drillhole ONK-PH28 – a method comparison. Posiva Working Report 2023-06, Posiva Oy, Finland.

Eklund S, Mattsson K-J, 2008. Oskarshamn site investigation. Quantitative mapping of fracture minerals in Laxemar. SKB P-08-38, Svensk Kärnbränslehantering AB.

Eklund S, Mattsson K-J, 2009. Forsmark site investigation. Quantitative mapping of fracture minerals in Forsmark. SKB P-08-47, Svensk Kärnbränslehantering AB.

Elert M, Gylling B, Lindgren M, 2004. Assessment model validity document FARF31. SKB R-04-51, Svensk Kärnbränslehantering AB.

Fabritius O, Fabritius A, Hellings M, Sorokina T, Sojakka T, Jakobsson A-M, Li X, Sammaljärvi J, Siitari-Kauppi M, 2024. Radium sorption on crystalline rock; spatial distribution and sorption modeling study. Applied Geochemistry 162, 105930. https://doi.org/10.1016/j.apgeochem.2024.105930

Ferreira C A S, Nick H M, 2024. On the influence of matrix flow in the hydraulic permeability of roughwalled fractures. Journal of Hydrology 645, 132192. https://doi.org/10.1016/j.jhydrol.2024.132192

Ferry M, 2019. PARTRACK. User's guide. Technical Report TR 19083, MFRDC, Orvault, France.

Follin S, 2008. Bedrock hydrogeology Forsmark. Site descriptive modelling, SDM-Site Forsmark. SKB R-08-95, Svensk Kärnbränslehantering AB.

Follin S (ed), 2019. Multidisciplinary description of the access area of the planned spent nuclear fuel repository in Forsmark prior to construction. SKB R-17-13, Svensk Kärnbränslehantering AB.

Follin S, Levén J, Hartley L, Jackson P, Joyce S, Roberts D, Swift B, 2007. Hydrogeological characterisation and modelling of deformation zones and fracture domains, Forsmark modelling stage 2.2. SKB R-07-48, Svensk Kärnbränslehantering AB.

Follin S, Hartley L, Jackson P, Roberts D, Marsic N, 2008. Hydrogeological conceptual model development and numerical modelling using CONNECTFLOW, Forsmark modelling stage 2.3. SKB R-08-23, Svensk Kärnbränslehantering AB.

Forsman I, Zetterlund M, Forsmark T, Rhén I, 2006. Forsmark site investigation. Correlation of Posiva Flow Log anomalies to core mapped features in KFM06A and KFM07A. SKB P-06-56, Svensk Kärnbränslehantering AB.

Fuller A J, Shaw S, Ward M B, Haigh S J, Mosselmans J F W, Peacock C L, Stackhouse S, Dent A J, Trivedi D, Burke I T, 2015. Caesium incorporation and retention in illite interlayers. Applied Clay Science 108, 128–134. https://doi.org/10.1016/j.clay.2015.02.008

Gaines G L, Thomas H C, 1953. Adsorption studies on clay minerals. II. A Formulation of the thermodynamics of exchange adsorption. The Journal of Chemical Physics 21, 714–718. https://doi.org/10.1063/1.1698996

Gelhar L W, 1993. Stochastic subsurface hydrology. Englewood Cliffs, NJ: Prentice-Hall.

Gelman A, Carlin J, Stern H, Rubin D, 2004. Bayesian data analysis. 2nd ed. Boca Raton, FL: Chapman & Hall/CRC.

Giffaut E, Grivé M, Blanc P, Vieillard P, Colàs E, Gailhanou H, Gaboreau S, Marty N, Madé B, Duro L, 2014. Andra thermodynamic database for performance assessment: ThermoChimie. Applied Geochemistry 49, 225–236. https://doi.org/10.1016/j.apgeochem.2014.05.007

Glover P W J, 2016. Archie's law – a reappraisal. Solid Earth 7, 1157–1169. https://doi.org/10.5194/se-7-1157-2016

Goldberg S, Criscenti L J, 2007. Modeling adsorption of metals and metalloids by soil components. In Violante A, Huang P M, Gadd G M (eds). Biophysico-chemical processes of heavy metals and metalloids in soil environments. New York: John Wiley & Sons, 215–264.

Goode D J, 1996. Direct simulation of groundwater age. Water Resources Research 32, 289–296. https://doi.org/10.1029/95WR03401

Goodfellow B W, Hilley G E, Webb S M, Sklar L S, Moon S, Olson C A, 2016. The chemical, mechanical, and hydrological evolution of weathering granitoid. Journal of Geophysical Research: Earth Surface 121, 1410–1435.https://doi.org/10.1002/2016JF003822

Grenthe I, Stumm W, Laaksoharju M, Nilsson A C, Wikberg P, 1992. Redox potentials and redox reactions in deep groundwater systems. Chemical Geology 98, 131–150. https://doi.org/10.1016/0009-2541(92)90095-M

Gylling B, Moreno L, Neretnieks I, 1999. The Channel Network Model—A Tool for Transport Simulations in Fractured Media. Groundwater 37, 367–375. https://doi.org/10.1111/j.1745-6584.1999.tb01113.x

- Haggerty R, 2012. Review of matrix diffusion and related properties of intact rock in SKB's licence application for a spent nuclear fuel repository in Forsmark, Sweden. SSM Technical Note 2012:44, Strålsäkerhetsmyndigheten (Swedish Radiation Safety Authority).
- **Haggerty R, Gorelick S M, 1995.** Multiple-rate mass transfer for modeling diffusion and surface reactions in media with pore-scale heterogeneity. Water Resources Research 31, 2383–2400. https://doi.org/10.1029/95WR10583
- **Haggerty R, McKenna S A, Meigs L C, 2000.** On the late-time behavior of tracer test breakthrough curves. Water Resources Research 36, 3467–3479. https://doi.org/10.1029/2000WR900214
- Hakanen M, Ervanne H, Puukko E, 2014. Safety case for the disposal of spent nuclear fuel at Olkiluoto. Radionuclide migration parameters for the geosphere. Posiva Report 2012-41, Posiva Oy, Finland.
- **Hallbeck L, Pedersen K, 2008.** Explorative analysis of microbes, colloids and gases. SDM-Site Forsmark. SKB R-08-85, Svensk Kärnbränslehantering AB.
- Hammond G E, Lichtner P C, Mills R T, 2014. Evaluating the performance of parallel subsurface simulators: An illustrative example with PFLOTRAN. Water Resources Research 50, 208–228. https://doi.org/10.1002/2012WR013483
- Hartley L, Appleyard P, Baxter S, Hoek J, Roberts D, Swan D, 2013a. Development of a hydrogeological discrete fracture network model for the Olkiluoto site descriptive model 2011. Posiva Working Report 2012-32, Posiva Oy, Finland.
- Hartley L, Hock J, Swan D, Appleyard P, Baxter S, Roberts D, Simpson T, 2013b. Hydrogeological modelling for assessment of radionuclide release scenarios for the repository system 2012. Posiva Working Report 2012-42, Posiva Oy, Finland.
- Hartley L, Baxter S, Hoek J, Joyce S, Mosley K, Williams T, Fox A, Cottrell M, La Pointe P, Gehör S, Darcel C, Le Goc R, Aaltonen I, Vanhanarkaus O, Löfman J, Poteri A, 2018. Discrete fracture network modelling (version 3) in support of Olkiluoto site description. Posiva Working Report 2017-32, Posiva Oy, Finland.
- Hartley L, Baxter S, Carty J, Libby S, 2021. Exploratory integration of discrete fracture network models and 1D stress models with data from hydraulic tests for the shallow bedrock at the Forsmark site. SKB R-21-13, Svensk Kärnbränslehantering AB.
- Hayes K F, Redden G, Ela W, Leckie J O, 1991. Surface complexation models: An evaluation of model parameter estimation using FITEQL and oxide mineral titration data. Journal of Colloid and Interface Science 142, 448–469. https://doi.org/10.1016/0021-9797(91)90075-J
- **Heberling F, Trainor T P, Lützenkirchen J, Eng P, Denecke M A, Bosbach D, 2011.** Structure and reactivity of the calcite-water interface. Journal of Colloid and Interface Science 354, 843–857, and Corrigendum 404, 230. https://doi.org/10.1016/j.jcis.2010.10.047
- **Hedqvist I, Degueldre C, 2008.** Oskarshamn site investigation. Granitic groundwater colloids sampling and characterisation. Colloids analysis from KLX17A (416.0 to 437.5 m) and KLX15 A (623.0 to 634.5 m). SKB P-08-101, Svensk Kärnbränslehantering AB.
- **Hermanson J, Petersson J, 2022.** Methodology for deterministic geological modelling of the Forsmark site. Application to the development of the final repository for spent nuclear fuel. SKB R-20-10, Svensk Kärnbränslehantering AB.
- **Hiemstra T, Van Riemsdijk W H, 1996.** A surface structural approach to ion adsorption: The charge distribution (CD) model. Journal of Colloid and Interface Science 179, 488–508. https://doi.org/10.1006/jcis.1996.0242
- **Hjerne C, Nordqvist R, Harrström J, 2010.** Compilation and analyses of results from cross-hole tracer tests with conservative tracers. SKB R-09-28, Svensk Kärnbränslehantering AB.
- **Idiart A, Pękala M, 2016.** Models for diffusion in compacted bentonite. SKB TR-15-06, Svensk Kärnbränslehantering AB.

- Idiart A, Coene E, Bagaria F, Román-Ross G, Birgersson M, 2019. Reactive transport modelling considering transport in interlayer water. New model, sensitivity analyses and results from the Integrated Sulfide Project inter-model comparison exercise. SKB TR-18-07, Svensk Kärnbränslehantering AB.
- Iraola A, Trinchero P, Voutilainen M, Gylling B, Selroos J-O, Molinero J, Svensson U, Bosbach D, Deissmann G, 2017. Microtomography-based Inter-Granular Network for the simulation of radionuclide diffusion and sorption in a granitic rock. Journal of Contaminant Hydrology 207, 8–16. https://doi.org/10.1016/j.jconhyd.2017.10.003
- **Iraola A, Trinchero P, Karra S, Molinero J, 2019.** Assessing dual continuum method for multicomponent reactive transport. Computers & Geosciences 130, 11–19. https://doi.org/10.1016/j.cageo.2019.05.007
- Ittner T, Torstenfelt B, Allard B, 1988a. Migration of the fission products strontium, technetium, iodine, cesium and the actinides neptunium, plutonium, americium in granitic rock. SKB TR 88-02, Svensk Kärnbränslehantering AB.
- Ittner T, Torstenfelt B, Allard B, 1988b. Diffusion of neptunium, plutonium and americium in granitic rock. Radiochimica Acta 44–45, 171–178. https://doi.org/10.1524/ract.1988.4445.1.171
- **IUPAC**, **1976**. Manual of symbols and terminology for physicochemical quantities and units Appendix II. Definitions, terminology and symbols in colloid and surface chemistry. Part II: Heterogenous catalysis. Pure and Applied Chemistry 46, 71–90. https://doi.org/10.1351/pac197646010071
- **Jackson C P, Hoch A R, Todman S, 2000.** Self-consistency of a heterogeneous continuum porous medium representation of a fractured medium, Water Resources Research 36, 189–202. https://doi.org/10.1029/1999WR900249
- **Jacobsson L, 2007.** Forsmark site investigation. Boreholes KFM01A and KFM02B. Micro crack volume measurements and triaxial compression tests on intact rock. SKB P-07-93, Svensk Kärnbränslehantering AB.
- **Jasak H, Jemcov A, Tukovic Z, 2007.** OpenFOAM: A C++ library for complex physics simulations. In Terze Z (ed). Proceedings of the International Workshop on Coupled Methods in Numerical Dynamics, Dubrovnik, Croatia, September 19–21 2007.
- Joyce S, Simpson T, Hartley L, Applegate D, Hoek J, Jackson P, Swan D, Marsic N, Follin S, 2010. Groundwater flow modelling of periods with temperate climate conditions Forsmark. SKB R-09-20, Svensk Kärnbränslehantering AB.
- Joyce S, Applegate D, Appleyard P, Gordon A, Heath T, Hunter F, Hoek J, Jackson P, Swan D, Woollard H, 2015a. Groundwater flow and reactive transport modelling in ConnectFlow. SKB R-14-19, Svensk Kärnbränslehantering AB.
- **Joyce S, Woollard H, Marsic N, Sidborn M, 2015b.** Future evolution of groundwater composition at Forsmark during an extended temperate period. SKB R-14-26, Svensk Kärnbränslehantering AB.
- Joyce S, Appleyard P, Hartley L, Tsitsopoulos V, Woollard H, Marsic N, Sidborn M, Crawford J, 2019. Groundwater flow and reactive transport modelling of temperate conditions. Report for the safety evaluation SE-SFL. SKB R-19-02, Svensk Kärnbränslehantering AB.
- Joyce S, Appleyard P, Gai G, Mather F, Williams T, 2021. Groundwater flow and transport modelling in support of the safety case for the operating licence application. Posiva Working Report 2021-20, Posiva Oy, Finland.
- **Kaplan D I, 2021.** Geochemical data package for performance assessment calculations related to the Savannah River Site. Report SRNL-STI-2021-00017, Savannah River National Laboratory, United States.
- **Kaukonen V, Hakanen M, Lindberg A, 1997.** Diffusion and sorption of HTO, Np, Na and Cl in rocks and minerals of Kivetty and Olkiluoto. Posiva Report 1997-07, Posiva Oy, Finland.
- Kelly M, Cliffe K A, 2006. Validity document for COMP23. SKB R-06-76, Svensk Kärnbränslehantering AB.

Kelokaski M, Oila E, Siitari-Kauppi M, 2001. Äspö Hard Rock Laboratory. TRUE Block Scale project. Investigation of porosity and microfracturing in granitic fracture wall rock and fault breccia specimens using the PMMA technique. SKB IPR-01-27, Svensk Kärnbränslehantering AB.

Kienzler B, Vejmelka P, Römer J, Schild D, Jansson M, 2009. Actinide migration in fractures of granite host rock: Laboratory and in situ investigations. Nuclear Technology 165, 223–240. https://doi.org/10.13182/NT09-A4088

Kim Y, Kirkpatrick R J, 1997. ²³Na and ¹³³Cs NMR study of cation adsorption on mineral surfaces: Local environments, dynamics, and effects of mixed cations. Geochimica et Cosmochimica Acta 61, 5199–5208. https://doi.org/10.1016/S0016-7037(97)00347-5

Kim Y, Kirkpatrick R J, 1998. NMR T₁ relaxation study of ¹³³Cs and ²³Na adsorbed on illite. American Mineralogist 83, 661–665. https://doi.org/10.2138/am-1998-5-625

Kim Y, Kirkpatrick R J, Cygan R T, 1996. ¹³³Cs NMR study of cesium on the surfaces of kaolinite and illite. Geochimica et Cosmochimica Acta 60, 4059–4074. https://doi.org/10.1016/S0016-7037(96)00257-8

Kinniburgh D G, Cooper D M, 2004. Predominance and mineral stability diagrams revisited. Environmental Science & Technology 38, 3641–3648. https://doi.org/10.1021/es0349271

Kosmulski M, 2009. Surface charging and points of zero charge. Boca Raton, FL: CRC Press.

Ku H H, 1966. Notes on the use of propagation of error formulas, Journal of Research of the National Bureau of Standards – C. Engineering and Instrumentation 70C, 263–273. https://doi.org/10.6028/jres.070C.025

Kulik D A, 2002. Sorption modelling by Gibbs energy minimisation: Towards a uniform thermodynamic database for surface complexes of radionuclides. Radiochimica Acta 90, 815–832. https://doi.org/10.1524/ract.2002.90.9-11 2002.815

Kulik D A, 2006. Chapter 7 – Standard molar Gibbs energies and activity coefficients of surface complexes on mineral-water interfaces (thermodynamic insights). In Lützenkirchen J (ed). Surface complexation modeling. Interface science and technology, Volume 11. Amsterdam: Elsevier, 171–250.

Laaksoharju M, Smellie J, Tullborg E-L, Gimeno M, Hallbeck L, Molinero J, Waber N, 2008. Bedrock hydrogeochemistry Forsmark. Site descriptive modelling, SDM-Site Forsmark. SKB R-08-47. Svensk Kärnbränslehantering AB.

Landström O, Tullborg E-L, Eriksson G, Sandell Y, 2001. Effects of glacial/post-glacial weathering compared with hydrothermal alteration - implications for matrix diffusion. Results from drillcore studies in porphyritic quartz monzodiorite from Äspö SE Sweden. SKB R-01-37, Svensk Kärnbränslehantering AB.

Langmuir D, 1997. Aqueous environmental geochemistry. Englewood Cliffs, NJ: Prentice-Hall.

Lavonen E, Lagerström M, Drake H, 2014. A comparative study of two rock crushing methods using quartz monzodiorite from Laxemar, Oskarshamn. Effects on oxygen consumption, sorption capacity, morphology and pore size distribution. SKB TR-14-18, Svensk Kärnbränslehantering AB.

Lichtner P C, 2000. Critique of dual continuum formulations of multicomponent reactive transport in fractured porous media. In Faybishenko B, Witherspoon P A, Benson S M (eds). Dynamics of fluids in fractured rock. Geophysical Monograph 122, American Geophysical Union.

Lichtner P C, Karra S, 2014. Modeling multiscale-multiphase-multicomponent reactive flows in porous media: Application to CO₂ sequestration and enhanced geothermal energy using PFLOTRAN. In Al-Khoury R, Bundschuh J (eds). Computational models for CO₂ geo-sequestration & compressed air energy storage. London: CRC Press, 81–136

Lichtner P C, Hammond G E, Lu C, Karra S, Bisht G, Andre B, Mills R, Kumar J, 2015. PFLOTRAN User Manual: A massively parallel reactive flow and transport model for describing surface and subsurface processes. Report LA-UR-15-20403, Los Alamos National Laboratory, United States.

Lindborg T (ed), 2010. Landscape Forsmark – data, methodology and results for SR-Site. SKB TR-10-05, Svensk Kärnbränslehantering AB.

Lindgren M, Lindström F, 1999. SR 97. Radionuclide transport calculations. SKB TR-99-23, Svensk Kärnbränslehantering AB.

Lindgren M, Gylling B, Elert M, 2002. FARF31 Version 1.2 User's Guide. TS-02-03, Svensk Kärnbränslehantering AB.

Lützenkirchen J, 1998. Comparison of 1-pK and 2-pK versions of surface complexation theory by the goodness of fit in describing surface charge data of (hydr)oxides. Environmental Science & Technology 32, 3149–3154. https://doi.org/10.1021/es980125s

Lützenkirchen J, Marsac R, Kulik D A, Payne T E, Xue Z, Orsetti S, Haderlein S B, 2015. Treatment of multi-dentate surface complexes and diffuse layer implementation in various speciation codes. Applied Geochemistry 55, 128–137. https://doi.org/10.1016/j.apgeochem.2014.07.006

Löfgren M, **2001.** Diffusive properties of granitic rock as measured by *in-situ* electrical methods. PhD thesis. Royal Institute of Technology (KTH), Stockholm, Sweden.

Löfgren M, 2014. Recommendation of rock matrix effective diffusivities for SR-PSU. Based on formation factor logging in situ by electrical methods in KFR102B and KFR105. SKB R-13-39, Svensk Kärnbränslehantering AB.

Löfgren M, 2015. Artefacts associated with electrical measurements of the rock matrix formation factor. With comments on handling in, and potential consequences for, the safety assessment SR-Site. SKB R-14-20, Svensk Kärnbränslehantering AB.

Löfgren M, Crawford J, 2014. Modelling of radionuclide retention by matrix diffusion in a layered rock model. Response to the request by SSM for supplementary information on retention of radionuclides (SSM2011-2426-110), items 4 and 6. SKBdoc 1421960 ver 1.0, Svensk Kärnbränslehantering AB.

Löfgren M, Neretnieks I, 2005. Forsmark site investigation. Formation factor logging *in-situ* by electrical methods in KFM01A and KFM02A. Measurements and evaluation of methodology. SKB P-05-29, Svensk Kärnbränslehantering AB.

Löfgren M, Sidborn M, 2010. Statistical analysis of results from the quantitative mapping of fracture minerals in Forsmark. Site descriptive modelling – complementary studies. SKB R-09-30, Svensk Kärnbränslehantering AB.

Löfgren M, Sidborn M, 2016. Quantitative mapping and statistical evaluation of fracture minerals in the granitic bedrock at Forsmark, Sweden. Mineralogy and Petrology 110, 663–680. https://doi.org/10.1007/s00710-016-0437-3

Mahmoudzadeh B, Liu L, Moreno L, Neretnieks I, 2013. Solute transport in fractured rocks with stagnant water zone and rock matrix composed of different geological layers – Model development and simulations. Water Resources Research 49, 1709–1727. https://doi.org/10.1002/wrcr.20132

Mahmoudzadeh B, Liu L, Moreno L, Neretnieks I, 2014. Solute transport in a single fracture involving an arbitrary length decay chain with rock matrix comprising different geological layers. Journal of Contaminant Hydrology 164, 59–71. https://doi.org/10.1016/j.jconhyd.2014.05.011

Makedonska N, Hyman J D, Karra S, Painter S L, Gable C W, Viswanathan H S, 2016. Evaluating the effect of internal aperture variability on transport in kilometer scale discrete fracture networks. Advances in Water Resources 94, 486–497. https://doi.org/10.1016/j.advwatres.2016.06.010

Malmström M E, Berglund S, Jarsjö J, 2008. Combined effects of spatially variable flow and mineralogy on the attenuation of acid mine drainage in groundwater. Applied Geochemistry 23, 1419–1436. https://doi.org/10.1016/j.apgeochem.2007.12.029

Mathur S, Dzombak D, 2006. Chapter 16 – Surface complexation modeling: goethite. In Lützenkirchen J (ed). Surface complexation modeling. Interface science and technology, Volume 11. Amsterdam: Elsevier, 443–468.

Meier D B, Waber H N, Gimmi T, Eichinger F, Diamond L W, 2015. Reconstruction of *in-situ* porosity and porewater compositions of low-permeability crystalline rocks: Magnitude of artefacts induced by drilling and sample recovery. Journal of Contaminant Hydrology 183, 55–71. http://doi.org/10.1016/j.jconhyd.2015.10.006

Metcalfe R, Milodowski A E, Field L P, Wogelius R A, Carpenter G, Yardley B W D, Norris S, 2021. Natural analogue evidence for controls on radionuclide uptake by fractured crystalline rock. Applied Geochemistry 124, 104812. https://doi.org/10.1016/j.apgeochem.2020.104812

Molinero J, Trinchero P, Ebrahimi H, de Vries L, Luna M, Svensson U, Lichtner P, 2016. The BRIDGE Project: Development, testing and application of a high performance computing framework for reactive transport modelling in crystalline roks (iDP). SKB R-15-17, Svensk Kärnbränslehantering AB.

Molins S, Soulaine C, Prasianakis N I, Abbasi A, Poncet P, Ladd A J C, Starchenko V, Roman S, Trebotich D, Tchelepi H A, Steefel C I, 2021. Simulation of mineral dissolution at the pore scale with evolving fluid-solid interfaces: review of approaches and benchmark problem set. Computational Geosciences 25, 1285–1318. https://doi.org/10.1007/s10596-019-09903-x

Molz F, 2015. Advection, dispersion, and confusion. Groundwater 53, 348–353. https://doi.org/10.1111/gwat.12338

Moreno L, Crawford J, 2009. Can we use tracer tests to obtain data for performance assessment of repositories for nuclear waste? Hydrogeology Journal 17, 1067–1080. https://doi.org/10.1007/s10040-008-0418-7

Moreno L, Neretnieks I, 1993. Fluid flow and solute transport in a network of channels. Journal of Contaminant Hydrology 14, 163–192. https://doi.org/10.1016/0169-7722(93)90023-L

Munier R, Stenberg L, Stanfors R, Milnes A G, Hermanson J, Triumf C-A, 2003. Geological Site Descriptive Model. A strategy for the model development during site investigations. SKB R-03-07, Svensk Kärnbränslehantering AB.

Möri A, Mazurek M, Adler M, Schild M, Siegesmund S, Vollbrecht A, Ota K, Ando T, Alexander W R, Smith P A, Haag P, Bühler C, 2003. Grimsel Test Site. Investigation Phase IV (1994–1996). The Nagra-JNC in situ study of safety relevant radionuclide retardation in fractured crystalline rock. IV: The in situ study of matrix porosity in the vicinity of a water conducting fracture. Nagra Technical Report 00-08, Nagra, Switzerland.

Nardi A, Idiart A, Trinchero P, de Vries L M, Molinero J, 2014. Interface COMSOL-PHREEQC (iCP), an efficient numerical framework for the solution of coupled multiphysics and geochemistry. Computers & Geosciences 69, 10–21. https://doi.org/10.1016/j.cageo.2014.04.011

Neretnieks I, 1983. A note on fracture flow dispersion mechanisms in the ground. Water Resources Research 19, 364–370. https://doi.org/10.1029/WR019i002p00364

Neretnieks I, 2002. A stochastic multi-channel model for solute transport--analysis of tracer tests in fractured rock. Journal of Contaminant Hydrology 55, 175–211. https://doi.org/10.1016/S0169-7722(01)00195-4

Neretnieks I, 2006. Channeling with diffusion into stagnant water and into a matrix in series. Water Resources Research 42, W11418. https://doi.org/10.1029/2005WR004448

Neretnieks I, 2023. Radionuclide transport in channel networks with radial diffusion in the porous rock matrix, Nuclear Technology 209, 604-621. https://doi.org/10.1080/00295450.2022.2136440

Neretnieks I, Moreno L, Liu L, Mahmoudzadeh B, Shahkarami P, Maskenskaya O, Kinnbom P, **2018.** Use of infrared pictures to assess flowing channel frequencies and flowrates in fractured rocks. A feasibility study. SKB R-17-04, Svensk Kärnbränslehantering AB.

Nielsen U, Ringgaard, J 2004. Forsmark site investigation. Geophysical borehole logging in borehole KFM01A, HFM01 and HFM02. SKB P-03-103, Svensk Kärnbränslehantering AB.

Nilsson A, Degueldre D, 2007. Forsmark site investigation. Granitic groundwater colloids sampling and characterisation. SKB P-07-169, Svensk Kärnbränslehantering AB.

Nilsson G, 2021. Borrning av kärnborrhål KFR117–120 och teleskopborrhål KFR121 i Forsmark. SKB P-20-32, Svensk Kärnbränslehantering AB. (In Swedish.)

Nilsson G, 2024. Borrning av kärnborrhål KFR90 och KFR91 under jord, SFR, Forsmark. SKB P-24-04, Svensk Kärnbränslehantering AB. (In Swedish.)

Nilsson K, Byegård J, Selnert E, Widestrand H, Höglund S, Gustafsson E, 2010. Äspö Hard Rock Laboratory Long Term Sorption Diffusion Experiment (LTDE-SD). Results from rock sample analyses and modelling. SKB R-10-68, Svensk Kärnbränslehantering AB.

Nordqvist R, 2008. Evaluation and modelling of SWIW tests performed within the SKB site characterisation programme. SKB R-08-104, Svensk Kärnbränslehantering AB.

Nordqvist R, Gustafsson E, Andersson P, Thur P, 2008. Groundwater flow and hydraulic gradients in fractures and fracture zones at Forsmark and Oskarshamn. SKB R-08-103, Svensk Kärnbränslehantering AB.

Norman S, Kjellbert N, 1990. FARF31 - A far field radionuclide migration code for use with the PROPER package. SKB TR 90-01, Svensk Kärnbränslehantering AB.

Ochs M, Talerico C, 2004. SR-Can. Data and uncertainty assessment. Migration parameters for the bentonite buffer in the KBS-3 concept. SKB TR-04-18, Svensk Kärnbränslehantering AB.

Odén M, Follin S, Öhman J, Vidstrand P, 2014. SR-PSU Bedrock hydrogeology. Groundwater flow modelling methodology, setup and results. SKB R-13-25, Svensk Kärnbränslehantering AB.

Odén M, Follin S, Werner K, 2025. Methodology for hydrological and hydrogeological modelling of the Forsmark site. SKB R-20-14, Svensk Kärnbränslehantering AB.

OECD/NEA, 2012. Thermodynamic sorption modelling in support of radioactive waste disposal safety cases. NEA Sorption Project Phase III. NEA Report No. 6914, OECD Nuclear Energy Agency (NEA), OECD Publishing, Paris, France.

OECD/NEA, 2020. TDB-2: Guidelines for the extrapolation to zero ionic strength. OECD Publishing, Paris, France.

Ogilvie S R, Isakov E, Glover P W J, 2006. Fluid flow through rough fractures in rocks. II: A new matching model for rough rock fractures. Earth and Planetary Science Letters 241, 454–465. https://doi.org/10.1016/j.epsl.2005.11.041

Ohlsson Y, 2001. Studies of ionic diffusion in crystalline rock. PhD thesis. Royal Institute of Technology (KTH), Stockholm, Sweden.

Okumura T, Tamura K, Fujii E, Yamada H, Kogure T, 2014. Direct observation of cesium at the interlayer region in phlogopite mica. Microscopy 63, 65–72. https://doi.org/10.1093/jmicro/dft045

Olin M, Valkiainen M, Aalto H, 1997. Matrix diffusion in crystalline rocks: coupling of anion exclusion, surface diffusion and surface complexation. Posiva Report 1996-25, Posiva Oy, Finland.

Olofsson I, Simeonov A, Stephens M, Follin S, Nilsson A-C, Röshoff K, Lindberg U, Lanaro F, Fredriksson A, Persson L, 2007. Site descriptive modelling Forsmark, stage 2.2. A fracture domain concept as a basis for the statistical modelling of fractures and minor deformation zones, and interdisciplinary coordination. SKB R-07-15, Svensk Kärnbränslehantering AB.

Painter S, Cvetkovic V, 2005. Upscaling discrete fracture network simulations: An alternative to continuum transport models. Water Resources Research 41, W02002. https://doi.org/10.1029/2004WR003682

Painter S, Mancillas J, 2013. MARFA user's manual: Migration analysis of radionuclides in the far field. Posiva Working Report 2013-01, Posiva Oy, Finland.

- **Painter S, Cvetkovic V, Mancillas J, Pensado O, 2008.** Time domain particle tracking methods for simulating transport with retention and first-order transformation. Water Resources Research 44, W01406. https://doi.org/10.1029/2007WR005944
- **Painter S, Trinchero P, Sanglas J, 2022.** MARFA user's manual: Migration analysis of radionuclides in the far field version 5.0. Revision nr. 2. Amphos 21 Consulting, Barcelona, Spain.
- **Parkhurst D L, Appelo C A J, 1999.** User's guide to PHREEQC (version 2) A computer program for speciation, batch-reaction, one-dimensional transport, and Inverse geochemical calculations. Water-Resources Investigations Report 99-4259, U.S. Geological Survey, United States.
- **Parkhurst D L, Appelo C A J, 2013.** Description of input and examples for PHREEQC version 3 A computer program for speciation, batch-reaction, one-dimensional transport, and inverse geochemical calculations. U.S. Geological Survey, Techniques and methods, book 6, chapter A43. Available at: https://pubs.usgs.gov/tm/06/a43/ [April 30 2025].
- **Penttinen L, Siitari-Kauppi M, Ikonen J, 2006.** Forsmark site investigation. Determination of porosity and micro fracturing using the ¹⁴C-PMMA technique in samples taken from Forsmark area. SKB P-06-60, Svensk Kärnbränslehantering AB.
- Pinnioja S, Jaakkola T, Miettinen J, 1983. Comparison of batch and autoradiographic methods in sorption studies of radionuclides in rock and mineral samples. MRS Online Proceedings Library 26, 979–984. https://doi.org/10.1557/PROC-26-979
- **Posiva, 2012.** Safety case for the disposal of spent nuclear fuel at Olkiluoto Features, events and processes 2012. Posiva Report 2012-07, Posiva Oy, Finland.
- **Posiva, 2013a.** Safety case for the disposal of spent nuclear fuel at Olkiluoto Performance assessment 2012. Posiva Report 2012-04, Posiva Oy, Finland.
- **Posiva, 2013b.** Safety case for the disposal of spent nuclear fuel at Olkiluoto Models and data for the repository system 2012. Posiva Report 2013-01, Posiva Oy, Finland.
- **Posiva, 2021.** Sulfide fluxes and concentrations in the spent nuclear fuel repository at Olkiluoto 2021 update. Posiva Working Report 2021-07, Posiva Oy, Finland.
- Poteri A, Andersson P, Nilsson K, Byegård J, Skålberg M, Siitari-Kauppi M, Helariutta K, Voutilainen M, Kekäläinen P, Ikonen J, Sammaljärvi J, Lindberg A, Timonen J, Kuva J, Koskinen L, 2018a. The first matrix diffusion experiment in the water phase of the REPRO Project: WPDE 1. Posiva Working Report 2017-23, Posiva Oy, Finland.
- Poteri A, Andersson P, Nilsson K, Byegård J, Skålberg M, Siitari-Kauppi M, Helariutta K, Voutilainen M, Kekäläinen P, 2018b. The second matrix diffusion experiment in the water phase of the REPRO Project: WPDE 2. Posiva Working Report 2017-24, Posiva Oy, Finland.
- **Probst H, Schröter H, Kraft E, Andersson P, 2005.** Forsmark site investigation. Geophysical borehole logging using the antares dual-laterolog in KFM01A and KFM02A. SKB P-05-110, Svensk Kärnbränslehantering AB.
- **Righetto L, Azimonti G, Missana T, Bidoglio G, 1995.** The triple layer model revised. Colloids and Surfaces A: Physicochemical and Engineering Aspects 95, 141–157. https://doi.org/10.1016/0927-7757(94)02990-A
- Román-Ross G, Trinchero P, Maia F, Molinero J, 2014. Hydrogeochemical modelling and evolution of the groundwater types and processes in geosphere of SFR, SR-PSU. SKB R-13-30, Svensk Kärnbränslehantering AB.
- Román-Ross G, Iraola A, Trinchero P, Molinero J, 2024. Site scale modelling of groundwater evolution at SFR. A modelling application with iDP. SKB R-23-19, Svensk Kärnbränslehantering AB.
- **Romero L, 1995.** The near-field transport in a repository for high-level nuclear waste. PhD thesis. Royal Institute of Technology (KTH), Stockholm, Sweden.

Ruiz Pestana L, Kolluri K, Head-Gordon T, Nielsen Lammers L, 2017. Direct exchange mechanism for interlayer ions in non-swelling clays. Environmental Science & Technology 51, 393–400. https://doi.org/10.1021/acs.est.6b04747

Saetre P, Nordén S, Keesmann S, Ekström P-A, 2013. The biosphere model for radionuclide transport and dose assessment in SR-PSU. SKB R-13-46, Svensk Kärnbränslehantering AB.

Sáinz-García A, Sampietro D, Abarca E, García D, Molinero J, 2022. Modelling of radionuclide transport and retention in the regolith above a hypothetical SFL repository location in the Laxemar area. SKB R-20-08, Svensk Kärnbränslehantering AB.

Salamon P, Fernandez-Garcia D, Gomez-Hernandez J J, 2006. A review and numerical assessment of the random walk particle tracking method. Journal of Contaminant Hydrology 87, 277–305. https://doi.org/10.1016/j.jconhyd.2006.05.005

Salas J, Gimeno M J, Auqué L, Molinero J, Gómez J, Juárez I, 2010. SR-Site – hydrogeochemical evolution of the Forsmark site. SKB TR-10-58, Svensk Kärnbränslehantering AB.

Sampietro D, Pool M, Abarca E, Molinero J, 2022. iCP version 2.0 – A numerical tool for solving reactive transport in discrete fractures with matrix diffusion. SKB R-21-10, Svensk Kärnbränslehantering AB.

Sanchez-Vila X, Guadagnini A, Carrera J, 2006. Representative hydraulic conductivities in saturated groundwater flow, Reviews of Geophysics 44, RG3002. https://doi.org/10.1029/2005RG000169

Sandström B, Stephens M, 2009. Mineralogy, geochemistry, porosity and redox properties of rocks from Forsmark. Compilation of data from the regional model volume for SR-Site. SKB R-09-51, Svensk Kärnbränslehantering AB.

Sandström B, Tullborg E-L, 2006. Forsmark site investigation. Mineralogy, geochemistry, porosity and redox capacity of altered rock adjacent to fractures. SKB P-06-209, Svensk Kärnbränslehantering AB.

Sandström B, Tullborg E-L, 2011. Site investigation SFR. Fracture mineralogy and geochemistry of borehole sections sampled for groundwater chemistry and Eh. Results from boreholes KFR01, KFR08, KFR10, KFR19, KFR7A and KFR105. SKB P-11-01, Svensk Kärnbränslehantering AB.

Sandström B, Tullborg E-L, Smellie J, MacKenzie A B, Suksi J, 2008. Fracture mineralogy of the Forsmark site. SDM-Site Forsmark. SKB R-08-102, Svensk Kärnbränslehantering AB.

Sandström B, Nilsson K, Tullborg E-L, 2011. Site investigation SFR. Fracture mineralogy including identification of uranium phases and hydrochemical characterisation of groundwater in borehole KFR106. SKB P-11-41, Svensk Kärnbränslehantering AB.

Sanglas J, Trinchero P, Painter S L, Cvetkovic V, Poteri A, Selroos J-O, Zou L, 2024. Significance of low-velocity zones on solute retention in rough fractures. Water Resources Research 60, e2023WR036221. https://doi.org/10.1029/2023WR036221

Schindler P W, Fuerst B, Dick R, Wolf P U, 1976. Ligand properties of surface silanol groups. I. surface complex formation with Fe³⁺, Cu²⁺, Cd²⁺, and Pb²⁺. Journal of Colloid and Interface Science 55, 469–475. https://doi.org/10.1016/0021-9797(76)90057-6

Selnert E, Byegård J, Widestrand H, 2008. Forsmark site investigation. Laboratory measurements within the site investigation programme for the transport properties of the rock. Final report. SKB P-07-139, Svensk Kärnbränslehantering AB.

Selnert E, Byegård J, Widestrand H, Carlsten S, Döse C, Tullborg E-L, 2009a. Bedrock transport properties. Data evaluation and retardation model. Site descriptive modelling, SDM-Site Laxemar. SKB R-08-100. Svensk Kärnbränslehantering AB.

Selnert E, Byegård J, Widestrand H, 2009b. Oskarshamn site investigation. Laboratory measurements within the site investigation programme for the transport properties of the rock. Final report. SKB P-07-179, Svensk Kärnbränslehantering AB.

Selroos J-O, Follin S, 2010. SR-Site groundwater flow modelling methodology, setup and results. SKB R-09-22, Svensk Kärnbränslehantering AB.

Selroos J-O, Painter S L, 2012. Effect of transport-pathway simplifications on projected releases of radionuclides from a nuclear waste repository (Sweden). Hydrogeology Journal 20, 1467–1481. https://doi.org/10.1007/s10040-012-0888-5

Selroos J-O, Cheng H, Painter S, Vidstrand P, 2013. Radionuclide transport during glacial cycles: Comparison of two approaches for representing flow transients. Physics and Chemistry of the Earth Parts A/B/C 64, 32–45. https://doi.org/10.1016/j.pce.2012.10.003

Selroos J-O, Mas Ivars D, Munier R, Hartley L, Libby S, Davy P, Darcel C, Trinchero P, 2022. Methodology for discrete fracture network modelling of the Forsmark site. Part 1 – concepts, data and interpretation methods. SKB R-20-11, Svensk Kärnbränslehantering AB.

Shahkarami P, 2017. Solute transport in fractured rocks. The effect of stagnant water zones and velocity dispersion. PhD thesis. Royal Institute of Technology (KTH), Stockholm, Sweden.

Shahkarami P, 2024. Verification of a model for calculating the dilute water penetration in fractured rock – a MATLAB implementation. SKB R-24-15, Svensk Kärnbränslehantering AB.

Shelton A, Sellin P, Missana T, Schäfer T, Červinka R, Koskinen K, 2018. Synthesis report: Colloids and related issues in the long term safety case. SKB TR-17-17, Svensk Kärnbränslehantering AB.

Sidborn M, Sandström B, Tullborg E-L, Salas J, Maia F, Delos A, Molinero J, Hallbeck L, Pedersen K, 2010. SR-Site: Oxygen ingress in the rock at Forsmark during a glacial cycle. SKB TR-10-57, Svensk Kärnbränslehantering AB.

Sidborn M, Marsic N, Crawford J, Joyce S, Hartley L, Idiart A, de Vries L M, Maia F, Molinero J, Svensson U, Vidstrand P, Alexander R, 2014. Potential alkaline conditions for deposition holes of a repository in Forsmark as a consequence of OPC grouting. Revised final report after review. SKB R-12-17, Svensk Kärnbränslehantering AB.

Siitari-Kauppi M, Lindberg A, Ikonen J, Kauppi L, 2010. Investigation of porosity and pore structure adjacent to fractures by PMMA method; samples taken from drill cores at Olkiluoto. Posiva Working Report 2010-66, Posiva Oy, Finland.

Silliman S E, 1989. An interpretation of the difference between aperture estimates derived from hydraulic and tracer tests in a single fracture. Water Resources Research 25, 2275–2283. https://doi.org/10.1029/WR025i010p02275

Skagius K, Neretnieks I, 1986. Diffusivity measurements and electrical resistivity measurements in rock samples under mechanical stress. Water Resources Research 22, 570–580. https://doi.org/10.1029/WR022i004p00570

SKB R-07-33. SKB 2007. Final repository facility. Underground design premises/D2. Svensk Kärnbränslehantering AB.

SKB R-24-01. SKB 2025. Baseline conditions of Forsmark prior to start of underground constructions. Baseline Forsmark. Svensk Kärnbränslehantering AB.

SKB TR-06-09. SKB 2006. Long-term safety for KBS-3 repositories at Forsmark and Laxemar – a first evaluation. Main Report of the SR-Can project. Svensk Kärnbränslehantering AB.

SKB TR-08-05. SKB 2008. Site description of Forsmark at completion of the site investigation phase. SDM-Site Forsmark. Svensk Kärnbränslehantering AB.

SKB TR-09-01. SKB 2009. Site description of Laxemar at completion of the site investigation phase. SDM-Site Laxemar. Svensk Kärnbränslehantering AB.

SKB TR-09-22. SKB 2009. Design premises for a KBS-3V repository based on results from the safety assessment SR-Can and some subsequent analyses. Svensk Kärnbränslehantering AB.

SKB TR-10-48. SKB 2010. Geosphere process report for the safety assessment SR-Site. Svensk Kärnbränslehantering AB.

SKB TR-10-50. SKB 2010. Radionuclide transport report for the safety assessment SR-Site. Svensk Kärnbränslehantering AB.

SKB TR-10-52. SKB 2010. Data report for the safety assessment SR-Site. Svensk Kärnbränslehantering AB.

SKB TR-11-01. SKB 2011. Long-term safety for the final repository for spent nuclear fuel at Forsmark. Main report of the SR-Site project. Svensk Kärnbränslehantering AB.

SKB TR-11-04. SKB 2013. Site description of the SFR area at Forsmark at completion of the site investigation phase. SDM-PSU Forsmark. Svensk Kärnbränslehantering AB.

SKB TR-14-01. SKB 2015. Safety analysis for SFR. Long-term safety. Main report for the safety assessment SR-PSU. Svensk Kärnbränslehantering AB.

SKB TR-14-05. SKB 2014. Geosphere process report for the safety assessment SR-PSU. Svensk Kärnbränslehantering AB.

SKB TR-14-09. SKB 2015. Radionuclide transport and dose calculations for the safety assessment SR-PSU. Revised edition. Svensk Kärnbränslehantering AB.

SKB TR-14-10. SKB 2014. Data report for the safety assessment SR-PSU. Svensk Kärnbränslehantering AB.

SKB TR-19-01. SKB 2019. Post-closure safety for a proposed repository concept for SFL. Main report for the safety evaluation SE-SFL. Svensk Kärnbränslehantering AB.

SKB TR-19-05. SKB 2019. Biosphere synthesis for the safety evaluation SE-SFL. Svensk Kärnbränslehantering AB.

SKB TR-19-06. SKB 2019. Radionuclide transport and dose calculations for the safety evaluation SE-SFL. Svensk Kärnbränslehantering AB.

SKB TR-21-01. SKB 2022. Post-closure safety for the final repository for spent nuclear fuel at Forsmark. Main report, PSAR version. Svensk Kärnbränslehantering AB.

SKB TR-21-03. SKB 2022. Post-closure safety for the final repository for spent nuclear fuel at Forsmark. Buffer, backfill and closure process report, PSAR version. Svensk Kärnbränslehantering AB.

SKB TR-21-04. SKB 2022. Post-closure safety for the final repository for spent nuclear fuel at Forsmark. Geosphere process report, PSAR version. Svensk Kärnbränslehantering AB.

SKB TR-21-06. SKB 2022. Post-closure safety for the final repository for spent nuclear fuel at Forsmark. Data report, PSAR version. Svensk Kärnbränslehantering AB.

SKB TR-21-07. SKB 2022. Post-closure safety for the final repository for spent nuclear fuel at Forsmark. Radionuclide transport report, PSAR version. Svensk Kärnbränslehantering AB.

SKB TR-23-01. SKB 2023. Post-closure safety for SFR, the final repository for short-lived radioactive waste at Forsmark. Main report, PSAR version. Svensk Kärnbränslehantering AB.

SKB TR-23-06. SKB 2023. Post-closure safety for SFR, the final repository for short-lived radioactive waste at Forsmark. Biosphere synthesis report, PSAR version. Svensk Kärnbränslehantering AB.

SKB TR-23-09. SKB 2023. Post-closure safety for SFR, the final repository for short-lived radioactive waste at Forsmark. Radionuclide transport and dose calculations, PSAR version. Svensk Kärnbränslehantering AB.

SKB TR-23-10. SKB 2023. Post-closure safety for SFR, the final repository for short-lived radioactive waste at Forsmark. Data report, PSAR version. Svensk Kärnbränslehantering AB.

Sposito G, 1981. Cation exchange in soils: an historical and theoretical perspective. In Dowdy R H, Ryan J A, Volk V V, Baker D E (eds). Chemistry in the soil environment. Madison, WI: American Society of Agronomy, 13–30.

Sposito G, 1989. The chemistry of soils. New York: Oxford University Press.

SSM, 2013. Begäran om komplettering av ansökan om slutförvaring av använt kärnbränsle och kärnavfall – Retardation av radionuklider. SSM2011-2426-110, Strålsäkerhetsmyndigheten (Swedish Radiation Safety Authority). (In Swedish.)

SSM, **2017**. SSM's external experts' review of SKB's safety assessment SR-PSU – dose assessment, K_d -values, and safety analysis methodology. Main review phase. SSM 2017:33, Strålsäkerhetsmyndigheten (Swedish Radiation Safety Authority).

SSM, **2018**. Strålsäkerhet efter slutförvarets förslutning. SSM 2018:07, Strålsäkerhetsmyndigheten (Swedish Radiation Safety Authority). (In Swedish.)

SSM, 2019. Granskningsrapport – Utbyggnad och fortsatt drift av SFR. SSM 2019:18, Strålsäkerhetsmyndigheten (Swedish Radiation Safety Authority). (In Swedish.)

Steefel C I, MacQuarrie K T, 1996. Approaches to modeling of reactive transport in porous media. This is chapter 2 of this book: Reviews in Mineralogy and Geochemistry 34, 85–129. https://doi.org/10.1515/9781501509797-005

Steefel C I, DePaolo D J, Lichtner P C, 2005. Reactive transport modeling: An essential tool and a new research approach for the Earth sciences. Earth and Planetary Science Letters 240, 539–558. https://doi.org/10.1016/j.epsl.2005.09.017

Stephens M B, Simeonov A, 2015. Description of deformation zone model version 2.3, Forsmark. SKB R-14-28, Svensk Kärnbränslehantering AB.

Stephens M B, Fox A, La Pointe P, Simeonov A, Isaksson H, Hermanson J, Öhman J, 2007. Geology Forsmark. Site descriptive modelling. Forsmark stage 2.2. SKB R-07-45, Svensk Kärnbränslehantering AB.

Stipp S L S, Eggleston C M, Nielsen B S, 1994. Calcite surface structure observed at microtopographic and molecular scales with atomic force microscopy (AFM). Geochimica et Cosmochimica Acta 58, 3023–3033. https://doi.org/10.1016/0016-7037(94)90176-7

Stipp S L S, Gutmannsbauer W, Lehmann T, 1996. The dynamic nature of calcite surfaces in air. American Mineralogist 81, 1–8. https://doi.org/10.2138/am-1996-1-201

Stockmann M, Schikora J, Becker D-A, Flügge J, Noseck U, Brendler V, 2017. Smart K_d -values, their uncertainties and sensitivities – Applying a new approach for realistic distribution coefficients in geochemical modeling of complex systems. Chemosphere 187, 277–285. https://doi.org/10.1016/j.chemosphere.2017.08.115

Stumm W, Morgan J J, 1996. Aquatic chemistry: chemical equilibria and rates in natural waters. 3rd ed. New York: Wiley Interscience.

Sudicky E A, Frind E, 1982. Contaminant transport in fractured porous media: Analytical solution for a system of parallel fractures. Water Resources Research 18, 1634–1642. https://doi.org/10.1029/WR018i006p01634

Svensson U, Kuylenstierna H-O, Ferry M, 2010. DarcyTools version 3.4 – Concepts, methods and equations. SKB R-07-38, Svensk Kärnbränslehantering AB.

Svensson U, Löfgren M, Trinchero P, Selroos J-O, 2018. Modelling the diffusion-available pore space of an unaltered granitic rock matrix using a micro-DFN approach. Journal of Hydrology 559, 182–191. https://doi.org/10.1016/j.jhydrol.2018.02.041

Sverjensky D A, 2003. Standard states for the activities of mineral surface sites and species. Geochimica et Cosmochimica Acta 67, 17–28. https://doi.org/10.1016/S0016-7037(02)01074-8

Söderlund M, Ervanne H, Muuri E, Lehto J, 2018. Sorption of alkaline earth metals on Olkiluoto bedrock biotite. Posiva Working Report 2017-41, Posiva Oy, Finland.

Söderlund M, Ervanne H, Muuri E, Lehto J, 2019. The sorption of alkaline earth metals on biotite. Geochemical Journal 53, 223–234. https://doi.org/10.2343/geochemj.2.0561

Tellinghuisen J, 2001. Statistical error propagation. Journal of Physical Chemistry A 105, 3917–3921. https://doi.org/10.1021/jp003484u

Torstenfelt B, Ittner T, Allard B, Andersson K, Olofsson U, 1982. Mobilities of radionuclides in fresh and fractured crystalline rock. SKBF/KBS TR 82-26, Svensk Kärnbränslehantering AB.

Tournassat C, Davis J A, Chiaberge C, Grangeon S, Bourg I C, 2016. Modeling the acid-base properties of montmorillonite edge surfaces. Environmental Science & Technology 50, 13436–13445. https://doi.org/10.1021/acs.est.6b04677

Trinchero P, Molinero J, Román-Ross G, 2014a. FASTREACT – A streamline-based approach for the solution of multicomponent reactive transport problems. SKB R-10-45, Svensk Kärnbränslehantering AB.

Trinchero P, Molinero J, Román-Ross G, Berglund S, Selroos J-O, 2014b. FASTREACT – An efficient numerical framework for the solution of reactive transport problems. Applied Geochemistry 49, 159-167. https://doi.org/10.1016/j.apgeochem.2014.04.004

Trinchero P, Painter S, Ebrahimi H, Koskinen L, Molinero J, Selroos J-O, 2016. Modelling radionuclide transport in fractured media with a dynamic update of *K*_d values. Computers & Geosciences 86, 55–63. https://doi.org/10.1016/j.cageo.2015.10.005

Trinchero P, Puigdomenech I, Molinero J, Ebrahimi H, Gylling B, Svensson U, Bosbach D, Deissmann G, 2017. Continuum-based DFN-consistent numerical framework for the simulation of oxygen infiltration into fractured crystalline rocks. Journal of Contaminant Hydrology 200, 60–69. http://doi.org/10.1016/j.jconhyd.2017.04.001

Trinchero P, Ebrahimi H, Colas E, Fernàndez-Garcia D, 2018a. Assessing nickel and molybdenum transport in the bedrock at SFL using a dynamic K_d approach. Report for the safety evaluation SE-SFL. SKB R-17-03, Svensk Kärnbränslehantering AB.

Trinchero P, Molinero J, Ebrahimi H, Puigdomenech I, Gylling B, Svensson U, Bosbach D, Deissmann G, 2018b. Simulating oxygen intrusion into highly heterogeneous fractured media using high performance computing. Mathematical Geosciences 50, 1–19. https://doi.org/10.1007/s11004-017-9718-6

Trinchero P, Sidborn M, Puigdomenech I, Svensson U, Ebrahimi H, Molinero J, Gylling B, Bosbach D, Deissmann G, 2019. Transport of oxygen into granitic rocks: Role of physical and mineralogical heterogeneity. Journal of Contaminant Hydrology 220, 108–118. https://doi.org/10.1016/j.jconhyd.2018.12.001

Trinchero P, Painter S L, Poteri A, Sanglas J, Cvetkovic V, Selroos J-O, 2020. A particle-based conditional sampling scheme for the simulation of transport in fractured rock with diffusion into stagnant water and rock matrix. Water Resources Research 56, e2019WR026958. https://doi.org/10.1029/2019WR026958

Trinchero P, Iraola A, Bruines P, Gylling B, 2021. Water-mineral reactions in a translated single realistic fracture: Consequences for contaminant uptake by matrix diffusion. Water Resources Research 57, e2021WR030442. https://doi.org/10.1029/2021WR030442

Trinchero P, Nardi A, Silva O, Bruch P, 2022. Simulating electrochemical migration and anion exclusion in porous and fractured media using PFLOTRAN^{NP}. Computers & Geosciences 166, 105166. https://doi.org/10.1016/j.cageo.2022.105166

Tsang C-F, Neretnieks I, 1998. Flow channeling in heterogeneous fractured rocks. Reviews of Geophysics 36, 275–298. https://doi.org/10.1029/97RG03319

Tsang Y W, 1992. Usage of "Equivalent apertures" for rock fractures as derived from hydraulic and tracer tests. Water Resources Research 28, 1451–1455. https://doi.org/10.1029/92WR00361

Turner D R, Pabalan R T, 1999. Abstraction of mechanistic sorption model results for performance assessment calculations at Yucca Mountain, Nevada. Waste Management 19, 375–388. https://doi.org/10.1016/S0956-053X(99)00198-1

Turner D R, Sassman S A, 1996. Approaches to sorption modeling for high-level waste performance assessment. Journal of Contaminant Hydrology 21, 311–332. https://doi.org/10.1016/0169-7722(95)00056-9

Vahlund F, Hermansson H, 2006. A direct numerical approach to solving the transport equations for radionuclide transport in fractured rock. SKB R-04-50, Svensk Kärnbränslehantering AB.

Vandergraaf T T, Abry D R M, 1982. Radionuclide sorption on drill core material from the Canadian Shield. Nuclear Technology 57, 399–412. https://doi.org/10.13182/NT82-A26306

Vilks P, 2007. Forsmark site investigation. Rock matrix permeability measurements on core samples from borehole KFM01D. SKB P-07-162, Svensk Kärnbränslehantering AB.

Vilks P, Miller N H, Stanchell F W, 2005. Laboratory program supporting SKB's Long Term Diffusion Experiment. Report 06819-REP-01300-10111-R00, Atomic Energy of Canada Limited.

Voutilainen M, Ikonen J, Sammaljärvi J, Siitari-Kauppi M, Lindberg A, Kuva J, Timonen J, Löfgren M, 2018. Investigation of rock matrix retention properties – Supporting laboratory studies II: Diffusion coefficient and permeability. Posiva Working Report 2017-39, Posiva Oy, Finland.

Voutilainen M, Miettinen A, Sardini P, Parkkonen J, Sammaljärvi J, Gylling B, Selroos J-O, Yli-Kaila M, Koskinen L, Siitari-Kauppi M, 2019. Characterization of spatial porosity and mineral distribution of crystalline rock using X-ray micro computed tomography, C-14-PMMA autoradiography and scanning electron microscopy. Applied Geochemistry 101, 50–61. https://doi.org/10.1016/j.apgeochem.2018.12.024

Voutilainen M, Sammaljärvi J, Ikonen J, Nenonen V, Kuva J, Siitari-Kauppi M, Lindberg A, 2022. Diffusivity and porosity of hydrogeological zones in ONK-PH8 and OL-KR25. Posiva Working Report 2022-10, Posiva Oy, Finland.

Waber H N, Smellie J A T, 2008. Characterisation of pore water in crystalline rocks. Applied Geochemistry 23, 1834–1861. https://doi.org/10.1016/j.apgeochem.2008.02.007

Waber H N, Smellie J A T, 2012. Forsmark site characterisation. Borehole KFM22 and KFM23: Derivation of porewater data by diffusion experiments. SKB P-12-18, Svensk Kärnbränslehantering AB.

Waber H N, Gimmi T, Smellie J A T, 2009. Porewater in the rock matrix. Site descriptive modelling SDM-Site Forsmark. SKB R-08-105, Svensk Kärnbränslehantering AB.

Waber H N, Gimmi T, Smellie J A T, 2011. Effects of drilling and stress release on transport properties and porewater chemistry of crystalline rocks. Journal of Hydrology 405, 316–332. https://doi.org/10.1016/j.jhydrol.2011.05.029

Wang F, Chen J, Forsling W, 1997. Modeling sorption of trace metals on natural sediments by surface complexation model. Environmental Science & Technology 31, 448–453. https://doi.org/10.1021/es960270a

Wang Z, Giammar D E, 2013. Mass action expressions for bidentate adsorption in surface complexation modeling: Theory and practice. Environmental Science & Technology 47, 3982–3996. https://doi.org/10.1021/es305180e

Watanabe N, Hirano N, Tsuchiya N, 2009. Diversity of channeling flow in heterogeneous aperture distribution inferred from integrated experimental-numerical analysis on flow through shear fracture in granite. Journal of Geophysical Research 114, B04208. https://doi.org/10.1029/2008JB005959

Weber J, 2017. Fundamental insights into the radium uptake into barite by atom probe tomography and electron microscopy. PhD thesis. RWTH Aachen University, Germany.

Westall J C, 1994. Modeling of the association of metal ions with heterogeneous environmental sorbents. MRS Online Proceedings Library 353, 937–950. https://doi.org/10.1557/PROC-353-937

Widestrand H, Byegård J, Ohlsson Y, Tullborg E-L, 2003. Strategy for the use of laboratory methods in the site investigations programme for the transport properties of the rock. SKB R-03-20, Svensk Kärnbränslehantering AB.

Widestrand H, Byegård J, Cvetkovic V, Tullborg E-L, Winberg A, Andersson P, Siitari-Kauppi M, 2007. Sorbing tracer experiments in a crystalline rock fracture at Äspö (Sweden): 1. Experimental setup and microscale characterization of retention properties, Water Resources Research 43, W10413. https://doi.org/10.1029/2006WR005277

Widestrand H, Byegård J, Selnert E, Skålberg M, Höglund S, Gustafsson E, 2010a. Long Term Sorption Diffusion Experiment (LTDE-SD). Supporting laboratory program – Sorption diffusion experiments and rock material characterisation. With supplement of adsorption studies on intact rock samples from the Forsmark and Laxemar site investigations SKB R-10-66, Svensk Kärnbränslehantering AB.

Widestrand H, Byegård J, Nilsson K, Höglund S, Gustafsson E, Kronberg M, 2010b. Long Term Sorption Diffusion Experiment (LTDE-SD). Performance of main *in situ* experiment and results from water phase measurements. SKB R-10-67, Svensk Kärnbränslehantering AB

Williams T, Sanglas J, Trinchero P, Gai G, Painter S L, Selroos J-O, 2021. Recovering the effects of subgrid heterogeneity in simulations of radionuclide transport through fractured media. Frontiers in Earth Science 8, 586247. https://doi.org/10.3389/feart.2020.586247

Willmann M, Carrera J, Sanchez-Vila X, Silva O, Dentz M, 2010. Coupling of mass transfer and reactive transport for nonlinear reactions in heterogeneous media. Water Resources Research 46, W07512. https://doi.org/10.1029/2009WR007739

Witherspoon P A, Wang J S Y, Iwai K, Gale J E, 1980. Validity of cubic law for fluid flow in a deformable rock fracture. Water Resources Research 16, 1016–1024. https://doi.org/10.1029/WR016i006p01016

Wold S, 2010. Sorption of prioritized elements on montmorillonite colloids and their potential to transport radionuclides. SKB TR-10-20, Svensk Kärnbränslehantering AB.

Yamashita R, Kimura H, 1990. Particle-tracking technique for nuclide decay chain transport in fractured porous media. Journal of Nuclear Science and Technology 27, 1041–1049. https://doi.org/10.1080/18811248.1990.9731289

Zavarin M, Roberts S K, Hakem N, Sawvel A M, Kersting A B, 2005. Eu(III), Sm(III), Np(V), Pu(V), and Pu(IV) sorption to calcite. Radiochimica Acta 93, 93–102. https://doi.org/10.1524/ract.93.2.93.59413

Öhman J, Odén M, 2018. SR-PSU (PSAR) Bedrock hydrogeology. TD18 – Temperate climate conditions. SKB P-18-02, Svensk Kärnbränslehantering AB.

Appendix A Derivation of transfer factors

A.1 Formulation for surface complexing solutes

In the present work, it is assumed that radionuclides that sorb by way of a surface complexation mechanism can be modelled using the following generalised reaction template (Lützenkirchen et al. 2015):

$$\alpha(>SOH) + M^{z+} + wH_2O \rightleftharpoons (>SO)_n M(OH)_w^{z-w} + (\alpha + w)H^+$$
 (A-1)

Here, it is assumed that sorption occurs by way of an inner-sphere surface complexation mechanism localised to the Stern layer. Although outer-sphere surface complexation can be treated in the same framework, this is neglected in the present derivation to simplify discussions.

The mass action equation for the sorbed surface species, k out of n_s possible sorption reactions can be written as:

$$K_{s(k)}^{int} = \frac{X_{s(k)} \cdot a_{H^{+}}^{n+\alpha}}{X_{soH}^{n} \cdot a_{M^{Z^{+}}}} \cdot E_{k}(y_{o})$$
(A-2)

where a_i represents the activity of aqueous species, i in the reaction, $X_{s(k)}$ is the mole fraction of surface complex k, and n is the denticity of the reaction. In this work, we adopt the convention of surface coverage fractions and treat formation of multidentate surface complexes as a reaction between separate hydroxyl ligands as described by Wang and Giammar (2013) which is the same as in the PHREEQC program (Parkhurst and Appelo 2013). In the present modelling framework, only monodentate and bidentate reactions are considered although the description is readily applicable to higher denticities if necessary. The electrostatic correction term, $E_k(y_0)$ is given by the customary Boltzmann factor (Parkhurst and Appelo 1999):

$$E_k(y_o) = \exp(\Delta z_{s(k)} y_o)$$
 where $y_o = \frac{F\Psi_o}{RT}$ (A-3)

Here, F is the Faraday constant, R is the universal gas constant, T is absolute temperature, and Ψ_o is the electric potential at the surface. The term $\Delta z_{s(k)}$ is equal to the net change in surface charge resulting from the surface complexation reaction k.

Hydroxyl groups (>SOH) at the mineral surfaces undergo protonation-deprotonation reactions, which in the 2-pK formalism (e.g. Lützenkirchen 1998) can be written as:

$$>SOH + H^+ \rightleftharpoons >SOH_2^+ \qquad \log_{10} K_{>SOH_2^+} = pK_{a1}$$
 (A-4)

$$>$$
SOH $\rightleftharpoons >$ SO⁻ + H⁺ $\log_{10} K_{>SO^-} = -pK_{a2}$ (A-5)

The mass action equations for the protonation-deprotonation equilibria can be written as:

$$K_{>SOH_2^+} = \frac{X_{>SOH_2^+}}{X_{>SOH} \cdot a_{H^+}} \cdot \exp(y_0)$$
 (A-6)

$$K_{>SO^{-}} = \frac{X_{>SO^{-}} \cdot a_{H^{+}}}{X_{>SOH}} \cdot \exp(-y_{o})$$
 (A-7)

The concentration (mol/l) of the surface sorbed species, k can then be given as:

$$c_{s(k)} = X_{s(k)} \cdot N_s = K_{s(k)}^{int} \cdot \left(\frac{X_{>SOH}^n \cdot a_{M}^{z+}}{a_{H}^{n+\alpha}}\right) \cdot E_k(y_o) \cdot N_s$$
(A-8)

or, more generally in the form:

$$c_{s(k)}^{M} = X_{s(k)} \cdot N_{s} = K_{s(k)}^{int} \cdot E_{k}(y_{o}) \cdot (X_{>SOH}^{n} \cdot N_{s}) \cdot \prod_{i=1}^{n_{c}} a_{i}^{\nu_{(k,i)}}$$
(A-9)

where $v_{(k,i)}$ is the stoichiometric coefficient of aqueous component, i with activity, a_i in surface complexation reaction, k. The mole fraction activities of all surface species associated with a given site type must sum to unity, thus:

$$1 = (X_{>SOH} + X_{>SOH_2^+} + X_{>SO^-}) + \sum_{k=1}^{n_s} X_{s(k)}$$
(A-10)

If the concentration of sorbed species is very low relative to the total concentration of binding sites, the mole fraction of un-reacted binding sites, $X_{>SOH}$ can be given to a good approximation as:

$$X_{>SOH} \approx \frac{1}{1 + K_{>SOH_{2}^{+}} \cdot 10^{-\text{pH}} \cdot \exp(y_{o}) + \frac{K_{>SO^{-}}}{10^{-\text{pH}}} \cdot \exp(-y_{o})}$$
 (A-11)

The total binding site concentration, $N_{s(j)}$ (mol/l) for a given site type, j is defined as:

$$S_{tot(j)} = \left(\frac{10^{18}}{N_a} \cdot \frac{m_j}{V}\right) \cdot \Gamma_{s(j)} \cdot A_{s(j)}$$
(A-12)

where Γ_s (sites/nm²) is the site density, N_a is Avogadro's number (6.022 × 10²³), $A_{s(j)}$ (m²/g) is the specific surface area of reactive sites in contact with the aqueous phase, and V/m_j (l/g) is the liquid to solid ratio for the mineral phase associated with site type j. The factor of 10¹⁸ in the numerator accounts for the conversion of site density in units of sites/nm² to sites/m².

For a sorption process involving k surface reactions with possibly differing denticity associated with each site type j, the surface area normalised sorption partitioning coefficient, K_A (m) for site type j can be written as:

$$K_{A(j)} = \frac{N_{s(j)} \sum_{k=1}^{n_{s(j)}} X_{s(j,k)}}{c_w} \cdot \frac{1}{A_{s(j)}} \cdot \frac{V}{m_j}$$
(A-13)

where c_w (mol/l) is the total concentration of the sorbing solute in the aqueous phase. Equation A-13 can be written out more fully as:

$$K_{A(j)} = \left(\frac{10^{18}}{N_o}\right) \cdot \Gamma_{S(j)} \cdot \frac{\sum_{k=1}^{n_S(j)} K_{S(j,k)}^{int} \cdot E_{(j,k)}(y_o) \cdot X_{>SOH(j)}^{n(j,k)} \cdot \prod_{i=1}^{n_c} a_{\xi}^{v_{k(j,i)}}}{c_w}$$
(A-14)

If there are n_m site types associated with multiple minerals in the rock matrix, the bulk K_A (m) for the rock can be calculated as the weighted sum of contributions from individual surfaces:

$$K_a = \sum_{i=1}^{n_m} \theta_i K_{a(i)} \tag{A-15}$$

where θ_j is the accessible surface area fraction for site type j:

$$\theta_i = A_{s(i)}/A_{tot} \tag{A-16}$$

Here, it should be noted that there may be more than one site type associated with a given mineral phase. In some surface complexation models (e.g. Dzombak and Morel 1990, Bradbury and Baeyens 2005a), for example, non-linear sorption effects are captured by combining a small population of sites featuring strong sorption (low sorption capacity) together with a larger population of weakly sorbing sites (high sorption capacity). This is not problematic for the present analysis provided the contributing surface area fractions of each site type can be assigned based on measurement data or mechanistic reasoning.

The average K_d (m³/kg) for the rock is:

$$K_d = A_{tot} \sum_{j=1}^{n_m} \theta_j K_{a(j)}$$
(A-17)

Thus far the analysis is not specific to any particular representation of the electrical double layer and may be considered general for whichever surface complexation model sub-type is being considered. A full discussion of the various assumptions in the different modelling approaches is beyond the scope of this Appendix, although good overviews of the various approaches may be found in, e.g. Dzombak and Morel (1990), Hayes et al. (1991), Goldberg and Criscenti (2007), Righetto et al. (1995) and Brendler et al. (2004). The principal difference between the different models is largely related to the conceptualisation of the electrical double layer, the localisation of interacting species at different planes within it, and thus the magnitude of corrections required to account for electrostatic effects on the mass action equations describing sorption reactions.

For inner-sphere surface complexation, specific adsorption is posited to occur within the Stern layer at the solid-water interface. The Stern layer contains the surface reactive groups and specifically adsorbed ions that are in close contact with the mineral surface and is only a few angstroms (2-10 Å) thick depending on the properties of the mineral surface, the electrolyte solution it is in contact with, and ions undergoing sorption. The Stern layer is usually conceptualised as consisting

of two layers; the inner Helmholtz plane (IHP) being the plane of adsorption of inner-sphere surface complexes, and the outer Helmholtz plane (OHP) which is the distance of closest approach of solvated cations featuring a hydration sphere. The outer boundary of the Stern layer is usually considered to reside at the outer the outer Helmholtz plane.

In the diffuse double layer model (DLM), the diffuse layer is assumed to extend all the way to the mineral surface and outer-sphere surface complexes are neglected. In the diffuse layer, ions are not specifically adsorbed but are electrostatically influenced by the charge on the surface. Ions with charge of the same sign as the net surface charge are repelled from the surface, whereas ions of opposite charge are attracted to the surface. This leads to a potential gradient extending into the water. The impact this has on the mass action equation for adsorption equilibrium is corrected for using the electrostatic Boltzmann factor.

In the implementation of the DLM model in PHREEQC (Parkhurst and Appelo 2013), the relation between the diffuse layer charge, σ_d (C/m²) and potential Ψ_s (V) is given by the general expression

$$\sigma_d = \pm (2 \times 10^3 \varepsilon RT)^{\frac{1}{2}} \cdot \left(\sum_{\xi=1}^{n_c} c_{\xi} \left(exp \left(-z_{\xi} \frac{F \Psi_d}{RT} \right) - 1 \right) \right)^{\frac{1}{2}}$$
(A-18)

where

$$\sigma_o = \frac{FN_s}{A_s m} \left(X_{>SOH_2^+} - X_{>SO^-} + \sum_{k=1}^{n_s} z_k X_{s(k)} \right)$$

$$\sigma_o + \sigma_d = 0 \qquad (A-20)$$

In Equation A-18, $\varepsilon(-)$ is the dielectric constant of water, c_i (mol/l) is the concentration of dissolved species i in the bulk solution, and z_i (–) is its charge. For the expression in Equation A-19, the variables have their previously established definitions while z_k (–) is the charge of surface species k. In principle, the DLM has three adjustable parameters for the 2-p K_a surface charge model consisting of the protonation-deprotonation constants and site density (i.e. p K_{a1} , p K_{a2} , Γ_s). This can be reduced to 2 parameters if a 1-p K_a description of protonation-deprotonation is used, although typically at the penalty of a less-good fit to measurement data (Lützenkirchen 1998).

The constant capacitance model (CCM) is approximate for low surface potentials and higher ionic strengths (I > 0.01 M) where the thickness of the electrical double layer is negligible. In this model, an additional parameter is introduced in the form of a capacitance to relate the approximately linear variation of charge and potential over the thickness of the Stern layer resulting in four adjustable parameters in the 2-p K_a case.

In the non-electrostatic model (NEM), the electrostatic correction is neglected entirely (i.e. $\Psi_s \approx 0$) implying that the intrinsic binding constants are typically interpreted as apparent constants rather than true thermodynamic quantities. This also means that the intrinsic binding constants are only strictly applicable for the ionic strength and bulk ion composition used in laboratory experiments. Although electrostatic corrections are neglected, the model still essentially has the same number of adjustable parameters as the DLM.

For phyllosilicates such as montmorillonite and illite, however, the NEM has been successfully used to model sorption (Bradbury and Baeyens 2005a, b, 2009a, b) since the customary Boltzmann factor for a flat planar surface incorrectly predicts the corrections required for the electrostatic potential at phyllosilicate edge sites. This is due to a combination of factors including the difficulty in quantifying reactive surface areas and binding site densities of edge sites, difficulties in obtaining unambiguous protonation-deprotonation constants, as well as the inability of Equation A-3 to properly capture spillover of permanent electrostatic charge from negatively charge basal planes to edge sites (see, e.g. Bourg et al. 2007).

Although Tournassat et al. (2016) have recently implemented a modification in PHREEQC to enable more accurate calculation of electrostatics at edges of single phyllosilicate platelets (based on the earlier work by Delhorme et al. 2010 and Bourg et al. 2007), this capability is yet to be included in the official release version of the code. In the work by Bradbury and Baeyens (2005a, b, 2009a, b), however, the NEM was found to adequately describe surface charging behaviour to an acceptable degree of accuracy over a range of ionic strengths from 0.01 to 0.5 M for modelling uptake of transition metal, lanthanide, and heavy metal cations.

In the standard triple layer model (TLM), an additional layer is added between the inner- and outer-Helmholtz planes in order to limit the concentration of ions near the surface (Bickmore et al. 2006) and permit the inclusion of outer-sphere surface complexes formed by the non-specific sorption (electrostatic interaction) of background electrolyte ions with charged surface groups. The inner and outer-Helmholtz planes are often referred to as the β - and d-planes in the literature. The non-specifically sorbed ions (outer-sphere complexes) are assumed to be sorbed in the layer between the inner- and outer Helmholtz planes, although they are assigned to the β -plane in the formal mathematical description of sorption while protonation-deprotonation and specific sorption reactions (inner-sphere complexes) occur at the o-plane. The binding constants for the outer-sphere reactions also require correction for electrostatic effects using a Boltzmann correction factor although evaluated at the potential of the β -plane.

The inclusion of non-specific sorption of electrolyte ions permits accurate modelling of sorption over a wider range of ionic strengths than the DLM or CC models. The triple layer model introduces additional parameters including capacitances of the o-plane and β -plane plus intrinsic binding constants of electrolyte ions as outer sphere complexes on the β -plane. This model contains at least 7 adjustable parameters including the protonation-deprotonation constants, site density, cation and anion electrolyte binding constants, as well as two capacitances (one each for the o- and β -planes).

A simplified version of the TLM, referred to as the Basic Stern model (BSM) neglects the potential drop between the inner- and outer-Helmholtz planes by assuming an infinitely large capacitance (the β -plane and d-plane are effectively coplanar in this model formulation). In this model version both protonation-deprotonation reactions and inner-sphere surface complexation reactions are posited to occur at the o-plane, while outer-sphere surface complexation reactions occur at the β -plane. The BSM is simpler than the TLM as it requires one less adjustable parameter, although it has been less widely adopted for modelling sorption of trace solutes with some notable exceptions (e.g. Britz 2018). It is considered more physically realistic than the DLM since the infinitely close approach of ions to the surface (ions are modelled as point charges) in the DLM is not physically reasonable and overestimates electrostatic corrections.

A far more comprehensive modelling approach is contained in the CD-MUSIC modelling framework (Hiemstra and van Riemsdijk 1996) where the surface complexes are considered to have a spatial distribution of charge within the electrical double layer structure. The model considers the fact that different hydrated and non-hydrated ions have different sizes and approach the mineral surface to different distances of closest approach. To account for this, fractional charge is assigned to the different planes of the electrical double layer. The model is essentially a TLM, however, it requires additional adjustable parameters relating to the distribution of charge over the o-plane and β -plane for ions interacting with the charged surface.

The Stern-layer capacitance is also treated as an adjustable parameter because the dielectric properties of water near the mineral surface deviate from the bulk owing to the preferred orientation of water-molecule dipoles at the interface. Although some of the model parameters can be optimised to fit macroscopic measurement data, the non-uniqueness of the model parameterisation means that many of the model parameter values need to be estimated using *ab initio* molecular dynamics simulations based on careful consideration of crystal structure and bond valences related to the coordination environment of sorbing species and surface reactive groups.

In the following discussions, we assume that the surface complexation reactions are defined according to the constant capacitance (CCM), diffuse layer (DLM) or non-electrostatic model (NEM) formulations, although the analysis can likely be expanded to the more comprehensive TLM-based surface complexation model sub-types if required. The focus is mostly on models which can be readily implemented in PHREEQC as this is the code of choice for hydrogeochemical calculations made within the present work due to its versatility and ease of coupling with external scripts in Python or Matlab.

PHREEQC has the capability of simulating DLM, NEM, and CD-MUSIC based sorption models. The CCM model is also available in the code and can be readily implemented, although it is undocumented in the user manual. The BSM model can be simulated in PHREEQC by assigning a large capacitance to the β -layer (e.g. Heberling et al. 2011, Britz 2018), although care must be taken to ensure that ionic charge is assigned to the correct plane in the model. The TPM implemented in

PHREEQC for CD-MUSIC is different from the standard TLM since charge can be specified for the d-plane which is not included in the standard TLM.

Although the triple plane-based models including CD-MUSIC have been proven very successful at reproducing experimental data over a broad range of experimental conditions, the need for multiple additional adjustable parameters and the risk of non-unique parameterisation means that they are difficult to apply to complex mineral assemblages in a consistent manner. For this reason, applications rooted in safety assessment have tended to favour the simpler DLM, NEM, and CCM approaches (e.g. Turner and Sassman 1996, Turner and Pabalan 1999, OECD/NEA 2012).

For some mineral surfaces, linear free energy relations (LFERs) have been described which can be used to correlate surface complexation binding constants and analogous hydrolysis reactions in the aqueous phase. It is noted that most LFERs reported in the literature have been developed for the DLM (Dzombak and Morel 1990, Mathur and Dzombak 2006), NEM (Bradbury and Baeyens 2005a, b, 2009a, b), and CCM (Schindler et al. 1976).

If there exists a unique LFER for each binding site type, j we would have:

$$\log_{10} K_{s(j,k)}^{\text{int}} = b_j + m_j \cdot \log_{10} K_{OH(k)}^{M^{z+}}$$
(A-21)

where b_j and m_j are, respectively, the intercept and slope of the linear regression relating the log binding constant, $\log_{10} K_{s(j,k)}^{int}$ for a specified surface complexation reaction k on site type j and $\log_{10} K_{OH(k)}^{M^{Z+}}$ is the log hydrolysis constant for the analogous aqueous phase hydrolysis reaction. LFERs are useful for estimating binding constants for radioelements which have not been studied experimentally. In general, the magnitude of the intrinsic binding constant $K_{s(j,k)}^{int}$ is dependent on the site density assumed in the fitted surface complexation model. Based on work by Kulik (2002, 2006) and Sverjensky (2003), normalisation formula for conversion of binding constants between different reference site densities can be given as:

$$\log_{10} K_0^{\text{int}} = \log_{10} K_{\text{exp}}^{\text{int}} + n \cdot \log_{10} \left(\Gamma_{\text{exp}} / \Gamma_0 \right)$$
(A-22)

where n is the denticity of the reaction, K_{exp}^{int} is the intrinsic binding constant determined for the surface complexation reaction at a given site density, Γ_{exp} measured (or, more typically assumed) in a laboratory experiment and K_0^{int} is the intrinsic binding constant for a different reference site density, Γ_0 . The conversion formula given by Equation A-22 is necessary since site densities are highly uncertain and strongly affect the magnitude and uncertainty of reported binding constants.

If data from different experiments are to be combined, it is necessary to be able to convert between different standard states to obtain an internally consistent description of sorption for a given mineral surface. When the denticity of the surface complexation reactions is identical for all surface reactions comprising the LFER, a change in the reference site density should only affect the intercept, b_i of the regression curve under the transformation implied by Equation A-22.

One of the interesting aspects of the LFER relationship given in Equation A-21 is that it seeks to separate intrinsic binding constants to a material specific contribution (the intercept, b_j) which is independent of the identity of the sorbing solute and a contribution related to intrinsic chemical properties of the sorbing solute (the product of the slope, m_j and $\log_{10} K_{OH(k)}^{M^{z+}}$).

Although all LFERs described in the literature (to the best knowledge of the author) are defined for monodentate surface complexation reactions only, it is noted that the data reported by Schindler et al. (1976) representing a mix of monodentate and bidentate reactions on fumed silica can be described with a single LFER. For bidentate reactions, however, the binding constants are paired with second hydrolysis constants to distinguish them from the monodentate reactions. It is not clear whether this generalises to other geological materials as there appears to be insufficient data to test this hypothesis.

Groundwater composition has a large impact on the magnitude of K_d values estimated from measurement data and frequently dominates over other factors. This occurs principally by way of speciation effects where dissolved ions are complexed by different ligands causing competition effects with surface binding reactions. The electrolyte composition also has an impact on activities

of dissolved solutes and thus the apparent equilibrium constant of sorption reactions. These issues are of particular importance when using an SCM calibrated against a given solution composition to extrapolate to different chemical conditions and ionic strengths. In the RES³T database (Brendler et al. 2003), for example, the Davies equation is used to extrapolate intrinsic binding constants from the ionic strength of solutions used in measurements to zero ionic strength as is standard practice in solution chemistry (see, e.g. OECD/NEA 2020). This has the potential to affect predictions made with CCM or NEM based models since fitted parameters (including capacitance for the CCM) are typically conditional to the ionic strength used in experiments and extrapolation to zero ionic strength may introduce significant inconsistencies and unquantified prediction errors.

Often it is arguably better to use identical equilibrium constants (including hydrolysis, protonation-deprotonation, and metal surface complexation reactions) to original authors and treat any extrapolation to differing chemical conditions with suspicion. Even then, additional aqueous-speciation reactions in the selected thermodynamic database can remain inconsistent with the SCM parameterisation. Although refitting the model with updated thermodynamic data is sometimes feasible, it is not always practical. Therefore, predictions made outside the model's calibration domain should be treated carefully, even when the model is well documented and supported by high-quality measurements.

Extrapolation to differing groundwater composition for constant mineralogy

If we have made an experiment at a given reference water composition, i where the contributions from individual minerals can be estimated by radiographic techniques (e.g. Fabritius et al. 2024), then the reactive surface area fractions, θ_i and intrinsic $K_{a(i,j)}$ values for the reference groundwater composition can be readily calculated for a component additivity model. Say we have two groundwater compositions (1) and (2) where composition (1) is the "anchor" for which we have a K_d measurement and composition (2) is the one for which we would like to estimate a K_d value. For a system with two mineral surfaces, we can now write:

$$\bar{K}_{a(1,a)} = K_{a(1,1)}\theta_{(1,a)} + K_{a(1,2)}\theta_{(2,a)} \tag{A-23}$$

$$\bar{K}_{a(2,a)} = K_{a(2,1)}\theta_{(1,a)} + K_{a(2,2)}\theta_{(2,a)} \tag{A-24}$$

Here it is implicitly assumed that the rock samples referred to by equations A-23 and A-24 are identical (thus the subscript index "a" in parentheses representing the same sample, only with differing water composition, i). Taking the ratio of equations A-24 and A-23 allows us to write the chemistry transfer factor, f_{chem} as:

$$f_{\text{chem}} = \frac{\bar{K}_{a(2,a)}}{\bar{K}_{a(1,a)}} = \frac{K_{a(2,1)}\theta_{(1,a)} + K_{a(2,2)}\theta_{(2,a)}}{K_{a(1,1)}\theta_{(1,a)} + K_{a(1,2)}\theta_{(2,a)}}$$
(A-25)

which can also be written as:

$$f_{\text{chem}} = \frac{\bar{K}_{a(2)}}{\bar{K}_{a(1)}} = \frac{\frac{K_{a(2,1)}}{K_{a(1,1)}} K_{a(1,1)} \theta_{(1,a)}}{K_{a(1,1)} \theta_{(1,a)} + K_{a(1,2)} \theta_{(2,a)}} + \frac{\frac{K_{a(2,2)}}{K_{a(1,2)}} K_{a(1,2)} \theta_{(2,a)}}{K_{a(1,1)} \theta_{(1,a)} + K_{a(1,2)} \theta_{(2,a)}}$$
(A-26)

which simplifies to the expression:

$$f_{\text{chem}} = \frac{\bar{K}_{a(2)}}{\bar{K}_{a(1)}} = f_{r(1,1)} \cdot \frac{K_{a(2,1)}}{K_{a(1,1)}} + f_{r(1,2)} \cdot \frac{K_{a(2,2)}}{K_{a(1,2)}}$$
(A-27)

where the variable $f_{r(1,j)}$ represents the sorbed fraction associated with site type j at the reference groundwater composition:

$$f_{r(1,j)} = \frac{K_{a(1,j)}\theta_j}{\sum_{\xi=1}^{n_m} K_{a(1,\xi)}\theta_\xi} = \frac{K_{a(1,j)}\theta_j}{\bar{K}_{a(1)}} = \frac{a_{(1,j)}}{\sum_{\xi=1}^{n_m} a_{(1,\xi)}}$$
(A-28)

Here, the symbol $a_{(1,j)}$ is used to represent the adsorbed activity of the radionuclide on surface j in contact with the reference groundwater composition labelled "1". If, instead of direct measurements of the sorbed fractions of solute on each site type, we have an estimate of the relative surface-area normalised sorptivity of each mineral at a given groundwater composition, we can write:

$$f_{r(1,j)} = \frac{R_{s(1,j)}\theta_j}{\sum_{\xi=1}^{n_m} R_{s(1,j)}\theta_{\xi}}$$
 (A-29)

Here, it is necessary to introduce an index mineral that is assigned a relative sorptivity of unity such that the sorptivity of all other contributing minerals can be related to it. As an example, we might choose feldspar as the index mineral with an $R_{s(Fs)} = 1$. If biotite sorbs 10 times as strongly as feldspar on a surface area normalised basis, we would then have $R_{s(Bi)} = 10$. It does not matter which mineral is chosen, provided it is used consistently throughout the calculation. It should be noted that this treatment implicitly assumes both a direct impact of differing solution chemistry on surface speciation as well as an indirect impact on sorptivity from aqueous phase reactions between the sorbing solute and dissolved ligands.

Equation A-27 can be easily generalised to a system comprised of n_m separate mineral surfaces, or site types:

$$f_{chem} = \frac{\bar{K}_{d(2)}}{\bar{K}_{d(1)}} = \frac{\bar{K}_{a(2)}}{\bar{K}_{a(1)}} = \sum_{j=1}^{n_m} f_{r(1,j)} \cdot f_{c(j)}$$
(A-30)

where

$$f_{c(j)} = \frac{K_{a(2,j)}}{K_{a(1,j)}} \tag{A-31}$$

Since the bulk surface area is the same for both groundwater compositions, the ratio of K_d and K_a values is the same in this case. As can be seen from the form of Equation A-30, it is not strictly necessary to estimate the θ_j values for individual mineral surfaces if the relative sorbed fractions of the radionuclide on each mineral surface can be estimated using radiographic measurements for the reference groundwater composition. A potential complication, however, arises where there are multiple binding site types associated with a given mineral that cannot be directly quantified by macroscopic measurements. An example here would be the strong and weak sites invoked in sorption modelling to capture non-linear, Langmuirian saturation effects at low concentrations. Equation A-30 can, in principle, be extended to an arbitrary number of binding sites for each mineral surface provided the relative fraction of each binding site can be estimated independently.

If contributions to sorptivity cannot be estimated from independent radiographic measurements, another possibility is to assume that the reactive surface area contributions are roughly proportional to the volume fractions of the minerals in the rock matrix and their individual specific surface areas:

$$\theta_j \approx f_S \cdot \frac{\rho_j \phi_j A_{S(j)}}{\rho_b A_{\text{tot}}}$$
 (A-32)

where ρ_j (kg/m³) is the density of the mineral, ρ_b (kg/m³) is the bulk density of the sample, ϕ_j (m³/m³) is the volume fraction, $A_{s(j)}$ (m²/kg) is the specific surface area of the mineral, and A_{tot} (m²/kg) is the total surface area (determined by for example BET). The f_s variable is a dimensionless normalisation factor used to empirically adjust for differences between estimated surface areas of individual minerals and that of the bulk sample. The relationship expressed in Equation A-32 is basically the same as that assumed in the conventional component additivity approach as described in OECD/NEA (2012).

Since reactive surface area cannot be estimated in any simple fashion, it is customary to use BET surface area of crushed minerals as a proxy measurement. Calculating reactive surface area contributions in this manner, however, suffers from the disadvantage that BET surface areas measured for crushed samples of pristine minerals may not be representative of the true reactive surface area in the rock matrix due to differing grain sizes, crushing damage, and occlusion of surfaces due to abutting minerals in non-decompacted samples.

Since the volume-fraction weighted sum of BET surface areas of constituent minerals may not exactly match the measured BET surface area of rock samples used in the laboratory, the normalisation factor f_s is introduced to ensure that the weighted surface area contributions of individual minerals match the measured BET surface area of the bulk sample:

$$f_s = \frac{\rho_b A_{\text{tot}}}{\sum_{i=1}^{n_m} \rho_j \phi_j A_{s(j)}}$$
(A-33)

Thin sections used in radiographic measurements may not be representative of the intact rock if significant damage occurs during sample cutting and polishing. There may also be differences between the representative pore spaces enclosed by minerals in a 3D sample relative to the 2D slice plane sampled in a thin section which renders it non-representative. Recent work by Demnitz et al.

(2022a, b) using vertical scanning interferometry techniques has demonstrated that it is feasible to quantify surface roughness on the scale of individual mineral grains at the surface of thin sections, thus permitting quantification of the role of surface roughness on sorption.

To extrapolate this information to the micro-surfaces in contact with water within the rock matrix would, however, require statistical estimation of roughness of grain boundaries in the rock matrix, techniques for which remain to be developed and require further study. In the absence of a suitable means of accounting for such features of the data, sensitivity studies will need to be conducted to ascertain the impact of this uncertainty in the component additivity framework.

Extrapolation to differing mineralogy at a fixed groundwater composition

Here, it is assumed that we have an experiment involving measurement of K_d for two different samples ("a" and "b") although using the same contact water composition including the same concentration of sorbing radionuclide. The rock samples may be of the same rock type although have differing mineralogy, surface area, etc. Returning to the two mineral surface example as given previously, the K_d value can be written out for two differing mineral compositions (here, denoted a and b) as:

$$\frac{\bar{K}_{d(1,a)}}{A_{\text{tot},a}} = K_{a(1,1)}\theta_{(1,a)} + K_{a(1,2)}\theta_{(2,a)} \tag{A-34}$$

$$\frac{\bar{K}_{d(1,b)}}{A_{\text{tot},b}} = K_{a(1,1)}\theta_{(1,b)} + K_{a(1,2)}\theta_{(2,b)} \tag{A-35}$$

We now define the surface area transfer factor, f_m as:

$$f_m = \frac{A_{\text{tot},b}}{A_{\text{tot},a}} \tag{A-36}$$

and a component-wise mineralogy transfer factor, $f_{q(j)}$ for each mineral/site type j defined as:

$$f_{q(j)} = \frac{\theta_{j,b} \Gamma_{s(j)}}{\theta_{j,a} \Gamma_{s(j)}} \tag{A-37}$$

If the same reference site density is assumed for each contributing mineral, Equation A-37 can be simplified to:

$$f_{q(j)} \approx \frac{\theta_{j,b}}{\theta_{j,q}}$$
 (A-38)

This allows us to rewrite Equation A-35 in the form:

$$\frac{\bar{K}_{d(1,b)}}{f_m A_{\text{tot},a}} = f_{q(1)} K_{a(1,1)} \theta_{(1,a)} + f_{q(2)} K_{a(1,2)} \theta_{(2,a)} \tag{A-39}$$

Taking the ratio of equations A-39 and A-34 gives:

$$\frac{\bar{K}_{d(1,b)}}{\bar{K}_{d(1,a)}} = f_m \left(\frac{f_{q(1)} K_{a(1,1)} \theta_{(1,a)}}{K_{a(1,1)} \theta_{(1,a)} + K_{a(1,2)} \theta_{(2,a)}} + \frac{f_{q(2)} K_{a(1,2)} \theta_{(2,a)}}{K_{a(1,1)} \theta_{(1,a)} + K_{a(1,2)} \theta_{(2,a)}} \right)$$
(A-40)

which can also be written as:

$$\frac{\tilde{K}_{d(1,b)}}{\tilde{K}_{d(1,a)}} = f_m \left(f_{q(1)} f_{r(1,1)} + f_{q(2)} f_{r(1,2)} \right) \tag{A-41}$$

As previously, this expression can be readily generalised to system comprised of n_m separate mineral surfaces/site types using the expression:

$$\frac{\tilde{K}_{d(1,b)}}{\tilde{K}_{d(1,a)}} = f_m \cdot f_q$$
 (A-42)

or in terms of K_A values as:

$$\frac{\bar{K}_{A(1,b)}}{\bar{K}_{A(1,a)}} = f_q$$
 (A-43)

where

$$f_q = \sum_{j=1}^{n_m} f_{q(j)} f_{r(1,j)} \tag{A-44}$$

In the laboratory programme the best estimate K_d value will be calculated for a reference mineralogy "b" based on a large number of individual K_d measurements, with "a" representing a broad range of BET surface areas and differing mineralogy.

Realistically, f_r values will only be known for a small number of thin section samples that may differ from the mineralogy of both the sample "a" used in a laboratory experiment to estimate a K_d point value and the pre-defined reference mineralogy "b" for which we would like to calculate K_d values for use in transport calculations. It is not yet clear how such situations should be handled in practice as the methodology requires further development and testing. Depending on the accuracy with which the sample specific mineralogy is known or if thin section data are unavailable, it may be necessary to simplify the treatment further.

As a calculation example, consider the case of rock where biotite, (Bi) is the main sorbing mineral with a smaller contribution from feldspar minerals (Fs, here including both K-feldspar and plagioclase), and minor contribution from quartz (Qz). To simplify the calculation, we define a relative sorptivity of minerals, R_s such that the surface area normalised sorptivity of biotite is $R_{s(Bi)} \sim 10$ times greater than that of feldspar while quartz is assumed to sorb 100 times more weakly than feldspar with ($R_{s(Qz)} \sim 0.01$) where the sorptivity on feldspar, is taken to be $R_{s(Fs)} = 1$.

Furthermore, consider that the K_d value that has been measured is for a rock sample with composition (Bi 11.6 %, Fs 57 %, Qz 30.8 %). If we want to extrapolate the K_d measurement to a value that reflects the average composition of Forsmark metagranite (Bi 5.1 %, Fs 58.1 %, Qz 35.6 %), we need to calculate an f_q value that accounts for the difference between the two mineralogical compositions.

Based on Equation A-28 (assuming $\theta_i \approx \phi_i$), the f_r values for each mineral can be written as:

$$f_{r(1,Bi)} = \frac{10(0.116)}{10(0.116) + 1(0.57) + 0.01(0.38)} \approx 0.669$$
(A-45)

$$f_{r(1,Fs)} = \frac{1(0.57)}{10(0.116) + 1(0.57) + 0.01(0.38)} \approx 0.329$$
 (A-46)

$$f_{r(1,Qz)} = \frac{0.01(0.38)}{10(0.0116) + 1(0.57) + 0.01(0.38)} \approx 2.19 \cdot 10^{-3}$$
(A-47)

For the specified relative sorptivities, we then estimate that biotite contributes roughly 67 % to the overall sorptivity, while feldspar minerals contribute 33 %, and quartz contributes less than 0.2 %. From equations A-44 and A-37, the f_q value can then be written as:

$$f_q = 0.669 \left(\frac{5.1}{11.6}\right) + 0.329 \left(\frac{58.1}{57}\right) + 2.19 \cdot 10^{-3} \left(\frac{35.6}{30.8}\right) \approx 0.632$$
 (A-48)

In this calculation example, to extrapolate the K_d value obtained for rock with 11.6 % biotite to a value appropriate for the *in-situ* rock with an average biotite content of 5.1 % requires a reduction of the measured K_d value by multiplying it by a factor of 0.6.

Although this example is very simple, it can be used to illustrate the impact of assumptions concerning the relative sorptivity of biotite. Figure A-1 shows the impact of varying the relative sorptivity of biotite $R_{s(Bi)}$ within a range 0.001 to 1000 times that of feldspar while maintaining the relative sorptivity of quartz at 1 % of that of feldspar (i.e. $R_{s(Oz)} = 0.01$).

For most radionuclides we would expect the sorptivity of biotite relative to that of feldspar to be greater than unity, and in some cases significantly greater. If we were to assume that biotite sorbs roughly equally as strongly as feldspar minerals, the f_q transfer factor would be close to unity (actually, $f_q = 0.92$) which suggests that the mineralogical transfer factor can probably be neglected. For a relative sorptivity of 10, the K_d should be reduced by multiplying by a factor of 0.6 as in the example discussed above. If the relative sorptivity of biotite is extremely high, on the other hand, then f_q approaches a value equal to the ratio of biotite in the reference rock and the lab sample, which in the present example implies $f_q = 0.44$.

As can be seen from the numerical examples, the mineralogical correction is relatively minor and, in some cases, could be reasonably neglected when extrapolating between different rock types at the same reference groundwater composition. When extrapolating to different groundwater compositions, however, the changes in sorptivity for some mineral surfaces may be much greater than others and the mineralogical transfer factor cannot be neglected since the f_{chem} correction factor (Equation A-30) will be incorrectly calculated.

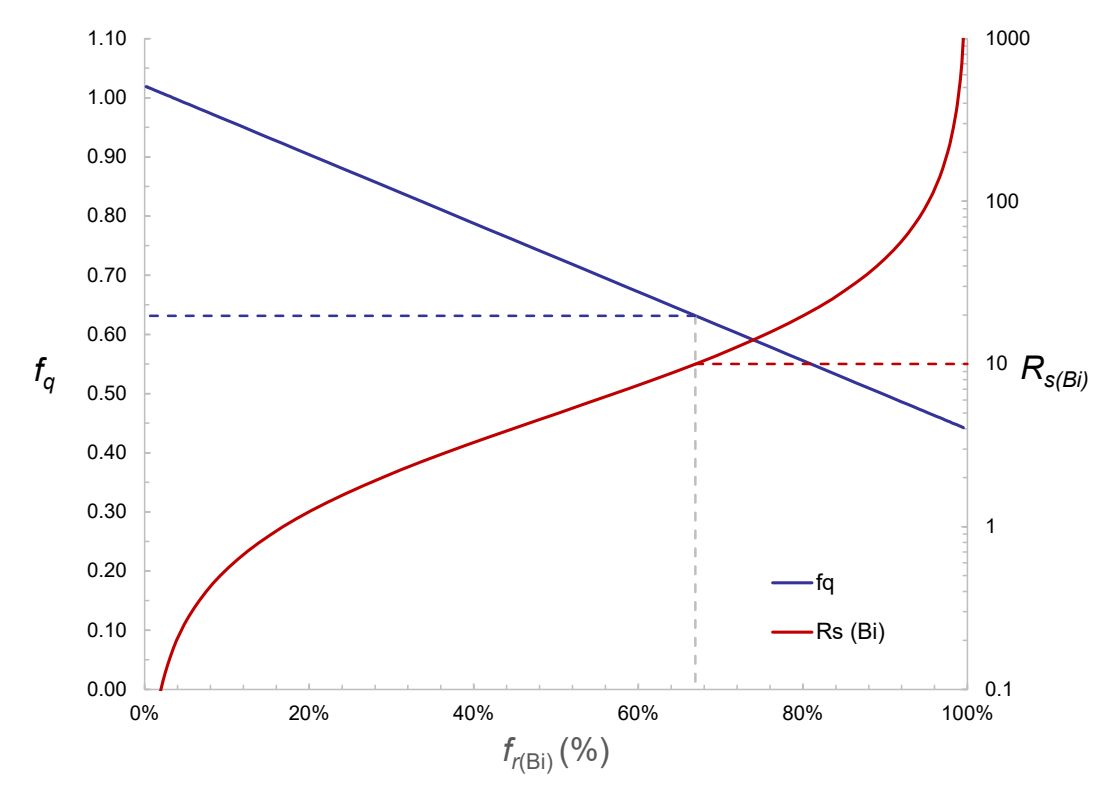


Figure A-1. Example calculation showing the theoretical impact of varying relative contributions of biotite to sorption of a radioelement on rock where sorption is assumed to occur on biotite and feldspar minerals and quartz (assuming the same relative mineral proportions discussed in the text for that of the reference rock type and that used in laboratory measurements of K_d). In the calculation, the relative sorptivity of biotite, $R_{s(Bi)}$ is varied from 0.001 to 1000 times that of feldspar (assuming a relative sorptivity for quartz of 0.01). The dotted lines indicate the f_q calculated for the example discussed in the text for a relative biotite sorptivity of $R_{s(Bi)} = 10$.

Simultaneous extrapolation to differing mineralogy and groundwater composition

For the more general case of extrapolation to simultaneously differing groundwater composition and mineralogy, we can write for the two-mineral example:

$$\frac{\bar{K}_{d(1,a)}}{A_{\text{tot},a}} = K_{a(1,1)}\theta_{(1,a)} + K_{a(1,2)}\theta_{(2,a)} \tag{A-49}$$

$$\frac{\bar{K}_{d(2,b)}}{A_{\text{tot},b}} = K_{a(2,1)}\theta_{(1,b)} + K_{a(2,2)}\theta_{(2,b)} \tag{A-50}$$

Taking the ratio of equation A-50 and A-49, and using the previously established definitions for f_m , $f_{q(j)}$, and $f_{c(j)}$ gives:

$$\frac{\bar{K}_{d(2,b)}}{\bar{K}_{d(1,a)}} = f_m \cdot \left(f_{q(1)} f_{r(1,1)} f_{c(1)} + f_{q(2)} f_{r(1,2)} f_{c(2)} \right) \tag{A-51}$$

For a generalised system comprised of n_m separate mineral surfaces/site types, we can then write:

$$\frac{\bar{K}_{d(2,b)}}{\bar{K}_{d(1,a)}} = f_m \cdot \sum_{j=1}^{n_m} f_{q(j)} f_{r(1,j)} f_{c(j)}$$
(A-52)

or in terms of K_a values as:

$$\frac{\bar{K}_{a(2,b)}}{\bar{K}_{a(1,a)}} = \sum_{j=1}^{n_m} f_{q(j)} f_{r(1,j)} f_{c(1,j)} \tag{A-53}$$

As can be seen from Equation A-52, it is not strictly possible to separate the effects of mineralogy from chemistry in the generalised extrapolation for simultaneous differences in mineralogy and chemistry unless one neglects mineralogical effects or if there is a single mineral or mineral group that dominates sorption. In the case of a single dominant mineral, we would have:

$$f_{r(1,1)} = 1$$
 (A-54)

Thus, for conversion from lab measurements to a specified reference mineralogical composition under *in-situ* conditions, we would have:

$$\frac{\bar{K}_{d(1,b)}}{\bar{K}_{d(1,a)}} = f_m \cdot f_q \tag{A-55}$$

where

$$f_q \approx \frac{\phi_{1,b}}{\phi_{1,a}} \tag{A-56}$$

$$f_m = \frac{A_{\text{tot},b}}{A_{\text{tot},a}} \tag{A-57}$$

For the conversion from the reference water composition to the application groundwater composition, we then have:

$$\frac{\bar{K}_{d(2,b)}}{\bar{K}_{d(1,b)}} = f_{\text{chem}} = \frac{K_{a(2,1)}}{K_{a(1,1)}} \tag{A-58}$$

For a monodentate surface complexation reaction and assuming negligible effect of electrostatics, the chemistry transfer factor has a linear dependency on binding site density which cancels out in both the numerator and denominator of Equation A-58. In the more general case of mixed reaction denticity and electrostatic effects, however, the f_{chem} value is not truly independent of site density, $\Gamma_{S(j)}$ which might have a non-negligible effect on calculated K_a ratios. The impact of this uncertainty on predictions of f_{chem} will need to be ascertained in further work. The direct effect of a mixed multi-dentate/monodentate reaction mechanism on the value of the intrinsic binding constant for a given sorption reaction, however, is expected to be the dominant effect and only minor deviations are expected for electrostatic corrections at low surface potentials (where electrostatic effects are approximately linear).

A.2 Formulation for cation exchanging solutes

The transfer factor formulation for a cation exchange reaction can be defined by analogy with the equations established in the previous section, although with some minor differences. The generalised cation exchange reaction for a binding site type, X can be written as:

$$z_A B^{z_B} + z_B \cdot A^{z_A} X \rightleftharpoons z_B \cdot A^{z_A} + z_A B^{z_B} X$$
 with the selectivity coefficient ${}^B_A K_{GT}$ (A-59)

In the Gaines-Thomas convention, the mass action equations are described in terms of the fraction of exchangeable cation equivalents, E_j on each site type. The mass action equation corresponding to the Gaines-Thomas selectivity coefficient ${}_{A}^{B}K_{GT}$ is:

$${}_{A}^{B}K_{GT(X)} = \frac{E_{B(X)}^{Z_{A}} \cdot a_{A}^{Z_{B}}}{E_{A(X)}^{Z_{B}} \cdot a_{B}^{Z_{A}}}$$
(A-60)

where $E_{k(X)}$ represents the fraction of exchangeable cation k (i.e. fractional occupancy of A and B) on site type X and a_j is the activity of the aqueous cation j. The fractional occupancy is defined as the number of charge equivalents of component k adsorbed per mass of solid (in mol/kg) divided by the cation exchange capacity, CEC_X (eq/kg) for the site type. Being defined as fractions, the sum of n_k exchangeable cation equivalents on each site type is unity:

$$\sum_{k=1}^{n_k} E_{k(X)} = 1 \tag{A-61}$$

The exchangeable fraction of each cation, i with charge z_i on site type X is defined as:

$$E_{i(X)} = \frac{z_i c_{s(i,X)}}{\sum_{k=1}^{n_k} z_k c_{s(k,X)}} = \frac{z_i c_{s(i,X)}}{cE c_X}$$
(A-62)

The K_d value for the exchanged cation i summed over all site types is then given by:

$$K_d = \frac{\sum_{X=1}^{n_X} (E_{(i,X)} \cdot CEC_X)}{z_i c_i}$$
(A-63)

while the total CEC is:

$$CEC_{\text{tot}} = \sum_{X=1}^{n_X} CEC_X \tag{A-64}$$

For biotite, there are at least three different site types associated with external surfaces of the mineral grains. By drawing an analogy with studies of illite (e.g. Bradbury and Baeyens 2000) these are:

- 1. FES (frayed edge sites). These account for about ~0.25 % of the total CEC and are associated with partially delaminated interlayers at disrupted platelet edges. They are related to the loss of K-intercalating cations and subsequent partial hydration of the interlayer region in the open wedge shaped nanopores formed by weathering processes.
- 2. Type II sites. These account for roughly 20 % of the total CEC and are of unclear origin. NMR studies (e.g. Kim et al. 1996, Kim and Kirkpatrick 1997, 1998) of Cs⁺ sorption on illite suggest an inner sphere process implying sorption in the compact (Stern) layer, although probably not associated with FES.
- 3. Planar sites. These are the most numerous sites, accounting for at least 80 % of the total CEC although are very loosely bound, hydrated cations residing in the diffuse layer (Gouy-layer) and are readily displaced by competing cations (equivalent to outer sphere surface complexes in a surface complexation framework).

Over extended time periods, weakly hydrated solutes such as Cs^+ can penetrate the non-hydrous interlayers and access additional sorption sites. This process is limited by diffusion kinetics, although unlike normal diffusive transport, the exchange fronts are typically very sharp (Ruiz Pestana et al. 2017). In Okumura et al. (2014) the diffusive replacement of interlayer K^+ with Cs^+ was measured in phlogopite samples with characteristic penetration depths of 10's of nm into the mica interlayers after as little as 24 h contact time with Cs^+ solution. Similar penetration depths were observed by Fuller et al. (2015) for illite although at longer contact times of up to a year. This exchange process, however, is only strictly relevant for non-muscovite micas as the K^+ interlayer cations in muscovite are not considered readily exchangeable.

The concept of FES as a special class of sorption site envisions relatively tight wedge spaces (i.e. few nm separation) between interlayers over very short distances at the boundary between hydrous and non-hydrous interlayer where steric effects give strong selectivity for weakly hydrated cations (e.g. Cs⁺, K⁺, Rb⁺). Most of the frayed edge area in contact with water, however, exhibits larger separation between adjacent tetrahedral sheets and the "true" FES, as abstracted in mechanistic modelling is likely to encompass a very small portion of the total area of frayed edges. The sorptive properties of these outer edges of disrupted platelets would bear greater similarity to hydrated interlayer spaces or basal planes.

A complication for characterisation of cation exchange, however, is that the surface area accessible to BET measurements made using N_2 or Kr gas probe molecules typically does not include interlayer sites. Furthermore, for minerals such as chlorite, the interlayer sites are replaced by a brucite-like structure which compensates the permanent negative charge of the flanking interlayers and nullifies their contribution to the overall CEC. The surface area of hydrated interlayers can be measured using EGME (e.g. Allard et al. 1983), although this does not say a great deal about the exchange capacity of non-hydrated interlayer sites of biotite that might be exchangeable with solutes such as Cs^+ .

A.3 Case for a single CEC-dominating mineral

In this case study we only consider three binding sites here taken to include two hypothetical binding site types associated with external surfaces and a binding site type assumed to correspond to non-hydrated interlayers. Since we are only attempting to establish a formal means of distinguishing surface area effects from mineralogy, however, the absence of additional site types is not crucial for the example. Assuming for the moment that the only cation exchanging mineral in the rock is biotite and only two out of the three binding sites are accessible to gas probe molecules, the relation between the total specific surface area of accessible biotite, A_{Bi}^* (m²/g) and that measurable by the BET-surface area, A_{Bi} (m²/g) is:

$$A_{\text{Bi}} = (\alpha_1 + \alpha_2)A_{\text{Bi}}^* = \theta_{\text{Bi}}A_{\text{tot}} \tag{A-65}$$

where the fractional surface area, α_X comprising the three site-types sum to unity:

$$\alpha_1 + \alpha_2 + \alpha_3 = 1 \tag{A-66}$$

The total sorptive surface area of biotite, A_{Bi} corresponding to the three site types can then be written in terms of the measurable BET surface area as:

$$A_{\text{Bi}}^* = \frac{A_{\text{Bi}}}{\alpha_1 + \alpha_2} = \frac{\theta_{\text{Bi}} A_{\text{tot}}}{\alpha_1 + \alpha_2} \tag{A-67}$$

The sorptive surface area and CEC of each binding site type, X is related by way of the equivalent site density, $\Gamma_{c(X)}$ of exchange sites in a similar fashion to binding site concentration for surface complexing solutes:

$$CEC_X \approx \frac{10^{18}}{N_A} \cdot \alpha_X \Gamma_{c(X)} A_{\text{Bi}}^*$$
 (A-68)

If it is assumed that all three exchange site types have the same "average" site density, Γ_c the total CEC is given by:

$$CEC_{\text{tot}} = \frac{10^{18}}{N_A} \Gamma_c A_{\text{Bi}}^*$$
 (A-69)

It does not actually matter if the true site density varies between each site type on the same mineral provided the α_X terms preserve the same overall proportionality of cation exchange capacity between each binding site type. Combining equations A-69 and A-67 then gives:

$$CEC_{\text{tot}} \approx \frac{10^{18}}{N_A} \cdot \left(\frac{1}{\alpha_1 + \alpha_2}\right) \Gamma_c \theta_{\text{Bi}} A_{\text{tot}}$$
 (A-70)

Here, we also assume that the CEC that is accessible to hydrated cations is less than the total CEC. This may, or may not be true, although is a reasonable working assumption for solutes such as Cs^+ that are expected to exchange with K^+ sequestered in interlayer sites of mica. The ratio of hydrated and total sites would then be given by:

$$\varphi_{\text{hyd}} = \frac{cEC_{\text{hyd}}}{CEC_{\text{tot}}} = \alpha_1 + \alpha_2 \tag{A-71}$$

For a solute that can access the non-hydrous interlayers, the K_d value for the exchanged solute i summed over all site types is:

$$K_{\rm d} = \frac{(E_{i(1)}\alpha_1 + E_{i(2)}\alpha_2 + E_{i(3)}\alpha_3) \cdot CEC_{\rm tot}}{z_i c_i}$$
(A-72)

which can also be expressed as:

$$K_{\rm d} = \frac{(E_{i(1)}\alpha_1 + E_{i(2)}\alpha_2 + E_{i(3)}\alpha_3)\beta_c\theta_{\rm Bi}A_{\rm tot}}{z_ic_i}$$
(A-73)

where

$$\beta_c = \frac{10^{18}}{N_A} \cdot \left(\frac{1}{\alpha_1 + \alpha_2}\right) \cdot \Gamma_c \tag{A-74}$$

or, as a surface area normalised K_a value:

$$K_{a} = \frac{K_{d}}{A_{\text{tot}}} = \frac{(E_{i(1)}\alpha_{1} + E_{i(2)}\alpha_{2} + E_{i(3)}\alpha_{3})\beta_{c}\theta_{\text{Bi}}}{z_{i}c_{i}}$$
(A-75)

Extrapolation to differing groundwater composition for constant mineralogy

Here, we again consider the case of two groundwater compositions (1) and (2) where composition (1) is the "anchor" for which we have a K_d measurement and composition (2) is the one for which we would like to estimate a K_d value. For the case where biotite overwhelmingly dominates the CEC of the rock, we can write:

$$K_{d(1,a)} = \left(E_{i(1,1)}\alpha_1 + E_{i(1,2)}\alpha_2 + E_{i(1,3)}\alpha_3\right)\beta_{c(a)}\theta_{Bi(a)}A_{tot,a} \tag{A-76}$$

$$K_{d(2,a)} = \left(E_{i(2,1)}\alpha_1 + E_{i(2,2)}\alpha_2 + E_{i(2,3)}\alpha_3\right)\beta_{c(a)}\theta_{Bi(a)}A_{tot,a}$$
(A-77)

Here, it is implicitly assumed that the rock samples referred to by equations A-76 and A-77 are identical (thus the subscript "a" representing the same sample). The only difference is the surface loading of solute i in groundwater composition j on site type k represented as $E_{i(j,k)}$. Taking the ratio of equations A-77 and A-76 allows us to write the chemistry transfer factor, f_{chem} as:

$$f_{chem} = \frac{K_{a(2,a)}}{K_{a(1,a)}} = \frac{K_{d(2,a)}}{K_{d(1,a)}} = \frac{E_{i(2,1)}\alpha_1 + E_{i(2,2)}\alpha_2 + E_{i(2,3)}\alpha_3}{E_{i(1,1)}\alpha_1 + E_{i(1,2)}\alpha_2 + E_{i(1,3)}\alpha_3}$$
(A-78)

Extrapolation to differing mineralogy at a fixed groundwater composition

As in the surface complexation example, we assume that we have an experiment involving measurement of K_d for two different samples ("a" and "b") although using the same contact water composition including solute concentration. The different rock samples may have differing mineralogy, surface area, etc. Returning to the two mineral surface example as given previously, the K_d value can be written out for two differing mineral compositions (denoted a and b) as:

$$K_{d(1,a)} = \left(E_{a(1,1)}\alpha_{a(1)} + E_{a(1,2)}\alpha_{a(2)} + E_{a(1,3)}\alpha_{a(3)}\right)\beta_{c(a)}\theta_{Bi(a)}A_{tot,a} \tag{A-79}$$

$$K_{d(1,b)} = \left(E_{b(1,1)}\alpha_{b(1)} + E_{b(1,2)}\alpha_{b(2)} + E_{b(1,3)}\alpha_{b(3)}\right)\beta_{c(b)}\theta_{Bi(b)}A_{tot,b} \tag{A-80}$$

If the relative distribution of surface area (and CEC) amongst each site type is roughly the same for rocks of similar origin, then the α - and β -terms should be identical in both the numerator and denominator. Furthermore, if the ratio of K_d values is calculated for the same equilibrated contact water composition, the fractional occupancy of each site type, $E_{i(m,k)}$ should also be the same provided the exchanging solute, i is sufficiently dilute. The ratio of K_d values given in equations A-80 and A-79 can then be written as:

$$\frac{K_{\mathbf{d}(1,b)}}{K_{\mathbf{d}(1,a)}} = f_m \cdot f_q \tag{A-81}$$

where

$$f_m = \frac{A_{\text{tot},b}}{A_{\text{tot},a}} \tag{A-82}$$

$$f_q = \frac{\theta_{\text{Bi}(b)}}{\theta_{\text{Bi}(a)}} \tag{A-83}$$

Under the same assumptions as established for surface complexation, the mineralogical transfer factor, f_q for cation exchange can be approximated as the ratio of biotite volume fractions in each sample for small variations in $\phi_{\rm Bi}$:

$$f_q = \frac{\theta_{\text{Bi}(b)}}{\theta_{\text{Bi}(a)}} \approx \frac{\phi_{\text{Bi}(b)}}{\phi_{\text{Bi}(a)}} \tag{A-84}$$

A direct consequence of this theoretical treatment is that the product of the f_m and f_q transfer factors can be shown to be equal to the ratio of CEC values:

$$\frac{K_{d(1,b)}}{K_{d(1,a)}} = \frac{CEC_b}{CEC_a} = f_m \cdot f_q \tag{A-85}$$

This suggests that for cation exchanging solutes, it may be more expedient to make K_d extrapolations using CEC ratios directly rather than computing f_m and f_q separately. Since CEC is a directly measurable property, this is likely to introduce less error than treating surface area and mineralogy effects separately.

Simultaneous extrapolation to differing mineralogy and groundwater composition

For the more general case of extrapolation to simultaneously differing groundwater composition and mineralogy, we can write:

$$K_{d(1,a)} = \left(E_{i(1,1)}\alpha_1 + E_{i(1,2)}\alpha_2 + E_{i(1,3)}\alpha_3\right)\beta_{c(a)}\theta_{Bi(a)}A_{tot,a} \tag{A-86}$$

$$K_{d(2,b)} = \left(E_{i(2,1)}\alpha_1 + E_{i(2,2)}\alpha_2 + E_{i(2,3)}\alpha_3\right)\beta_{c(b)}\theta_{\text{Bi}(b)}A_{\text{tot},b}$$
(A-87)

As previously, if the relative distribution of surface area (and CEC) amongst each site type is roughly the same for rocks of similar origin, then the α - and β -terms should be identical in both the numerator and denominator. In this case, however, the fractional site occupancy, $E_{i(m,k)}$ may differ considerably due to the differing contact water composition. The ratio of K_d values can now be given as:

$$\frac{K_{\mathbf{d}(2,b)}}{K_{\mathbf{d}(1,a)}} = f_{chem} \cdot f_m \cdot f_q \tag{A-88}$$

$$f_{chem} = \frac{E_{i(2,1)}\alpha_1 + E_{i(2,2)}\alpha_2 + E_{i(2,3)}\alpha_3}{E_{i(1,1)}\alpha_1 + E_{i(1,2)}\alpha_2 + E_{i(1,3)}\alpha_3}$$
(A-89)

$$f_m = \frac{A_{\text{tot},b}}{A_{\text{tot},a}} \tag{A-90}$$

$$f_q = \frac{\theta_{\text{Bi}(b)}}{\theta_{\text{Bi}(a)}} \approx \frac{\phi_{\text{Bi}(b)}}{\phi_{\text{Bi}(a)}} \tag{A-91}$$

A.4 Case for multiple CEC-contributing minerals

As shown in the previous section, the relations for extrapolation of K_d for a cation exchanging radionuclide are relatively simple and can be applied independently provided a single CEC-dominating mineral determines the sorptive properties of the rock. More generally, however, we might expect minor contributions from other CEC-bearing minerals which are either phyllosilicates with broadly similar properties to biotite or pH-dependent outer sphere surface complexes associated with surfaces lacking permanent structural charge (e.g. quartz and feldspar minerals). For mixtures of phyllosilicates of similar structure, it may be sufficient to assume a generic proportion of site types (i.e. α_1 , α_2 , α_3) in the sorption model and consider total CEC of phyllosilicate minerals taken as a group.

In any case, we can write for the more general case of a mix of $n_{\rm m}$ CEC-contributing minerals:

$$CEC_{\text{tot}} = A_{\text{tot}} \sum_{j=1}^{n_m} \beta_{c(j)} \theta_j$$
(A-92)

where

$$\beta_{c(j)} = \frac{10^{18}}{N_A} \cdot \left(\frac{1}{\alpha_{j(1)} + \alpha_{j(2)}}\right) \cdot \Gamma_{c(j)} \tag{A-93}$$

$$\varphi_{\text{hyd}(j)} = \alpha_{j(1)} + \alpha_{j(2)} \tag{A-94}$$

The CEC of the hydrated binding sites only is:

$$CEC_{\text{hyd}} = A_{\text{tot}} \sum_{i=1}^{n_m} \varphi_{\text{hyd}(i)} \beta_{c(i)} \theta_i$$
(A-95)

For a cation, *i* that can access interlayer sites (e.g. Cs^+) the K_d value averaged over all minerals and site types is then (introducing an additional subscript for mineral type):

$$\bar{K}_{d} = \frac{A_{tot} \sum_{j=1}^{n_{m}} (E_{i(j,1)} \alpha_{j(1)} + E_{i(j,2)} \alpha_{j(2)} + E_{i(j,3)} \alpha_{j(3)}) \cdot \beta_{c(j)} \theta_{j}}{z_{i} c_{i}}$$
(A-96)

Extrapolation to differing groundwater composition for constant mineralogy

For two mineralogically identical samples in contact with differing equilibrium contact water composition, we can write the ratio of K_d values by analogy with the corresponding case for surface complexation:

$$f_{\text{chem}} = \frac{\bar{K}_{d(2,a)}}{\bar{K}_{d(1,a)}} = \frac{\bar{K}_{a(2,a)}}{\bar{K}_{a(1,a)}} = \sum_{j=1}^{n_m} f_{r(1,j)} \cdot f_{c(j)}$$
(A-97)

where

$$f_{c(j)} = \frac{E_{i(j,2,1)}\alpha_{j(1)} + E_{i(j,2,2)}\alpha_{j(2)} + E_{i(j,2,3)}\alpha_{j(3)}}{E_{i(j,1,1)}\alpha_{j(1)} + E_{i(j,1,2)}\alpha_{j(2)} + E_{i(j,1,3)}\alpha_{j(3)}}$$
(A-98)

$$f_{r(1,j)} = \frac{K_{a(1,j)}\theta_j}{\sum_{\xi=1}^{n_m} K_{a(1,\xi)}\theta_\xi} = \frac{K_{a(1,j)}\theta_j}{\bar{K}_{a(1)}} = \frac{a_{(1,j)}}{\sum_{\xi=1}^{n_m} a_{(1,\xi)}}$$
(A-99)

Here, the mineral and site-specific occupancy for sorbing solute i is given by $E_{i(j,\xi,k)}$ for mineral j, in contact with equilibrium water composition ξ , and site type k.

Extrapolation to differing mineralogy at a fixed groundwater composition

For two samples featuring differing mineralogy in contact with the same equilibrium contact water composition, we can write the ratio of K_d values as:

$$\frac{K_{d(1,b)}}{K_{d(1,a)}} = f_m \cdot \sum_{j=1}^{n_m} f_{r(1,j)} \cdot f_{q(j)}$$
(A-100)

where

$$f_m = \frac{A_{\text{tot},b}}{A_{\text{tot},a}} \tag{A-101}$$

$$f_{q(j,a\to b)} = \frac{\theta_{j(b)}}{\theta_{j(a)}} \approx \frac{\phi_{j(b)}}{\phi_{j(a)}} \tag{A-102}$$

$$f_{r(1,j)} = \frac{K_{a(1,j)}\theta_j}{\sum_{\xi=1}^{n_m} K_{a(1,\xi)}\theta_\xi} = \frac{K_{a(1,j)}\theta_j}{\bar{K}_{a(1)}} = \frac{a_{(1,j)}}{\sum_{\xi=1}^{n_m} a_{(1,\xi)}}$$
(A-103)

This is the same relation as derived previously for surface complexing solutes, although its applicability depends on the feasibility of separating sorptive contributions, $f_{r(1,j)}$ for individual minerals comprising the rock.

Simultaneous extrapolation to differing mineralogy and groundwater composition

For the more general case of extrapolation to simultaneously differing groundwater composition and mineralogy, we can write by analogy with Equation A-52:

$$\frac{\bar{K}_{d(2,b)}}{\bar{K}_{d(1,a)}} = f_m \cdot \sum_{j=1}^{n_m} f_{q(j)} f_{r(1,j)} f_{c(j)}$$
(A-104)

where

$$f_m = \frac{A_{\text{tot},b}}{A_{\text{tot},a}} \tag{A-105}$$

$$f_{q(j,a\to b)} = \frac{\theta_{j(b)}}{\theta_{j(a)}} \approx \frac{\phi_{j(b)}}{\phi_{j(a)}} \tag{A-106}$$

$$f_{r(1,j)} = \frac{\kappa_{a(1,j)}\theta_j}{\sum_{\xi=1}^{n_m} \kappa_{a(1,\xi)}\theta_{\xi}} = \frac{\kappa_{a(1,j)}\theta_j}{\bar{\kappa}_{a(1)}} = \frac{a_{(1,j)}}{\sum_{\xi=1}^{n_m} a_{(1,\xi)}}$$
(A-107)

$$f_{c(j)} = \frac{E_{i(j,2,1)}\alpha_{j(1)} + E_{i(j,2,2)}\alpha_{j(2)} + E_{i(j,2,3)}\alpha_{j(3)}}{E_{i(j,1,1)}\alpha_{j(1)} + E_{i(j,1,2)}\alpha_{j(2)} + E_{i(j,1,3)}\alpha_{j(3)}}$$
(A-108)

Appendix B Handling of uncertainties related to transfer factor calculations

B.1 Rescaling of measured R_d^0 values to reference K_d^0 values for specific rock types

Since the treatment of sorption data involves multiple steps of interpretation and correction for known biases, the rigorous treatment of uncertainties and their propagation in calculations is of central importance to this work. The basic rescaling equation for estimation of reference K_d^0 values from R_d^0 values measured in laboratory studies is given in Chapter 5 as:

$$\log_{10} K_{\rm d}^0 = \log_{10} R_{\rm d}^0 + \log_{10} f_m + \log_{10} f_q \tag{B-1}$$

As discussed previously in Appendix A, it is not strictly possible to separate the effects of chemistry from mineralogy in the more general case, so this assumes an extrapolation of K_d at a constant groundwater composition corresponding to the reference composition used in the laboratory study.

For any function that can be written in the form $y = f(x_1 \cdots x_n)$, the generalised expression for error-propagation (Tellinghuisen 2001) can be written down as the matrix expression:

$$\sigma_{\nu}^2 = g^T V g \tag{B-2}$$

where σ_y^2 is the variance (uncertainty) of the function, g is the vector of partial derivatives $\partial y/\partial x_i$ of the function y, and V is the covariance matrix of the parameters $\bar{x} = \langle x_1, \dots, x_n \rangle$.

For comparison of a rock sample "L" studied in the laboratory with the *in-situ* reference rock "R", the surface area transfer factor, f_m is defined (cf. Equation A-36) as:

$$f_m = \frac{A_R}{A_L} \tag{B-3}$$

Since the measured BET surface areas for rock "L" and "R" can have large errors, it is convenient to assume that the ratio given by Equation B-3 has a lognormally distributed uncertainty where the measured BET surface areas also have lognormally distributed uncertainties. The calculation of f_m and the subsequent error propagation calculation is therefore carried out on the \log_{10} -transformed data. From the definition of the moment generating function of a lognormal distribution (e.g. Crow and Shimizu 1988), the location and scale parameter (base 10) for a lognormally distributed variable, x, can be given as:

$$\mu_{x} = \frac{1}{\ln(10)} \cdot \left(\ln\left(E[x]\right) - \frac{1}{2} \cdot \ln\left(1 + \left(\frac{s_{x}}{E[x]}\right)^{2}\right) \right)$$
(B-4)

$$\sigma_{x} = \frac{1}{\ln(10)} \cdot \sqrt{\ln\left(1 + \left(\frac{S_{x}}{E[x]}\right)^{2}\right)}$$
(B-5)

where E[x] is the expected value (i.e. arithmetic mean) and s_x is the associated standard deviation. The surface area transfer factor is then calculated in logarithmic space as:

$$\log_{10} f_m = \mu_m = \mu_{AR} - \mu_{AL} \tag{B-6}$$

where μ_{AR} and μ_{AL} are the central estimates for the *in-situ* rock and laboratory samples, respectively calculated using Equation B-4 based on the measured BET surface areas and their reported standard errors.

The error estimate for the difference of two normally distributed (in log-space), uncorrelated variables is given by (e.g. Ku 1966):

$$\sigma_m = \sqrt{\sigma_{AR}^2 + \sigma_{AL}^2} \tag{B-7}$$

We can then write for the location parameter, μ_m :

$$\mu_m = \log_{10}\left(\frac{A_R}{A_L}\right) - \frac{\Lambda_m}{\ln(10)} \tag{B-8}$$

where A_R and A_L are the measured BET surface areas and the variable Λ_m is a convexity correction factor defined as:

$$\Lambda_m = \frac{1}{2} \cdot \left(\ln \left(1 + \left(\frac{s_R}{A_R} \right)^2 \right) - \ln \left(1 + \left(\frac{s_L}{A_L} \right)^2 \right) \right)$$
(B-9)

where s_R and s_L are the standard errors of the measurements. The standard error associated with μ_m is calculated from:

$$\sigma_m = \frac{1}{\ln(10)} \cdot \sqrt{\ln\left(1 + \left(\frac{s_R}{A_R}\right)^2\right) + \ln\left(1 + \left(\frac{s_L}{A_L}\right)^2\right)}$$
(B-10)

For the mineralogical transfer factor, f_q we have for n_m distinct minerals (here, neglecting different site types on a mineral surface to simplify the arithmetic description):

$$f_q = \sum_{j=1}^{n_m} f_{q(j)} f_{r(0,j)}$$
 (B-11)

where

$$f_{r(0,j)} \approx \frac{R_{s(0,j)}\phi_{j,L}}{\sum_{\xi=1}^{n_m} R_{s(0,\xi)}\phi_{\xi,L}}$$
 (B-12)

$$f_{q(j)} pprox \frac{\phi_{j,R}}{\phi_{j,L}}$$
 (B-13)

Here, the relative sorptivities, $R_{s(0,j)}$ for each mineral j in the assemblage are defined for the reference groundwater (thus the subscript "0"). As noted previously in Appendix A.1, an approximate proportionality of mineral-specific reactive surface with mineral volume fraction is taken as an a priori assumption since the reactive surface areas of constituent minerals cannot be measured directly. If we accept the validity of this assumption, the uncertainty of the f_q transfer factor can be estimated from the underlying uncertainties of the mineral specific relative sorptivities, $R_{s(1,j)}$ and mineral volume fractions in the lab samples and the *in-situ* rock (i.e. $\phi_{j,L}$ and $\phi_{j,R}$, respectively).

In the more general case where multiple minerals contribute to the K_d value in a non-negligible way, this requires a simulation-based approach since the uncertainty distributions for the $f_{q(j)}$ factors cannot be written down simply in terms of elementary functions. The relative sorptivities, $R_{s(1,j)}$ compared to the index mineral can be reasonably assumed to have a lognormal distribution since they are specified as a ratio of K_a values which are *a priori* assumed to be lognormally distributed. For a mix of n_m minerals, the uncertainty of the $f_{q(j)}$ factors is described by a Dirichlet distribution given that the mineral volume fractions must sum to unity.

In the case where a single mineral such as biotite dominates the sorption properties, however, the overall f_q transfer factor can be simplified to (as per Equation A-56):

$$f_q \approx \frac{\phi_R}{\phi_L}$$
 (B-14)

At the relatively low volume fractions of biotite in Forsmark rock, the uncertainty distribution of f_q can then be approximated as a lognormal distribution in an analogous fashion to that for the surface area transfer factor:

$$\mu_q = \log_{10} \left(\frac{\phi_R}{\phi_I} \right) - \frac{\Lambda_q}{\ln(10)} \tag{B-15}$$

The convexity correction factor, Λ_q is now defined as:

$$\Lambda_{q} = \frac{1}{2} \cdot \left(\ln \left(1 + \left(\frac{s_{\phi R}}{\phi_{R}} \right)^{2} \right) - \ln \left(1 + \left(\frac{s_{\phi L}}{\phi_{L}} \right)^{2} \right) \right)$$
(B-16)

where $s_{\phi R}$ and $s_{\phi L}$ are the standard errors of the measurements of mineral volumetric fraction. The standard error, σ_q is then calculated from:

$$\sigma_{q} = \frac{1}{\ln(10)} \cdot \sqrt{\ln\left(1 + \left(\frac{S_{\phi R}}{\phi_{R}}\right)^{2}\right) + \ln\left(1 + \left(\frac{S_{\phi L}}{\phi_{L}}\right)^{2}\right)}$$
(B-17)

Since biotite is a minor component of the rock, it typically has a much larger relative variation than that of feldspar or quartz minerals and the value of σ_q calculated using Equation B-17 should therefore establish an upper limit to the relative uncertainty of the transfer factor, f_q .

For the calculation of uncertainty, it is convenient to write out the rescaling Equation B-1 in terms of the location parameters:

$$\log_{10} K_d^0 = \mu_0 + \mu_{AR} - \mu_{AL} + \mu_{\phi R} - \mu_{\phi L}$$
(B-18)

Here, the reference R_d^0 value is assumed to be lognormally distributed with a location parameter, μ_0 and standard error, σ_0 .

From first principles, we would expect mutual correlation between $\langle R_d^0, A_L \rangle$ and $\langle R_d^0, \phi_L \rangle$. In fact, the use of a scaling relation such as Equation B-1 requires this to be true. On the other hand, we would not expect any correlation between the parameter pairs $\langle A_R, A_L \rangle$, $\langle \phi_R, \phi_L \rangle$, $\langle A_R, \phi_L \rangle$, nor $\langle A_L, \phi_R \rangle$ since they are physically different samples of rock. The parameter pair $\langle A_L, \phi_L \rangle$, however, could exhibit correlation as might $\langle A_R, \phi_R \rangle$ if BET surface area is correlated with mineralogy in a non-trivial way. After zeroing out elements of the covariance matrix, V that can be presumed to have no covariance, the covariance matrix V associated with Equation B-2 can then be defined as:

$$V = \begin{pmatrix} \sigma_0^2 & \rho_{\langle A_R, R_d^0 \rangle} \sigma_{AR} \sigma_0 & 0 & \rho_{\langle \phi_R, R_d^0 \rangle} \sigma_{\phi R} \sigma_0 & 0 \\ \rho_{\langle R_d^0, A_R \rangle} \sigma_0 \sigma_{AR} & \sigma_{AR}^2 & 0 & \rho_{\langle q_R, A_R \rangle} \sigma_{\phi R} \sigma_{AR} & 0 \\ 0 & 0 & \sigma_{AL}^2 & 0 & \rho_{\langle \phi_L, A_L \rangle} \sigma_{\phi L} \sigma_{AL} \\ \rho_{\langle LR_d^0, q_R \rangle} \sigma_0 \sigma_{\phi R} & \rho_{\langle A_R, q_R \rangle} \sigma_{AR} \sigma_{\phi R} & 0 & \sigma_{\phi R}^2 & 0 \\ 0 & 0 & \rho_{\langle A_L, q_L \rangle} \sigma_{AL} \sigma_{\phi L} & 0 & \sigma_{\phi L}^2 \end{pmatrix}$$
(B-19)

For broadly similar rock types it is conceivable that any correlation between $\langle A_R, \phi_R \rangle$ is identical to that for $\langle A_L, \phi_L \rangle$, which would allow us to simplify the expression in Equation B-2 to:

$$\sigma_K^2 = \sigma_0^2 + \sigma_{A_R}^2 + \sigma_{A_L}^2 + \sigma_{q_R}^2 + \sigma_{q_L}^2 + \varepsilon_{cv}^2$$
(B-20)

where σ_K^2 is the variance of the $\log_{10} K_{\rm d}^0$ estimate after application of the transfer factors, and the off-diagonal effects are gathered in the parameter, ε_{cv}^2 defined as:

$$\varepsilon_{cv}^2 = 4\rho_{\langle A_L, \phi_L \rangle} \sigma_{AL} \sigma_{\phi L} + 2\left(\rho_{\langle R_d^0, A_L \rangle} \sigma_0 \sigma_{AL} + \rho_{\langle R_d^0, \phi_L \rangle} \sigma_0 \sigma_{\phi L}\right)$$
(B-21)

If all off-diagonal terms in the covariance matrix (Equation B-19) are zero, or if these are neglected then the uncertainty is given by the familiar error propagation expression for summation of normally distributed uncertainties:

$$\sigma_K^2 \approx \sigma_0^2 + \sigma_{AR}^2 + \sigma_{AL}^2 + \sigma_{\phi R}^2 + \sigma_{\phi L}^2$$
 (B-22)

B.2 Handling of uncertainties related to the chemistry correction factor

In Chapter 5, an expression of the following form is given for the chemistry transfer factor:

$$K_{\rm d} = K_{\rm d}^0 \cdot f_{\rm chem} \tag{B-23}$$

Equation B-23 is used to extrapolate the $K_{\rm d}^0$ value estimated for a given reference mineralogy and sorptive surface area in intact rock to groundwater compositions deviating from the reference groundwater composition (i.e. one of the synthetic groundwater types used in laboratory experiments). As shown in Appendix A, when extrapolating to different groundwater chemistry it is necessary to calculate a weighted average of transfer factors for each mineral contributing towards the overall sorptivity. For a system comprised of n_m separate mineral surfaces, or site types $f_{\rm chem}$ is defined for an *in-situ* groundwater composition, i (cf. equations A-30 and A-31) as:

$$f_{\text{chem}(i)} = \frac{\kappa_{d(i)}}{\kappa_d^0} = \frac{\kappa_{a(i)}}{\kappa_a^0} = \sum_{j=1}^{n_m} f_{r(0,j)} \cdot f_{c(i,j)}$$
(B-24)

where

$$f_{c(i,j)} = \frac{K_{a(i,j)}}{K_{a(j)}^0}$$
 (B-25)

Assuming that the $f_{r(0,j)}$ weights and their uncertainties are already known (see Equation B-12) from the evaluation of laboratory measurement data, it remains to estimate the mineral specific chemistry transfer factors, $f_{c(i,j)}$ from a suitable thermodynamic model for each mineral component. As noted previously in Appendix A, the formulation of the chemistry correction transfer factor is not dependent on any particular thermodynamic sorption model and any suitable model can be substituted in the workflow without changing the basic premise of the transfer factor approach.

Since the $f_{c(i,j)}$ factors generally need to be estimated using a numerical modelling tool such as PHREEQC (Parkhurst and Appelo 2013) any uncertainty analysis needs to be performed numerically in the context of the modelling tool being used. For a specified groundwater composition i, the uncertainty of $f_{c(i,j)}$ depends on the uncertainty of the various parameters comprising the underlying thermodynamic model. Some of these uncertainties (e.g. site density, surface area, etc.) mutually cancel in the computation of $f_{c(i,j)}$, although others remain. It is reasonable to expect that point values of $f_{c(i,j)}$ for a single groundwater composition will have a lognormally distributed uncertainty deriving from the uncertain parameterisation of the model. These uncertainties can be assessed quantitatively by calculating $f_{c(i,j)}$ using a stochastic sampling approach if the uncertainties associated with each parameter can be adequately estimated.

A similar approach was adopted in Crawford (2010) where randomly perturbed values of the half-reaction constants for cation exchange reactions were used in numerical simulations to assess parameter uncertainty in addition to spatial variability of groundwater composition. Although the uncertainty of individual reaction constants was in many cases unknown, this was addressed by assuming an uncertainty based on the number of significant figures reported in the references used to parameterise the model. In this way it is possible to assess the relative contribution of spatial variability of groundwater compositions (i.e. statistics of major component concentrations, etc.) and uncertainty in the thermodynamic modelling of sorption by stochastically varying parameters in Monte-Carlo calculations. An account of how such calculations might be incorporated in variance-based sensitivity analyses is given in Ciffroy (2020).

For a generalised system comprised of n_m separate mineral surfaces/site types, we have contributions to the overall uncertainty of $f_{\text{chem}(i)}$ from multiple mineral surfaces. The overall uncertainty depends on the uncertainties in each of the models used to calculate the weighted average and depends also on the accuracy with which the relative weights, $f_{r(0,j)}$ can be specified (i.e. in terms of best estimate $f_{r(0,j)}$ values and their standard errors). It is expected that the uncertainty will be dominated by how much the application groundwater composition differs from the reference synthetic groundwater used in laboratory experiments.

For small extrapolations within a similar groundwater type, the uncertainty is likely to be relatively low. For large extrapolations, particularly to higher pH levels and significantly different redox conditions, however, the uncertainties are likely to be large.

In a broader context, there is a component of variable groundwater composition in the geosphere that we seek to capture in the computation of f_{chem} where a large number of point values, i are calculated for a range of different compositions. This is essentially an integration of the probability distribution representing f_{chem} over a range of application groundwater compositions. The calculation of the marginal distribution of f_{chem} can be represented as:

$$p(f_{\text{chem}}) = \frac{\int p(f_{\text{chem}}|\varphi) \cdot p(\varphi) d\varphi}{\int p(\varphi) d\varphi}$$
(B-26)

Although the uncertainty of an individual point estimate of $f_{\rm chem}$ might be reasonably lognormally distributed as described previously, there is no requirement for statistics of groundwater composition for a particular application to conform to a lognormal distribution and the marginal probability distribution for $f_{\rm chem}$ can, at least in principle, take on a range of different forms depending on its context. The general case for computation of $f_{\rm chem}$ reflecting a range of groundwater compositions therefore requires a numerical computation of Equation B-23 which essentially implies a convolution of the uncertainty distributions for $f_{\rm chem}$ and K_d^0 . Although a nontrivial calculation, this can be readily implemented at the point of calculation using a scripting language such as Python or Matlab and calls to iPhreeqc calculation modules (Charlton and Parkhurst 2011).

In the case where a single mineral such as biotite dominates the sorption properties, the f_{chem} transfer factor and its uncertainty for different application types can be readily calculated without needing to specify the relative contributions of different minerals. This, however, is a very rough approximation and care must be taken, particularly at higher pH levels where different mineral surfaces can contribute to sorption differently to that assessed at normal groundwater pH levels. The approximation is useful, however as it allows us to develop application areas in prototype form to test the overall methodology in a simplified fashion. Some calculation examples showing potential data delivery types are given in Appendix C.

In the more general case where we seek to simultaneously extrapolate for deviating chemistry and mineralogy from the reference rock, the chemistry transfer factor cannot be completely decoupled from the mineralogy transfer factor, and we have (as per Equation A-52):

$$\frac{K_{d(i,k)}}{K_d^0} = f_{m(k)} \cdot \sum_{j=1}^{n_m} f_{q(k,j)} f_{r(0,j)} f_{c(i,j)}$$
(B-27)

Here, we introduce an additional subscript k to represent the extrapolated K_d value to a deviating mineralogy k and groundwater composition, i. In most application cases, this is an unnecessary complication as the reference K_d^0 value should already be calculated in such a way that it adequately reflects the target rock *in-situ* including its surface area and mineralogical variability.

The correction implied by Equation B-27 therefore should only really be used in situations where a suitable K_d^0 estimate for the target rock is unavailable. Such a situation might arise where laboratory measurement data are lacking for a specific alteration type, or where one seeks to model a potential trend in K_d over an alteration rim with a continuous (systematic) spatial variation in mineralogy. Since the contribution of different minerals towards the overall sorptivity is more uncertain for rocks which have not been studied in the laboratory, the extrapolation implied by Equation B-27 is associated with a larger uncertainty than rocks where an appropriate K_d^0 value for the "average" material type can be specified.

Appendix C Prototype calculation examples for the chemistry transfer factor

C.1 Simple examples involving a single anchor

An example of a typical calculation involving extrapolation from an anchor point is given in Figure C-1 for Am(III) measurement data from the SDM-Site lab campaign (Selnert et al. 2008, 2009b). Although Am(III) and Eu(III) are typically considered together as geochemical analogues, data for Eu(III) are excluded in this plot to make the comparison as internally consistent as possible for the present example. The R_d data plotted for each groundwater composition are based on the average of measured values for the largest crushed size fraction (1-2 mm) and longest contact time (177–188 days). The data represent a mix of unaltered rock types from both site investigation areas and are not corrected for surface area effects, mineralogy, or diffusive disequilibrium. This is sufficiently accurate for demonstration of the anchoring concept, however, since we are mostly interested in accounting for relative changes in sorptivity. For safety assessment calculations, on the other hand, the calculations would ideally be based on estimated reference equilibrium K_d^0 values for each reference rock type and groundwater composition.

In this analysis, the $R_{\rm d}$ data are plotted against pH with circular markers representing data for Forsmark samples, and triangular markers representing samples from the Laxemar-Simpevarp site. Measured $R_{\rm d}$ values for Am(III) sorption on Laxemar site-specific rocks are generally higher than those for the Forsmark site which might be indicative of a non-negligible impact of mineralogy since the crushed rock samples from both sites have roughly the same BET surface area. It is difficult to draw specific conclusions, however, since mineralogy is not recorded for all borehole sections represented in the Am data sets for the different groundwater types. Where mineralogical data does exist, however, the Laxemar samples frequently contain larger proportions of chlorite, hornblende, and magnetite which are mostly recorded as being absent from the Forsmark rock samples. Each of these minerals are typically considered to be relatively sorbing when present.

The pH values for the measurement data are plotted at the end-point pH estimated for the groundwater at the conclusion of the experiments which was roughly 1.0–1.5 pH units higher than the initial pH. As discussed previously, this was interpreted as most likely due to outgassing of CO₂ from the contact solutions due to the low pCO₂ in the glovebox. For modelling the R_d measurements made in SDM-Site, the partial pressure of oxygen was arbitrarily set to 10⁻²⁵ atm. to obtain a redox potential in the range 300-400 mV which is roughly in the same range as Eh measurements that were made at the conclusion of the sorption experiments. Calibration calculations using PHREEQC suggest that the pH changes were consistent with a headspace pCO₂ on the order of about ~15 ppm (with a 95 % confidence interval of 4-60 ppm). Error bars on the horizontal and vertical axes represent the studentised 95 % confidence interval of the mean (i.e. not the standard deviation of the raw data).

The curves shown in Figure C-1 represent titrations of the Am(III)-illite system (based on the BB09 model) made by varying the unknown pCO₂ over a limited range to obtain a match with the endpoint pH of the corresponding synthetic groundwater. The theoretical titration curves were calculated with PHREEQC using the fitted binding constants for Am(III) given in Bradbury and Baeyens (2009a, b) together with the Thermochimie v9.0 thermodynamic database (Giffaut et al. 2014). In this example, the measured $R_{\rm d}$ value for Forsmark saline groundwater is assumed to be the anchor and thus the red titration curve passes exactly through this data point (i.e. $f_{\rm chem} = 1$). The blue, green, and orange curves on the other hand are predictions for the corresponding synthetic groundwaters assuming the Forsmark saline composition as an anchor.

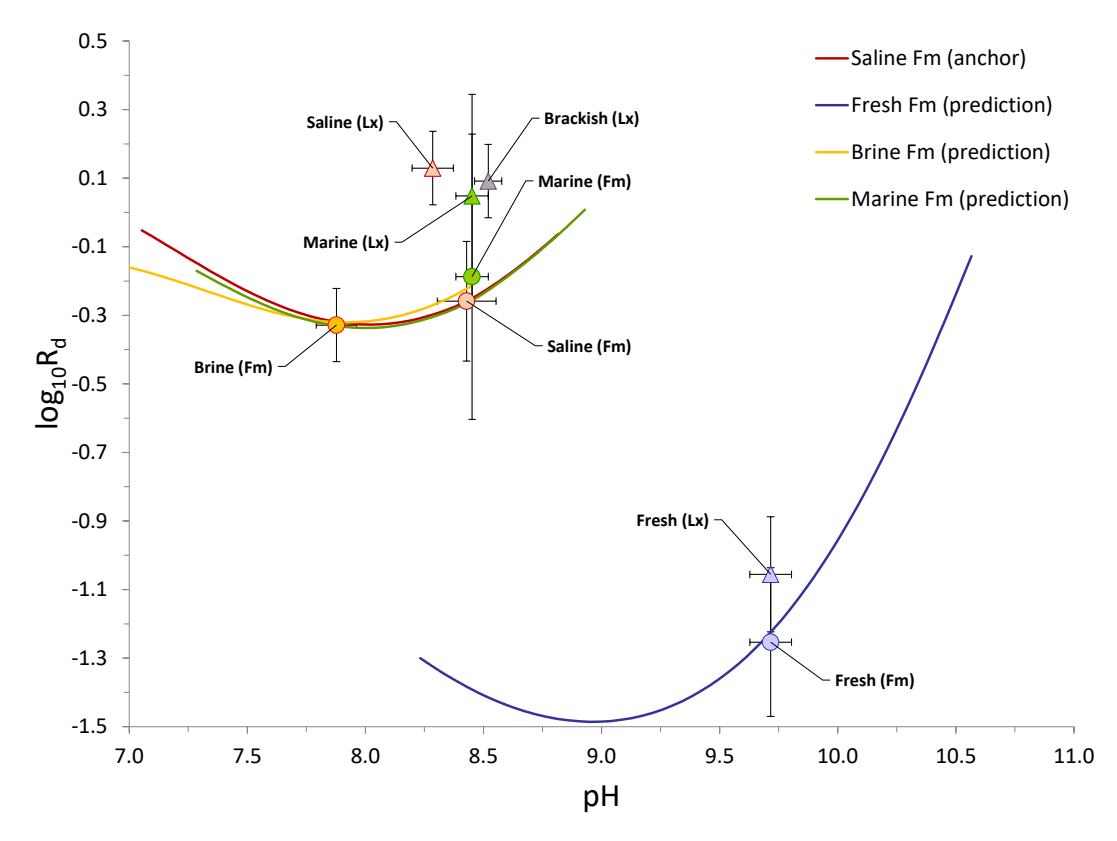


Figure C-1. Example of the anchoring procedure for sorption of Am(III) on Forsmark (circular markers) and Laxemar (triangular markers) rock types in contact with site-specific synthetic groundwater compositions. Markers indicate R_d values for the 1-2 mm size fraction (mean values) measured at the longest contact time for saline (red), fresh (blue), marine (green), and brine (orange) type synthetic groundwaters. Forsmark saline groundwater composition is assumed to be the anchor and predictions are made for other groundwater types as indicated by the coloured curves. Since the pCO_2 in the headspace was unknown, the curves show the trajectory of R_d predictions where pCO_2 is varied in an interval (see main text for details).

All modelled cases assume a picomolar concentration of radioelement and significantly higher concentration of surface sites to avoid non-linearity related to sorption site saturation. In Figure C-1, the prediction for the fresh groundwater extrapolated from the saline anchor (blue curve) is very good and correctly predicts the roughly order of magnitude reduction in R_d for Am(III) relative to that for the Forsmark saline composition. The predictions for the marine and brine groundwaters in contact with Forsmark rock are also very good and suggest only very small deviations from the saline reference anchor.

Another example of the anchoring procedure is shown in Figure C-2 for Ni(II) sorption. As for the previous example, $R_{\rm d}$ data are plotted against pH with circular markers representing data for Forsmark samples, and triangular markers representing samples from the Laxemar-Simpevarp site. Error bars on the horizontal and vertical axes represent the studentised 95 % confidence interval of the mean. Owing to the small sample sizes, however, the error bars are proportionally much larger than for the Am(III) example. The measured $R_{\rm d}$ values represent 3 replicates of rock samples taken from single borehole sections, except for the Forsmark saline data set which is based on 6 replicates representing rock from 2 borehole sections. The theoretical titration curves for Ni are calculated using the same procedure as for Am, although with the fitted binding constants for Ni surface complexation given in Bradbury and Baeyens (2009a, b).

The prediction made for Ni(II) sorption on Forsmark rock in contact with fresh groundwater is satisfactory (within the error range of the measured R_d values), although clearly not as good as that calculated for Am(III) and appears to underpredict the measured R_d value. The prediction for the Forsmark marine groundwater is also within the error bounds of the measured value. The prediction for brine groundwater is not good, although this might be partly due to the overestimation of aqueous Ni²⁺ activity at the high ionic strength of the brine (1.3 mol/l) which is roughly twice that of standard oceanic seawater.

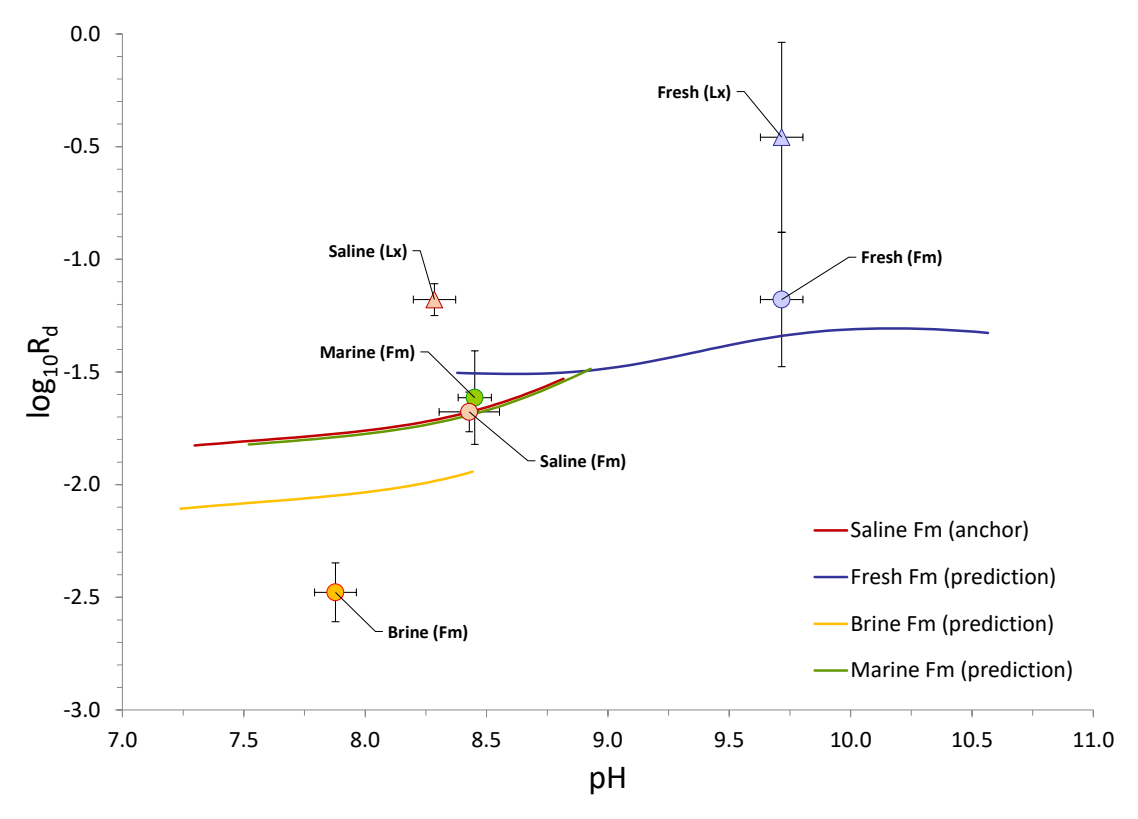


Figure C-2. Example of the anchoring problem for sorption of Ni(II) on Forsmark (circular markers) and Laxemar (triangular markers) rock types in contact with site-specific synthetic groundwater compositions. Markers indicate R_d values for the 1-2 mm size fraction (mean values) measured at the longest contact time for saline (red), fresh (blue), marine (green), and brine (orange) type synthetic groundwaters. Forsmark saline groundwater composition is assumed to be the anchor and predictions are made for other groundwater types as indicated by the coloured curves. Since the pCO2 in the headspace was unknown, the curves show the trajectory of R_d predictions where pCO2 is varied in an interval (see main text for details).

C.2 Higher dimensional extrapolations based on multiple anchors

Although the example given in the previous section is illustrative and the extrapolations show good predictive skill relative to measurement data, they ultimately have limited value for safety assessment applications. Typically, in the geosphere there is a continuum of groundwater compositions where the groundwaters described in the previous section comprise typical compositional types. For the more general problem where there is a large range of intermediate compositions, it is necessary to make predictions outside the range of compositions for which there are measured $R_{\rm d}$ values.

The general picture of present-day groundwater compositional variation at Forsmark as described in the site descriptive model (Laaksoharju et al. 2008) is that groundwater in the upper ~ 50 m of the bedrock is predominantly meteoric in character and similar to the fresh groundwater type used in the laboratory programme. For depths greater than ~ 100 m, on the other hand, the groundwater becomes more representative of a marine (Littorina) origin with an increasingly large proportion of saline content with increasing depth to about ~ 500 m. Although there is evidence of water featuring deep saline influences already at intermediate levels ($\sim 300-500$ m), this groundwater type is mostly found at greater depths (~ 600 m).

The brine groundwater used in the laboratory programme can be assumed to be approximately the same as deep saline groundwater discussed in the site descriptive model. Based on this description of depth dependent compositional variation, one can infer that a large proportion of the compositional variation could be modelled by assuming mixing of the various groundwater types in various proportions together with reasonable assumptions concerning which aquifer minerals should be approximately in equilibrium with the groundwater.

With a focus on the upper 400–500 m of the geosphere, the present-day compositional variation can then be represented in a simplified fashion as a ternary mixing system where the fresh, marine, and saline groundwater types constitute approximate end-members for hydrodynamic mixing processes in the subsurface. Here, it is necessary to distinguish between the end-members defined above for modern groundwater mixing processes and paleo-origin end-members as identified by principal component analysis in the site descriptive modelling work (Laaksoharju et al. 2008).

The groundwater origin end-members are used to initialise early Holocene compositions in large scale transport simulations of hydrochemical evolution made in the site scale hydrogeological model (e.g. Joyce et al. 2015b) and consist of a deep saline water, Littorina water, an altered meteoric water, a water of glacial origin, as well as two variants referred to as "old meteoric" and "dilute meteoric". Theoretically, the three end-members used in this work to represent the modern groundwaters (i.e. fresh, marine, and Forsmark saline) could be reconstituted from the original end-members although this is redundant for the present purpose and need not be considered.

A complicating issue for the present data set is the fact that the synthetic groundwater compositions used in the laboratory investigations are perturbed relative to their original definitions due to the pH drift related to pCO₂ readjustment. This is problematic since the task of interpolating between K_d^0 values for mixed proportions of well-defined groundwater laboratory compositions now becomes an exercise in extrapolation. This is because the *in-situ* groundwater compositions are mostly outside the mixing envelope of the three originally defined end-members. The mixing process is illustrated in Figure C-3 in terms of pH and total dissolved carbonate concentration where the three groundwater compositions corresponding to fresh (blue diamond marker), marine (green diamond marker), and Forsmark saline (red diamond marker) are mixed in various proportions to obtain a sequence of intermediate mixed compositions ("+" symbols).

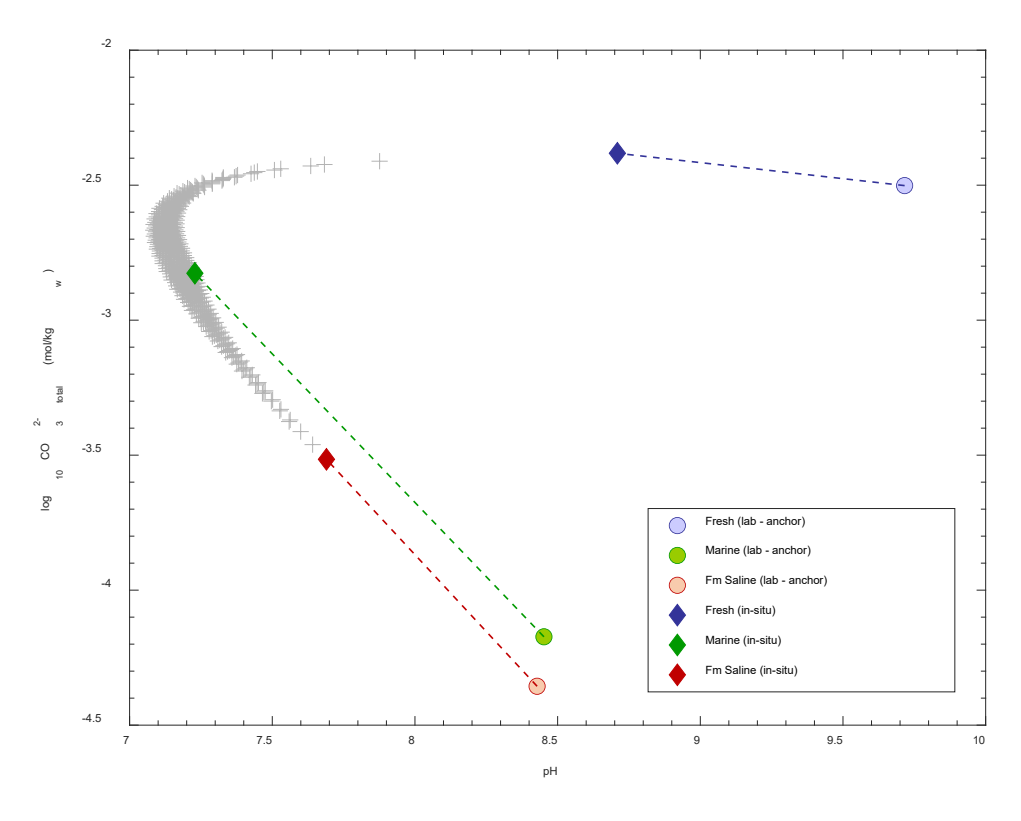


Figure C-3. Example of a multi-anchor problem for sorption of Ni(II) on Forsmark mixed groundwaters. Total carbonate concentration vs. pH is plotted for intermediate compositions ("+" symbols) formed by hydrodynamic mixing of the three end-members: fresh (blue markers), marine (green markers), and saline (red markers). Since the synthetic groundwaters used in laboratory investigations (circular markers) are perturbed relative to the in-situ mixing end-members (diamond markers), the problem involves extrapolation outside the locus of points describing all possible mixing trajectories.

In this calculation the *in-situ* groundwaters are assumed to be in equilibrium with calcite, quartz and hydroxyapatite. For the Fe³⁺/Fe²⁺ redox pair, equilibrium with the crystalline ferric-oxy-hydroxide, Fe(OH)₃ is assumed to control the Fe³⁺ concentration using equilibrium constants consistent with the calibration model derived by Grenthe et al. (1992). Here, the reduced species Fe(II), S(-II), and Mn(II) were included in the initial definition of the *in-situ* groundwater compositions, although for the laboratory synthetic groundwaters a pO₂ of 10^{-25} atm was used to specify redox as in the previous example.

In the top left-hand corner of Figure C-3 it is interesting to note that the equilibrium state of mixed compositions ("+" symbols) can have lower pH than the original end-members that are mixed. This result, although counterintuitive, is a consequence of the assumed mineral phase equilibrium (i.e. calcite precipitation-dissolution) in a closed system which results in a non-linear deviation from what would be obtained for a concentration-conservative mixing process. The three-component mixing model can also be represented more intuitively in a ternary diagram as shown in Figure C-4. Here, the K_d is estimated for the Forsmark rock *in-situ* for the site-specific conditions defined by hydrodynamic mixing of the 3 end-members (saline-marine-fresh).

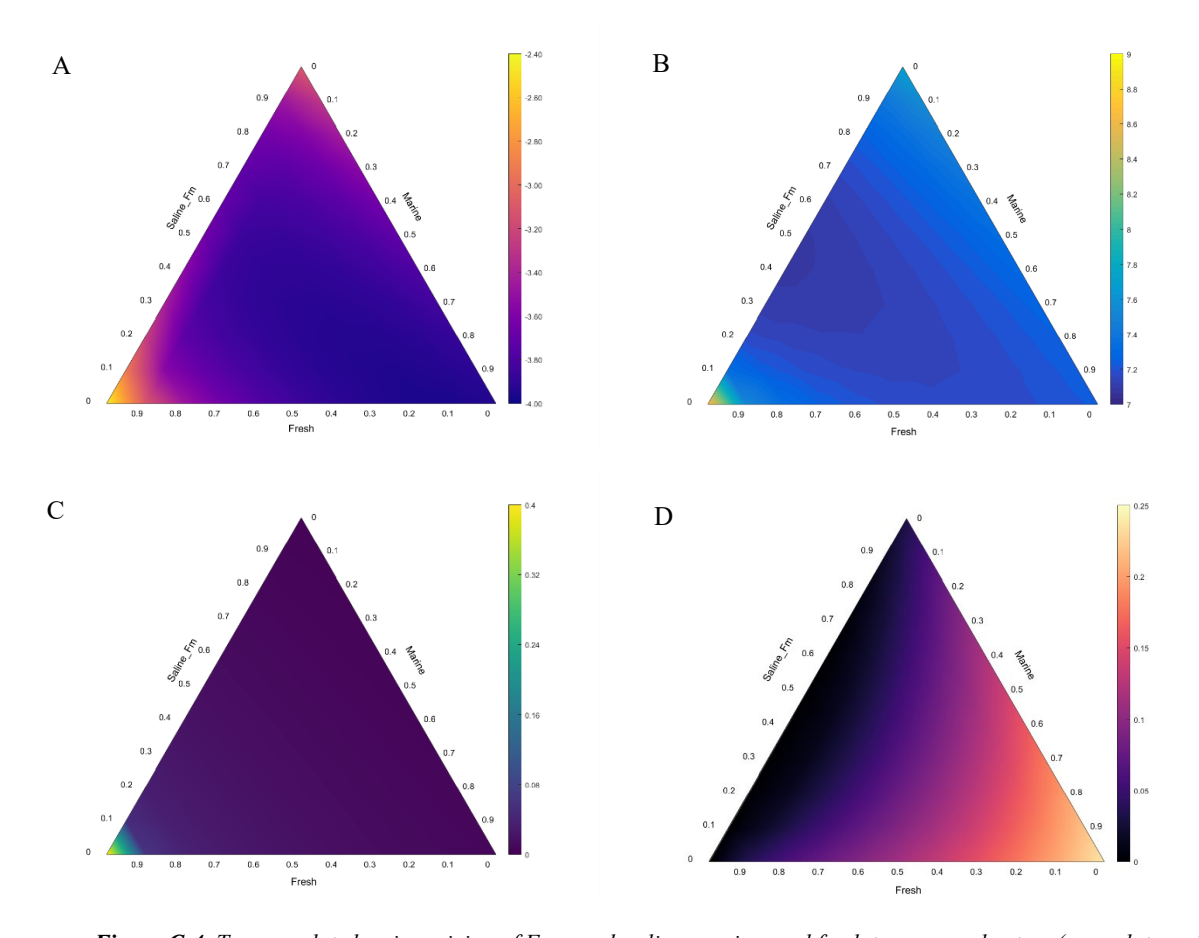


Figure C-4. Ternary plot showing mixing of Forsmark saline, marine, and fresh type groundwaters (same data as in Figure C-3). Plotted data: A) estimated $log_{10}K_d$ value (m^3/kg) for Ni(II) sorption on in-situ rock using the Forsmark saline composition as a single anchor; B) pH as a function of different groundwater mixed compositions; C) fraction of total Ni(II) concentration complexed by carbonate, and; D) fraction of total Ni(II) complexed by HS^- .

In this representation, the K_d values are extrapolated assuming the Forsmark saline anchor at the end-point pH and estimated pCO₂ achieved in the laboratory (red circular marker in Figure C-2). The vertices of the ternary diagram for the *in-situ* mixing problem, on the other hand, correspond to the unperturbed groundwater compositions (diamond markers) which have different pH, pCO₂, and Eh values to the lab values. Since we are not attempting to demonstrate consistency with measured R_d values in this example, the extrapolation uses the recommended K_d^0 value for Forsmark saline groundwater after the lab-to-field correction for surface area and mineralogy (i.e. f_m and f_q).

As can be seen from Figure C-4A, the extrapolated K_d calculated using the BB09 model implemented in PHREEQC varies by a factor of ~35 over the range of variation implied by hydrodynamic mixing of the three end-members. The model predicts the highest K_d values for the fresh groundwater type which is mostly related to the higher pH (Figure C-4B) of this groundwater relative to the saline and marine end-members. The effect of pH on the surface complexation outweighs the effect of increased solution complexation by dissolved carbonate in the fresh groundwater (Figure C-4C) which should otherwise lead to a decrease in K_d (compare the left-hand bottom vertex of the ternary diagrams for the fresh synthetic groundwater).

Chloride complexation has a minor impact on Ni(II) sorption, although this is mostly only relevant for highly saline groundwaters such as the brine reference composition and is not important for the three end-member ternary mixing example considered here. The surface complexation model only considers simple monodentate reactions with surface hydroxyl groups and ternary surface complexation reactions with carbonate and chloride are neglected, so may underestimate K_d in cases where such reactions make significant contributions to sorptivity.

After pH, however, the parameter which appears to have the largest impact on the modelled K_d in this example is the presence or absence of significant amounts of sulphide, HS– which forms solution complexes with Ni²⁺ according to the thermodynamic calculations made using the Thermochimie database (Giffaut et al. 2014). At high concentrations NiS may precipitate, thus limiting Ni mobility. However, at the trace concentrations considered for K_d calculations the effect is primarily disadvantageous due to the formation of Ni(HS)₂ which reduces the availability of Ni²⁺ for surface complexation. In the present context, Ni(II) is an interesting test case for the methodology since, while not *intrinsically* redox sensitive, it appears to exhibit *indirect* redox sensitivity due to sulphide complexation. The lowest K_d values for Ni(II) sorption are associated with the saline end-member which is at least partly owing to higher concentrations of HS– relative to the other groundwater types.

In the original concept for K_d extrapolation using chemistry correction factors as described in Crawford (2010), the justification for using the Forsmark saline groundwater as a main reference anchor was twofold. Firstly, the Forsmark saline groundwater was deemed to be most like the expected composition at repository depth during much of the temperate period when radionuclide release would have the greatest dose impact for surface communities (see Figure C-5). It is also projected to be representative of the dominant groundwater at repository depth for the first 1000 y post closure which is the period with the highest demand for quantitative safety assessment as stipulated by the radiation protection authority (SSM).

The use of the saline groundwater data as an anchor point would therefore imply smaller extrapolations for this period, and consequently reduced error if used as an anchor rather than the other groundwater compositions. Secondly, for most of the SDM-Site data sets there were significantly more measurements made for the saline groundwater than other groundwater types. The reference K_d^0 value estimated for the saline groundwater might therefore be reasonably expected to be more statistically representative than K_d^0 values derived for the other groundwater types. This was not applied uniformly for all data sets, however, and in the case of Sr(II) the measured R_d values for the saline groundwater were sufficiently close to the quantification limit that the fresh groundwater type was deemed a more appropriate reference anchor.

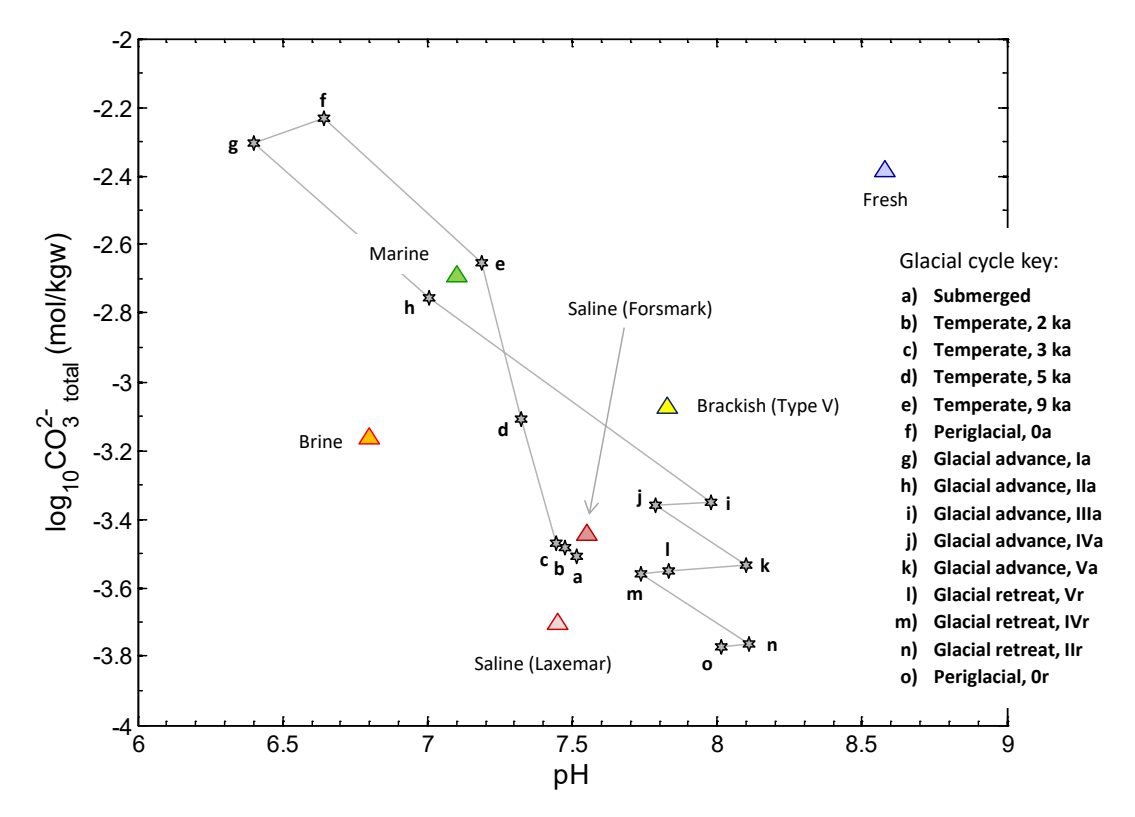


Figure C-5. Groundwater composition (total carbonate vs. pH) at the location associated with first canister failure in SR-Site (hexagram markers) compared with the groundwater types defined for the site descriptive modelling laboratory investigations (triangular markers). The groundwater composition at this location is expected to evolve over the reference glacial cycle as indicated by the legend key. Compositions corresponding to temperate climate conditions, periglacial, as well as different times during glacial advance and retreat are taken from calculations made by Salas et al. (2010).

Given that R_d measurement data for sorption often exhibit a range of variation that differs from predictions made using an assumed thermodynamic sorption model, there is a reasonable expectation that the use of multiple anchors representing several different synthetic groundwaters might give a better overall view of uncertainty than the use of a single anchor value. Since the underlying sorption model is identical regardless of which anchor is assumed, the net effect is simply to shift the response surface up or down depending on which reference K_d^0 is chosen for the calculation.

One way of approaching the problem of harmonising predictions for multiple (possibly conflicting) anchors would be to calculate a simple logarithmic mean and standard deviation taken over all predictions. This would give some indication of potential model uncertainty and preserve the shape of the response surface, thus honouring the underlying model constrained covariance of key variables. If there is greater confidence in data for certain anchors and lesser confidence in others, then the calculation could be modified to give greater weight to those which are deemed more accurate. For inaccuracies related to small sample sizes and standard errors associated with each K_d^0 anchor, a simple weighting function based on the uncertainty of individual anchor values might be used to give greater emphasis to extrapolations from more reliable anchors. Other, more sophisticated interpolation techniques are feasible, although it requires further investigation to determine whether they would reduce the overall extrapolation uncertainty.

C.3 Smart K_d estimates based on detailed groundwater modelling

While the calculations shown in the previous section are useful for demonstrating the basic methodology for K_d extrapolation, the example of ternary groundwater mixing is a simplified scoping-type representation and might not be appropriate for site descriptive or comprehensive safety assessment calculations. In SR-Site, however, detailed calculations of hydrogeochemical evolution of the Forsmark site were made for open repository conditions, temperate and submerged time periods, as well as a sequence of hydrochemical snapshots representative of a glacial cycle (see Figure C-6, which shows modelling results from Salas et al. 2010). The PHREEQC program was used for these calculations using the (paleo-origin) end-member mixing fractions calculated with the site-scale hydrogeological model in ConnectFlow (Joyce et al. 2010) and a minimal set of mineral phases thought to control equilibrium concentrations of key groundwater components.

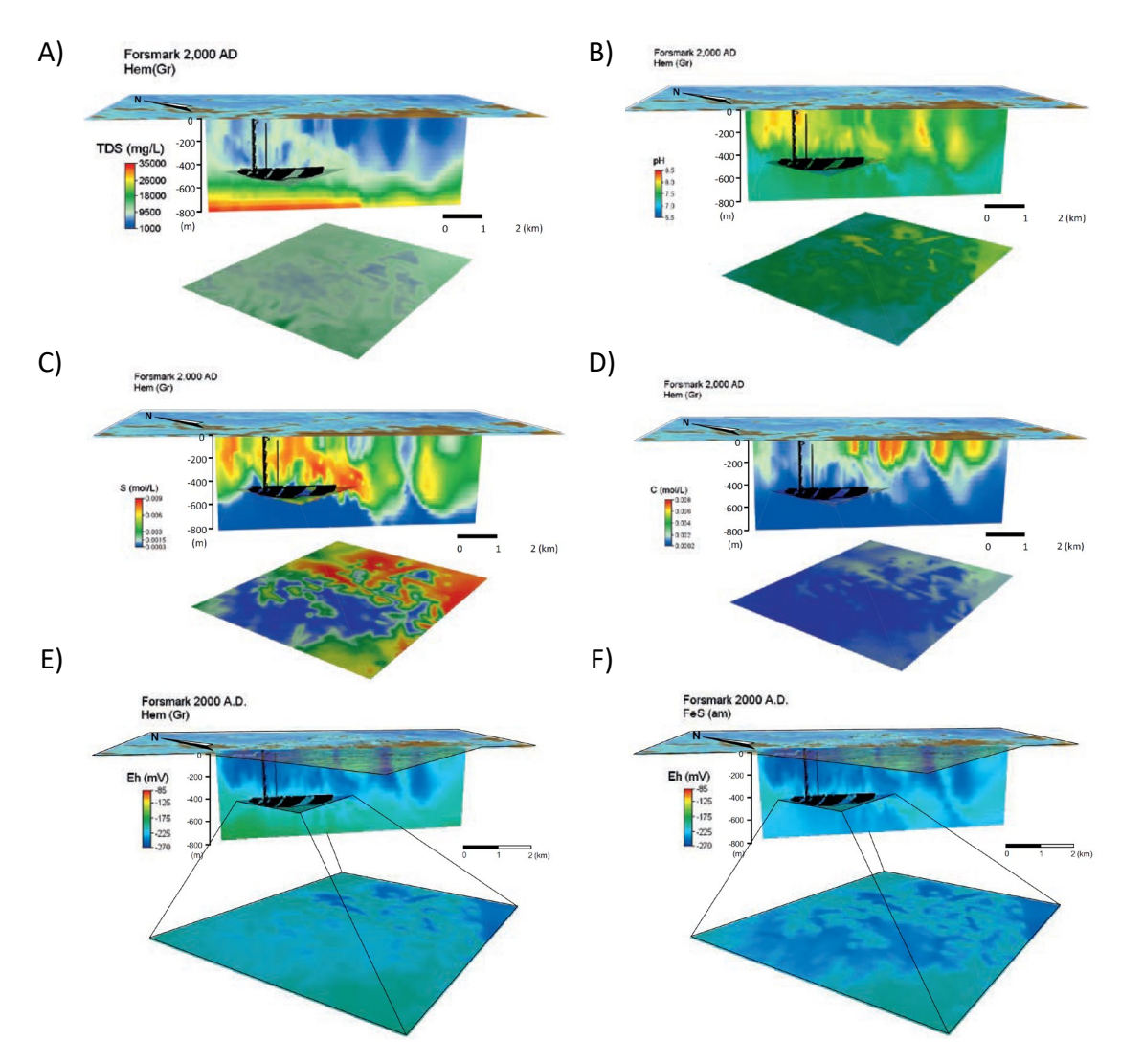


Figure C-6. Data snapshot of a vertical depth profile taken from Salas et al. (2010) for the groundwater situation at 2000 AD with different panels showing A) salinity, B) pH, C) total sulphur, D) total carbonate, as well as E) redox potential, Eh (mV) assuming $Fe(OH)_3$ control or, F) $FeS_{(am)}$ redox control.

As an extended methodological demonstration, the hydrogeochemical data from SR-Site are used to make simulations of Smart K_d in this section using the procedures outlined in the previous section. Since an updated thermodynamic database, Thermochimie v9b (Giffaut et al. 2014) has been used for these calculations, the *in-situ* groundwater compositions have been recalculated from the original end-member mixing fractions using the same modelling assumptions as in the reference (Salas et al. 2010).

The in-data for the calculation consisted of two text files for each timestep record with rows of output data extracted from the ConnectFlow simulations corresponding to a vertical and horizontal slice (respectively) through the local model volume at Forsmark and indexed by spatial coordinate triplets. The data are comprised of mixing fractions for the five paleo-origin end-members (deep saline, Littorina, altered meteoric, glacial, and an old meteoric end-member). The horizontal slice consists of 65 237 rows of data centred at repository depth in the elevation range -450 m to -490 m, while the vertical slice consists of 116 577 rows of data along a NW-SE transect approximately parallel to the shoreline. The details of the data extraction are described in Salas et al. (2010), although are not of great importance for the present demonstration. In the present demonstration calculations, only the vertical slice is considered since this is most like the previous scenario for the simplified ternary mixing model.

Two limiting cases for redox control were considered in the SR-Site hydrogeochemical simulations; one variant assuming Fe(III) oxy-hydroxide, Fe(OH)₃ using the calibrated equilibrium constant from Grenthe et al. (1992) and a variant assuming an amorphous Fe(II) mono-sulphide, FeS_(am) precipitate corresponding to a significant activity of sulphate reducing bacteria. In all *in-situ* groundwater calculations, equilibrium with calcite, quartz, and hydroxyapatite was assumed. The temperature of the *in-situ* groundwaters was taken to be 15 °C in accordance with the previous work by Salas et al. (2010). For the synthetic groundwater anchors used in the laboratory investigations, the same assumptions were made as used in previous examples.

The results of the SR-Site groundwater simulations are shown in Figure C-7 for Fe(OH)₃ redox control. The plot shows the calculated Smart K_d values versus pH and pCO₂ for 5000 randomly sampled compositions taken from the Salas et al. (2010) data set (filled markers). For illustrative purposes, extrapolated K_d data are shown for the marine anchor only. For comparison, a simply calculated response surface is shown for extrapolation from the marine anchor assuming the marine synthetic groundwater as a starting composition and adjusting pH and pCO₂ while other chemical parameters are held roughly constant (calcite equilibrium assumed). The response surface was calculated using the PHREEPLOT program (Kinniburgh and Cooper 2004).

As can be seen clearly from Figure C-7, the calculations for detailed *in-situ* compositions do not line up neatly on a single, low-dimensional response surface. This behaviour implies that simple parametric variation of pH and pCO₂ for a representative groundwater type does not capture the full complexity of sorptive variation for mixing of groundwaters of different origin even when evaluated using the same thermodynamic sorption model.

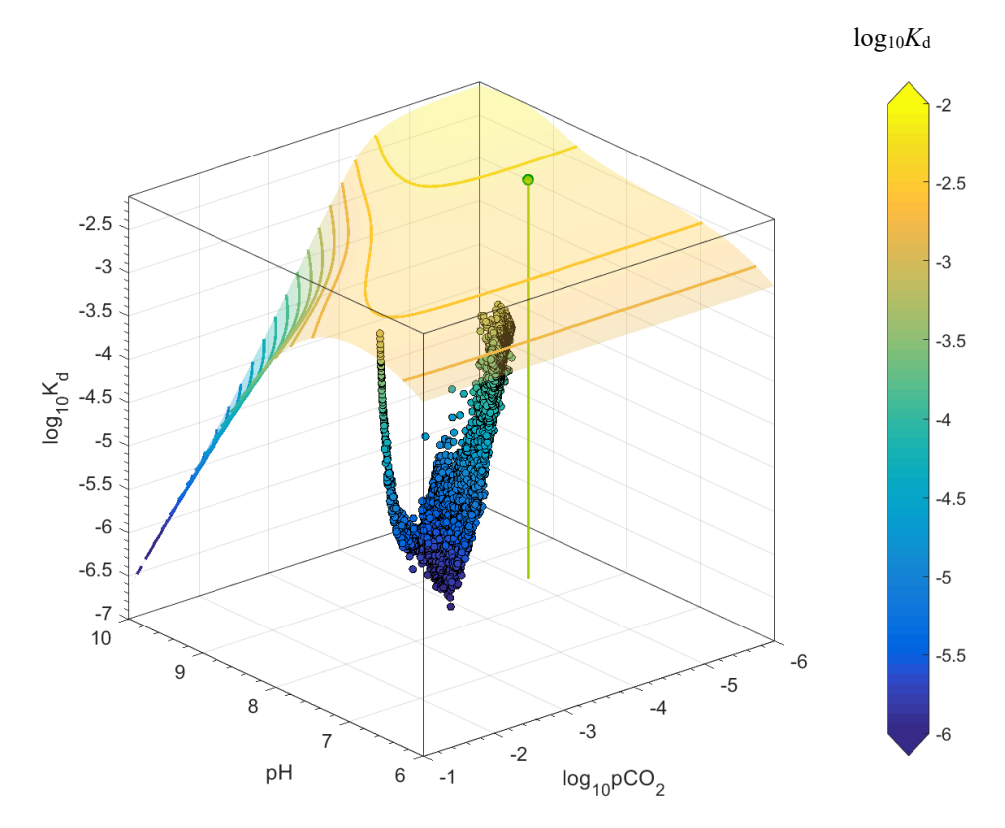


Figure C-7. Smart K_d (m^3/kg) values (log-values) calculated for Ni(II) sorption (circular markers) estimated for 5000 randomly sampled in-situ groundwater compositions for the present-day groundwater situation (2000 AD) at Forsmark based on the SR-Site hydrogeochemistry calculations by (Salas et al. 2010) assuming $Fe(OH)_3$ for redox control (see text for explanation). The response surface shows a simple extrapolation from the marine anchor varying pH and pCO2 only. The reference K_d^0 value for the marine groundwater is shown as a single circular marker embedded in the top surface with contextual stem showing the pH and pCO2 of the reference composition.

The same data can be plotted in different ways. Figure C-8, for example, shows the Smart K_d values mapped to the vertical NW-SE profile transecting the site as modelled by Salas et al. (2010). Figure C-9 on the other hand, shows the same data presented as a probability distribution (smoothed kernel density estimate) showing a stratification into two distinct sub-populations, one with a moderate sorptivity and another exhibiting very low sorptivity. Figure C-9 also shows the impact of assuming different groundwater anchors in the calculation.

The function describing the relative variation of K_d is similar for each case since it is calculated using the same thermodynamic sorption model. The only difference between the different cases is the reference K_d^0 value and the chosen synthetic groundwater composition used to estimate the K_d value in the denominator of the f_{chem} equation. Since both of these values are constants, this corresponds to a constant shift in the predicted Smart K_d probability density function with a magnitude dependent on the different anchors used to rescale the modelled data. The K_d variability implied by the offset between different K_d values calculated with different anchors should be considered part of the overall prediction uncertainty for the extrapolated values and only a lower bound on the true uncertainty.

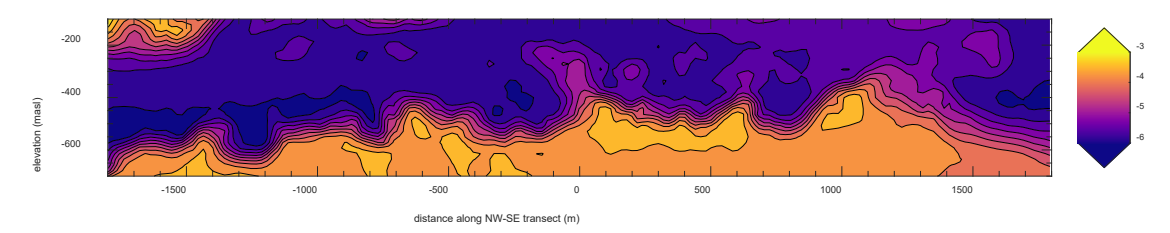


Figure C-8. Same data for Ni(II) sorption (5000 randomly sampled values) as shown in the previous figure, although mapped to the vertical NW-SE profile modelled by Salas et al. (2010).

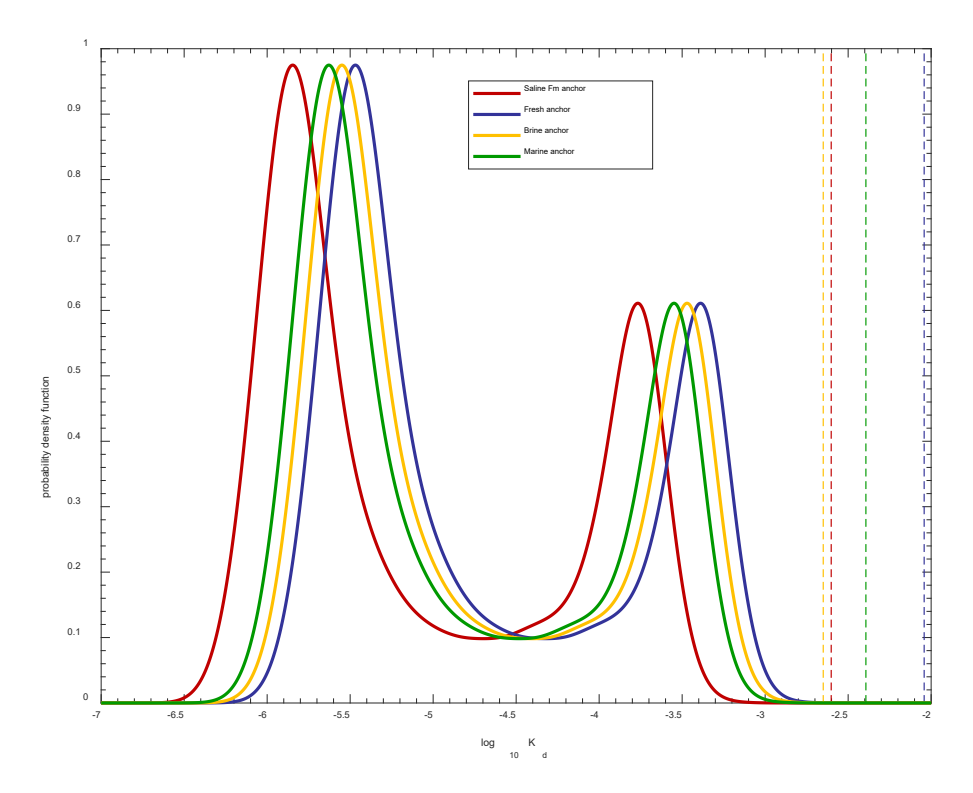


Figure C-9. Same data for Ni(II) sorption (5000 randomly sampled values) as shown in the previous figure, although presented as a kernel density estimate. Data are shown for each of the groundwater anchors illustrating an offset between predictions depending on which synthetic groundwater type is assumed as an anchor. The K_d^0 for each anchor is indicated by vertical broken lines on the right-hand side of the figure. Note that the extrapolated Smart K_d values do not necessarily follow the same order (smallest to largest) as the anchor values. The Smart K_d values are stratified into 2 distinct groups: one exhibiting a moderate sorptivity, and a larger population exhibiting very low sorptivity.

The present calculations shown in this section should only be considered a prototype demonstration of the methodology for estimation of Smart K_d values using chemistry correction factors. It is difficult to make reasonable extrapolations outside a narrow range of groundwater compositional variation where the underlying anchor values are based on a very limited data set that may not be fully representative of the sorption process, nor adequately span the region of parameter variation implied by the application groundwater compositional data. Furthermore, the use of a very simple non-electrostatic model of sorption for a single surface complexation binding site type as is the case with the BB09 model is likely not an accurate assumption outside its range of calibration. It is likely to be even more inaccurate for prediction of sorption where multiple mineral surfaces might contribute in a non-negligible fashion towards measured K_d values in laboratory measurements.

It is intended that a more detailed component additivity-based model will be produced and tested for those radioelements where non-mica minerals make significant contributions towards the overall sorptivity of the rock. It is envisaged that this modelling work will be informed by quantitative measurements of sorption on thin sections using digital autoradiographic techniques. This should result in a more accurate description of sorptive variability than can be otherwise achieved using first principles assumptions concerning the distribution of reactive surface areas.

Despite the inherent simplifications, the modelling results are useful since they clearly indicate an impact of speciation giving very low K_d values in some parts of the geosphere and much higher values in other parts. Since the multimodal probability density describing K_d variation reflects considerable spatial variability, it therefore would not be recommended to simply sample from the probability density directly without consideration of the trend of groundwater chemistry along individual migration paths. This represents a major shift in thinking relative to the previous limited handling of Smart K_d within SR-Site (i.e. for the cation exchanging solutes Cs, Sr, Ra). In transport calculations using codes such as MARFA (Painter and Mancillas 2013), Smart K_d values should ideally be supplied for individual migration paths mapped from the database of values calculated for the entire geosphere with additional consideration given to the timescale of evolving groundwater composition relative to the travel time of the radioelement.

C.4 Estimation of Smart K_d for radioelements lacking measurement data

As discussed in Chapter 5, it is difficult to envisage a laboratory campaign sufficiently comprehensive that one could quantify K_d values for all radionuclides of relevance to safety assessments including all relevant geological materials and contact water compositions. For this reason, the focus in SDM-Site was on quantifying the sorption of radioelements representing specific classes of sorptivity (Widestrand et al. 2003) with the aim of invoking geochemical analogies to assign K_d values for radioelements that were not studied.

An example calculation is shown in Figure C-10 showing how the K_d value for Pb(II) sorption varies relative to that for Ni(II) for a range of pH values and different groundwater types. The calculations are made using the BB09 model as previously. As can be seen from the plot there are significant variations in the K_d calculated for Pb(II) sorption relative to that for Ni(II) for different synthetic groundwaters over the range of pH values studied.

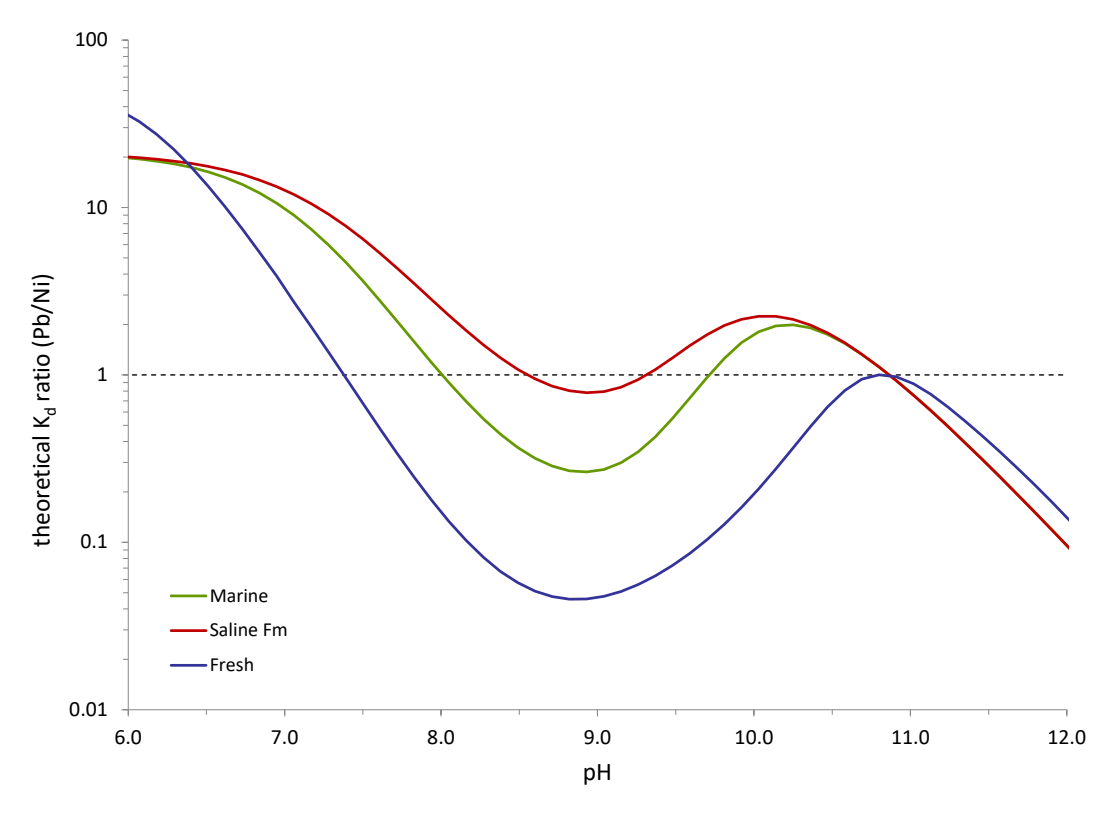


Figure C-10. Theoretically calculated K_d ratio for Pb(II) sorption relative to that of Ni(II) for different synthetic groundwaters where the pH is varied over a range by titration with HCl.

When invoking a geochemical analogy for extrapolation of data for Pb(II) sorption, however, we are not necessarily interested in comparing the K_d for Pb(II) and Ni(II) sorption at the same pH. Instead, we need to relate the calculated K_d for Pb(II) to the K_d value for Ni(II) at the reference composition (anchor point) of the groundwater corresponding to the K_d^0 value evaluated for Ni(II). The resulting f_{chem} curves are shown in Figure C-11 and are based on the same simulation data as in Figure C-10 except that the K_d ratio is now defined relative to the fixed anchor point for Ni(II) sorption in Forsmark saline groundwater at pH 8.43.

The calculations indicate that the K_d for Pb(II) is roughly in parity with that for Ni(II) in the Forsmark saline groundwater at the reference pH of 8.43, although for the fresh groundwater type the K_d for Pb(II) should be about 10 times lower than the K_d for Ni(II) in the saline groundwater. Here, it should be noted that the reference state is the K_d value for Ni(II) in Forsmark saline groundwater at the reference pH, and all f_{chem} values shown for Pb(II) in Figure C-11 for the plotted groundwater types are defined relative to this value.

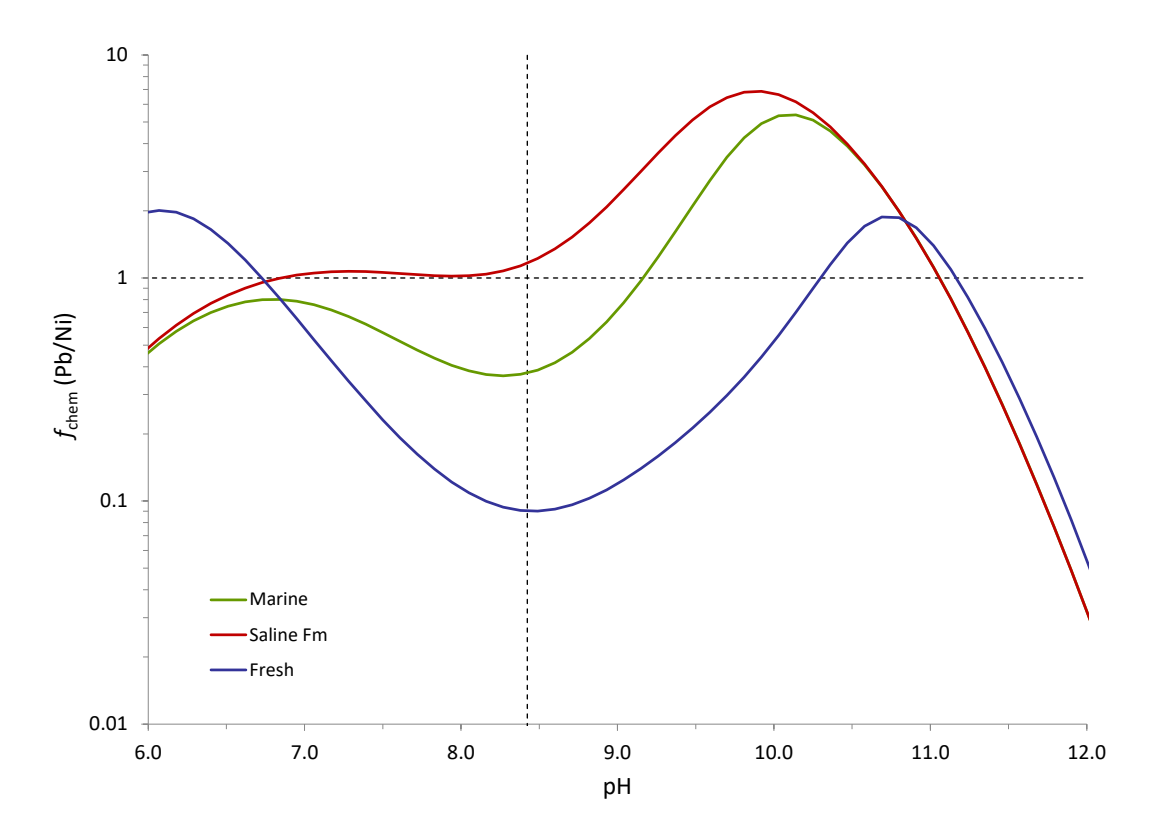


Figure C-11. Theoretically calculated f_{chem} curves for extrapolation of K_d values for Pb(II) sorption from measurement data obtained for Ni(II) in contact with Forsmark saline groundwater (anchor) at the pH where measurement data are obtained (pH \sim 8.43).

Appendix D Transport modelling using the time domain random walk approach

This appendix presents the modelling algorithm and transport equations for solute transport calculations with the time domain (TD) random walk approach introduced in Section 7.2.3. Note that the description below uses the β and τ notation for the main flow-related parameters that is common in the scientific literature; β and τ correspond to F and t_w , respectively, in the notation usually used by SKB and Posiva.

For each fracture segment, the mass discharge at the outlet can be written as a convolution of the time-dependent mass input f_{in} to the segment and a transit (travel) time distribution:

$$r_{out}(t) = \int_0^t f_{tran}(t - t') f_{in}(t') dt'$$
 (D-1)

where f_{tran} is the probability density for the solute transit time t_{tran} . The random variable t_{tran} [y] is the sum of two other random variables:

$$t_{tran} = \tau + t_{ret} \tag{D-2}$$

where τ [y] is the travel time of a non-sorbing species not affected by matrix diffusion and t_{ret} [y] is the retention time in the matrix, which has a related pdf (f_{ret}). The retention time distribution is conditioned on β (Equation 3-3, i.e. F in SKB notation) and thus f_{tran} can be expressed as the following convolution

$$f_{tran}(t_{tran}) = \int_0^\infty \int_0^\infty f_{ret}(t_{tran} - \tau | \beta) f_{\tau,\beta}(\tau,\beta; \bar{\tau},\bar{\beta}) d\tau d\beta$$
 (D-3)

where $f_{\tau,\beta}$ is the joint probability for τ and β and f_{ret} is the retention time distribution. The quantities $\bar{\tau}$ and $\bar{\beta}$ are averaged quantities over the considered fracture segment. The joint probability $f_{\tau,\beta}$ can be expressed as $f_{\tau}(\tau)f_{\beta|\tau}(\beta|\tau)$, i.e. the probability density for τ multiplied by the probability density for β conditioned on τ . The mass discharge at the fracture outlet is then given by the triple integral:

$$r_{out}(t) = \int_0^t \int_0^\infty \int_0^\infty f_{ret}(t_{tran} - \tau - t'|\beta) f_{\beta|\tau}(\beta|\tau) f_{\tau}(\tau) f_{in}(t') d\tau d\beta dt'$$
 (D-4)

However, the TD random walk method can be simplified by neglecting spatial variability inside each segment. Then, we get that $\tau/\bar{\tau} = \beta/\bar{\beta}$, which leads to $f_{\tau,\beta}(\beta|\tau) = \delta\left(\beta - \bar{\beta}\frac{\tau}{\bar{\tau}}\right)$. This simplifies the mass discharge formula by avoiding the integration over β :

$$r_{out}(t) = \int_0^t \int_0^\infty f_{ret} \left(t_{tran} - \tau - t' \middle| \bar{\beta} \frac{\overline{\tau}}{\overline{\tau}} \right) f_{\tau}(\tau) f_{in}(t') \, d\tau dt'$$
 (D-5)

In the TD framework this integral is solved as a sequence of Monte Carlo steps:

- 1. The *i*-th particle is launched by randomly sampling a starting pathline and a starting start time t_0 . The starting time t_0 is sampled from the normalised source function (f_{in}) , whereas the pathline is uniformly sampled from the (predefined) equiprobable set of particle pathlines.
- 2. The (precomputed) $\bar{\tau}$ is randomised to account for longitudinal dispersion; that is, τ is sampled from the appropriate distribution $f_{\tau}(\tau; \bar{\tau})$ accounting for longitudinal dispersion.
- 3. Given the τ sample, β is then sampled from the conditional distribution $f_{\beta,\tau}(\beta|\tau)$. If within-fracture variability in aperture is neglected, then $\beta = \tau/b = \tau \bar{\beta}/\bar{\tau}$.
- 4. The arrival time for the *i*-th particle and the *j*-th pathway segment is then calculated as $t_{ar.i}^{j} = t_{ar.i}^{j-1} + \tau + t_{ret}$.
- 5. Steps (2)-(4) are repeated until the particle hits the outlet segment (j = M).

The cumulative breakthrough curve (cumulative mass discharge) can then be computed using this Monte Carlo estimate:

$$R_{out}(t) = \frac{S_0}{N} \sum_{i} H[t - t_{ar,i}^M]$$
 (D-6)

where H[-] is the Heaviside function and S_0 (mol) is the total injected amount, which is evenly distributed among all the particles. The instantaneous breakthrough curve can be reconstructed using kernel-based methods. This algorithm along with a broad range of retention models are implemented in the numerical code MARFA.